Universitat Autònoma de Barcelona

Printed Graphene for Energy Storage and Sensing Applications

Bhawna Nagar

Universitat Autònoma de Barcelona

Institut Català de Nanociència i Nanotecnologia

Ph.D THESIS

Printed Graphene for Energy Storage and Sensing Applications

Bhawna Nagar

For the Degree of ***Doctor of Philosophy***

In Material Science programme of

Universitat Autònoma de Barcelona (UAB)

Thesis advisors:

Prof. Dr. Pedro Gómez-Romero, CSIC

&

Prof. Dr. Arben Merkoçi, ICREA

UAB Tutor: Prof. Manel del Valle Zafra

Institut Català de Nanociència I Nanotecnologia (ICN2)

Bellaterra-08193, Barcelona, Spain

May, 2019

Declaration

Prof. Pedro Gómez-Romero and Prof. Arben Merkoçi, Research professors at Catalan Institute of Nanoscience and Nanotechnology.

We hereby certify that the thesis entitled “Printed Graphene for Energy storage and Sensing applications” submitted by Bhawna Nagar in partial fulfilment of the requirements for the degree of Doctor of Philosophy was carried out under our supervision and we authorize its submission for oral defense.

Prof. Pedro Gomez-Romero

(Director)

Prof. Arben Merkoçi

(Director)

Prof. Manel del Valle Zafra

(UAB Tutor)

Declaration

I hereby declare that the work in this thesis entitled “Printed Graphene for Energy storage and Sensing Applications”, is the result of research carried out by me at the ‘Catalan Institute of Nanoscience and Nanotechnology (ICN2)’ under the supervision of Prof. Pedro Gomez-Romero (thesis director), Prof. Arben Merkoçi (thesis director) and, Prof. Manel del Valles Zafra (tutor). In keeping with the general practices of reporting scientific observation, due acknowledgments have been made whenever the work described is based on the findings of other investigators. Any omission which might have occurred by oversight or error of judgment is regretted.

Bhawna Nagar

Acknowledgements

I would like to start by thanking and showing utmost gratitude to my Professors, Prof. Pedro Gomez-Romero and Prof. Arben Merkoçi for their constant guidance and help throughout the journey of this thesis. Along with sharing their knowledge and experience, they provided me the freedom to work on my own, try my own ideas and grow as a researcher. They have been really encouraging, understanding and supporting all this while. I would like to acknowledge the Spanish Government and ICN2 for the Severo Ochoa (SO) grant which covered my salary, part of the UAB tuition fees, expenses to attend conferences and also to pursue research to other laboratories. I thank my tutor Prof. Manel del Valle Zafra from UAB.

I would like to thank Dr. Deepak P.Dubal for teaching and guiding me all about the designing and working of supercapacitors. All the discussions, endless possibilities of trying different materials strategies etc. and the way of working all helped me in one way or the other. A big thanks to Dr. Alfredo de la Escosura, it was a pleasure working with him.

Special thanks goes to my groupmates, colleagues and friends from Spain as well as from India with whom I had shared my bad and good moments, cried and laughed with, had conversations about life and science and so on. Finishing the thesis would have been much more difficult and monotonous without all of them. Love you guys and thank you!!

I cannot thank enough my parents (Sanjay and Harshi Nagar), brothers (Karan Nagar), and my husband (Cyril Daniel) for their unconditional love, for believing in me, for being there for me no matter what. They have been a continuous source of encouragement and joy. A special thanks to my darling Kittu, the difference you made by coming to our lives is undefineable, thank you for everything. We will love you and miss you forever. I wouldn't have been where I am without my parents. Mummy, papa I love you!

Abstract

The focus of this thesis has been the design and preparation of flexible graphene-based electrodes and their printing using different techniques for applications in energy storage, specifically supercapacitors and electrochemical sensing devices. Different strategies have been employed keeping in mind the end application and accordingly graphene or its hybrids were prepared using different synthetic routes along with careful selection of the available printing techniques as well as the substrates. For energy storage part (Chapter 2), Supercapacitor devices with high capacitances, energy and power density have been demonstrated over Cloth (Carbon), Paper (Common A4 paper) and Plastic substrates using different printing techniques, graphene hybrids as well as hybrid electrolytes. In the case of Sensing applications (Chapter 3), two sensors have been demonstrated over plastic substrates. A high sensitivity DNA (Bio)sensor for viruses using one step facile printing is shown, the structure and operation of which in principle can be extended to other bio-analytes with interest for applications in various areas. In another study, extremely high concentration yet stable graphene inkjet printable ink has been prepared and its use as a bacterial sensor has been demonstrated as a proof of concept. The graphene ink prepared could produce highly conducting patterns that in principle can offer other bio or chemical sensing with high sensitivities.

Studies of different printing techniques were carried out and suitable inks were formulated and tested for each technique with optimization of the printing parameters in order to obtain reproducible films and hence reproducible device fabrication has been the focus. The main printing/coating techniques used in this Thesis are Doctor blade coating, Inkjet printing, screen printing and wax stamping technique. The project therefore involved a very important part of synthesis and characterization of graphene and derivatives, formulation of inks and finally device integration and testing.

List of Abbreviations

AC - Activated Carbon
AM - Active Material
CIJ - Continuous Inkjet
CV - Cyclic Voltammetry
CVD - Chemical Vapor deposition
DET - Direct Electron Transfer
DNA - Deoxyribonucleic Acid
DoD - Drop on Demand
EC - Ethyl Cellulose
EDLC - Electric double layer capacitance
EIS - Electrochemical Impedance Spectroscopy
EPPG - Edge Plane Pyrolytic Graphite
ESR - Electrochemical Series Resistance
ETK - Electron transfer kinetcics
GCD - Galvanostatic charge/Dicharge
GCE - Glassy Carbon Electrodes
GIC - Graphene Intercalation Compounds
GO - Graphite Oxide
GPE - Gel Polymer electrolytes
HOPG - Highly Ordered Pyrolytic Graphite
IL - Ionic Liquid
IoT - Internet of Things
ITO - Indium Tin Oxide
LAPS - Light addressable Potentiometric Sensors
LPE - Liquid Phase Exfoliation
LSV - Linear Sweep Voltammetry
NPs - Nanoparticles
OFET - Organic Field Effect Transistor
Oh - Ohnesorge Number
PANI - Polyaniline
POM - Polyoxometalates
PPy - Polypyrrole
rGO - reduced Graphene Oxide
Re - Reynolds Number
RNA - Ribonucleic Acid
SC - Supercapacitors
SPE -Screen Printed Carbon Electrodes
TFT - Thin Film Transistor
We – Zeber Number

Table of Contents

CHAPTER 1
Introduction to Graphene and its Printing

1.1. Printing: From Bibles to High-tech Devices

Putting things down in black and white has never been easier. Since the 15th century, we have come a long way from using highly sophisticated and expensive tools for printing towards easy to handle, high performance and low cost printing techniques that are not only useful in printing graphics or writing texts on a paper, but also highly advantageous at laboratory level i.e. for printing of nanoscale materials into devices. This art of reproducing texts or images to pass-on or preserve information is used for completely different purposes in scientific research areas. Here, the same established techniques are adapted for depositing inks containing functional micro or nanomaterials over a desired substrate with the aim of coating, precisely studying the behavior and application of that specific material and for device fabrication. Metallization on hard substrates have garnered huge interest for fabrication of electronic devices like transistors, chemical/bio sensors, energy devices etc. Several metals, their oxides or semiconductors are used for coating of the substrate material in form of thin films or nanoparticle films[1][2][3] so as to impart their electrical, thermal or optical properties depending on the type of application. For instance Hui Ling et al patterned gold nanoparticles over Si substrate using Self-assembly and soft Lithography patterns for OFET applications [4], and a review article by S.N.Arifin *et al* talks about several metal oxide thin films used for phototelectrochemical splitting of water [5]. Although these coatings on hard substrates have shown excellent functioning, the focus has significantly shifted to printed flexible devices for advancements of next generation devices. This change emanates in order to meet the need of small size, flexible, easy to use and low cost devices. Many reviews have discussed the emergence of devices based on flexible substrates highlighting their importance and need in each area and a lot of work has been done on the deposition of metal films or nanoparticles over flexible substrates

namely polymers, papers, textiles, and metal foils [6][7][8][9][10]. However, the research of all these devices is incomplete without the incorporation of graphene into the system as an alternative of expensive energy-critical and scarce elements or as a base to design hybrids able to provide enhanced properties [11] [12]

1.2. Motivation and Objective

Printing 2-D materials, and particularly Graphene, has gained much interest in electronic and medical industries in the last 10-15 years [13]. Evidently, graphene has shown its exceptional potential in numerous applications, and therefore it is reasonable to invest resources for finding ways to use it for mass applications, especially in terms of production and processability. For this, printing has shown several advantages over conventional photo-lithography, electroless platings or vacuum deposition methods. Recent works dealing with these multi-step and complex processes, require sophisticated and expensive instruments and specific atmospheric conditions. Furthermore, conventional methods involve the use of harsh chemicals, large material requirements, need of a specialized person performing the task, and most importantly they cannot be applied on all types of substrates, thus difficulting their use in mass production [14][15]. On the other hand, printing techniques are additive manufacturing processes as opposed to the above subtractive processes. Selective layer by layer material deposition takes place which allows the use of minimum material quantity, providing different features depending on the end applications. Printing techniques offer several advantages and are comparatively easy to handle whilst providing high-resolution and precise patterns [16][17][17], but it wouldn't be justified to say that these are achievable without any obstacles. The best results are achieved by combination of the whole manufacturing process, starting from Graphene production until the sintering process. The first step is the Graphene preparation method. It is very important to select a bulk production method that leads to the required properties at the end and it is also particularly important to be able to limit or control the amount and nature of defects or heteroatoms in graphene, For instance, pristine graphene that is

needed to make electrodes with the sole purpose of conducting electrons in applications like semiconductors or transistors etc.[18][19], having defective sites or edges may break the connections resulting in decreased conductivity whereas in some other applications, graphene with high oxygen functionalities is needed to make modifications on the electrodes or some might even require specific functionalization of the graphene sheets [20][21][22].

With these considerations comes the challenge of preparing devices that offer not only high performance but also are industrially feasible, eco-friendly as well as cost effective. This is the challenge that has been tackled in the thesis, i.e. to integrate research with the simple printing / coating techniques in order to bring the devices closer to real applications.

The structure of the Thesis is graphically summarized in the following diagram:

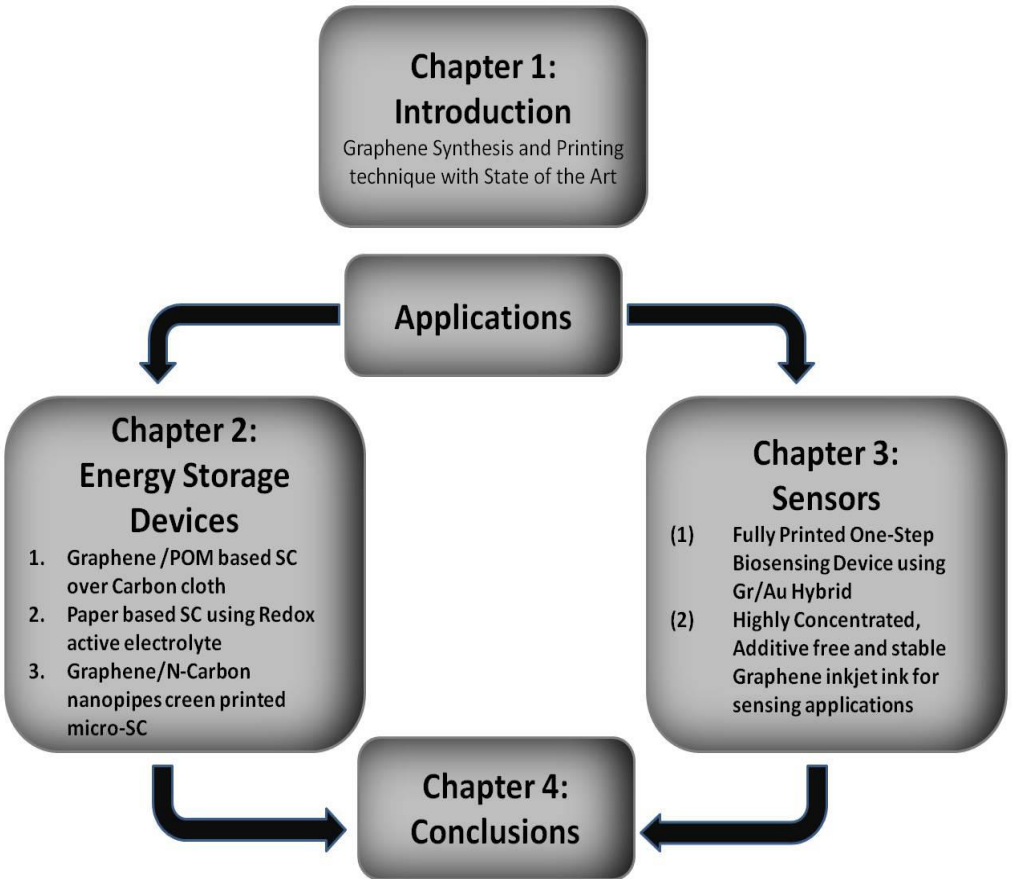

1.3. Graphene

Research on graphene for various different applications has been going on at a relentless pace. Graphene as per the International Union of Pure and Applied Chemistry (IUPAC) is an atom thick layer of carbon atoms arranged in hexagonal lattice. It began with the theoretical study made by a Canadian physicist Philip Russel Wallace where he reported for the first time electronic band structure of Graphene. In his pursuit of studying properties of 3-D graphite, he conceived a 2 dimensional analog (graphene) for comparison[23]. Later the term 'Graphene' was coined by Hanns-Peter Boehm and colleagues in the IUPAC nomenclature in 1986 which was a combination of Graphite and suffix –ene for the presence of polycyclic aromatic hydrocarbon [24]. Long before that, Boehm along with A. Clauss and U. Hoffmann had produced and identified the single layer carbon foil (thinnest carbon layers of the reduced graphite oxide) based on TEM contrast in 1962 [25]. But it wasn't until 2004 that for the first time, Andre Geim and Konstantin Novoselov isolated, characterized and studied the electronic properties of stable graphene sheets that were pristine and without any defective planes using a very simple approach famously known as the "scotch tape method" [26]. This major breakthrough which was duly awarded the Nobel prize in Physics in 2010 [27] started a pool of research on graphene, and studies on its unique properties could be finally made. It was shown it is 300 times harder than steel with a Young's modulus of 1 TPa and intrinsic strength of 130 GPa [28], has high electron mobility (charge carrier mobility of 200000 cm^2/V s)[29][30], is thermally more conducting than diamond with thermal conductivity up to 5000 W/mK [31], has a very high theoretical surface area of 2630 m^2/g [32], along with being flexible and transparent (optical transparency of 97% or absorption of 2.3%) [33][34]. All these exceptional properties just in one atom thin layer of carbon.

1.3.1. Graphene Preparation Methods

There are various ways by which Graphene can be produced, for specific research applications or for mass production. The synthesis methods can be broadly categorized into top down and bottom up approaches, as shown in fig. 1.

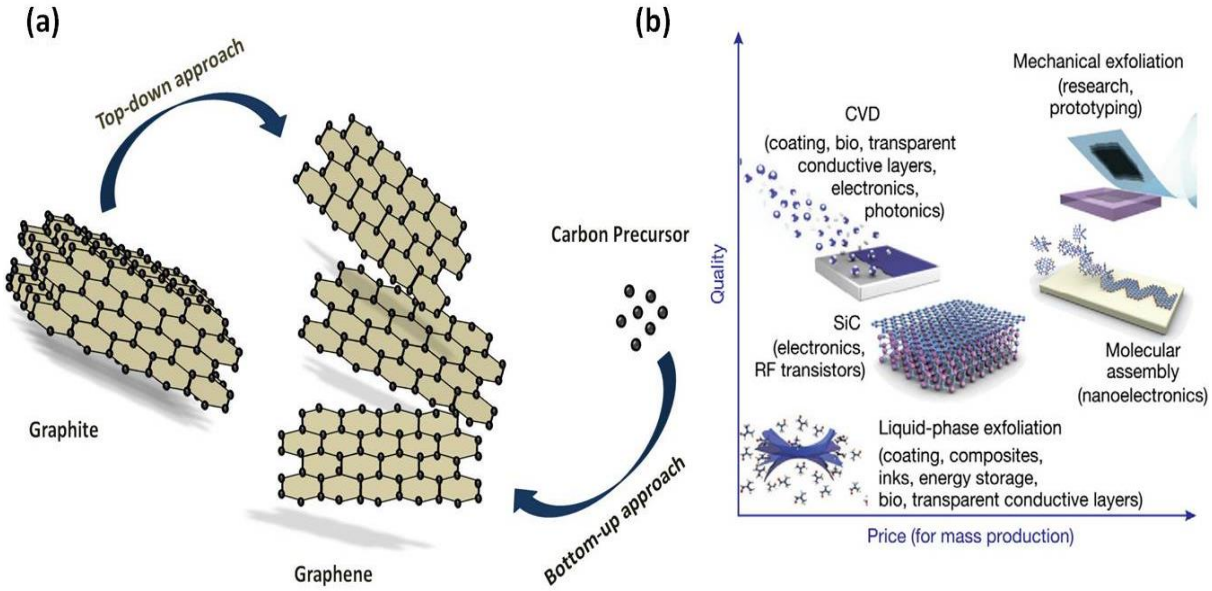

Figure 1: top down and bottom approach for the synthesis of graphene (a) and comparison of quality and price using these techniques [35](b)

1.3.1.1. Bottom-up approach

In applications like electronic devices, where high quality graphene is needed, the fabrication methods used are- **Epitaxial Growth**, in which Silicon carbide is thermally decomposed at elevated temperatures (usually above 1200 °C) under ultra-High vacuum or atmospheric pressure (under Ar atmosphere) causing Si to sublime, leaving only carbon for graphitization. These carbon atoms segregate on the surface forming interfacial, single layer, bi-layer or few-layer graphene. Depending on the growth of Carbon on either Si or carbon terminated SiC, different growth rates and electronic properties are obtained [36][37][38]. **Chemical Vapor Deposition (CVD)** which uses decomposition

of gaseous or liquid precusors (Methane, acetylene, ethylene or hexane) or sometimes polymers to form graphene patterns in presence of a transition metal catalyst (such as Cu and Ni) that also acts as a substrate at high temperatures (650 – 1000 °C). The hydrocarbon or other precursors dissociate into free carbon and Hydrogen atoms where the C atoms diffuse to the catalyst to form the graphene structure. Large polycrystalline graphene films with low defects can be grown using this technique, however it is expensive method and requires the transfer of grown film from metallic substrate to dielectric or other substrate of interest, this can result in addition of impurities [39][40][41].

But, for mass production purposes, Top down approaches like Chemical route and exfoliation [42] methods are of interest, are favorable for graphene solution based processing as well as for ink formulations, however , the quality obtained from these methods are not as high as the quality obtained from the bottom-up methods described above.

1.3.1.2. Top-Down approach

Scotch Tape method

Here, an adhesive cellophane tape is used to mechanically peel off the graphene layers from graphite repeatedly, Fig. 5(b). Later, the thin sheets attached to the adhesive are removed in acetone and transferred to a smooth Si substrate [43][26].

Chemical Oxidation of graphite to form graphite oxide :

It is based on the oxidation of graphite forming graphite oxide using strong acids and oxidizing agents and later the complete delamination of 3D graphite oxide (frequently with ultrasounds) to obtain 2D graphene oxide, this is generally followed by a reduction step to remove (at least some of) the oxygen functionalities. Four different chemical oxidation procedures are generally referred to in the literature: (i) Brodie method (ii) Staudenmaier method, (iii) Hofmann method and (iv) Hummers method (Fig. 2).

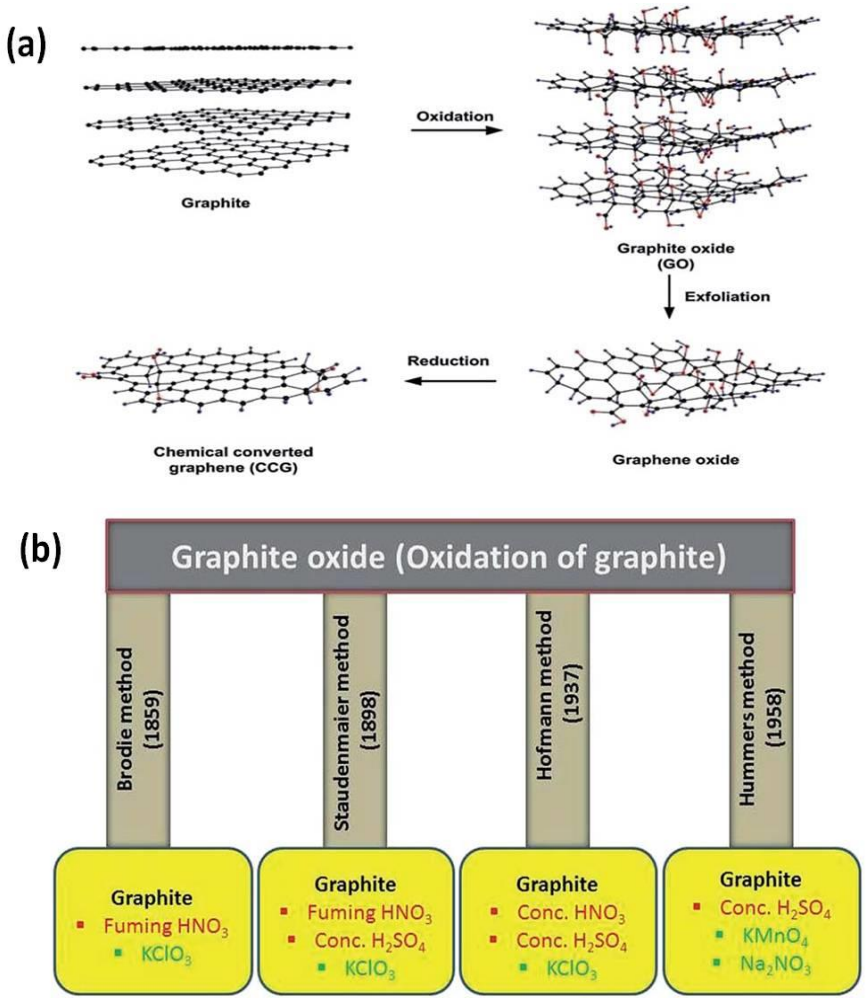

Figure 2 : (a) schematic of formation of reduced Graphene Oxide (rgO) from graphite using oxidative exfoliation of Graphite [44] and (b) Method used for chemical oxidation [45].

Brodie in 1859 studied a series of chemical reactions on graphite in order to calculate its weight and properties. For this purpose graphite was treated with potassium chlorate and solubilised in fuming nitric acid. This treatment was repeated after drying the material at 100 °C continuously many times until the limit of oxidation was achieved (no difference in appearance was observed after the fourth or fifth time). This created an oxidized product that was dispersible in pure water but not in the acidic medium or mediums containing salts, with his observations on the formed materials, he named it graphic acid. The resulting product had a percent composition of C: H: O ratio 61. 04 : 1.85 : 37.11. There were many downsides of using this method some of which included long reaction time

(3-4 days), use of harsh chemicals, production of toxic gases etc [46]. Staudenmaier in 1898 made improvements in Brodies work by using concentrated H_2SO_4 and aliquots of potassium chlorate during the whole reaction time. He could prepare a highly oxidized Graphite oxide (C : O ~2 : 1) in a single procedure, contrary to Brodie's procedure where several oxidation steps were performed. Nevertheless, it suffered the same drawbacks like long reaction times and evolution of toxic gases that was a cause of frequent explosions[47]. While Hoffmann in 1937 made a slight change in Staudenmaier procedure by using concentrated nitric acid instead of fuming nitric[48], much bigger difference in the synthesis route was brought in by Hummers and Offeman in 1958. In their procedure they mixed graphite with concentrated H_2SO_4, $NaNO_3$ and $KMnO_4$, the obtained brownish paste was then mixed with H2O2 to eliminate the residual permanganate species (by converting the permanganate and manganese dioxide to soluble manganese sulphate). They eliminated the use of potassium chlorate and nitric acid and improved the preparation procedure drastically in terms of time and safe operating conditions, however it holds the negative point of long and time consuming separation and purification process[49]. Dimiev and Tour explained the mechanism of formation of graphene oxide in their study and concluded that there are three distinct and independent stages of graphene oxide formation. Stage one is the formation of graphite intercalation compounds, second is the conversion of these GIC into oxidized product with third stage being the conversion of graphite oxide into graphene oxide with water exposure [50]. Marcano et al from Tour's group in 2010 produced GO by modifying some parameters from Hummers' method. They used a mixture of sulphuric and phosphoric acid (H_2SO_4:H_3PO_4 9:1) instead of sodium nitrate, which eliminated the evolution of harmful gases along with providing easy control over temperature. Also, higher volumes of well oxidized GO was obtained in this case compared to Hummers method [51]. Benzyl peroxide [52] and (H_2CrO_4/H_2SO_4) [53] have also been used as oxidizing agents for oxidative exfoliation of graphite.

Exfoliation

Liquid Phase Exfoliation

In **liquid phase**, two adjacent layers of graphite are detached from each other by providing shear force stronger than the inherently weak van der Waals force of attraction between them in presence of an organic solvent. The mixture is generally sonicated for long hours and was first reported by Hernandez et al [54]for the exfoliation of Graphite in NMP. The changes in pressure arising from propagating sonic waves create localized cavitations (micro-bubbles). These, upon collapse (under the effect of continuous sound waves) produce micro explosions generating shockwaves that separate the sheets. Since then, a lot of work has been published using this technique. The mechanism and possible forces acting during liquid phase exfoliation are presented in Fig. 3(a). Here, the rate of exfoliation depends on the sonication power and the solvent medium used. Graphite crystals can be dispersed and sonicated in different liquid media, that can be (Fig. 3(b)) , **(i) organic solvents** having surface tensions in the range of 40-50 mJ/m^2 [54], these media have surface energies closer to that of Graphite which helps in a better exfoliation and dispersion of the graphene sheets. Commonly used organic solvents for this purpose are NMP, DMAc, DMF etc. and the resulting graphene concentration is typically <0.01mg/ml. Some work has also been carried out using solvents of perfluorinated aromatic molecules like hexafluorobenzene (C_6F_6), octafluorotoluene ($C_6F_5CF_3$), pentafluorobenzonitrile (C_6F_5CN), and pentafluoropyridine (C_5F_5N) that achieved higher concentration of exfoliated graphene (0.1mg/ml) [55], Other works also reported the addition of organic or inorganic salts to the organic solvents [56][57]. In addition to the relatively small concentration reached, the organic solvents used in graphene exfoliation present as main drawback their high boiling points and various degrees of toxicity, which could limit their use. **(ii) Ionic liquids**, these are organic salts whose melting point is <100 ºC. Reported works have shown the concentration of up to 5.33 mg/ml using sonication. These provide high concentrations but also have high boiling points and are expensive and difficult to remove later [58][59]. **(iii) Addition of Surfactants or polymers to water.**

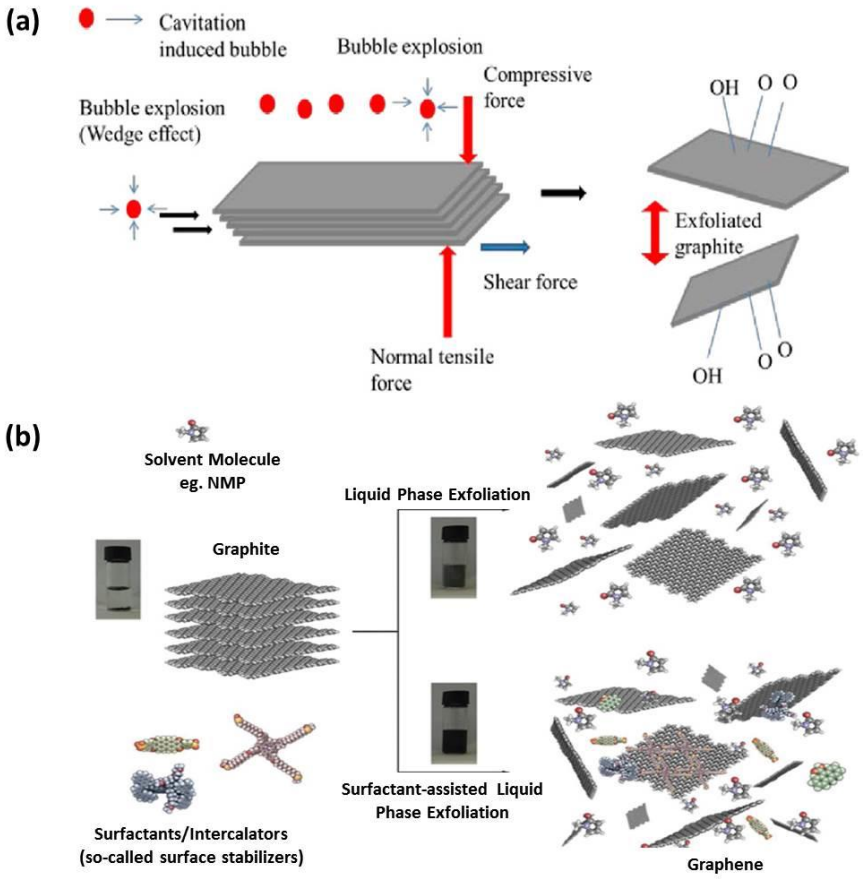

Figure 3: (a)different possibilities that can cause liquid phase exfoliation [60] and (b) LPE in presence of just solvents or with surfactants/polymer stabilizers[61]

Surfactants are generally added to lower the surface tension of water in order to smooth up the exfoliation process and at the same time stabilizes graphene sheets using hydrophilic interactions whereas polymers interact with graphene sheets using non-covalent interactions and avoid the re-stacking process. In both cases, an additional step is needed for their removal which is difficult when compared with organic media which can affect the properties of Graphene. Any kind of surfactant (non-ionic, cationic and anionic) can be used for the exfoliation and dispersion process while the commonly used ones are CTAB, SDS, SDBS, Pluronic ®127 etc. Concerning polymers, non-ionic and non-toxic polymers like PVP, PS and cellulose based polymers like ethyl cellulose and cellulose etc. are mostly used. Strong interactions of polymers with graphene sheets is a cause of concerns as it make them difficult to be removed [61][62].

Electrochemical Exfoliation

This process takes advantage of the conductive properties of graphite for its exfoliation. Here, graphite is used as the working electrode and is immersed into an electrolyte media, after which the electrode is set to a given potential (either oxidizing or reducing) and a positive or negative electric current flows resulting in either cathodic reduction or anodic oxidation of graphite as shown in Fig. 4. This causes intercalation and exfoliation of the layers. This method is rather simple and straightforward when compared to chemical exfoliation that also works on the same mechanism of exfoliation of graphite using strong oxidizing agents as well as other harsh chemicals. It is also less time consuming giving benefits of acquiring pristine few-layered graphene or functionalized graphene depending on the parameters and intercalating ions used [63]. Common anionic intercalants used are H_2SO_4, H_3PO_4, $FeCl_3$ and HNO_3 in aqueous media. In this case, electrolysis of water firstly forms strong nucleophilic groups like OH- that attack sp^2 domains of graphite resulting in its oxidation and increased interlayer spacing, which further aids in intercalation of the anions (eg. SO_4^{2-}). Graphite exfoliation can also be aided by possible gases evolution during electrolysis. This case would normally produce fully/partially oxidized or functionalised graphene and require an additional step of reduction if needed, this technique rely on formation of oxygenated functional groups to overcome the van der Waals forces. Su et al, first reported a method of subsequent electrochemical reduction of the formed graphene oxide sheets by using an electrolyte mixture of H_2SO_4 and KOH and applying an alternating voltage of + and – 10V. At first the +10V is used for the graphite exfoliation whereas the subsequent -10V reduced the formed functional groups [64]. In case of cathodic reduction, common cathodic intercalants like Li, K, Rb etc. are used along with other intercalating molecules. Positive ions along with organic solvents can be used for this purpose, for instance Wang et al studied and used the Li+/Polycarbonate (PC) electrolyte and exfoliated few layered graphene after applying a high voltage of 15 ± 5V, this procedure was inspired by the destructive behaviour of PC used in Lithium ion batteries where the Li+/PC forms a ternary intercalation compound that causes fragmentation of graphite interlayers or the ability of PC

decomposition products to form a stable solid electrolyte interface [65]. Other examples are collected in references [66][67][68].

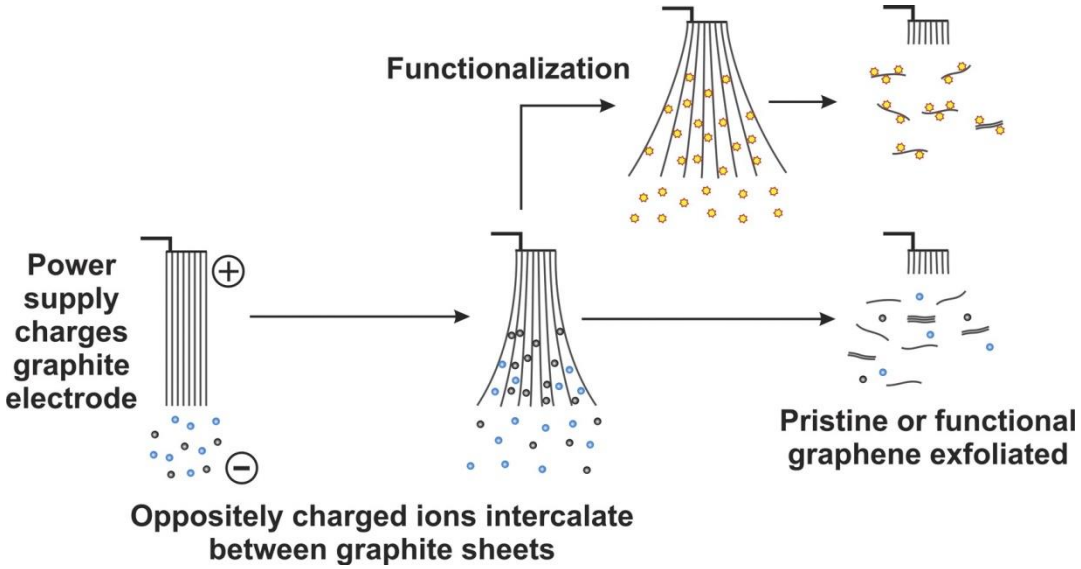

Figure 4: Mechanism of anodic exfoliation of graphite, where the oppositely charged (-ve) intercalating ions are attracted towards the charged electrode (+ve electrode). The same procedure occurs in cathodic exfoliation with +ve ions causing the exfoliation of –vely charged graphite electrode [69]

Mechanical Exfoliation

Apart from the scotch tape method described earlier, graphene can be mass produced by mechanical exfoliation using the shear forces and other forces (Fig.5(a)) for example in ball milling, possible ways of exfoliation using ball milling are shown in Fig.5(c). The beads create impact and attrition to form nano-thick graphene flakes and can simultaneously mix graphene with other nanomaterial or simply functionalize it. It was firstly utilized with the intention of breaking down graphite, and flakes down to10nm could be obtained [70]. Later in 2010, the idea was adopted by Knieke *et al.* [84] and Zhao *et al.* [8] to prepare graphene. The different properties of the formed graphene are dependent on the matrix used, weight, size and type of beads used, milling time and speed etc. [70][71][72][73].

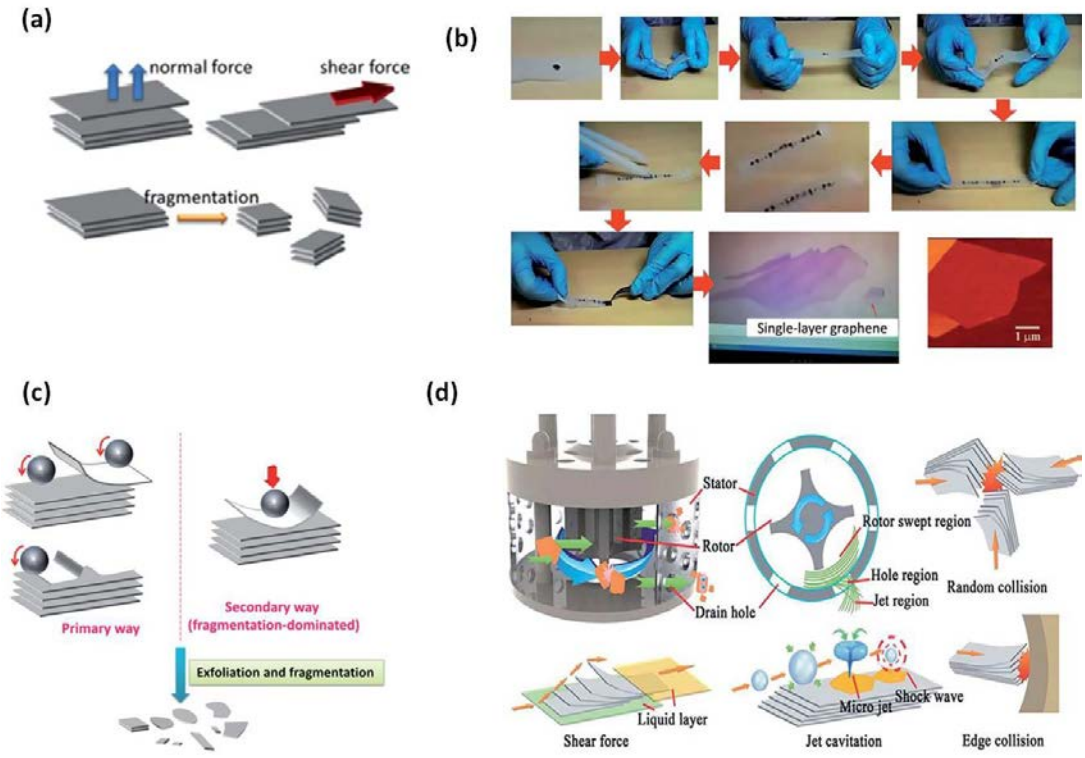

Figure 5: (a) Forces acting during Mechanical exfoliation. Mechanical exfoliation done using (a) typical scotch tape procedure, (c) ball milling and the direction of forces acting, and (d) high- shear mixer [74]. [70]

Sometimes the balls can impact vertically on the graphite that forms either amorphous or non-uniform graphene distribution and with more defects which must be avoided by controlling the rotation of the jars. Ball milling can be done in wet (in organic solvents, aqueous surfactants etc.) or dry state. Planetary ball mills are commonly used for this purpose as they provide high energy which is beneficial for exfoliation as well as simultaneous functionalization, but the disadvantage of using this high energy milling is the lack of complete control over the temperatures, long hours and the need for post milling treatments, as well as the difficulty of large scaling up. Zhao et al used organic solvents for (planetary) ball milling of graphite for ~30 h at low rpm (300 rpm), while , Aparna *et al.et alet al* Used the same technique but with strong exfoliant, 1-pyrene carboxylic acid and methanol and they achieved faster exfoliations compared to DMF. In contrast to the planetary milling, Knieke et al used vertically stirred media mill to form graphene flakes in aqueous surfactant (SDS) media. 50% of the total graphite was exfoliated to give graphene sheets of thickness less than 3 nm in 5 h

[75]. On the other hand is the dry milling in which Graphite is mixed with usually chemically inert materials, where a removal step by washing or heating is performed to obtain graphene sheets, for example Liu et al prepared graphene sheets of ≤5nm using ammonia borane using planetary ball milling [76]. Lin et al used the electronegativity of sulfur matching that of graphene to readily exfoliate and functionalize graphene. They mixed graphite and sulfur powders to mix in a planetary mill for 3-6 h at 500 rpm and obtained high conductivity (1820 S/cm) graphene sheets and Gr-S composite which was then used to prepare Lithium sulfur batteries [77]. Although Ball milling seems like a good option for mass production and functionalization of graphene, there is very limited control over the side effects caused like temperature rise, defects in graphene, breaking of graphene sheets etc. Some exfoliation based on shearing using fluid dynamics like Vortex fluid films pressure driven and Mixer driven fluid dynamics (Fig. 5(d))have been also exploited. As the name suggests, graphene is exfoliated in different locations by the fluid dynamics using rotational forces [78].

Arc discharge method

In **arc discharge method** the anode and cathode (Graphite) are submerged in either a gas or liquid medium in a reaction chamber in H_2, NH_3 and He, air atmosphere. The discharge current is generally kept constant between 100 - 150 A. The electric current that is applied creates high temperature plasma due to the dissociation of the medium and sublimates the precursor. The drawbacks that hinders its application for mass production are the high process control and safety concerns [79][80][81].

1.3.2. GO Reduction techniques:

After the preparation of graphite oxide, it is necessary to de-laminate the sheets, which is mostly performed by sonication or by providing thermal shock. The last steps include the reduction of oxidized species i.e. to reduce the functional groups present and to make attempts for the restoration of the carbon sp2 structure. Herein, the produced graphite oxide is sonicated in water

giving uniformly dispersed graphene oxide sheets (due to the oxygen functionalities it contains), which are then treated with a strong reducing agent. This eliminates most of the functional groups like hydroxyl, carbonyl and carboxyl on GO and partially restores the π electron configuration of the aromatic structure. Again, this can be achieved through several routes [82]:

Chemical reduction:

The transformation of GO to rGO can be easily detected by the simple observation of physical changes, either by the change in color from brown to black or the increase in hydrophobicity, when the dispersed GO starts to precipitate and/or aggregate and is no longer dispersible in water. However, more detailed analyses can be carried out to verify the oxygen content (C:O ratio) and the conductivity of the material. Use of hydrogen sulphide (H_2S) as a reductant for reducing graphite oxide was first reported in 1937 [83]. Later in 1963, Brauer treated graphite with few reducing agents namely hydrazine hydroxylamine, hydroiodic acid, iron(II) and tin (II) ions [84]. Today, we have a pool of reducing agents for the reduction purposes that include Hydrazine, Hydroxylamine, Sodium borohydride, Aluminium borohydride metal acids and alkaline based etc. Hydrazine is the most commonly used reducing agent for this purpose and is the most effective in producing rGO with electrical properties and restored sp^2 domains comparable to pristine graphene. Another reducing agent commonly used is sodium borohydride. Numerous reports have successfully employed these reducing agents to chemically reduce graphene oxide, however, their environmental and human toxicity and expensive handling led to research for alternative green routes. Researchers have used environmentally friendly reducing agents to reduce the graphene oxygen functionalities and produce good quality sheets [85]. Ascorbic acid (AA) which is known as Vitamin C is an important example in green reductants, it has shown reduction capabilities comparable to that of hydrazine. Chang et al in their work showed the efficiency of lemon juice in reducing GO and achieved a C/O ratio of 8.2, they carried on with the AA rGO to fabricate solar cells and compared its efficiency with that of hydrazine reduced GO which was found to be similar[86]. In addition, GO reduced using AA has shown applications in both bio-medical as well as electronics

area. Broadly green reductants can be classified into organic acids, plants extracts, micro-organisms, proteins, amino acids, hormones, saccharides etc. These are environmentally friendly compounds which provide comparable results, although, limitation for large scale fabrication due to several washing and centrifuging steps along with the need of a supporting agent cannot be overlooked [87][86].

Thermal reduction:

This reduction procedure is carried out by subjecting the material (Graphene/graphite oxide) to high temperatures (<300 °C) in vacuum, inert or reducing atmosphere. The high temperature causes the removal of intercalated water molecules and oxygen functional groups. Along with this, rapid heating of graphite oxide causes decomposition of the oxygen groups causing formation and expansion of CO/CO_2 gases that finally leads to further exfoliation of the sheets and to the production of very low density porous powders. This however is accompanied by structural defects like carbon sp^3 and vacancies due to high pressure between the sheets. Hamaker constant predicts and evaluate that a pressure of 2.5 MPa is sufficient for exfoliating graphene sheets. Actually, a pressure of 1 or 2 orders of magnitude larger than the van der Waals binding forces is applied generally, 40 and 130 MPa are created at 200 and 1000 °C respectively [88]. Doblin et al investigated the effect of temperature for thermal reduction and exfoliation of graphite oxide in their work and demonstrated that at ~300 °C the removal of labile oxygen functionalities and intercalated water is favoured causing pores and defects (structural and lattice defects), at 500 ºC pyrolysis of the carbon material initiates and at around 700 °C partial restoration of sp^2 domains takes place and the pores are diminished but big voids are created instead. Finally, at 900 °C, there is simultaneous mass loss due to pyrolysis, removal of oxygen functionalities along with partial restoration of the sp2 structure, this creates additional topological defects on the carbon sheet. They proved this by using the GO reduced at different temperatures and verified their ability for gas sorption [89]. This is less time consuming than the chemical reduction routes but the use of such high temperatures limits its

application and increases the cost for industrial applications. Along with this, the defects inevitably reduce the electronic performance of graphene by shrinking the transport ballistic path.

Microwave or photo reduction:

Microwave or photo irradiation are alternate ways of thermally annealing and reducing the sample (GO). It is an efficient and rapid way of producing and/or exfoliating rGO sheets. The immediate heating of the reactant causes the internal temperature to rise instantaneously which shortens the reaction time thereby improving efficiency of the procedure. rGO was exfoliated and obtained within 1 min of heating of GO powders in a microwave oven by Zhu et al[90]. The production of graphene can be obtained in powder state while the reduction can be obtained in suspension or heating of GIC. It is a rapid reduction technique but it might result in unwanted re-oxidation if an inert atmosphere is not provided. Photo-reduction can be performed either photo-thermally or photo chemically to obtain clean and high quality rGO. These have the advantages of being able to show good and tuneable degree of reduction in ambient conditions, high efficiency, rapidity and compatibility with possible flexible substrates; in addition, photothermal processes are additive/chemical free whereas photochemical processes require a catalyst. UV light has been most commonly used for the photo reduction of GO[91][92] [93]Park et al first reported the use of flashing lights in the order of milliseconds for reduction of GO using Xenon laser lamps. They flashed the GO samples in the range of 20 to 40 J cm^{-2} obtained 96% pure rGO at the energy of 40 J cm^{-2} with a pulse width of 20ms [94] later, Seon-Jin Choi et al used the technique and modified the parameters to reduce GO directly over a flexible KI substrate to make a wearable chemicals (gas) sensor [95], a lot of other work shows the use of Xenon lamps for GO reduction [96][97]. Preferential absorption of the photons by the active material allows localized heating preventing damage to the underlying substrate. Further improvements have been done using femto-second laser irradiation that created higher power density than the xenon lamp[98] or excimer laser radiation [99][100][101]. Photochemical reduction requires the use of a catalyst for generation of electron hole pairs in order to remove the OFG and for restoration of graphene sp2 structure. TIO_2 is a well-

known photo-catalyst and has been widely employed for water splitting and degradation of organic contaminants [102]. It was first employed for GO reduction by Kamat *et al* in 2008 where they showed that ethoxy radicals are formed and electrons are build up within TiO2 when its colloidal suspension is irradiated by UV light, which reduces the OFG of GO. Since then several groups used the technique for reduction of graphene or even for the preparation of composites (rGO/TiO_2) [103][104]. Other catalysts used for this purpose are ZnO, $BiVO_4$, WO_3, $H_3PW_{12}O_{40}$ etc. A review published by Zhang et al gives detailed insights on the works and mechanism of photo reduction of graphene oxide [105]. The inorganic photocatalyst removal can be a predicament when pristine graphene sheets are needed for an application, for this reason recently Mangadlao et al use ketyl radicals (generated by I-2959 or (1-[4-(2-hydroxyethoxy)phenyl]-2-hydroxy-2-methyl-1-propan-1-one) for photochemically reducing GO and prepared its composite with metal NPs in less than 10 min and demonstrated further its use as a catalyst for degradation of environmental pollutant [106].

Electrochemical reduction:

Herein, the reduction is caused by mere exchange of electrons between the electrode and GO in an electrochemical cell containing a suitable electrolyte. A thin GO film is deposited over conducting (Indium Tin oxide, ITO; Glassy carbon electrode, GCE; screen printed carbon electrodes, SPE etc) [107] or non-conducting substrates (quartz or flexible plastic) [108] and electrodes are then placed at each end of it to form a circuit and perform the measurement electrochemically by either cyclic voltammetry [109][110][108], linear sweep voltammetry [111] or constant potential mode[112][113]. Different media can be used to perform the reduction procedure, that includes HCl, NaCl, Na3PO4 , Na2SO4 [114], H2SO4 [115], KOH [116] $NaNO_3$ [110], PBS (K_2HPO_4/KH_2PO_4) [109], KNO_3 [117] and KCl aqueous solutions, eutectic melts [118], organic solvents [119] or ionic liquids [120][112]. The biggest advantage of the technique is that it avoids the use of hazardous chemicals or solvents. Guo et al reported the production of high quality graphene sheets at large scale from exfoliated graphite oxide in PBS (K_2HPO_4/KH_2PO_4) solution at a constant potential of -1.5 or -1.3 V vs SCE. They obtained ErGO sheets with a conductivity of ~3.5 x 10^3 S/m which was slightly higher than

chemically reduced GO ~3.2 x 10^3 S/m [121]. Use of these high potentials allows overcoming the energy barriers of OFGs, removing them electrochemically. Reduction potential and electrolyte are the main factors influencing the degree of reduction in this process which is why different reduction potentials are applied depending on the respective experiment. Jussi Kauppila *et al* in their work compared the reduction of GO in aqueous media at different pH and organic media (Acetonitrile and Propylene carbonate) and demonstrated that with the use of higher pH or organic media, the working potential window can be increased thereby allowing application of higher reduction potentials that provide much more efficient GO reduction[119]. Apart from pH, conductivity of the media also determined the quality of produced graphene sheets. Hilder et al showed that the optimal conductivity ranges for neutral pH media (0.5 mg/ml GO and 0.25 M NaCl) is between 4 and 25 mS cm^{-1} at a reduction potential of -1.2 V w.r.t SCE [113].

Hydrothermal/Solvothermal reduction:

This method has advantages over chemical reduction routes such as mild synthesis conditions, scalability, straightforwardness and low defects content. Since the nineteenth century when it was used for producing synthetic minerals till date, it has been continuously studied and used for various applications including synthesis of carbon nanospheres[122] and CNTs [123]. For graphene, this procedure has been widely used for preparing graphene oxide[124], graphene based composites[125][126][127], and GO reduction[128][129][130]. In the case of GO reduction, exposure to moderate temperatures and internal pressure favours the π conjugation recovery after dehydration with minimum defects. Zhou et al demonstrated in their work that supercritical water can act as a reducing agent under hydrothermal conditions offering a green reduction route [131]. Recently Huang *et al* studied the changes in GO in detail by subjecting GO prepared by modified Hummers method to hydrothermal process from 0.5 to 10 h at 200 °C and showed how differently formed rGO can be tuned and used for desired applications by this route [132], whereas previously, Niu et al studied the structural changes occurring during reduction of GO at different temperatures between 180 - 200 °C, and concluded that optimal conditions were 180 °C for 24 h [133]. For

Solvothermal processes, the reduction of GO occurs by induced surface chemistries and the enhanced reactivity in presence of a solvent inside a sealed container resulting from the temperature-pressure conditions. Most common solvents used for this purpose are N, N dimethylformamide (DMF) and N-methyl-2-pyrrolidone (NMP) [134][135][136]. Alcohols like ethanol, butanol, ethylene glycol (EG) etc have also been used successfully [137] [138].

1.4. Graphene processing and its printing

1.4.1. Basic ink composition:

Ink preparation is a major step that defines the quality of printed patterns formation, their adhesion and drying process as well the resolution. The optimal physical and rheological properties of inks differ for each printing technique. Thus, an ink formulated for one particular technique might not work for another. An ink is basically a composition of various materials, namely, the active material (graphene or its derivatives), binder, additives and a solvent. Active material (AM) is the main component of the ink that is required in the final prints/depositions. It is of the main interest and is often tested and studied. These play the role of pigments when compared to conventional inks where these are used as colorants, provide resistance against the environmental conditions like moisture, heat abrasion, chemicals etc. Binders play a very significant role in the ink formulations. They bind together AM particles to each other and are a cause of adherence of the AM to the substrate. Binders can simply dry off and stay along with the AM over the substrate or can be removed through curing using annealing, UV radiations etc. after the printing procedure. Examples of typical binders are polyvinyl alcohol (PVA), Polyvinyl Pyrollidone, Cellulose based polymers, rubber resins etc. Additives are used in much smaller quantities (<10 wt%) for modifying/tailoring the ink properties or imparting additional ones. These can be surfactants or defoamers to change the fluid properties, stabilizers or other materials like acetylene black, activated carbon for filling the tiny

voids created by deposition of large graphene sheets for better conductivity etc. Solvents are responsible for fluidity of the ink. They are used for dispersing all the ink components and provide specific required rheological properties to the ink. Solvents can be practically any liquid ranging from water to organic liquids, although their selection is based on the type of printing technique, evaporation rate, viscosity, compatibility with the ink components as well as with the substrate and the end application. Water based ink formulations are attracting increasing attention due to environmental considerations compared to organic solvent based formulations [139][140][141]. Ink properties like its viscosity, surface tension etc. need to be precisely controlled for specific techniques as these can affect the printability directly.

1.4.2. Graphene based inks

With all the properties of graphene mentioned, it makes it an excellent material for flexible electronic devices. In addition, different graphene (pristine graphene and GO), functionalized graphene and its composites give us a broad range of possibilities to process and print it. The task of ink formulation and printing in order to get satisfactory results is nevertheless quite challenging. A conductive ink includes a primary conducting material that is dispersed in an aqueous or organic solvent. Dispersion is not straightforward for typically non-dispersible hydrophobic carbon materials like graphene. Thus, polymer or surfactant based additives are added to facilitate easy printing and avoid graphene agglomeration. Pristine graphene inks are prepared with or without using stabilizers. Polymer-based stabilizers such as ethyl cellulose, surfactants etc. are normally added during ultrasonic preparation of graphene to avoid sheets restacking. Work done by Secor *et al* in 2013 [142], includes sonication of Graphite in presence of EC for producing a stable ink for inkjet printing application. They showed successful patterning over different flexible substrates with good conductivities: the ink however needed annealing later at 250 °C for 30 min for effective EC removal. This made them refine their work in 2015 [143] and modify the ink composition with higher

graphene loading and good conductivities over different substrates was achieved by changing the composition of EC and using shear mixing technique instead of sonication as well as changing the thermal annealing step with photonic curing using intense pulsed laser. Majee *et al*, also prepared their graphene flakes using mechanical shear exfoliation in organic solvents and used EC as the stabilizer to prepare a stable inkjet ink with a concentration of 3.2 mg/ml. According to their report[144], EC provides steric stabilization to the exfoliated graphene sheets[145]. Other examples of ink using EC and polymers as the stabilizers are reported in references [146] [147] [148] [149]. Aside from polymeric stabilizers, surfactants are also widely employed for modifying the ink properties along with stabilizing graphene, for instance Lee *et al* prepared graphene dispersions that were stable for more than a month by using Sodium n-dodecyl sulfate surfactant for stabilization and by adjusting the pH to 10 for changing the charge density of graphene sheets [150]. Pristine graphene can be also dispersed in some organic solvents without the use of any stabilizers due to their matching Hansen solubility parameter, work was done by Torrisi *et al*, where he exfoliated and prepared inkjet printable ink in NMP without the use of any additives, they successfully printed conducting (~30kΩ/sq) and transparent (~ 80 % transmittance) patterns to fabricate a thin film transistor that showed charge carrier mobility of ~95 $cm^2 V^{-1} s^{-1}$ [151]. Miao *et al* also used organic solvent DMF for dispersion of their electrochemically exfoliated graphene sheets, but in order to obtain proper viscosity, they added ethylene glycol and glycerol in the ratio, DMF: ethylene glycol: glycerol - 50:45:5 vol%, and achieved a concentration of 2.8mg/ml [152]. The disadvantage of this is that organic solvents are toxic and they frequently have low vapor pressures and high boiling temperatures that can be sometimes incompatible with the desired flexible substrates [141][153]. Recently Kewen Pan *et al* prepared screen-printed graphene inks at a very high concentration of 70 mg/ml using a non-toxic, environmentally friendly cellulose derived solvent 'Cyrene'. Cyrene has appropriate polarity, surface tension that not only helped them to achieve dispersion with higher concentration, but also aided in efficient and fast exfoliation compared to the solvent commonly used for this purpose, NMP. Expanding that, they used the ink to produce wireless connectivity

antenna that worked from MHz to tens of GHz and the conductivity of the patterns attained was 7.13×10^4 S m^{-1} [154].

An interesting alternative to using pristine graphene or rGO dispersions is the use of GO as an active ink component, the presence of oxygen functionalities makes it hydrophilic which makes its solution based processing highly convenient. It is readily dispersible in water and other polar solvents like NMP, DMF, ethylene glycol etc without the need of any dispersing agents. In this case, the reduction step to obtain conductive patterns is done post printing. Water based GO/acrylic ink was prepared and inkjet printed by Porro *et al*, where they used photonic curing UV light to simultaneously reduce GO and polymerise the resin. The GO dispersion at different concentrations can be directly used for stamping technique (described in the later sections) as an alternative to toxic approaches. In one of our approaches, we used this technique for patterning GO and later the reduction was carried out at 80 °C using citrate [155]. Graphene/polymer or Graphene/metal NPs inks are also very common, in most cases, composites of graphene, GO or rGO are prepared with conducting polymers[156] or metal nanoparticles for enhancing the conductivity of the final prints or to have synergistic properties beneficial for the end application. For example, a water-based ink of Graphene/Polyannilne was prepared by Xu *et al* using SDBS and was inkjet printed over Quartz and fabric (carbon) substrates and used it for Supercapacitor application since graphene exhibits inherent double layer capacitance whereas conducting polymers like Polyaniline (PANI) or Polypyrrole (PPy) show pseudocapacitance[157]. Another example is the GO/PANI, and rGO ink using PEDOT:PSS as stabilizer, that not only enhanced the fluid property for extrusion printing but also enhanced the conductivity of the printed electrode. These enhanced performance were utilised in fabricating a symmetric and asymmetric Supercapacitor by Liu *et al* [158]. Also, in chapter 2 we will discuss the formulation, printing and performance of screen printable Graphene/polypyrrole ink for the same application. Metal nanoparticles can be simply added to enhance the conductivity of the overall print [159] or they can have specific function, for instance, we have prepared dispersion of graphene/Au NPs for stamping of graphene for sensing application where Au NPs played the role

for attachment of thiolated DNA [155]. Another example of functional NPs are the composites of Nitrogen-doped reduced Graphene oxide and Cobalt oxide nanocrystals (N-rGO/Co_2O_4) formulated for inkjet printing and used as oxygen reduction catalyst in the work by Bassetto *et al* [160].

The formulation of graphene-based inks presents several specific challenges. For instance, the use of additives like polymers/surfactants needed for tailoring the fluid rheology sometimes reduces the conductivity of the printed films which then require high temperature annealing, frequently incompatible with flexible polymer substrates. Besides, low graphene concentrations are generally used to avoid aggregation or blocking of the printheads but these low concentrations lead to poor printed solid networks, directly affecting the conductivity. Dimitrios Konios *et al* made an investigation on how the dispersibility of GO in different solvents changes upon reduction. In their study they considered different critical parameters like surface tension, Hansen and Hilderbrand solubility parameters [161][162][163] and polarity of the solvents to determine their dispersion behavior since just one property cannot define it. That study give us some insights on how the two different material behave in different solvents, which is crucial for ink formulation [164]. The dispersion behavior of graphene in 40 different solvents based on the above 3 parameters was also investigated by the group of Colmen in 2010. They suggested that the surface tension and Hilderband solubility parameter of the solvents must be close to 40 mJ/m^2 and 23 MPa respectively with non-zero values, well defined values of polarity and hydrogen bonding Hansen Parameters. This study can help us find and create new solvents based on these parameters for efficient exfoliation or dispersion of graphene[165].

1.5. Graphene Printing/Deposition techniques

This is the step where formulated inks are used for patterning onto the desired substrate. Different printing techniques have different operating parameters hence require different fluid properties. We

will now discuss a few printing techniques for different graphenes directly related to the thesis as well as some previous relevant works:

1.5.1 Doctor blade/tape casting method:

It is a widely used technique for forming thin films over large area substrates. A very simple approach where slurry (ink) is prepared with the AM, binder additive and solvent and placed on the substrate. A blade is then used to spread the slurry by either a constant movement along the stationary substrate or by the movement of the substrate where the blade remains stationary. Dual doctor blades can be used further to have better control over the film thickness. Sometimes, a reservoir is used along the process for continuous ink deposition as shown in Fig. 6 (a and b). Furthermore, for coating over uneven surfaces like cloth, flexible plastic surfaces, leather etc., the doctor blade can be modified with a spiral applicator (also known as Mayer rod), the spiral gap size, geometry, gap-spiral ratio define the thickness of the coated layer along with the particle size, and fluid properties of the ink Fig. 6(c and d). Also, the thickness depends on the height of the doctor blade edge [166].

This technique has so far been frequently used for uniform coating of graphene or graphene-based composites for several applications like solar cells [167][168], photovoltaics [169], supercapacitors [170], filtration membranes[171], batteries [172] etc. Wang *et al* even prepared thin film coating of GO using Mayer rods followed by reduction at room temperature to produce transparent and conducting rGO thin films for touch screen applications [173]. Akbari *et al* in their work prepared graphene antennas using also the doctor blade technique. The prints were made over cardboard substrates that showed excellent processability with an efficiency of 40% [174].

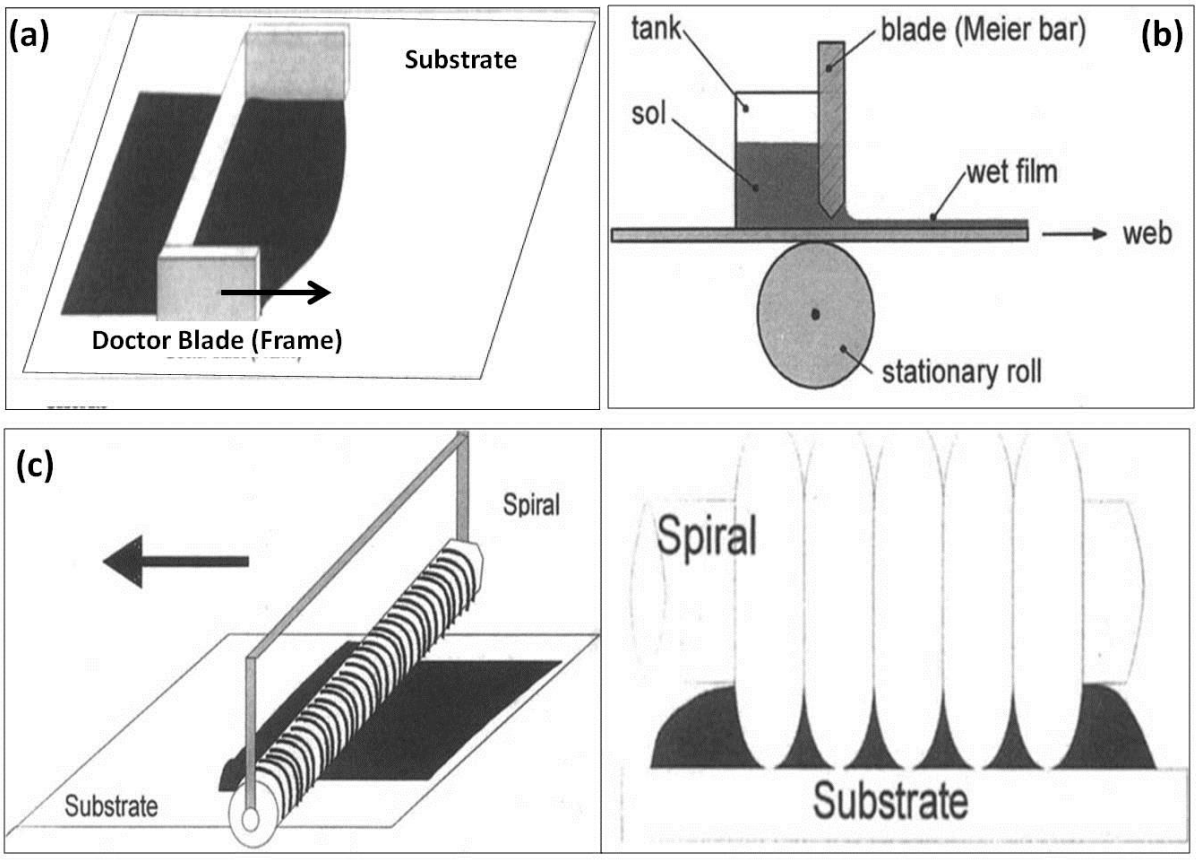

Figure 6: Doctor blade coating technique (a)top view, (b) cross sectional view showing the dependency of the thickness with distance between blade and the substrate, (c) coating using Mayer rod and (d) dependency of film thickness on the geometry of rod rings.

1.5.2. Screen Printing

It is considered to be the most conventional and at the same time versatile printing technique. It has been used since the 19th century and a huge amount of publications have reported the use of this technique for various device fabrications. It is a stencil based technique where a patterned stencil mesh, made up of fine porous mesh of fabric, silk, metal threads or synthetic fibers is used for squeezing the ink through the open pores of its patterns. Photopolymerized resin is used to block the unwanted open pores (i.e. to make patterns). It generally requires squeegees or rollers to be moved in a direction in order to push/force the ink through the mesh onto the underlying substrate. At the time of ink transfer, due to the force applied, the stencil makes contact with the substrate so as to effectively receive the ink and leave it as soon as the force is removed, leaving the patterns in

just one pass. Fig. 7 shows the mechanism of screen printing. Once optimized, the procedure can be used for different substrates reproducibly.

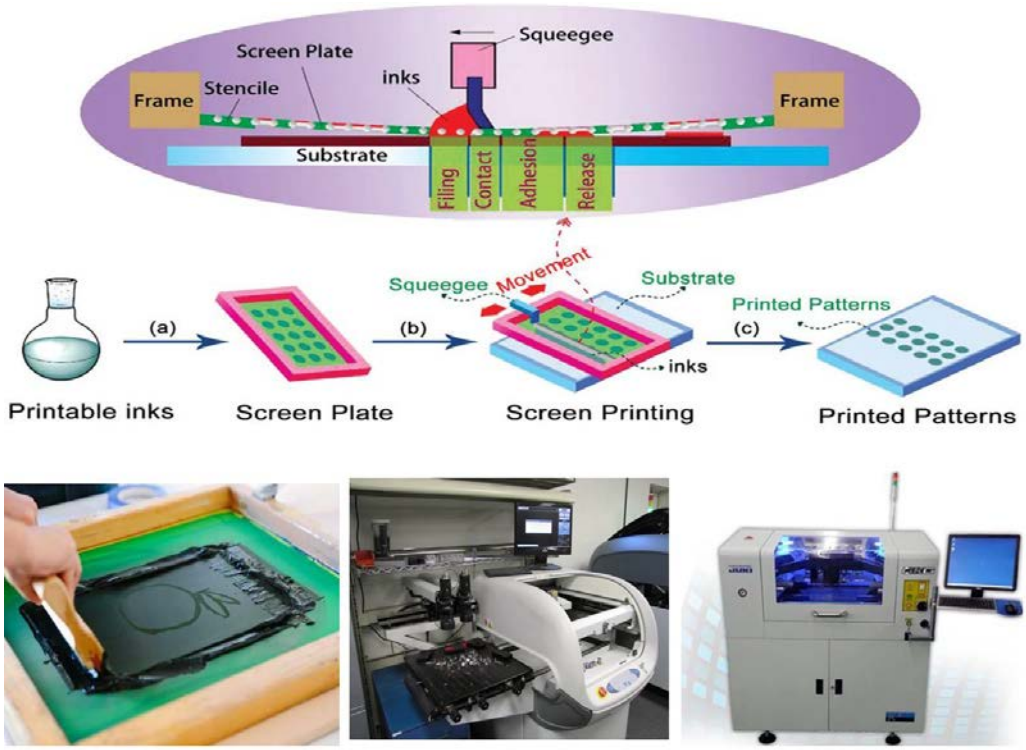

Figure 7: Screen Printing Mechanism [14] and different types of printers available for this purpose: hand-operated/manual, semi-automated (DEK 248 Semi-Automatic Screen Printer) and Fully automated (JUKI K3-II Extra Large Fully Automatic Screen Printer)

Screen-printing is the technology with a widest implementation amongst printing techniques and has been continuously automated for easy handling and mass production. Several groups prefer to prepare their own screen-printed electrodes in the lab rather than buying commercial ones since reproducible results can be readily achieved. This can be done using semi-automated machines where the substrates are put and removed and ink is fed manually, or by using fully automated versions where automatic feed and delivery system does the work instead (Fig. 7). Nevertheless, less automated units are much handier and preferable when series of optimization tests or new formulations are involved, or in cases when the substrate is either too thick or too thin. Screen-

printing offers several advantages like simplicity, compatibility with various substrates and a comparatively wide range of parameters concerning ink formulations. The quality of the printed patterns depends on several factors like the speed, force and angle applied to the squeegees, thickness of the stencil, pore size of the mesh, substrate quality, etc. Yet, the most important factor is the ink rheology, essentially its viscosity. An ideal screen printing ink is a paste that must have a high viscosity at rest and low viscosity at high shear rate with fast recovery time and values between 50 to 5000 cPs. This is achieved by using high graphene concentrations [154], using cellulose based or polymeric binders [175] or by gelating graphene dispersions [176]. Woo Jin Hyu *et al* in 2015 achieved a resolution of ~40µm in screen-printed graphene electrodes by carefully designing a Si-based stencil with proper pore sizes and ink formulation containing ethyl cellulose (EC) as the binder (also for enhancing the viscosity) [175]. As a matter of fact, ethyl cellulose is a popular binder and has been utilised in several ink formulations. Other binders commonly used are PVP, PVA, ionic liquids [177], etc. Also in 2015, Arapov *et al* prepared graphene ink with a high concentration of 52 mg/ml using polymeric binders that caused gelation, thereby increasing the overall viscosity of the ink. The resulting patterns not only exhibited low resistivity of 30 Ω sq^{-1} in just 5 min of annealing at 100 °C (thicknesss 25 µm) but also showed patterning of lines of 40 µm [176]. The work mentioned above by Pang *et al* to prepare high concentration graphene using Cyrene solvent [154] could also be highlighted here. A few downsides of scree-printing techniques include the resolutions of the printed patterns which are restricted to 50 -150 µm [175], values comparatively lower than the digital printing techniques, difficulty in preparing concentrated graphene inks without aggregation of the nanosheets, ink drying during the process, requirement of several masks if the pattern is not straightforward. Also, since it is a contact printing, additional impurities or defects are occasionally found.

1.5.3. Inkjet printing

This printing method is very useful for printing high resolution films by precisely monitoring the drop volume and firing parameters. By controlling parameters like jetting frequency, drop volume and applied voltage, very clean and high resolution films can be obtained that can be used in very different areas of applications like manufacturing of ceramics, molecular electronics, Solar cells devices, Energy storage and biosciences [178][179]. There is a complete list of materials that can be inkjet printed on suitable substrates including conducting polymers, nanoparticles, metals or their oxides, ceramics and also biomaterials like proteins or nucleic acid etc. [180].This printing method offers a straightforward fabrication of low cost, highly scalable, flexible films as an alternative to the conventional expensive and complex electrode fabrication methods like etching, lithography etc. Furthermore, Inkjet printing of graphene inks can be used as an alternative to expensive metal nanoparticle inks. The challenge is to prepare stable and size-controlled graphene sheets to be compatible with the inkjet printer. Many reports have shown successful printing of pristine graphene [181][148][182]

1.5.3.1. Inkjet mechanism

The drops in the inkjet can be formed by two different mechanism-Continuous Inkjet Printing (CIJ) or Drop on Demand (DOD) [183]. In CIJ, A liquid is pushed through a column and droplets are formed from them by Rayleigh instability phenomenon, this way series of droplets are ejected resulting in continuous stream and printing occurs sometimes even where it is not required. The nozzles are kept at a constant voltage relative to the ground that causes small charge formation on the droplets and allows for flowing droplets to be steered by passing them through an electrostatic field, the unwanted droplets are collected and recycled, Fig. 8(a).

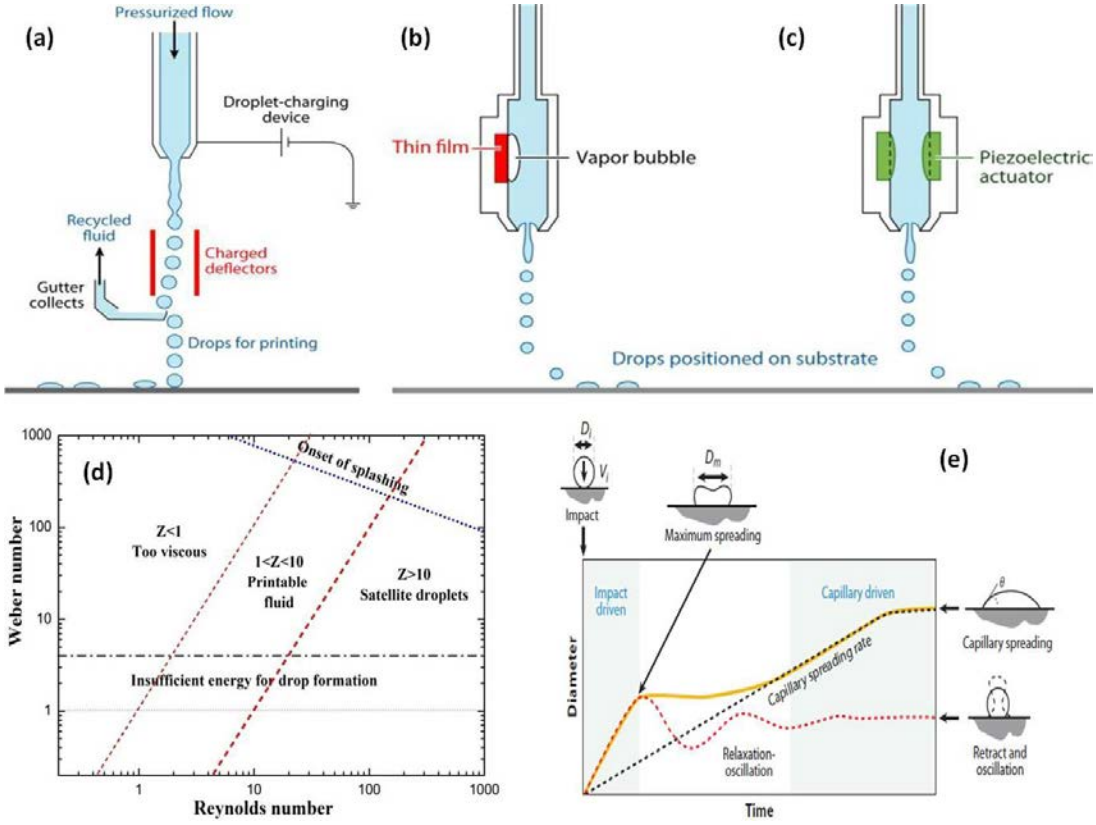

Figure 8 : Mechanism of (a) Continuous Inkjet Printing and (b) thermal and (c) piezoelectric Drop on Demand (DOD) Inkjet printing. (d) Limits of stable drop formation on the basis of Ohnesorge number derived from Weber and Reynolds numbers. (e) Drop impact and spreading behaviour at the substrate occurring with an initial impact followed by damped oscillations and capillary flow spreading. Here Di and Dm are the drop diameter before and after spreading and Vi is the velocity of the impacting drop. [184]

Drop-on-Demand (DoD) involves a more sophisticated mechanism. It relies on generating individual droplets and demands less restrictions providing high accuracy. In simple terms, picolitre drops are generated by applying pressure pulses to the chamber containing the ink and as soon as the pulse pressure increases beyond a threshold value for the liquid ink, drops are jetted out from the nozzle openings. Liquid ink stays in the chamber due to the surface tension, therefore a stable nozzle meniscus must be maintained. Pressure in the fluid can be applied in two ways to allow drop formation – by heating (Fig. 8(b)) or by applying voltage to a piezoelectric actuator (Fig. 8(c)). In the thermal mode, a thin film heater/resistor causes the ink to heat up to its boiling point causing rapid formation of bubbles and consequently bubble vapors that leads to ejection of ink from the nozzle, whereas, in the other case, a voltage is applied to a piezoelectric actuator that expands and creates a

pressure momentarily surpassing the surface tension of the ink at the nozzle, resulting in drop evacuation [185].

For DoD printing, three main conditions must be carefully considered and properly addressed (i) Formulation of ink with proper rheological requirements, (ii) Drop formation and ejection and (iii) Drop impact and interaction with the substrate.

1.5.3.2. Ink Formulation and challenges

An ideal ink for inkjet printing is the one that can easily form droplets. The main properties that influence drop formation and spreading are the viscosity(η), surface tension(γ), density (ρ) as well as wettability and surface adhesion of the prepared ink with the substrate [186]. These parameters that determine the way in which fluids behave can be represented by Ohnesorge (Oh) numbers which are derived using the physical constant parameters that determine Reynolds (Re) and Weber (We) numbers [187] :

$$Re = \frac{\upsilon \rho a}{\eta}$$

$$We = \frac{\upsilon^2 \rho a}{\gamma}$$

$$Oh = \frac{\sqrt{We}}{Re} = \frac{\eta}{\sqrt{\gamma \rho a}}$$

Z number (i.e 1/Oh) is another parameter that is used for determining the printability of an ink. According to the literature, Z>2 is the best condition for stable drop formation, although drops can be formed in the range of 14>Z>1. For lower Z values, the ink is too viscous and at high values there are a lot of satellite drops (Fig. 8(d)) (small drops that accompany the big drop *en route* to the substrate)[151][184] [188]. As per the specifications of Dimatix printer, optimum viscosity and surface tension of inkjet printable ink is recommended between 10-12 cPs and 28 – 33 mN/m respectively [189]; then again, the values could be different for different printers or devices. These values determine the shape factor of the drop and they can normally be adjusted with the help of

surfactants. Also for conductive inks, the particle size should be at least 1/50 than the nozzle opening to prevent clogging during printing[151]. Other challenges involving ink formulation concern the stability of the suspension. The particles should form a stable dispersion in the solvent with the help of stabilizing agents like polymers or surfactants if necessary. However these stabilizing agents frequently reduce the conductivity when highly conducting prints are needed; therefore their concentration should be finely adjusted to an optimum in order not to clog the nozzle, while keeping to a minimum the modification of the active material and preserving the compatibility with the substrate.

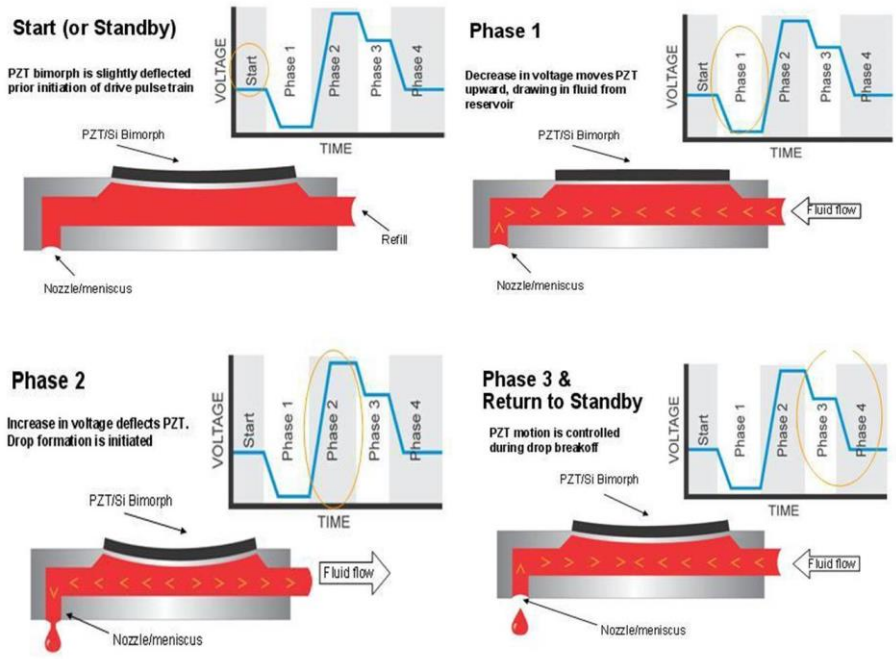

Figure 9: The four phases in the Inkjet DImatix Waveform drop formation [190].

Drop Formation and ejection in piezoelectric DOD mechanism also relies on the application of voltage to the piezoelectric membrane and it takes place in four stages that can be explained and controlled in form of a waveform, shown in Fig. 9. Each of the four segments in the waveform controls three properties- Duration of applied voltage, It tells us how long the transducer will stay in a particular position, second is level or magnitude, it is the amplitude of how far the transducer will be bending and third is the slew rate, which is the slope of applied voltage and determines how fast

the transducer will bend. The first and the last segment are connected and are just there for the ease of users understanding about the inception and ending of each drop formation process. Segment 1 and 2 are indicative of drop formation and jetting. In this, the voltage is reduced for the piezoelectric membrane to relax and let the chamber fill with the ink and then the voltage is increased to create pressure inside the chamber by compressing the membrane. This transient pressure forces the fluid to steer out of the nozzle in the form of a droplet. During Segment 3, the amount of liquid that leaves the chamber causes the chamber to relax and then in segment 4, it goes back to its relaxing position thereby initiating next cycle [190].

Contact of the drop and substrate: The mechanism is shown in Fig. 8(e), when the drop interacts with the substrate, its behaviour is controlled by a number of factors like capillary and inertial forces, velocity and viscosity of the ink droplet, contact angle as well as the type of substrate. At first, when the drop impacts the substrate, the Kinetic forces dominate for a short time (<1μs) followed by spreading, recoiling and oscillations. Shortly (about 0.1 to 1ms) capillary forces dominate the spreading until reaching equilibrium [184] Then, in order to get an optimised coalescence of the drops, drop spacing plays an important role. In the study of Soltman and Subramanian, [191] they showed that no overlaps are observed at high drop spacing values whereas gradually decreasing the spacing results either in bead-shaped (at slightly smaller drop spacing than the diameter of a single drop) or perfect end lines (with approximately the size of single droplet radius). Decreasing the drop spacing further results in non-uniform areas with some bulging parts containing excess fluid. Detailed information of how each factor effects the formation, spreading and drying of the inkjet droplets can be found in the review by Derby [184]

The final solidification of the inks can be achieved by either annealing, gelation of the polymer precursors, chemical reactions etc. This is the step done to allow for the display of the useful inherent properties of the nanomaterial used, for instance conductivity. It is the final step of the printing process in which phase transformation of droplet from liquid to solid occurs. As the ink is dropped onto the substrate by the printer, it needs to be solidified in order to make electrical

contacts between the nanomaterials that are otherwise floating in the solvent. Sometimes, drying of the droplets results in a ring-like formation which is known as the infamous Coffee Ring or coffee stain effect [192][193]. This is the phenomenon where solute from the solvent diffuses towards the initial contact line or the circumference forming a ring like structure during solvent evaporation and it occurs due to two reasons- First, at the edges, it is easier to transport heat vapors from the bulk to the neighboring dry substrate area because of difference in evaporation rate on the substrate vs. the bulk of the drop . And the second reason is that the surface area of the edges of a drop is higher compared to that in the bulk and hence the rate of evaporation in both areas are different (it is higher at the edges), this higher evaporation rate causes the solvent to flow towards the edges, resulting in segregation of solute upon heating around the edges, i.e. the solvent from the bulk replaces the evaporated solvent from the corners. This segregation is the cause of ring formation that is seen at the end of drying process. This can be avoided either by changing substrate temperature and make it comparable to the drops as carried out by Saoltman & Subramanian. (they used a cold substrate to deposit PEDOT ink resulting in reduced coffee ring effect), or by selecting compositions that have solvents with different vapor pressures (evaporation rate) [191]. Other ways of reducing this effect are by freezing the drops as soon as they interact with the substrate. This helps in freezing the composition of the drop impeding the bias movement. Important factors that need to be optimized in order to reduce the coffee ring effect are boiling points and heat of vaporization (that should be more than that of water) and by viscosity, surface tension, contact angle, flow of the fluid and impact speed [194][195]. Major challenges with this printing techniques are that it has a very narrow range of conditions for optimizing parameters. Also, Graphene dispersions are generally in very low concentration and as consequence several layers need to be printed in order to obtain good conductivity, and finally, the need for small graphene flakes, which come frequently associated to graphene with a relatively high concentration of defects-

1.5.4. Wax stamping method

Quite recently developed by Luis Pires and colleagues at Merkoçi's group, wax stamping is an environmentally friendly technique, free of solvents additives and stabilizers, which can be used to prepare Graphene oxide (GO) patterns on practically any type of substrate. They used nitrocellulose membranes with a pore size of 25 nm for the process and printed negative patterns on it using a wax ink printer. Later, different concentrations of GO dispersions in water were vacuum-filtered through the membrane. The membrane pores were blocked selectively by the inverse hydrophobic wax patterns and so that the GO dispersion is driven to the non-hydrophobic regions on the membrane under the influence of pressure from vacuum filtration, leaving a thin GO film on them. This thin layer was then transferred to a desired substrate by the pressure induced by the built-in roll-to-roll mechanism of the printer.

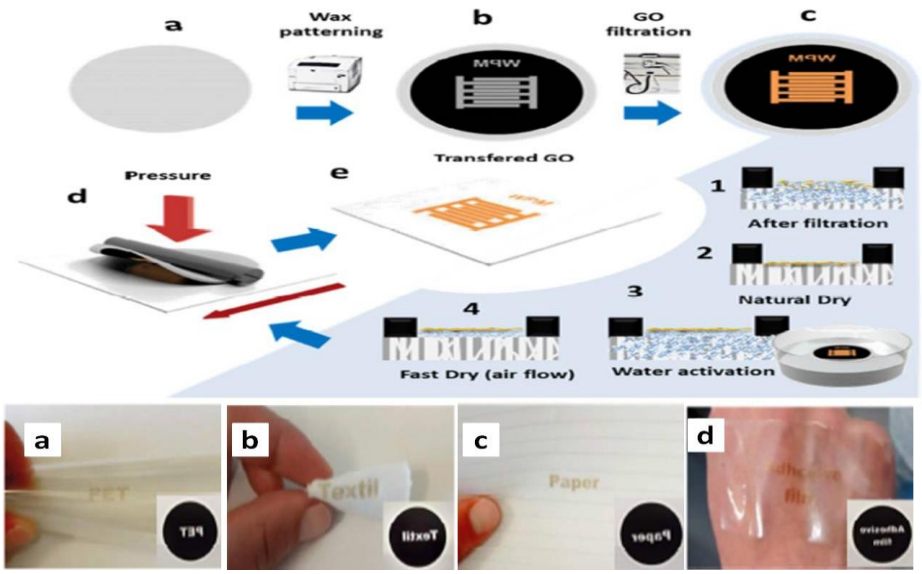

Figure 10: Top (a-d) steps for patterning graphene that includes wax negative patterning over nitrocellulose membranes, filtering GO dispersions through it and then its transfer over desired substrates. Below (a-d) are the transferred patterns over PET, Cloth, Paper and an adhesive film respectively [196].

Stepwise GO patterning using the technique is shown in fig. 10. With this methodology, they were able to achieve a pattern resolution of 50 µm, albeit, this resolution was attributed to the printer as

they showed that only the wax prints that were printed perpendicularly to the printer feed could show this resolution. Thus, in the future, higher resolutions could be possibly achieved with advances in the hardware. They were able to prepare stable patterns over paper, textile, adhesive and normal plastic substrates. This technique provides a rapid and green solution compared to other techniques along with pattern stability, high resolution, control over thickness, and ability to print diverse patterns over different kind of substrates, however, the use of additional step to reduce GO after patterning remains an issue. In their work, they immersed the patterned substrate directly into the solution containing ascorbic acid (Vitamin C) at room temperature for 48 h, which is very time consuming. They went on to prepare interdigitated patterns for fabrication of a touch sensitive device [196]. Progressing on their work, very recently they prepared rGO foam by autoclaving GO with ascorbic acid. The formed agglomerates were sonicated and showed stable dispersions in water. This dispersion was used to print on a plastic substrate using the wax printing technique and was used for electrocatalytic applications [197]. This makes the method much more interesting and useful, as it makes it possible for rGO to be printed over flexible substrates without considering any further thermal or chemical treatments.

1.5.5. Other printing techniques

Overall, there are several ways for depositing or printing graphene. Just to mention a few more, we could consider roll–to-roll techniques like gravure or flexographic techniques, Fig. 11 (a and b). In Gravure printing, the substrate is in direct contact with an engraved cylinder. It basically consists of two cylinders, one which collects the ink and is responsible for the pattern and the other that presses the substrate along. Substrate is passed between the cylinders while a doctor blade is fixed to the engraved cylinder intended for getting rid of the excess ink. A schematic diagram is shown in fig. 11(a). The technique is highly useful for commercial purposes since large volumes at very high speeds (up to 15 m/s) and low costs can be achieved [198]. The cost effectiveness is however only

applicable if printing in high volumes. Also, since it is a contact based printing process, scratching, creasing or damages on the substrates or prints can be expected. Secor *et al* used this method to successfully print graphene patterns at a resolution of ~30 μm [199]. The flexographic technique [198], can be described as a modified version of gravure method. It works on the same fundaments but utilizes 4 cylinders (Fig. 11(b)) that are made up of polymers, rubbers or metal cylinder covered with a photopolymer. The first cylinder carries the ink from a reservoir and transfers it to the second cylinder, Anilox, which has the engraved patterns; these patterns are then transferred to a third polymeric or rubber cylinder which is finally transferred to the substrates using the pressure applied from the 4th cylinder. The change of cylinder material is advantageous in reducing the impact and scratching of the substrate. Baker *et al* prepared flexographic graphene nanoplatelet inks and printed over flexible ITO sheet at a speed of 0.4 m/s and used it as a catalyst for solar cells [200]. Aerosol jet printing is a non-contact printing process and it differs from inkjet printing process in the way of jetting the ink. The ink is aerosolized and jetted onto the substrate using a carrier gas. A schematic of the process is shown in fig.11 (c), where at first the ink is atomized to form ink droplets followed by its transfer to the deposition head using a carrier gas. The aerosol beam is collimated using a sheath gas and finally the aerodynamic focusing of aerosol is achieved using inertial effects for diverting the droplets. A final resolution of as low as 10 μm can be achieved. More details on the mechanism can be found on the recent review by Ethan B. Secor [201]. The method is claimed to work with a wide range of viscosities (1- 1000 cP) [202] which enables the formulation of different graphene based inks, and since the ink is atomized, it can prevent graphene from agglomeration [203][204][205]. A comparison of speeds and print resolution obtained for different printing techniques is displayed in fig. 11(d)

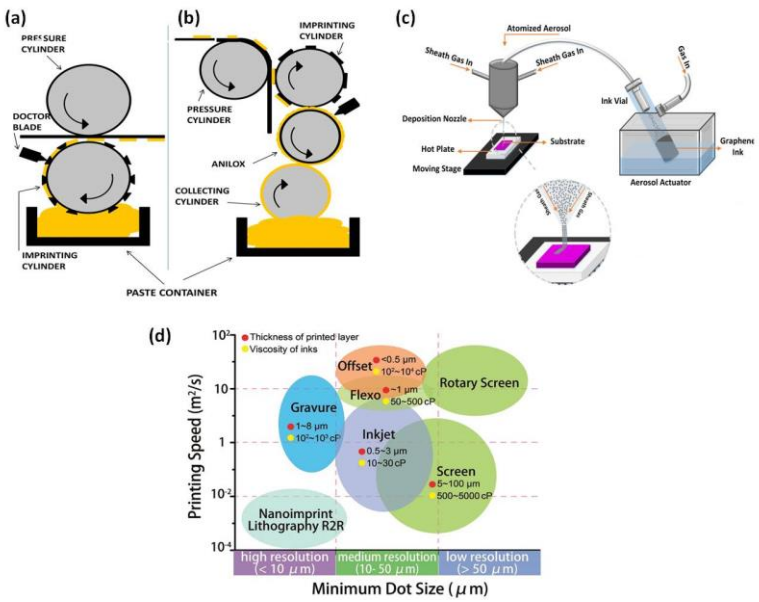

Figure 11: Schematic of roll-to-roll Processes (a)Gravure Printing and (b) flexographic printing [206]. (c) Aerosol-jet Printing [203], (d) is the comparison of speed and resolution obtained for different printing techniques [14]

1.6. Applications of Printed Graphene

All the printing technologies above promise efficient printing of graphene for various electronic applications, and a few ink compositions are already commercially available. Sigma-Aldrich is selling Graphene-based inks for inkjet (900695), screen (798983), gravure (796115) or flexographic printing. There is also a Graphene and EC (2.4 wt%) ink in terpineol/cyclohexanone for inkjet printouts which can be cured at 250-350°C for 20-30min, giving a conductivity of 0.003-0.008 Ω-cm at appropriate conditions and thickness (ink ID - 793663). They also have available water based graphene inks for inkjet (808288) and screen (808261) printing with ~0.1 and 10 wt. % solid content in water respectively. The inks can be used for various applications ranging from transparent conducting touch screen films transistors, OLEDs [207][208], Photodetectors [209], to energy conversion and storage devices [210][211] and Sensors [212][213]. In printed electronics, the main requirements of a device are to show high conductivity, mobilities, on/off ratios at ambient conditions and flexibility

1.7. References

[1] V. Musat, E. Fortunato, M. Purica, M. Mazilu, A. M. B. do Rego, B. Diaconu, and T. Busani, "Multifunctional zinc oxide nanostructures for a new generation of devices," *Mater. Chem. Phys.*, vol. 132, p. 339–346., 2012.

[2] M. E. A. Warwick, L.-M. Romero-Nunez, A. J. T. Naik, and R. Binions, "Electric Field–Assisted Chemical Vapor Deposition for Nanostructured Thin Films," in *Comprehensive Materials Processing*, S. Hashmi, G. F. Batalha, C. J. Van Tyne, and B. Yilbas, Eds. Oxford: Elsevier, 2014, pp. 171–190.

[3] S. Khan, R. Dahiya, and L. Lorenzelli, "Technologies for Printing Sensors and Electronics Over Large Flexible Substrates: A Review," *IEEE Sens. J.*, vol. PP, 2014.

[4] H. Ling Huang, J.-K. Chen, and M. Phon Houng, "Using soft lithography to fabricate gold nanoparticle patterns for bottom-gate field effect transistors," *Thin Solid Films*, vol. 524, pp. 304–308, 2012.

[5] S. N. Ariffin, H. N. Lim, Z. A. Talib, A. Pandikumar, and N. M. Huang, "Aerosol-assisted chemical vapor deposition of metal oxide thin films for photoelectrochemical water splitting," *Int. J. Hydrogen Energy*, vol. 40, no. 5, pp. 2115–2131, 2015.

[6] J. Li, W. Tang, Q. Wang, W. Sun, Q. Zhang, X. Guo, X. Wang, and F. Yan, "Solution-processable organic and hybrid gate dielectrics for printed electronics," *Mater. Sci. Eng. R Reports*, vol. 127, pp. 1–36, 2018.

[7] L. Liu, Y. Feng, and W. Wu, "Recent progress in printed flexible solid-state supercapacitors for portable and wearable energy storage," *J. Power Sources*, vol. 410–411, pp. 69–77, 2019.

[8] W. B. K. Deepak P. Dubal, Jong Guk Kim, Youngmin Kim, Rudolf Holze, Chandrakant D. Lokhande, "Supercapacitors Based on Flexible Substrates : An Overview," *Energy Technol.*, vol. 2, pp. 325–341, 2014.

[9] H. Shafiee, W. Asghar, F. Inci, M. Yuksekkaya, M. Jahangir, M. H Zhang, N. Gozde Durmus, U. Gurkan, D. R Kuritzkes, and U. Demirci, "Paper and Flexible Substrates as Materials for Biosensing Platforms to Detect Multiple Biotargets," *Sci. Rep.*, vol. 5, p. 8719, 2015.

[10] S.-J. Son, Y.-S. Cho, J.-J. Rha, and C.-J. Choi, "Fabrication of metal electrodes on flexible substrates by controlled deposition of conductive nano-ink," *Mater. Lett.*, vol. 117, pp. 179–183, 2014.

[11] R. Arvidsson and B. A. Sandén, "Carbon nanomaterials as potential substitutes for scarce metals," *J. Clean. Prod.*, vol. 156, pp. 253–261, 2017.

[12] F. Torrisi and T. Carey, "Graphene, related two-dimensional crystals and hybrid systems for printed and wearable electronics," *Nano Today*, vol. 23, pp. 73–96, 2018.

[13] E. P. Randviir, D. A. C. Brownson, and C. E. Banks, "A decade of graphene research: production, applications and outlook," *Mater. Today*, vol. 17, no. 9, pp. 426–432, 2014.

[14] W. Wu, "Inorganic nanomaterials for printed electronics: a review," *Nanoscale*, vol. 9, no. 22, pp. 7342–7372, 2017.

[15] K. Kwon and W. Kim, "A waveform design method for high-speed inkjet printing based on self-sensing measurement," vol. 140, pp. 75–83, 2007.

[16] T. S. Tran, N. K. Dutta, and N. R. Choudhury, "Graphene inks for printed flexible electronics: Graphene dispersions, ink formulations, printing techniques and applications," *Adv. Colloid Interface Sci.*, vol. 261, pp. 41–61, 2018.

[17] I. V Antonova, "2D printing technologies using graphene-based materials," *Physics-Uspekhi*, vol. 60, no. 2, pp. 204–218, Feb. 2017.

[18] Y. Zhang, L. Zhang, and C. Zhou, "Review of Chemical Vapor Deposition of Graphene and Related Applications," *Acc. Chem. Res.*, vol. 46, no. 10, pp. 2329–2339, 2013.

[19] E. Bayaya, D. Waldmann, M. Krieger, and H. B. Weber, "Epitaxial graphene as an electrode material: a transistor testbed for organic and all-carbon semiconductors," *RSC Adv.*, vol. 4, no. 65, pp. 34474–34478, 2014.

[20] S. Basu and P. Bhattacharyya, "Recent developments on graphene and graphene oxide based solid state gas sensors," *Sensors Actuators B Chem.*, vol. 173, pp. 1–21, 2012.

[21] H. Xu, L. Ma, and Z. Jin, "Nitrogen-doped graphene: Synthesis, characterizations and energy applications," *J. Energy Chem.*, vol. 27, no. 1, pp. 146–160, 2018.

[22] R. Yadav and C. K. Dixit, "Synthesis, characterization and prospective applications of nitrogen-doped graphene: A short review," *J. Sci. Adv. Mater. Devices*, vol. 2, no. 2, pp. 141–149, 2017.

[23] P. R. Wallace, "The Band Theory of Graphite," *Phys. Rev.*, vol. 71, no. 9, pp. 622–634, 1947.

[24] and E. S. Hanns-Peter Boehm, Ralph Setton, "Nomenclature and Terminology of Graphite," *Carbon N. Y.*, vol. 24, no. 2, pp. 241–245, 1986.

[25] H. P. Boehm, A. Clauss, G. O. Fischer, and U Hoffman., "Das Adsorptionsverhalten sehr dunner Kohlenstoff-Folien," *Zeitschrift für Anorg. und Allg. Chemie*, vol. 316, no. 3–4, pp. 119–127, 1962.

[26] A. A. F. K. S. Novoselov, A. K. Geim, S. V. Morozov, D. Jiang, Y. Zhang, S. V. Dubonos, I. V. Grigorieva, "Electric Field Effect in Atomically Thin Carbon Films," *Science (80-.).*, vol. 306, no. 5696, pp. 666–669, 2004.

[27] Andre Geim and Konstantin Novoselov, "The Nobel Prize in Physics 2010." [Online]. Available: https://www.nobelprize.org/prizes/physics/2010/summary/.

[28] C. Lee, X. Wei, J. W. Kysar, and J. Hone, "Measurement of the elastic properties and intrinsic strength of monolayer graphene," *Science (80-.).*, vol. 321, no. 5887, pp. 385–388, 2008.

[29] A. S. Mayorov, R. V. Gorbachev, S. V. Morozov, L. Britnell, R. Jalil, L. A. Ponomarenko, P. Blake, K. S. Novoselov, K.

Watanabe, T. Taniguchi, and A. K. Geim, “Micrometer-scale ballistic transport in encapsulated graphene at room temperature,” *Nano Lett.*, vol. 11, no. 6, pp. 2396–2399, 2011.
[30] S. V. Morozov, K. S. Novoselov, M. I. Katsnelson, F. Schedin, D. C. Elias, J. A. Jaszczak, and A. K. Geim, “Giant intrinsic carrier mobilities in graphene and its bilayer,” *Phys. Rev. Lett.*, vol. 100, no. 1, pp. 11–14, 2008.
[31] A. A. Balandin, S. Ghosh, W. Bao, I. Calizo, D. Teweldebrhan, F. Miao, and C. N. Lau, “Superior Thermal Conductivity of Single-Layer Graphene,” *Nano Lett.*, vol. 8, no. 3, pp. 902–907, 2008.
[32] M. D. Stoller, S. Park, Z. Yanwu, J. An, and R. S. Ruoff, “Graphene-Based ultracapacitors,” *Nano Lett.*, vol. 8, no. 10, pp. 3498–3502, 2008.
[33] T. R. R. Nair, P. Blake, A. N. Grigorenko, K. S. Novoselov, T. J. Booth, Stauber and A. K. G. N. M. R. Peres, “Fine Structure Constant Defines Visual Transparency of Graphene,” *Science (80-.).*, vol. 330, p. 1308, 2008.
[34] A. Peigney, C. Laurent, E. Flahaut, R. R. Bacsa, and A. Rousset, “Specific surface area of carbon nanotubes and bundles of carbon nanotubes,” *Carbon N. Y.*, vol. 39, no. 4, pp. 507–514, 2001.
[35] K. S. Novoselov, V. Falko, L. Colombo, P. R. Gellert, M. G. Schwab, and K. A. Kim, “A Roadmap for graphene,” *Nature*, vol. 490, pp. 192–200, 2012.
[36] C. Çelebi, C. Yanik, A. G. Demirkol, and I. I. Kaya, “The effect of a SiC cap on the growth of epitaxial graphene on SiC in ultra high vacuum,” *Carbon N. Y.*, vol. 50, no. 8, pp. 3026–3031, 2012.
[37] K. V. Emtsev, A. Bostwick, K. Horn, J. Jobst, G. L. Kellogg, L. Ley, J. L. McChesney, T. Ohta, S. A. Reshanov, J. Röhrl, E. Rotenberg, A. K. Schmid, D. Waldmann, H. B. Weber, and T. Seyller, “Towards wafer-size graphene layers by atmospheric pressure graphitization of silicon carbide,” *Nat. Mater.*, vol. 8, no. 3, pp. 203–207, 2009.
[38] G. G. Jernigan, B. L. VanMil, J. L. Tedesco, J. G. Tischler, E. R. Glaser, A. Davidson, P. M. Campbell, and D. K. Gaskill, “Comparison of epitaxial graphene on si-face and C-face 4H SiC formed by ultrahigh vacuum and RF furnace production,” *Nano Lett.*, vol. 9, no. 7, pp. 2605–2609, 2009.
[39] A. Reina, X. Jia, J. Ho, D. Nezich, H. Son, V. Bulovic, M. S. Dresselhaus, and K. Jing, “Large area, few-layer graphene films on arbitrary substrates by chemical vapor deposition,” *Nano Lett.*, vol. 9, no. 1, pp. 30–35, 2009.
[40] S. Bae, H. Kim, Y. Lee, X. Xu, J. S. Park, Y. Zheng, J. Balakrishnan, T. Lei, H. Ri Kim, Y. Il Song, Y. J. Kim, K. S. Kim, B. Özyilmaz, J. H. Ahn, B. H. Hong, and S. Iijima, “Roll-to-roll production of 30-inch graphene films for transparent electrodes,” *Nat. Nanotechnol.*, vol. 5, no. 8, pp. 574–578, 2010.
[41] J. Campos-Delgado, A. R. Botello-Méndez, G. Algara-Siller, B. Hackens, T. Pardoen, U. Kaiser, M. S. Dresselhaus, J. C. Charlier, and J. P. Raskin, “CVD synthesis of mono- and few-layer graphene using alcohols at low hydrogen concentration and atmospheric pressure,” *Chem. Phys. Lett.*, vol. 584, pp. 142–146, 2013.
[42] D. A. C. Brownson and C. E. Banks, “The electrochemistry of CVD graphene: Progress and prospects,” *Phys. Chem. Chem. Phys.*, vol. 14, no. 23, pp. 8264–8281, 2012.
[43] K. S. Novoselov, D. Jiang, F. Schedin, T. J. Booth, V. V Khotkevich, S. V Morozov, and A. K. Geim, “Two-dimensional atomic crystals,” vol. 102, no. 30, pp. 10451–10453, 2005.
[44] H. Bai, C. Li, and G. Shi, “Functional Composite Materials Based on Chemically Converted Graphene,” *Adv. Mater.*, vol. 23, no. 9, pp. 1089–1115, 2011.
[45] R. K. Singh, R. Kumar, and D. P. Singh, “Graphene oxide: strategies for synthesis, reduction and frontier applications,” *RSC Adv.*, vol. 6, no. 69, pp. 64993–65011, 2016.
[46] B. C. Brodie, “On the atomic weight of graphite.,” *Philos. Trans. R. Soc. A*, vol. 149, pp. 249–259, 1859.
[47] S. L, “Verfahren zur Darstellung der Graphitsäure,” *Berichte der Dtsch. Chem. Gesellschaft*, vol. 31, pp. 1481– 1487, 1898.
[48] U. Hofmann and E. König, “Untersuchungen über Graphitoxyd,” *Zeitschrift für Anorg. und Allg. Chemie*, vol. 234, no. 4, pp. 311–336, 1937.
[49] W. S. Hummers and R. E. Offeman, “Preparation of Graphitic Oxide,” *J. Am. Chem. Soc.*, vol. 80, no. 6, p. 1339, 1958.
[50] A. M. Dimiev and J. M. Tour, “Mechanism of graphene oxide formation,” *ACS Nano*, vol. 8, no. 3, pp. 3060–3068, 2014.
[51] D. C. Marcano, D. V Kosynkin, J. M. Berlin, A. Sinitskii, Z. Sun, A. Slesarev, L. B. Alemany, W. Lu, and J. M. Tour, “Improved Synthesis of Graphene Oxide,” *ACS Nano*, vol. 4, no. 8, pp. 4806–4814, 2010.
[52] J. Shen, Y. Hu, M. Shi, X. Lu, C. Qin, C. Li, and M. Ye, “Fast and Facile Preparation of Graphene Oxide and Reduced Graphene Oxide Nanoplatelets,” *chem. Mater.*, vol. 21, no. 15, pp. 3514–3520, 2009.
[53] D. R. Dreyer, S. Park, W. Bielawski, and R. S. Ruoff, “The chemistry of graphene oxide,” *Chem. Soc. Rev.*, vol. 39, pp. 228–240, 2010.
[54] Y. Hernandez, V. Nicolosi, M. Lotya, F. M Blighe, Z. Sun, S. De, I. Mcgovern, B. Holland, M. Byrne, Y. Gun’ko, J. Boland, P. N. Nirmalraj, G. Duesberg, S. Krishnamurthy, R. Goodhue, J. Hutchison, V. Scardaci, A. Ferrari, and J. Coleman, “High-yield production of graphene by liquid-phase exfoliation of graphite,” *Nat. Nanotechnol.*, vol. 3, pp. 563–568, 2008.
[55] A. B. Bourlinos, V. Georgakilas, R. Zboril, T. A. Steriotis, and A. K. Stubos, “Liquid-Phase Exfoliation of Graphite Towards Solubilized Graphenes,” *Small*, vol. 5, no. 16, pp. 1841–1845, 2009.
[56] W. W. Liu and J. N. Wang, “Direct exfoliation of graphene in organic solvents with addition of NaOH,” *Chem. Commun.*, vol. 47, no. 24, pp. 6888–6890, 2011.
[57] W. Du, J. Lu, P. Sun, Y. Zhu, and X. Jiang, “Organic salt-assisted liquid-phase exfoliation of graphite to produce high-quality graphene,” *Chem. Phys. Lett.*, vol. 568–569, pp. 198–201, 2013.

[58] X. Wang, P. F. Fulvio, G. A. Baker, G. M. Veith, R. R. Unocic, S. M. Mahurin, M. Chi, and S. Dai, "Direct exfoliation of natural graphite into micrometre size few layers graphene sheets using ionic liquids," *Chem. Commun.*, vol. 46, no. 25, pp. 4487–4489, 2010.

[59] D. Nuvoli, L. Valentini, V. Alzari, S. Scognamillo, S. B. Bon, M. Piccinini, J. Illescas, and A. Mariani, "High concentration few-layer graphene sheets obtained by liquid phase exfoliation of graphite in ionic liquid," *J. Mater. Chem.*, vol. 21, no. 10, pp. 3428–3431, 2011.

[60] Z. Lin, P. S. Karthik, M. Hada, T. Nishikawa, and Y. Hayashi, "Simple Technique of Exfoliation and Dispersion of Multilayer Graphene from Natural Graphite by Ozone-Assisted Sonication," *Nanomaterials*, vol. 7, no. 6, 2017.

[61] A. Ciesielski and P. Samorì, "Graphene via sonication assisted liquid-phase exfoliation," *Chem. Soc. Rev.*, vol. 43, no. 1, pp. 381–398, 2014.

[62] Y. Xu, H. Cao, Y. Xue, B. Li, and W. Cai, "Liquid-Phase Exfoliation of Graphene: An Overview on Exfoliation Media, Techniques, and Challenges," *Nanomaterials*, vol. 8, p. 942, 2018.

[63] A. Abdelkader, A. Cooper, R. Dryfe, and I. Kinloch, "How to Get Between the Sheets: A Review of Recent Works on the Electrochemical Exfoliation of Graphene Materials from Bulk Graphite," *Nanoscale*, vol. 7, 2015.

[64] C.-Y. Su, A.-Y. Lu, Y. Xu, F.-R. Chen, A. N. Khlobystov, and L.-J. Li, "High-Quality Thin Graphene Films from Fast Electrochemical Exfoliation," *ACS Nano*, vol. 5, no. 3, pp. 2332–2339, 2011.

[65] J. Wang, K. K. Manga, Q. Bao, and K. P. Loh, "High-Yield Synthesis of Few-Layer Graphene Flakes through Electrochemical Expansion of Graphite in Propylene Carbonate Electrolyte," *J. Am. Chem. Soc.*, vol. 133, no. 23, pp. 8888–8891, 2011.

[66] H. Wang, C. Wei, K. Zhu, Y. Zhang, C. Gong, J. Guo, J. Zhang, L. Yu, and J. Zhang, "Preparation of Graphene Sheets by Electrochemical Exfoliation of Graphite in Confined Space and Their Application in Transparent Conductive Films," *ACS Appl. Mater. Interfaces*, vol. 9, no. 39, pp. 34456–34466, 2017.

[67] A. J. Cooper, N. R. Wilson, I. A. Kinloch, and R. A. W. Dryfe, "Single stage electrochemical exfoliation method for the production of few-layer graphene via intercalation of tetraalkylammonium cations," *Carbon N. Y.*, vol. 66, pp. 340–350, 2014.

[68] T. Achee, W. Sun, J. T. Hope, S. G. Quitzau, C. Brandon Sweeney, S. Shah, T. Habib, and M. J. Green, "High-yield scalable graphene nanosheet production from compressed graphite using electrochemical exfoliation," *Sci. Rep.*, vol. 8, 2018.

[69] P. Yu, S. E. Lowe, G. P. Simon, and Y. L. Zhong, "Electrochemical exfoliation of graphite and production of functional graphene," *Curr. Opin. Colloid Interface Sci.*, vol. 20, no. 5, pp. 329–338, 2015.

[70] M. Yi and Z. Shen, "A review on mechanical exfoliation for the scalable production of graphene," *J. Mater. Chem. A*, vol. 3, no. 22, pp. 11700–11715, 2015.

[71] M. Bastwros, G. Y. Kim, C. Zhu, K. Zhang, S. Wang, X. Tang, and X. Wang, "Effect of ball milling on graphene reinforced Al6061 composite fabricated by semi-solid sintering," *Compos. Part B Eng.*, vol. 60, pp. 111–118, 2014.

[72] X. Fan, D. W. Chang, X. Chen, J. B. Baek, and L. Dai, "Functionalized graphene nanoplatelets from ball milling for energy applications," *Curr. Opin. Chem. Eng.*, vol. 11, pp. 52–58, 2016.

[73] S. Zhuang, B. B. Nunna, J. A. Boscoboinik, and E. S. Lee, "Nitrogen-doped graphene catalysts: High energy wet ball milling synthesis and characterizations of functional groups and particle size variation with time and speed," *Int. J. Energy Res.*, vol. 41, no. 15, pp. 2535–2554, 2017.

[74] L. Liu, Z. Shen, M. Yi, X. Zhang, and S. Ma, "A green, rapid and size-controlled production of high-quality graphene sheets by hydrodynamic forces," *RSC Adv.*, vol. 4, 2014.

[75] C. Knieke, A. Berger, M. Voigt, R. N. K. Taylor, J. Röhrl, and W. Peukert, "Scalable production of graphene sheets by mechanical delamination," *Carbon N. Y.*, vol. 48, no. 11, pp. 3196–3204, 2010.

[76] L. Liu, Z. Xiong, D. Hu, G. Wu, and P. Chen, "Production of high quality single- or few-layered graphene by solid exfoliation of graphite in the presence of ammonia borane," *Chem. Commun.*, vol. 49, no. 72, pp. 7890–7892, 2013.

[77] T. Lin, Y. Tang, Y. Wang, H. Bi, Z. Liu, F. Huang, X. Xie, and M. Jiang, "Scotch-tape-like exfoliation of graphite assisted with elemental sulfur and graphene–sulfur composites for high-performance lithium-sulfur batteries," *Energy Environ. Sci.*, vol. 6, pp. 1283–1290, 2013.

[78] M. Yi and Z. Shen, "Fluid dynamics: an emerging route for the scalable production of graphene in the last five years," *RSC Adv.*, vol. 6, no. 76, pp. 72525–72536, 2016.

[79] S. Karmakar, N. V. Kulkarni, A. B. Nawale, N. P. Lalla, R. Mishra, V. G. Sathe, S. V. Bhoraskar, and A. K. Das, "A novel approach towards selective bulk synthesis of few-layer graphenes in an electric arc," *J. Phys. D. Appl. Phys.*, vol. 42, no. 11, 2009.

[80] Y. Li, Q. Chen, K. Xu, T. Kaneko, and R. Hatakeyama, "Synthesis of graphene nanosheets from petroleum asphalt by pulsed arc discharge in water," *Chem. Eng. J.*, vol. 215–216, pp. 45–49, 2013.

[81] K. S. Subrahmanyam, L. S. Panchakarla, A. Govindaraj, and C. N. R. Rao, "Simple method of preparing graphene flakes by an arc-discharge method," *J. Phys. Chem. C*, vol. 113, no. 11, pp. 4257–4259, 2009.

[82] S. Pei and H.-M. Cheng, "The reduction of graphene oxide," *Carbon N. Y.*, vol. 50, 2012.

[83] A. F. Von Ulrich Hofmann, "Die reduction von graphitoxyd mit schwefelwasserstoff.," *Kolloid-Zeitschrift*, vol. 2, pp. 149–151, 1934.

[84] G. Brauer, *Handbook of Preparative Inorganic chemistry*. New York: Academic Press, 1963.

[85] S. Eigler, S. Grimm, M. Enzelberger-Heim, P. Müller, and A. Hirsch, "Graphene oxide: efficiency of reducing

agents," *Chem. Commun.*, vol. 49, no. 67, pp. 7391–7393, 2013.
[86] S. W. Chong, C. W. Lai, and S. B. Abdul Hamid, "Green preparation of reduced graphene oxide using a natural reducing agent," *Ceram. Int.*, vol. 41, no. 8, pp. 9505–9513, 2015.
[87] K. K. H. De Silva, H.-H. Huang, R. K. Joshi, and M. Yoshimura, "Chemical reduction of graphene oxide using green reductants," *Carbon N. Y.*, vol. 119, pp. 190–199, 2017.
[88] M. J. Mcallister, J. Li, D. H. Adamson, H. C. Schniepp, A. A. Abdala, J. Liu, O. M. Herrera-alonso, D. L. Milius, R. Car, R. K. Prud, and I. A. Aksay, "Single Sheet Functionalized Graphene by Oxidation and Thermal Expansion of Graphite," *chem. Mater.*, vol. 19, no. 4, pp. 4396–4404, 2007.
[89] A. V. D. M. V. K. V. B., E. V. G. G. N. A. V. R. M., B. I. M. W. K. M. A. M., and Benito, "The effect of the thermal reduction temperature on the structure and sorption capacity of reduced graphene oxide materials," *Appl. Surf. Sci.*, vol. 361, 2015.
[90] Y. Zhu, S. Murali, M. D. Stoller, A. Velamakanni, R. D. Piner, and R. S. Ruoff, "Letter to the Editor Microwave assisted exfoliation and reduction of graphite oxide for ultracapacitors," *Carbon N. Y.*, pp. 8–11, 2010.
[91] J. M. D. Tasco, L. Guardia, J. I. Paredes, R. Rozada, and A. Martı, "UV light exposure of aqueous graphene oxide suspensions to promote their direct reduction , formation of graphene – metal nanoparticle hybrids and dye degradation," vol. 0, 2011.
[92] A. You, M. A. Y. Be, and I. In, "In-situ investigation of graphene oxide under UV irradiation : Evolution of work function," vol. 067154, no. May, 2015.
[93] Y. H. Ding, P. Zhang, Q. Zhuo, H. M. Ren, Z. M. Yang, and Y. Jiang, "A green approach to the synthesis of reduced graphene oxide nanosheets under UV irradiation," vol. 215601, 2011.
[94] S. H. Park and H. S. Kim, "Environmentally benign and facile reduction of graphene oxide by flash light irradiation," *Nanotechnology*, vol. 26, no. 20, p. 205601, 2015.
[95] S. J. Choi, S. J. Kim, and I. D. Kim, "Ultrafast optical reduction of graphene oxide sheets on colorless polyimide film for wearable chemical sensors," *NPG Asia Mater.*, vol. 8, no. 9, pp. 1–10, 2016.
[96] C. L. J, C.-S. R, and H. J, "Flash Reduction and Patterning of Graphite Oxide and Its Polymer Composite," *J. Am. Chem. Soc.*, vol. 131, no. 31, pp. 11027–11032, 2009.
[97] E. B. Secor, T. Z. Gao, M. H. Dos Santos, S. G. Wallace, K. W. Putz, and M. C. Hersam, "Combustion-Assisted Photonic Annealing of Printable Graphene Inks via Exothermic Binders," *ACS Appl. Mater. Interfaces*, vol. 9, no. 35, pp. 29418–29423, 2017.
[98] Y. Zhang, L. Guo, S. Wei, Y. He, H. Xia, Q. Chen, H. Sun, and F. Xiao, "Direct imprinting of microcircuits on graphene oxides film by femtosecond laser reduction," pp. 15–20, 2010.
[99] P. Kumar, K. S. Subrahmanyam, and C. N. R. Rao, "Graphene produced by radiation-induced reduction of graphene oxide."
[100] E. Kymakis, C. Petridis, T. D. Anthopoulos, and E. Stratakis, "Laser-Assisted Reduction of Graphene Oxide for Flexible , Large-Area Optoelectronics," no. January, 2014.
[101] D. A. Sokolov, C. M. Rouleau, D. B. Geohegan, and T. M. Orlando, "Excimer laser reduction and patterning of graphite oxide," vol. 3, pp. 1–9, 2012.
[102] S.-Y. Lee and S.-J. Park, "TiO2 photocatalyst for water treatment applications," *J. Ind. Eng. Chem.*, vol. 19, no. 6, pp. 1761–1769, 2013.
[103] O. Akhavan, M. Abdolahad, A. Esfandiar, and M. Mohatashamifar, "Photodegradation of Graphene Oxide Sheets by TiO 2 Nanoparticles after a Photocatalytic Reduction," pp. 12955–12959, 2010.
[104] G. S. and Z. L. Zeyu Lu, Guochang Chen, Wenbin Hao, "Mechanism of UV-assisted TiO2/reduced graphene oxide composites with variable photodegradation of methyl orange," *RSC Sdvances*, vol. 5, pp. 72916–72922, 2015.
[105] Y. Zhang, L. Guo, H. Xia, Q. Chen, J. Feng, and H. Sun, "Photoreduction of Graphene Oxides : Methods , Properties , and Applications," pp. 1–19, 2013.
[106] and R. C. A. Joey Mangadlao, Diana Choi, Peng-Fei Cao, "Photoreduction of Graphene Oxide and Photochemical Synthesis of Graphene – Metal Nanoparticle Hybrids by Ketyl Radicals," *ACS Appl. Mater. Interfaces*, vol. 9(29), pp. 24887–24898, 2017.
[107] M. Zhou, Y. Wang, Y. Zhai, J. Zhai, W. Ren, F. Wang, and S. Dong, "Controlled synthesis of large-area and patterned electrochemically reduced graphene oxide films," *Chem. - A Eur. J.*, vol. 15, no. 25, pp. 6116–6120, 2009.
[108] D. Manoj, K. Theyagarajan, D. Saravanakumar, S. Senthilkumar, and K. Thenmozhi, "Aldehyde functionalized ionic liquid on electrochemically reduced graphene oxide as a versatile platform for covalent immobilization of biomolecules and biosensing," *Biosens. Bioelectron.*, vol. 103, pp. 104–112, 2018.
[109] A. G. Marrani, R. Zanoni, R. Schrebler, and E. A. Dalchiele, "Toward Graphene/Silicon Interface via Controlled Electrochemical Reduction of Graphene Oxide," *J. Phys. Chem. C*, vol. 121, no. 10, pp. 5675–5683, 2017.
[110] M. Velmurugan, P. Balasubramanian, and S. M. Chen, "Determination of caffeic acid in wine samples based on the electrochemical reduction of graphene oxide modified screen printed carbon electrode," *Int. J. Electrochem. Sci.*, vol. 12, no. 5, pp. 4173–4182, 2017.
[111] J. Ping, Y. Wang, K. Fan, J. Wu, and Y. Ying, "Direct electrochemical reduction of graphene oxide on ionic liquid doped screen-printed electrode and its electrochemical biosensing application," *Biosens. Bioelectron.*, vol. 28, no. 1, pp. 204–209, 2011.
[112] C. Fu, Y. Kuang, Z. Huang, X. Wang, N. Du, J. Chen, and H. Zhou, "Electrochemical co-reduction synthesis of graphene/Au nanocomposites in ionic liquid and their electrochemical activity," *Chem. Phys. Lett.*, vol. 499, no. 4–

6, pp. 250–253, 2010.
[113] M. Hilder, B. Winther-Jensen, D. Li, M. Forsyth, and D. R. MacFarlane, "Direct electro-deposition of graphene from aqueous suspensions," *Phys. Chem. Chem. Phys.*, vol. 13, no. 20, pp. 9187–9193, 2011.
[114] Y. Shao, J. Wang, M. Engelhard, C. Wang, and Y. Lin, "Facile and controllable electrochemical reduction of graphene oxide and its applications," *J. Mater. Chem.*, vol. 20, no. 4, pp. 743–748, 2010.
[115] J. Yang and S. Gunasekaran, "Electrochemically reduced graphene oxide sheets for use in high performance supercapacitors," *Carbon N. Y.*, vol. 51, no. 1, pp. 36–44, 2013.
[116] W. J. Basirun, M. Sookhakian, S. Baradaran, M. R. Mahmoudian, and M. Ebadi, "Solid-phase electrochemical reduction of graphene oxide films in alkaline solution," *Nanoscale Res. Lett.*, vol. 8, no. 1, pp. 1–9, 2013.
[117] H. Tong, J. Zhu, J. Chen, Y. Han, S. Yang, B. Ding, and X. Zhang, "Electrochemical reduction of graphene oxide and its electrochemical capacitive performance," *J. Solid State Electrochem.*, vol. 17, no. 11, pp. 2857–2863, 2013.
[118] V. S. Dilimon and S. Sampath, "Electrochemical preparation of few layer-graphene nanosheets via reduction of oriented exfoliated graphene oxide thin films in acetamide-urea-ammonium nitrate melt under ambient conditions," *Thin Solid Films*, vol. 519, no. 7, pp. 2323–2327, 2011.
[119] J. Kauppila, P. Kunnas, P. Damlin, A. Viinikanoja, and C. Kvarnström, "Electrochemical reduction of graphene oxide films in aqueous and organic solutions," *Electrochim. Acta*, vol. 89, pp. 84–89, 2013.
[120] X. Feng, W. Chen, and L. Yan, "Electrochemical reduction of bulk graphene oxide materials," *RSC Adv.*, vol. 6, no. 83, pp. 80106–80113, 2016.
[121] H. Guo, X. Wang, Q. Qian, F. Wang, and X. Xia, "A Green Approach to the Synthesis of Graphene Nanosheets," *ACS Nano*, vol. 3, no. 9, pp. 2653–2659, 2009.
[122] Xiaoming Sun and Yadong Li, "Colloidal Carbon Spheres and Their Core/Shell Structures with Noble-Metal Nanoparticles**," *Angew. Chemie - Int. Ed.*, vol. 43, pp. 597–601, 2004.
[123] L. Luo, S. Yu, H. Qian, and T. Zhou, "Large-Scale Fabrication of Flexible Silver / Cross-Linked Poly (vinyl alcohol) Coaxial Nanocables by a Facile Solution Approach," no. 10, pp. 2822–2823, 2005.
[124] G. Huang, W. Kang, Q. Geng, B. Xing, and Q. Liu, "One-Step Green Hydrothermal Synthesis of Few-Layer Graphene Oxide from Humic Acid," *nanomaterials*, vol. 8, pp. 1–9, 2018.
[125] W. Hong, L. Li, R. Xue, X. Xu, H. Wang, J. Zhou, H. Zhao, Y. Song, Y. Liu, and J. Gao, "One-pot hydrothermal synthesis of Zinc ferrite/reduced graphene oxide as an efficient electrocatalyst for oxygen reduction reaction," *J. Colloid Interface Sci.*, 2016.
[126] D. Zhang, A. Liu, H. Chang, and B. Xia, "Room-temperature high-performance acetone gas sensor based on hydrothermal synthesized SnO2- reduced graphene oxide hybrid composite," *RSC Adv.*, vol. 5, pp. 3016–3022, 2015.
[127] M. Shi, J. Shen, H. Ma, Z. Li, X. Lu, N. Li, and M. Ye, "Preparation of graphene-TiO2 composite by hydrothermal method from peroxotitanium acid and its photocatalytic properties," *Colloids Surfaces A Physicochem. Eng. Asp.*, vol. 405, pp. 30–37, 2012.
[128] X. Mei, X. Meng, and F. Wu, "Hydrothermal method for the production of reduced graphene oxide GO colloidal solution GO lamellar solid sample for conductivity test," *Phys. E Low-dimensional Syst. Nanostructures*, vol. 68, pp. 81–86, 2015.
[129] J. L. Shi, W. C. Du, Y. X. Yin, Y. G. Guo, and L. J. Wan, "Hydrothermal reduction of three-dimensional graphene oxide for binder-free flexible supercapacitors," *J. Mater. Chem. A*, vol. 2, no. 28, pp. 10830–10834, 2014.
[130] and G. S. Yuxi Xu, Kaixuan Sheng, Chun Li, "Self-Assembled Graphene Hydrogel via a One-Step Hydrothermal Process," *ACS Nano*, vol. 4, no. 7, pp. 4324–4330, 2010.
[131] Y. Zhou, Q. Bao, L. Ai, L. Tang, Y. Zhong, and K. P. Loh, "Hydrothermal Dehydration for the ' Green ' Reduction of Exfoliated Graphene Oxide to Graphene and Demonstration of Tunable Optical Limiting Properties," no. 17, pp. 2950–2956, 2009.
[132] H. Huang, K. K. H. De Silva, G. R. A. Kumara, and M. Yoshimura, "Structural Evolution of Hydrothermally Derived Reduced Graphene Oxide," *Sci. Rep.*, no. April, pp. 2–10, 2018.
[133] Y. Niu, "Reduction and structural evolution of graphene oxide sheets under hydrothermal treatment," *Phys. Lett. A*, vol. 1, pp. 1–5, 2016.
[134] S. Kim, K. Choi, and S. Park, "Solvothermal reduction of graphene oxide in dimethylformamide," *Solid State Sci.*, vol. 61, pp. 40–43, 2016.
[135] D. S., G. S., W. K., T. V.C., C. K., H. A.S., F. J., V. R., Y. Y., and K. R.B., "A one-step, solvothermal reduction method for producing reduced graphene oxide dispersions in organic solvents.," *ACS Nano*, vol. 4, no. 7, pp. 3845–3852, 2010.
[136] L. Lin and S. Zhang, "Effective solvothermal deoxidization of graphene oxide using solid sulphur as a reducing agent," *J. Mater. Chem.*, vol. 22, no. 29, pp. 14385–14393, 2012.
[137] C. Nethravathi and M. Rajamathi, "Chemically modified graphene sheets produced by the solvothermal reduction of colloidal dispersions of graphite oxide," *Carbon N. Y.*, vol. 46, no. 14, pp. 1994–1998, 2008.
[138] P. K. Sahoo, S. Sahoo, A. K. Satpati, and D. Bahadur, "Solvothermal synthesis of reduced graphene oxide/Au nanocomposite-modified electrode for the determination of inorganic mercury and electrochemical oxidation of toxic phenolic compounds," *Electrochim. Acta*, vol. 180, pp. 1023–1032, 2015.
[139] S. Lee, J. Koo, S.-K. Kang, G. Park, Y. J. Lee, Y.-Y. Chen, S. A. Lim, K.-M. Lee, and J. A. Rogers, "Metal microparticle – Polymer composites as printable, bio/ecoresorbable conductive inks," *Mater. Today*, vol. 21, no. 3, pp. 207–215, 2018.

[140] D. W. Johnson, B. P. Dobson, and K. S. Coleman, "A manufacturing perspective on graphene dispersions," *Curr. Opin. Colloid Interface Sci.*, vol. 20, no. 5, pp. 367–382, 2015.
[141] J. Li, M. C. Lemme, and M. Östling, "Inkjet printing of 2D layered materials," *ChemPhysChem*, vol. 15, no. 16, pp. 3427–3434, 2014.
[142] E. B. Secor, P. L. Prabhumirashi, K. Puntambekar, M. L. Geier, and M. C. Hersam, "Inkjet printing of high conductivity, flexible graphene patterns," *J. Phys. Chem. Lett.*, vol. 4, no. 8, pp. 1347–1351, 2013.
[143] E. B. Secor, B. Y. Ahn, T. Z. Gao, J. A. Lewis, and M. C. Hersam, "Rapid and Versatile Photonic Annealing of Graphene Inks for Flexible Printed Electronics," *Adv. Mater.*, vol. 27, no. 42, pp. 6683–6688, 2015.
[144] S. Majee, M. Song, S. L. Zhang, and Z. Bin Zhang, "Scalable inkjet printing of shear-exfoliated graphene transparent conductive films," *Carbon N. Y.*, vol. 102, pp. 51–57, 2016.
[145] Yu Teng Liang and Mark C. Hersam, "Highly Concentrated Graphene Solutions via Polymer Enhanced Solvent Exfoliation and Iterative Solvent Exchange," *J. Am. Chem. Soc.*, vol. 132, pp. 17661–17663, 2010.
[146] J. Li, F. Ye, S. Vaziri, M. Muhammed, M. C. Lemme, and M. Östling, "Efficient inkjet printing of graphene," *Adv. Mater.*, vol. 25, no. 29, pp. 3985–3992, 2013.
[147] L. Dybowska-Sarapuk, K. Kielbasinski, A. Arazna, K. Futera, A. Skalski, D. Janczak, M. Sloma, and M. Jakubowska, "Efficient Inkjet Printing of Graphene-Based Elements: Influence of Dispersing Agent on Ink Viscosity," *Nanomaterials*, vol. 8, no. 8, p. 602, 2018.
[148] N. Karim, S. Afroj, A. Malandraki, S. Butterworth, C. Beach, M. Rigout, K. S. Novoselov, A. J. Casson, and S. G. Yeates, "All inkjet-printed graphene-based conductive patterns for wearable e-textile applications," *J. Mater. Chem. C*, vol. 5, no. 44, pp. 11640–11648, 2017.
[149] J. Li, S. Sollami Delekta, P. Zhang, S. Yang, M. R. Lohe, X. Zhuang, X. Feng, and M. Östling, "Scalable Fabrication and Integration of Graphene Microsupercapacitors through Full Inkjet Printing," *ACS Nano*, vol. 11, no. 8, pp. 8249–8256, 2017.
[150] C. L. Lee, C. H. Chen, and C. W. Chen, "Graphene nanosheets as ink particles for inkjet printing on flexible board," *Chem. Eng. J.*, vol. 230, pp. 296–302, 2013.
[151] F. Torrisi, T. Hasan, W. Wu, Z. Sun, A. Lombardo, T. S. Kulmala, G. W. Hsieh, S. Jung, F. Bonaccorso, P. J. Paul, D. Chu, and A. C. Ferrari, "Inkjet-printed graphene electronics," *ACS Nano*, vol. 6, no. 4, pp. 2992–3006, 2012.
[152] F. Miao, S. Majee, M. Song, J. Zhao, S. L. Zhang, and Z. Bin Zhang, "Inkjet printing of electrochemically-exfoliated graphene nano-platelets," *Synth. Met.*, vol. 220, pp. 318–322, 2016.
[153] L. Cseri, M. Razali, P. Pogany, and G. Szekely, "Chapter 3.15 - Organic Solvents in Sustainable Synthesis and Engineering," in *Green Chemistry*, B. Török and T. Dransfield, Eds. Elsevier, 2018, pp. 513–553.
[154] K. Pan, Y. Fan, T. Leng, J. Li, Z. Xin, J. Zhang, L. Hao, J. Gallop, K. S. Novoselov, and Z. Hu, "Sustainable production of highly conductive multilayer graphene ink for wireless connectivity and IoT applications," *Nat. Commun.*, vol. 9, no. 1, p. 5197, 2018.
[155] B. Nagar, M. Balsells, A. de la Escosura-Muñiz, P. Gomez-Romero, and A. Merkoçi, "Fully printed one-step biosensing device using graphene/AuNPs composite," *Biosens. Bioelectron.*, 2018.
[156] C. Bardpho, P. Rattanarat, W. Siangproh, and O. Chailapakul, "Ultra-high performance liquid chromatographic determination of antioxidants in teas using inkjet-printed graphene-polyaniline electrode," *Talanta*, vol. 148, pp. 673–679, 2016.
[157] Y. Xu, I. Hennig, D. Freyberg, A. James Strudwick, M. Georg Schwab, T. Weitz, and K. Chih-Pei Cha, "Inkjet-printed energy storage device using graphene/polyaniline inks," *J. Power Sources*, vol. 248, pp. 483–488, 2014.
[158] Y. Liu, B. Zhang, Q. Xu, Y. Hou, S. Seyedin, S. Qin, G. G. Wallace, S. Beirne, J. M. Razal, and J. Chen, "Development of Graphene Oxide/Polyaniline Inks for High Performance Flexible Microsupercapacitors via Extrusion Printing," *Adv. Funct. Mater.*, vol. 28, no. 21, pp. 1–12, 2018.
[159] W. Zhang, E. Bi, M. Li, and L. Gao, "Synthesis of Ag/RGO composite as effective conductive ink filler for flexible inkjet printing electronics," *Colloids Surfaces A Physicochem. Eng. Asp.*, vol. 490, pp. 232–240, 2016.
[160] V. Costa Bassetto, J. Xiao, E. Oveisi, V. Amstutz, B. Liu, H. H. Girault, and A. Lesch, "Rapid inkjet printing of high catalytic activity Co3O4/N-rGO layers for oxygen reduction reaction," *Appl. Catal. A Gen.*, vol. 563, pp. 9–17, 2018.
[161] Joel H. Hildebrand and Robert L. Scott, *The Solubility of Nonelectrolytes*, 3rd Editio. New York: Reinhold, 1950.
[162] G. H. Brown, "Regular Solutions. By Joel H. Hildebrand and Robert L. Scott," *Inorg. Chem.*, vol. 2, no. 2, pp. 431–432, 1963.
[163] C. M. Hansen, *Hansen Solubility Parameters: A User's Handbook, Second Edition*. 2012.
[164] D. Konios, M. M. Stylianakis, E. Stratakis, and E. Kymakis, "Dispersion behaviour of graphene oxide and reduced graphene oxide," *J. Colloid Interface Sci.*, vol. 430, pp. 108–112, 2014.
[165] Y. Hernandez, M. Lotya, D. Rickard, S. D. Bergin, and J. N. Coleman, "Measurement of Multicomponent Solubility Parameters for Graphene Facilitates Solvent Discovery," vol. 3, no. 9, pp. 3208–3213, 2010.
[166] A. Berni, M. Mennig, and H. Schmidt, "Doctor Blade," in *Sol-Gel Technologies for Glass Producers and Users*, M. A. Aegerter and M. Mennig, Eds. Boston, MA: Springer US, 2004, pp. 89–92.
[167] J. O. Huiqin Zheng, Chin Yong Neo, Xiaoguang Mei, Jun Qiu, "Reduced graphene oxide films fabricated by gel coating and their application as platinum-free counter electrodes of highly efficient iodide/triiodide dye-sensitized solar cells," *J. Mater. Chem.*, vol. 22, pp. 14465–14474, 2012.
[168] F. W. Low and C. W. Lai, "Recent developments of graphene-TiO2composite nanomaterials as efficient photoelectrodes in dye-sensitized solar cells: A review," *Renew. Sustain. Energy Rev.*, vol. 82, no. August 2017, pp.

103–125, 2018.
[169] P. Ranjan, S. Agrawal, A. Sinha, T. R. Rao, J. Balakrishnan, and A. D. Thakur, "A Low-Cost Non-explosive Synthesis of Graphene Oxide for Scalable Applications," *Sci. Rep.*, vol. 8, no. 1, pp. 1–13, 2018.
[170] T. Purkait, G. Singh, M. Singh, D. Kumar, and R. S. Dey, "Large area few-layer graphene with scalable preparation from waste biomass for high-performance supercapacitor," *Sci. Rep.*, vol. 7, no. 1, pp. 1–14, 2017.
[171] D. Mahalingam, S. Wang, and S. P. Nunes, "Graphene Oxide Liquid Crystal Membranes in Protic Ionic Liquid for Nanofiltration," *ACS Appl. Nano Mater.*, p. acsanm.8b00927, 2018.
[172] J. Garofalo, J. Lawler, D. Walczyk, and N. Koratkar, "Analysis of Deposition Methods for Lithium-Ion Battery Anodes Using Reduced Graphene Oxide Slurries on Copper Foil," *J. Manuf. Sci. Eng.*, vol. 140, no. 9, p. 094501, 2018.
[173] J. Wang, M. Liang, Y. Fang, T. Qiu, J. Zhang, and L. Zhi, "Rod-coating: Towards large-area fabrication of uniform reduced graphene oxide films for flexible touch screens," *Adv. Mater.*, vol. 24, no. 21, pp. 2874–2878, 2012.
[174] M. Akbari, M. W. A. Khan, M. Hasani, T. Bjorninen, L. Sydanheimo, and L. Ukkonen, "Fabrication and Characterization of Graphene Antenna for Low-Cost and Environmentally Friendly RFID Tags," *IEEE Antennas Wirel. Propag. Lett.*, vol. 15, no. c, pp. 1569–1572, 2016.
[175] W. J. Hyun, E. B. Secor, M. C. Hersam, C. D. Frisbie, and L. F. Francis, "High-resolution patterning of graphene by screen printing with a silicon stencil for highly flexible printed electronics," *Adv. Mater.*, vol. 27, no. 1, pp. 109–115, 2015.
[176] K. Arapov, E. Rubingh, R. Abbel, J. Laven, G. De With, and H. Friedrich, "Conductive Screen Printing Inks by Gelation of Graphene Dispersions," *Adv. Funct. Mater.*, vol. 26, no. 4, pp. 586–593, 2016.
[177] N. Maleki, A. Safavi, and F. Tajabadi, "Print - High-Performance Carbon Composite Electrode Based on an Ionic Liquid as a Binder - Analytical Chemistry (ACS Publications).pdf," vol. 78, no. 11, pp. 3820–3826, 2006.
[178] P. J. Smith and J. Stringer, "Applications in Inkjet Printing," in *Fundamentals of Inkjet Printing*, John Wiley & Sons, Ltd, 2015, pp. 397–418.
[179] M. Singh, H. M. Haverinen, P. Dhagat, and G. E. Jabbour, "Inkjet Printing—Process and Its Applications," *Adv. Mater.*, vol. 22, no. 6, pp. 673–685, 2010.
[180] P. Calvert, "Inkjet Printing for Materials and Devices," pp. 3299–3305, 2001.
[181] V. Dua, S. P. Surwade, S. Ammu, S. R. Agnihotra, S. Jain, K. E. Roberts, S. Park, R. S. Ruoff, and S. K. Manohar, "All-organic vapor sensor using inkjet-printed reduced graphene oxide," *Angew. Chemie - Int. Ed.*, vol. 49, no. 12, pp. 2154–2157, 2010.
[182] D. J. Finn, M. Lotya, G. Cunningham, R. J. Smith, D. McCloskey, J. F. Donegan, and J. N. Coleman, "Inkjet deposition of liquid-exfoliated graphene and MoS<inf>2</inf> nanosheets for printed device applications," *J. Mater. Chem. C*, vol. 2, no. 5, pp. 925–932, 2014.
[183] G. D. Martin, S. Hoath, and I. M. Hutchings, "Inkjet printing - The physics of manipulating liquid jets and drops," *J. Phys. Conf. Ser.*, vol. 105, p. 12001, 2008.
[184] B. Derby, "Inkjet Printing of Functional and Structural Materials: Fluid Property Requirements, Feature Stability, and Resolution," *Annu. Rev. Mater. Res.*, vol. 40, no. 1, pp. 395–414, 2010.
[185] B. Derby, "Inkjet printing ceramics: From drops to solid," *J. Eur. Ceram. Soc.*, vol. 31, no. 14, pp. 2543–2550, 2011.
[186] S. Magdassi, *The chemistry of inkjet inks*, Magdassi,. Singapore: World Scientific Publishing Company, 2010.
[187] J. E. Fromm, "Numerical Calculation of the Fluid Dynamics of Drop-on-Demand Jets," *IBM J. Res. Dev.*, vol. 28, no. 3, 1984.
[188] D. Jang, D. Kim, and J. Moon, "Influence of fluid physical properties on ink-jet printability," *Langmuir*, vol. 25, no. 5, pp. 2629–2635, 2009.
[189] "Materials Printer Jettable Fluid Formulation Guidelines," 2013. .
[190] Anonymous, "FUJIFILM Dimatix Materials Printer DMP-2800 Series User Manual," *2010*. User Manual ed. U.S.A.: FUJIFILM Dimatix, Inc., 2010.
[191] D. Soltman and V. Subramanian, "Inkjet-Printed Line Morphologies and Temperature Control of the Coffee Ring Effect," *Langmuir*, vol. 24, no. 5, pp. 2224–2231, 2008.
[192] R. D. Deegan, O. Bakajin, T. F. Dupont, G. Huber, S. R. Nagel, and T. A. Witten, "Capillary Flow as the Cause of Ring Stains From Dried Liquid Drops," *Nature*, vol. 389, pp. 827–829, 1997.
[193] R. D. Deegan, O. Bakajin, T. Dupont, G. Huber, S. Nagel, and T. A. Witten, "Pattern formation in drying drops," *Phys. Rev. E*, vol. 62, 2000.
[194] Y. Zhang, S. Yang, L. Chen, and J. R. G. Evans, "Shape Changes during the Drying of Droplets of Suspensions," *Langmuir*, vol. 24, no. 8, pp. 3752–3758, 2008.
[195] L. Zhang, H. Liu, Y. Zhao, X. Sun, Y. Wen, Y. Guo, X. Gao, C. Di, G. Yu, and Y. Liu, "Inkjet Printing High-Resolution, Large-Area Graphene Patterns by Coffee-Ring Lithography," *Adv. Mater.*, vol. 24, no. 3, pp. 436–440, 2012.
[196] L. Baptista-Pires, C. C. Mayorga-Martínez, M. Medina-Sánchez, H. Montón, and A. Merkoçi, "Water Activated Graphene Oxide Transfer Using Wax Printed Membranes for Fast Patterning of a Touch Sensitive Device," *ACS Nano*, vol. 10, no. 1, pp. 853–860, 2016.
[197] L. Baptista-pires, A. De Escosura-muñiz, M. Balsells, J. C. Zuaznabar-gardona, and A. Merkoçi, "Production and printing of graphene oxide foam ink for electrocatalytic applications," *Electrochem. commun.*, vol. 98, pp. 6–9, 2019.
[198] B. Roth, R. R. Søndergaard, and F. C. Krebs, "7 - Roll-to-roll printing and coating techniques for manufacturing large-area flexible organic electronics," in *Handbook of Flexible Organic Electronics*, S. Logothetidis, Ed. Oxford:

Woodhead Publishing, 2015, pp. 171–197.
[199] E. B Secor, S. Lim, H. Zhang, C. Frisbie, L. Francis, and M. C Hersam, "Gravure Printing of Graphene for Large-Area Flexible Electronics," *Adv. Mater.*, vol. 26, 2014.
[200] J. Baker, D. Deganello, D. T. Gethin, and T. M. Watson, "Flexographic printing of graphene nanoplatelet ink to replace platinum as counter electrode catalyst in flexible dye sensitised solar cell," *Mater. Res. Innov.*, vol. 18, no. 2, pp. 86–90, 2014.
[201] E. B. Secor, "Principles of aerosol jet printing," *Flex. Print. Electron.*, vol. 3, no. 3, p. 35002, Jul. 2018.
[202] B. Kahn, "The M3D aerosol jet system, an alternative to inkjet printing for printed electronics," *Org. Print. Electron.*, vol. 1, pp. 14–17, 2007.
[203] E. Jabari and E. Toyserkani, "Micro-scale aerosol-jet printing of graphene interconnects," *Carbon N. Y.*, vol. 91, pp. 321–329, 2015.
[204] E. Jabari and E. Toyserkani, "Aerosol-Jet printing of highly fl exible and conductive graphene / silver patterns," *Mater. Lett.*, vol. 174, pp. 40–43, 2016.
[205] E. Jabari and E. Toyserkani, "Laser heat treatment of aerosol-jet additive manufactured graphene patterns," *J. Phys. D. Appl. Phys.*, vol. 48, no. 37, p. 375503, Aug. 2015.
[206] P. Mariani, L. Vesce, and A. Di Carlo, "The role of printing techniques for large-area dye sensitized solar cells," *Semicond. Sci. Technol.*, vol. 30, no. 10, p. 104003, Sep. 2015.
[207] J.-W. Shin, J.-H. Han, H. Cho, J. Moon, B.-H. Kwon, S. Cho, T. Yoon, T.-S. Kim, M. Suemitsu, J.-I. Lee, and N. S. Cho, "Display process compatible accurate graphene patterning for {OLED} applications," *2D Mater.*, vol. 5, no. 1, p. 14003, Dec. 2017.
[208] T.-W. L. and S. Y. Jaeho Lee, Tae-Hee Han, Min-Ho Park, Dae Yool Jung, Jeongmin Seo, Hong-Kyu Seo, Hyunsu Cho, Eunhye Kim, Jin Chung, Sung-Yool Choi, Taek-Soo Kim, "Synergetic electrode architecture for efficient graphene-based flexible organic light-emitting diodes," *Nat. Commun.*, vol. 7, no. 11791, 2016.
[209] J. Oliveira, R. Brito-Pereira, B. F. Gonçalves, I. Etxebarria, and S. Lanceros-Mendez, "Recent developments on printed photodetectors for large area and flexible applications," *Org. Electron.*, vol. 66, pp. 216–226, 2019.
[210] K. Chen, Q. Wang, Z. Niu, and J. Chen, "Graphene-based materials for flexible energy storage devices," *J. Energy Chem.*, vol. 27, no. 1, pp. 12–24, 2018.
[211] X. Zhao, J. E, G. Wu, Y. Deng, D. Han, B. Zhang, and Z. Zhang, "A review of studies using graphenes in energy conversion, energy storage and heat transfer development," *Energy Convers. Manag.*, vol. 184, pp. 581–599, 2019.
[212] S. Cinti and F. Arduini, "Graphene-based screen-printed electrochemical (bio)sensors and their applications: Efforts and criticisms," *Biosens. Bioelectron.*, vol. 89, pp. 107–122, 2017.
[213] S. J. Rowley-Neale, E. P. Randviir, A. S. A. Dena, and C. E. Banks, "An overview of recent applications of reduced graphene oxide as a basis of electroanalytical sensing platforms," *Appl. Mater. Today*, vol. 10, pp. 218–226, 2018.

Chapter 2
Printed Supercapacitor

2.1. Introduction

Energy storage devices conform a peculiar part of our modern day lives. We are all highly dependent on them, especially since the advent of cell phones. Yet, we are going to witness even more intense growth of storage technologies in the near future, from large, high-power applications like renewable energy storage or electric vehicles to ever smaller, flexible, wearable devices [1]. In order to keep up the pace with the growing needs and harder demands from these new niches, new materials, devices and methods are being developed constantly. Main technologies for electrochemically storing energy focus mostly on rechargeable batteries and supercapacitor. Batteries fundamentally rely on bulk storage mechanisms, ions from the electrolyte are intercalated into the material (for example between the graphite sheets in lithium-ion anodes) during charging and are de-intercalated during discharging (fig. 2 (e and f)). This mechanism has limitations due to slow ion diffusion compared to transfer of electrons. This leads to relatively high energy densities but it also means low power densities and slow charge and discharge [2]. Nevertheless, research for overcoming theses kinetic and other limitations of the batteries for industrial purposes is continuously pursued, investigated and upgraded by using novel materials and techniques. For example, researchers at Samsung Advanced Institute of technology (SAIT) have recently published a paper in which they have used 'graphene balls' claiming to boost the capacity by 45% compared to the currently used Li-ion technology along with five times faster charging (in 12 minutes) and was found stable at 60 °C [3]. Other examples include Aluminium-air batteries [4], Zinc, Air [5], Sodium ion batteries [6] etc.

On the other hand we have supercapacitors that work on storing charges electrophysically. Electrochemical capacitors (ECs) also known as ultra- or supercapacitors (SCs) evolved from conventional dielectric capacitors when porous carbon electrodes in contact with an electrolyte were empirically tested in symmetrical capacitor cells. The formation of the Helmholtz double layer at the electrode-electrolyte interface upon polarization is at the heart of these devices providing larger capacitances thanks to their increased active area and reduced dimension of the charge separation. To these so-called Electric Double Layer Capacitors (EDLC) followed a new generation of electrode materials, with transition metal oxides or conducting polymers as representative examples of the so-called pseudocapaciotrs. Contrary to carbons (purely capacitive), these new materials featured electroactivities of intrinsical faradaic nature. Yet, could be used in both electrodes of symmetrical capacitors featuring behaviour characteristic of capacitors (i.e. nearly linear charge-discharge). These pesudocapacitive materials (like RuO2 or MnO2) work through redox reactions taking place at the surface leading to voltage-independent processes and led to higher capacitances and energy densities.

Finally, it should be noted that the final performance of supercapacitor devices will depend on many factors in addition to the nature of the electrode material, its storage mechanism and intrinsic properties. Thus, one of the most relevant will be the porosity (key to maximizing electrode-electrolyte interface, but also the electrical conductivity of the (composite) electrodes, the electrolytes (with emphasis on the size of the ions in relation with pore size distribution), separators, ink composition and rheology (in the case of printed devices) etc.

Bridging the gap between batteries and supercapacitors, a whole new breed of devices are being researched and developed: i) Hybrid devices with one capacitive (i.e. supercapacitor-like) and one faradaic (I.e. battery-like) electrode which are known as Metal-Hybrid Capacitors and ii) hybrid electrode materials combining both types of mechanisms in the same electrode (Figure 1).[1]

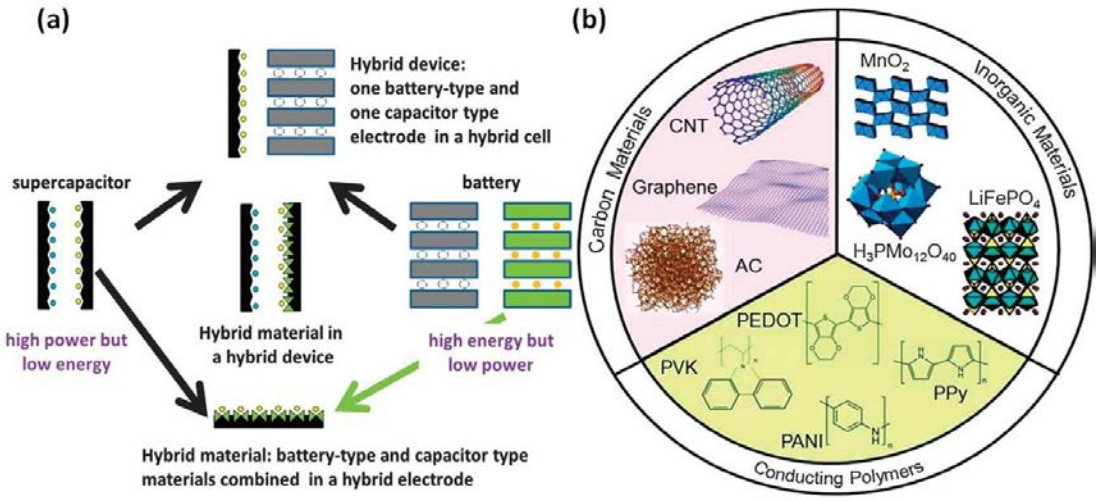

Figure 1 : (a) strategies employed for hybridisations in SCs and (b) main categories of materials used for SC applications [2]

2.2. Mechanism

2.2.1. Electric Double Layer Capacitors (EDLC)

In EDLC, two identical electrodes are polarized by applying a given voltage wich drives ions of opposite charges to be stored at the surface or the pores of the material through the formation of the Helmholtz double layer. Helmholtz provided a very simple phenomenon that the charges of an electrically conducting electrode are balanced and neutralised by adsorption of ions with the opposite charge, forming a double layer at the electrode-electrolyte interface (fig. 2(a)) [7][8]. Later, Guoy [9] and Chapman [10] proposed that the ionic charges are not adsorbed rigidly to the surface and rather move towards the surface by diffusion and electrostatic forces (fig. 2(b)). They used Boltzman distribution to develop theory between the ionic concentration and the local electric potential in the diffusion layer. Stern [11] went on to modify the above theories and proposed that there is a combination of two layers within the diffused layer, that can be divided into inner Helmholtz layer (IHP) or stern layer in which the ions strongly adsorbed to the surface and the outer Helmholtz layer (OHP) or the Gouy-Chapman layer

that consists of non-specifically bound counter ions (fig. 2(C)). The three models together are shown in fig. 2

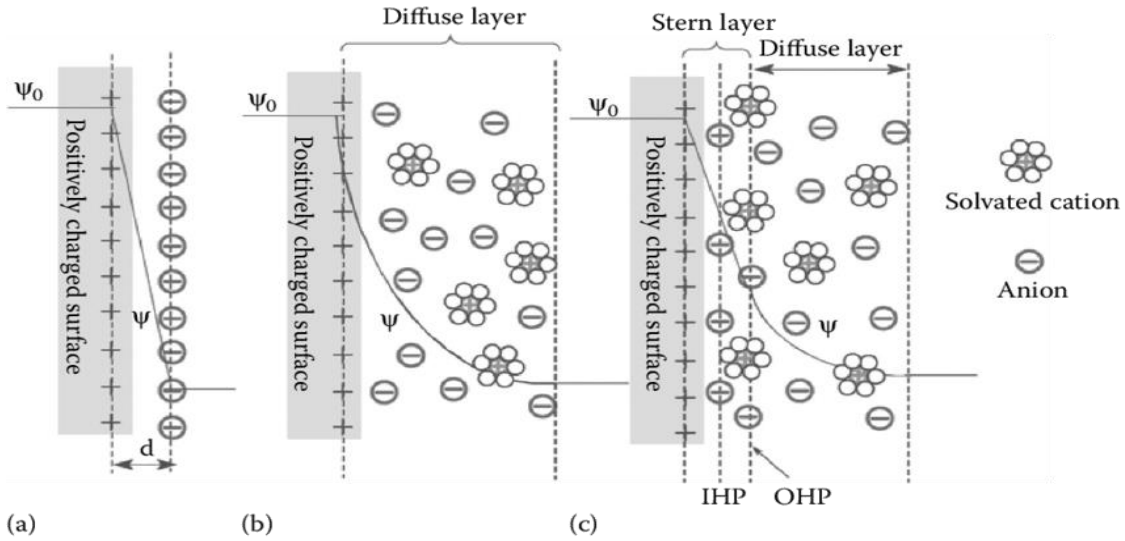

Figure 2: Formation of Electric double layer at Positive electrode (a) Helmholtz model, (b) Guoy-Chapman Model and (c) is the Stern model depicting IHP and OHP. d is the thickness of double layer formed according to Helmholtz, Ψ_0 and Ψ are the electrode and electrode/electrolyte interface potential respectively.

During charging of a Supercapacitor, the electrons move from the positive to negative electrode through an external circuit making the cations and anions in the electrolyte to concentrate at the negative and positive electrode respectively. At the time of discharging, the reverse process occurs reducing the polarisation. Charges are stored on the surface reversibly and no chemical reactions are taking place. Normally, an electrode with high surface area with pore size double the diameter of the corresponding electrolyte ion is considered to be the best to obtain maximum capacitance, since a too small pore diameter could effectively prevent the adsorption of ions, especially solvated ions. On the other hand, a review article by Wang et al described some examples leading to the conclusion that the capacitance determining factors are in fact the pore size and type of carbon nanomaterial used rather than the specific surface area [12]. Work done by Chmiola and colleagues [13] showed that the capacitance increased anomalously by decreasing the carbon nanomaterial pore size. They elucidated it using the finding of Dzubiella and Hansen [14] which suggested that the ions disintegrate or de-solvate to squeeze

through the pores under the influence of a potential when the size of the pore is smaller than the solvation shell, as under these conditions, ions have movement with almost negligible dielectric permittivity. Other works have also been reported to show the same results as above [15][16][17]. Monte Carlos simulations were performed [18] to understand the behaviour of ions theoretically and was proved that the superionic state ions are responsible for anomalous increase in capacitance at smaller pores. The superionic state develops due to exponential screening of electrostatic interaction between the ions inside the pore, which, itself is caused by the image forces, this facilitates the incorporation of more ions of the same charges [18].

Carbon materials like activated carbon (AC), carbon nanotubes (CNTs), Graphene etc. are of high interests for their application in double layer supercapacitors due to their chemical and thermal stabilities, high conductivity and large surface-to volume ratios (specific surface area). Graphene possesses very high theoretical surface area of 2630 m^2/g which hints of its great potential in this field, however, in actual materials, the great difficulty in utilising the whole graphene active area precludes the devices to perform as expected [19]. For this reason graphene in different forms, structures and hybrids are thoroughly researched, like 3-D graphene [20][21], vertically oriented graphenes [22], porous [23] and hybrid graphene[24][25]etc. These devices exhibit fast charging as well as long cycle life (~ 10^6 cycles) and this can be attributed to the electrophysical charge storage mechanism that doesn't require any chemical transformation of the material or transfer of charges [26].

2.2.2. Pseudocapacitance and Hybrids

In Pseudocapacitance, the charges are stored from the fast and reversible redox reactions occurring at the electrode-electrolyte interface in presence of an electrochemically active material. Apart from oxidation-reduction reactions, doping and de-doping of conducting polymers and electrosorption and intercalation can also cause pseudocapacitance (i.e. voltage-independent discharge). When compared to

EDLC, this shows better performance in terms of obtained capacitance and energy densities but poorer stability (exhibit shorter cycling lives) than EDLCs. Materials that exhibit pseudocapacitance can be conducting polymers (Polyaniline, Polypyrrole, polythiophene etc.), transition metal oxides (RuO_2, MnO_2, V_2O_5 etc.) or sulphides (MoS_2); but also carbon materials possessing oxygen or Nitrogen functionalities [27][12]. The mechanisms of EDLC and psedocpacitance are shown in fig. 3. Making a hybrid between EDLC and Pseudocapacitive material is the most common strategy employed these days to enhance the overall performance of a supercapacitor. Three strategies can be employed for this purpose, (i) anchoring or preparing a hybrid pseudocapacitive materials onto a high surface area carbon material as an electrode material, (ii) using an asymmetric system where one electrode exhibits purely EDLC and the other shows purely psedocapacitive behaviour, (iii) by using asymmetric system where one electrode is pseudocapacitive whereas the other is a rechargeable battery type material (fig.1) or iv) introducing an electroactive species in the electrolyte. These strategies can enhance the overall capacitance (due to the two charge storing mechanism involved), energy density (by increasing the effective voltage window of the device), long and fast cyclability.

2.3. Device Electrochemical Assessment

SC device performance is judged on the values obtained for capacitance, energy and power densities (gravimetric, areal or volumetric) that are measured with the help of electrochemical techniques like cyclic voltammetry, Galvanostatic charge/discharge (GCD) at particular current density and electrochemical impedance spectroscopy. Using these values, electrochemical performance of either the electrode material (in three-electrode cell measurements) or the device (in two-electrode cell measurements) is assessed [28][29].

With Cyclic voltammetry (CV), the nature of the energy-storage mechanism taking place at the electrode can be deduced. In this case a three-electrode cell is used and a stepwise changing potential is applied between the working and the reference electrode while the current is measured between the working and counter electrode and hence a current vs potential trace is plotted In the cyclic voltamogram for which a three electrode system is needed. CV is also used for primary investigation of the working potential ranges of the material. This can be assessed by eyeing the changes in shapes and sizes of the CV with different cycles. Typical rectangular shaped CVs are obtained in case of EDLCs due to the reversible and voltage-independent adsorption and de-sorption of ions, having symmetrical shapes around the zero current along with vertical current values at their two extreme potential values, whereas, pseudocapacitance displays distorted rectangular shape with appearance of voltage dependent current peaks arising from the redox reactions at the interface, shown in fig. 2(a and c) [2][28]. A CV can be used for calculating the specific capacitance (C, F/g) of the electrode material in a three- electrode system by the following equation [30]:

$$C = \frac{\oint I \, dV}{m \, \upsilon \, \Delta V}$$

Where I is the instantaneous current (mA), ΔV is the applied potential window, m is weight of the material (g) and υ is the scan rate (mV/s).

Using GCD in a two-electrode cell, capacitance behavior in response to the current density of the device can be calculated using the following equation [30]:

$$C = \frac{I \, \Delta t}{m \Delta V}$$

Where C is the capacitance (F/g), I is the current density (A/g), ΔV is the operating potential window (V), m is the mass of active material (g) and t is the charging/discharging time (s). The charge discharge

profiles of a double layer capacitive material shows linear slopes with symmetrical charging and discharging curves whereas, the profile for Pseudocapacitaive device exhibits unsymmetrical and distorted profiles as can be seen from fig 2. (b and d). Using GCD, equivalent series resistance (ESR; V=2IR, where V, I and R are Voltage, current and resistance respectively) and changes in the electrode (maybe due to over-oxidation of the electrode) can be seen from the CD profiles.

Ragone plot, which is a plot of power density vs. energy density provides a definitive view of the overall device performance instead of behaviour of a single electrode or the device. Energy and power densities are calculated using the following formulas:

$$E = \frac{1}{2} C \mathrm{V}^2$$

$$P = \frac{V^2}{2R}$$

Where E is energy density (Wh/Kg), P is power density (W/Kg), V is the voltage, C is the capacitance (F/g) and R is the equivalent series resistance (ESR) [26].

Finally, transportation of charges to the capacitive electrode is usually characterized by Electrochemical Impedance Spectroscopy (EIS) and Impedance of the SC at a particular potential can be obtained using this. Impedance of the device is obtained by applying amplitude voltage, the range of which is generally low (5-10 mV) to the corresponding wide frequency ranges used (0.01 Hz to 100 kHz). Nyquist plot shows the impedance (Z) value of the device in terms of real (Z') and imaginary (Z'') impedances that can be related by Z = Z' + jZ'' [29]. It consists of mainly two regions: high and low frequency regions. At higher frequency regions, the formed semi-circle is indicative of the interfacial resistance (and the ESR) while the vertical line extending in the imaginary impedance (y-axis) (Z) making an angle of about 90° with the X plane indicates the capacitive behavior of the system. Capacitance (C) from this plot using the frequency (f) can be calculated using the following formula [28]:

$$C = \frac{1}{2\pi f\ |Z|}$$

An inverse relation of capacitance and frequency can be obtained by using Bode plot that is the Log (Z) vs Log (f).

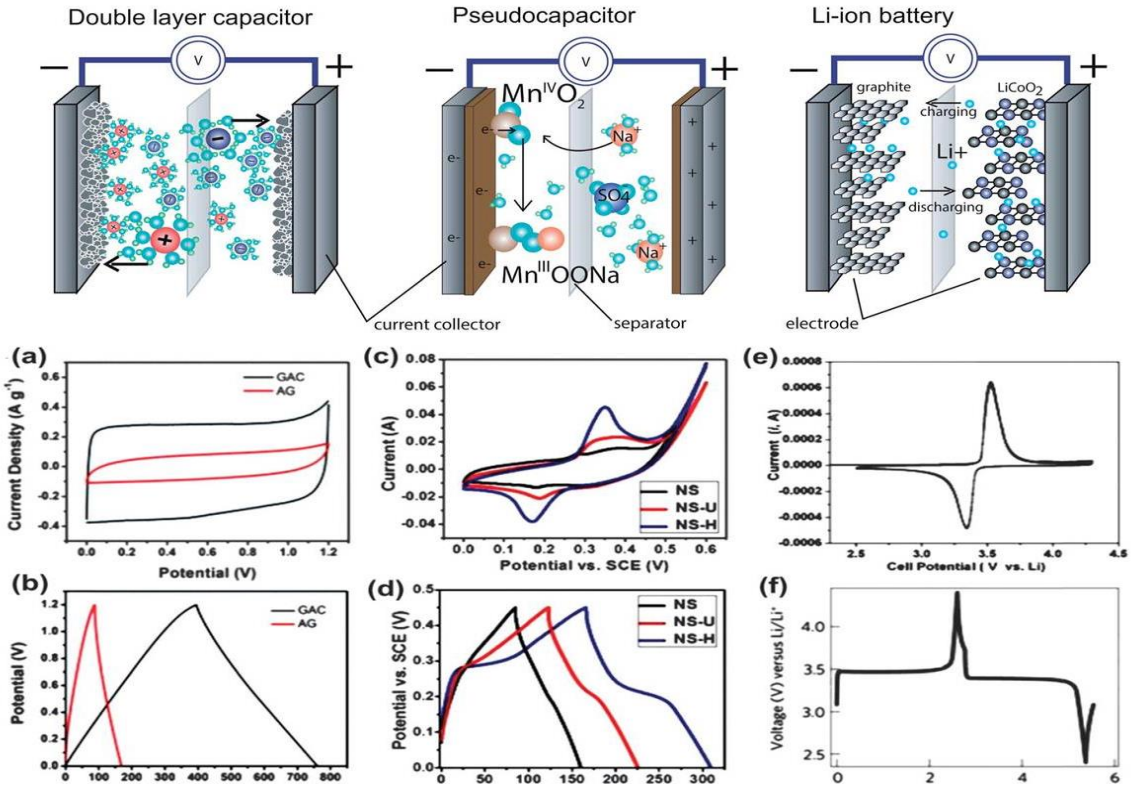

Figure 3: Top is the schematic of EDLC, Pseudocapacitive and Li-ion batteries [31]. Below are the corresponding typical Cyclic voltammetry and Charge/discharge profiles exhibited by (a and b) EDLC, (c and d) pseudocpacitance and (e and f) for Li ion battery[2].

2.4. Graphene Electrode Materials

As previewed in the previous chapter, graphene is very well suited for the manufacturing of printed devices due to its ease of production and processability. It has high specific surface area and possesses

inherent capacitive properties due to which it is widely applied in this field. Another advantage of having graphene is its stability in comparative wide potential windows (although the potential window is determined also by the electrolyte). For Supercapacitor applications, it has been used in various forms, like in 2 D sheets, 0 D graphene dots or particles, 1D fibers or yarns, 3 D foams or structures, vertically aligned graphene or its composites [20-25][32][33]. The theoretical capacitance calculated for single layer graphene and its specific capacitance was ~21 uF/cm^2 and ~550 F/g respectively, however, in practice, these values cannot be attained due to the limitation of accessible graphene area to accommodate electrolyte ions. The main reason for this is its agglomeration, both during preparation and application due to the Van der Waals interaction between sheets. This also lowers the initial columbic efficiency of the device. The best results when using graphene are achieved usually by playing with graphene surface to make most of the area accessible to the electrolyte by aligning or preparing different graphene structures as described above or by doping graphene chemically with electron accepting or donating groups [34][35][36][37].

Other works focus on making graphene-based hybrids to enhance the overall device performances as described in hybrid electrodes. These hybrids can be formed with either organic or inorganic nanomaterials. For organic materials, conducting polymers are the most common choice as they present high conductivity, and in addition provide pseudocapacitance by reversibly doping and de-doping of charges throughout their entire volume [25][24]. The π conjugated conducting polymers like polyaniline, polypyrrole, polythiophene are commonly used SC electrode materials that not only exhibit enhanced capacitance but their easy processability or ability to form uniform thin films electrochemically is an added benefit. Examples of other carbon materials used for making hybrid with graphene are CNTs, Carbon black etc [38][39]. Among the inorganic nanomaterials, most commonly used are metal oxide nanomaterials to make a composite with graphene. These together exhibit a synergistic effect of both EDLC and pseudocapacitance. Besides inhibiting the restacking of graphene sheets, they help to expose

more surface area of graphene, while graphene too help prevents its agglomeration and volume change during preparation along with uniform and controlled morphology [40]. Polyoxometalates (POMs), another class of electroactive soluble (early transition) metal oxide has garnered much interest in the supercapacitor applications since last decade. The research initially commenced with the great work done by Gomez-Romero et al by anchoring POMs over conducting polymers substrates as the electrodes for electrochemical energy storage [41]. POMs are needed to be anchored or wired to some conducting substrates as these are typically salts with negligible conductivities, extremely small size and solubility which restricts its use as the sole electrode material [42][43]. This approach of utilising the electroactivity of these molecular materials was then extended by using other carbon matrices like activated carbon (AC) [44], CNTs [45] and graphene [46]. In one of the studies made by Suarez-Guevara et al using activated carbon (AC) decorated with phosphotungstic acid ($H_3PW_{12}O_{40}$), the performance of the hybrid material displayed expected response in enhancing the capacitance but it also enhanced the working potential window of the device (up to 1.6V in 1M H_2SO_4 thanks to large over-potentials for hydrogen evolution) and led to remarkably improved cyclability (more than 30000 cycles as compared to less than 10000 for pure AC under the same conditions) [47]. Work carried out using graphene substrates showed similar response [48][49][50].

2.5. Electrolytes

Electrolytic media used for supercapacitors can be broadly classified into aqueous, organic,and ionic liquids. The nature of the electrolytic media (including ion sizes, concentration, solvent, working potential range, interaction with the electrode material etc.) plays an important role in defining performance of the device, namely capacitance, energy density and cycle life [51].

2.5.1. Aqueous electrolytes

These can be acidic, neutral or basic. These electrolytes provide an advantage of high conductivity, eg. 1M H_2SO_4 has a conductivity of 0.8 s/cm at 25 °C [52], leading to higher capacitance values but are limited with the voltage window due to their narrow decomposition potentials leading to less energy and power densities. Potential window of acidic and basic electrolytes is normally not extended more than 1.3 V of purely EDLCs as the water decomposition starts by oxygen evolution on the positive electrode at about 1.23V and hydrogen evolution at negative electrode at around 0V vs the SHE [53], whereas these values can reach upt o 2.2V by using neutral electrolytes [54].

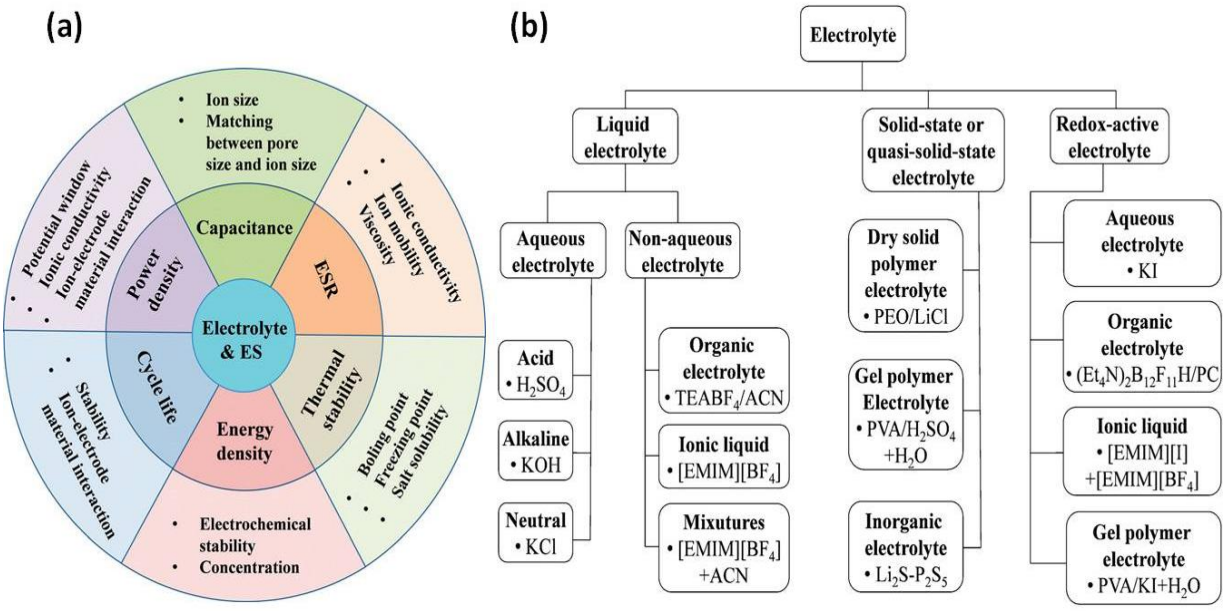

Figure 4: Electrolyte effect (a) and categories (b) for SC application [51]

Due to lower concentrations of H+ and OH- ions, these need higher overpotentials for the gas evolutions, but have lower conductivities. In addition, neutral electrolytes are less corrosive compared to the acidic and basic ones that overcome one of the major issue of metal conductors getting corroded

during long-term cycling [55]. Aqueous media are impractical for commercial purposes mainly because of the narrow potential window, leading to low energy densities but despite this and other limitations, aqueous electrolytes have been extensively studied and reported for research and development purposes [51].

2.5.2. Organic Electrolytes

Organic electrolytes are conductive salts like tetraethylammonium tetrafluoroborate ($TEABF_4$) that are dissolved in organic solvents like Acetonitrile or Polycarbonate solvents. These have a working potential ranging from 2.5 to 2.8V [51], that provides the benefit of higher energy and power densities of the device than that of aqueous based electrolytes because of which these are highly favoured for commercial purposes. The downside of using organic electrolytes is their higher costs and safety concerns for its processing, flammability, toxic nature and volatility [56]. As the system works under high potentials, it can lead to rise in the device temperature causing damages and also sometimes the electrode material can undergo oxidation causing unwanted gas evolution. From the point of view of their performance, these electrolytes show smaller capacitances and this can be either due to the electrolyte conductivity itself, which is at least one order of magnitude smaller than for aqueous electrolytes (1 M $TEABF_4$ /ACN exhibits a conductivity of 0.06 S/cm)[52] or because the solvated ion size is generally bigger with low dielectric constants that restricts its accessibility to the pores of the carbon nanomaterial [57][58]. Also, it was shown that the Pseudocapacitive activity of carbon materials was almost negligible in $TEABF_4$ /ACN, which can be due to the absence of protons in these aprotic media. Different solvents, or their mixtures with conducting salts have been employed, eg. $SBPBF_4$/ACN, $LiPF_6$/(EC–DEC 1:1), TEAODFB/PC, M $LiPF_6$/(EC–DEC 1:1), $LiClO_4$/PC, $Bu4NBF_4$/ACN, $LiPF_6$/EC–DMC (1:1), LiTFSI/CAN etc. [51].

2.5.3. Ionic liquid electrolytes

These are environmentally friendly liquids that are composed purely of salts and are liquid at room temperature, or at least with a melting point under 100 °C. These are also called room temperature molten salts and are liquid at room temperature owing to the asymmetry and special combination of the composing cation and anion. ILs have a very high thermal, chemical and electrochemical stability and very low vapor pressures, due to which they make excellent candidates as supercapacitor electrolytes [52]. The working potential window of ILs can be as high as ~6V, but this was studied using inert Pt electrodes. For carbon based electrodes, the ranges observed were much narrower (3-4V), possibly due to the carbon surface irregularities [59]. In one of the study, atomically thin graphene layer was tested using an IL that showed the working potential in the range of 4-10 V. There was a deposition of passivation layer which further helped in increasing the conductivity of the films [60]. Apart from these they are volatile, non-flammable and environmentally friendly when compared to the safety concerns of organic liquids. This solvent free approach seems to be ideal, however their high costs, very high viscosity and low ionic conductivities (lower than aqueous or organic electrolytes) limits their use [61][62] . A commonly used IL electrolyte [EMIM][BF4]showed ionic conductivity of 0.014 s/cm at 25 °C which is significantly lower than that of aqueous (0.8 S/cm) and organic (0.06 S/cm) electrolytes. This causes the increase in ESR affecting the rate and power performance of the system as well as lowering the capacitance values. ILs can be protic, aprotic and zwitterionic and the most commonly used cations are are 1-ethyl3-methylimidazolium (EMI), 1-butyl-3-methylimidazolium (BMI), NPropyl-N-methylpyrrolidinium (PYR13), 1-Butyl-1-methylpyrrolidinium (PYR14), Tetraethylammonium (Et4N), etc. Studies have shown that imidazolium based ILs possess higher ionic conductivities whereas pyrrolidinium provide larger working potential ranges [52][63]. Common anions used are chloride (Cl), bromide (Br), tetrafluoroborate (BF4), hexafluorophosphate (PF6), bis(fluorosulfonyl)imide (FSI), bis(trifluoromethylsulfonyl)imide (TFSI), etc.

2.5.4. Redox active electrolytes

It is a comparatively new strategy of mixing a redox active component into an ionic electrolyte in order to have a hybrid electrolyte system. In this case the electrolyte (apart from the electrode) is capable of providing pseudocapacitance to the device. These have shown to increase not only the capacitance but also potential windows in some cases [47]. They have also shown to accelerate the faradaic reaction of a pseudocapacitor by acting as an additional electron source [64][65]. Hydroquinone and Potassium Iodide (KI) have been used in this thesis and will be described in the following sections. As shown by Lota and Frackowiak [66], the first example was the use of Potassium Iodide as the component of an electrolyte system to enhance the supercapacitor performance. Capacitance of the positive carbon electrode was able to achieve a very high value of 1840 F/g using 1 M KI in the electrolyte solution with a narrow potential range whereas, capacitance of the device using 2 electrodes calculated was 125 F/g. They showed that KI didn't just showed pseudocapacitance but also enhanced the ionic conductivity of the electrolyte. The following reactions might occur on the electrode surface causing the pseudocapacitance from KI

$$3I^{-1} \leftrightarrow I_3^{-1} + 2e^-$$

$$2I^{-1} \leftrightarrow I_2 + 2e^-$$

$$2I_3^{-1} \leftrightarrow 3I_2 + 2e^-$$

$$I_2 + 6H_2O \leftrightarrow 2IO_3^{-1} + 12H^+ + 10e^-$$

Frackowiak and co-workers also studied the effect of Hydroquinine (HQ) redox activity. In their report they showed the dependency of HQ over different pH, with maximum capacitance of 283 F/g using 1M H_2SO_4 compared to 275 F/g obtained in 6M KOH. In acidic media, the reaction of quinone (Q)/hydroquinone (QH2)occurring are as follows [67].

$$Q + e^- \leftrightarrow Q^{\cdot -}$$

$$Q^{\cdot -} + H^{+} \leftrightarrow QH^{\cdot}$$

$$QH^{\cdot} + e^{-} \leftrightarrow QH^{-}$$

$$QH^{-} + H^{+} \leftrightarrow QH_2$$

Finally, $$Q + 2H^{+} + 2e^{-} \leftrightarrow QH_2$$

Other commonly used redox species are Heteropolyacids like phosphotungstic acid ($H_3PW_{12}O_{40}$), $VOSO_4$, $CuCl_2$, $K_3Fe(CN)_6$ etc. Addition of redox active materials can degrade the device performance in terms of cyclability and stability (self-discharge), this is due to the fact that these redox active materials might shuttle between the two electrodes [51]. It can be resolved by either using ion exchange separator membranes [68], by using species that can be reversibly become insoluble[51] or by strong adsorption of the ionic species to the electrode surface [69]. In addition to these, the following points must be considered before using the redox active species for SC applications that has direct effect on their performance: (i) carbon electrode material must be porous enough to retain the oxidized or reduced product formed by the charging, (ii) redox reactions of the species must be carefully studied before applying the potentials using Pourbaix diagram as the applied potentials will determine if the pseudocapacitance is caused by the electrosorbed metallic ions or whether the ions have reacted (chemisorbed) with the functional groups (eg. carbonyl) of carbon electrode and facilitated the electron transfer process, entrapment of these species into the carbon pores can be an alternative to this, (iii) concentration of the redox species in the supporting electrolyte, it directly determines fast reversibility as well as stability of the device over repeated cycles, for instance, concentrations of $K_3Fe(CN)6$ and $K_4Fe(CN)_6$ in Aq.KOH has shown a direct effect on the performance of the device [70] and (iv) pH, temperature and electrolyte composition [71].

2.5.5. Solid electrolyte

Solid state or quasi-solid state electrolytes are non-flowing, non-liquid electrolytes that not just serve the purpose of ion conductivities but also act as separator. These give the advantage of leakage-free, simplified processing of the supercapacitor device. Broadly, the solid state electrolytes are either organic (Polymer) or inorganic (eg. Ceramic). Polymer based electrolytes are mostly employed for SC applications and are further classified into solid, gel and polyelectrolytes. Solid polymer electrolytes are formed by a polymer and a salt in the absence of a solvent, and the salt ions are transported through the polymer providing the ionic conductivity. In Gel Polymer electrolytes (GPE; most common type) the, polymer is mixed with the electrolyte (aq.) or a conducting salt and the ion conductivity takes place through the solvent instead of the polymer whereas in Polyelectrolytes, being highly charged, the polymer itself provides the ionic conductivities. GPEs are most commonly studied as their ionic conductivities are relatively high due to the presence of a solvent but depending upon the composition they may suffer from poor mechanical and thermal stabilities for which solid electrolytes are better suited[51][72]. The solid electrolytes face the disadvantage of limited contact with the electrode surface limiting the transfer most possibly causing high ESR values. Therefore, it is always considered that the solid electrolyte system provide high ionic conductivities, mechanical, thermal, electrochemical and chemical stabilities. Examples of GPE includes a polymer matrix that can be Polyvinyl alcohol (PVA) [49], Polymethylmethacrylate (PMMA) [73], poly(ethylene) oxide (PEO) [74] etc. and a solvent that can be any aqueous (H_2SO_4, KOH etc), organic (PC, EC, DMF etc.) or IL ([BMIM][Cl], [BMIM][TFSI], [EMIM][SCN] etc.) liquid [75] [76][77]. Examples of inorganic solid electrolytes used are ceramics [78], Al_2O_3 [79] based etc., however, due to non-flexibility, these are not favored for printed and flexible SC applications.

2.6. Device Fabrication

A supercapacitor device is assembled by placing two electrodes in parallel separated by a separator membrane, immersed in or impregnated by an electrolytic medium. Separators membranes are the ones that electrically insulates the two electrodes meanwhile allowing ions to pass between them (they are ion-permeable). Features of a perfect separator are high electrical resistance, high ionic conductivity and low thickness, while thermal and mechanical stabilities are desired. Separator can be polymeric, paper, fiber or glass based and its selection is usually based on the electrolyte used. Shulga et al even used GO films as the separator for their Polyaniline based supercapacitor [80].

Current collectors are another component in a SC. They act as electron conducting materials that transport the electrons from an external source to the active electrode material and vice-versa while dispersing the heat generated within the cell. The active material is usually coated over stainless steel, copper, Aluminium, Iron, Gold etc. electrodes that provide a highly conducting surface in order to reduce the ESR values. One of the most important features of a collector electrode must be its chemical resistivity as its oxidation in presence of electrolytes is extremely common, especially when porous carbon is used as the active coated material. This can be avoided also if the active material is strongly coated to the collector which is usually done with the help of a binder during ink formulation. Polymeric binders such as Nafion, PVDF, PTFE etc. are commonly used for this purpose, they effectively help the adhesion of the materials together with the collector and inhibits their disintegration during long cycling, retaining the capacitance and performance for longer time [53]. Addition of binders in principle could reduce the conductivity of active material since they are intrinsically insulating, which is why they are used in very low percentage in the ink (<10%), however, it actually helps in binding the AM to the collector electrode indirectly helping with continuous flow of electrons the conductivity. In some cases,

Carbon materials are directly grown over the collectors (Al or Cu) that are attached strongly with the collectors improving the mechanical stability of the active material as well as its conductivity [81][82].

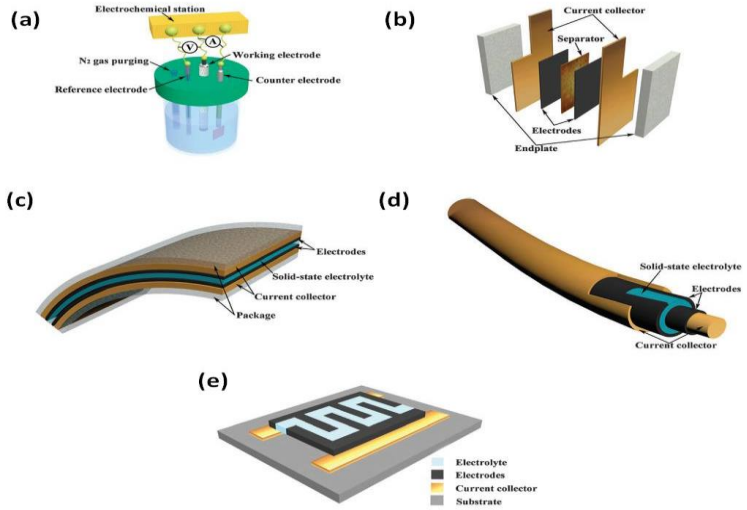

Figure 5 : Different setups of testing SCs (a and b) three and two electrode setup , (c) flexible sandwich type, (d) fibre type and (e) printed interdigitated micro-supercapacitor setup [51].

2.7. References

[1] D. P. Dubal, N. R. Chodankar, D.-H. Kim, and P. Gomez-Romero, "Towards flexible solid-state supercapacitors for smart and wearable electronics," *Chem. Soc. Rev.*, vol. 47, no. 6, pp. 2065–2129, 2018.

[2] D. P. Dubal, O. Ayyad, V. Ruiz, and P. Gómez-Romero, "Hybrid energy storage: The merging of battery and supercapacitor chemistries," *Chem. Soc. Rev.*, vol. 44, no. 7, pp. 1777–1790, 2015.

[3] I. H. Son *et al.*, "Graphene balls for lithium rechargeable batteries with fast charging and high volumetric energy densities," *Nat. Commun.*, vol. 8, no. 1561, pp. 1–10, 2017.

[4] J. Ryu, H. Jang, J. Park, Y. Yoo, and M. Park, "Seed-mediated atomic-scale reconstruction of silver manganate nanoplates for oxygen reduction towards high-energy aluminum-air flow batteries," *Nat. Commun.*, vol. 9, no. 3715, pp. 1–10, 2018.

[5] L. Wei *et al.*, "Amorphous Bimetallic Oxide–Graphene Hybrids as Bifunctional Oxygen Electrocatalysts for Rechargeable Zn–Air Batteries," *Adv. Mater.*, vol. 29, no. 38, p. 1701410, 2017.

[6] L. E. Marbella *et al.*, "Sodiation and Desodiation via Helical Phosphorus Intermediates in High-Capacity Anodes for Sodium-Ion Batteries," *J. Am. Chem. Soc.*, vol. 140, no. 25, pp. 7994–8004, 2018.

[7] H. Helmholtz, "Ueber einige Gesetze der Verlheiiung elektrischcr Strdme in kdrperlichen Leitern mit Anwendung auf die thierisch - elektrischen Versuche," *Ann. Der Phys. Und Chemie*, vol. 165, no. 6, pp. 211–233, 1853.

[8] H. Helmholtz, "Studien über electrische Grenzschichten.," *Ann. Der Phys. Und Chemie*, vol. 273, no. 7, pp. 337–382, 1879.

[9] M. Gouy, "Sur la constitution de la charge électrique à la surface d ' un électrolyte," *J. Phys. Theor. Appl.*, vol. 9, no. 4, pp. 457–67, 1910.

[10] D. L. Chapman, "LI. A contribution to the theory of electrocapillarity," *London, Edinburgh, Dublin Philos. Mag. J. Sci.*, vol. 25, no. 148, pp. 475–481, 1913.
[11] O. Stern, "ZUR THEORIE DER ELEKTROLYTISCHEN DOPPELSCHICHT," *Zeitschrift für Elektrochemie und Angew. Phys. Chemie*, vol. 30, no. 21-22, pp. 508–516, 1924.
[12] S. L. Fu, Q. Zhou, and Y. Wu, "Latest advances in supercapacitors : from new electrode materials to novel device designs," *Chem. Soc. Rev.*, vol. 46, pp. 6816–6854, 2017.
[13] J. Chmiola, G. Yushin, Y. Gogotsi, C. Portet, and P. L. Taberna, "Anomalous Increase in Carbon Capacitance at Pore Sizes Less Than 1 Nanometer," *Science (80-.).*, vol. 313, no. 5794, pp. 1760–1764, 2006.
[14] J. Dzubiella and J. Hansen, "Electric-field-controlled water and ion permeation of a hydrophobic nanopore Electric-field-controlled water and ion permeation of a hydrophobic nanopore," *J. Chem. Phys.*, vol. 122, no. 234706, 2005.
[15] H. Wang and L. Pilon, "Accurate Simulations of Electric Double Layer Capacitance of Ultramicroelectrodes," *J. Phys. Chem. C*, vol. 115, pp. 16711–16719, 2011.
[16] M. Endo, T. Takeda, Y. J. Kim, K. Koshiba, and K. Ishii, "High Power Electric Double Layer Capacitor (EDLC ' s); from Operating Principle to Pore Size Control in Advanced Activated Carbons," *Carbon Sci.*, vol. 1, no. 3, pp. 117–128, 2001.
[17] C. Largeot, C. Portet, J. Chmiola, P. Taberna, Y. Gogotsi, and P. Simon, "Relation between the Ion Size and Pore Size for an Electric Double-Layer Capacitor," *J. Am. Chem. Soc.*, vol. 130, no. 9, pp. 2730–2731, 2008.
[18] M. V. F. and A. A. K. S. Kondrat, N. Georgi, "Superionic state in nano-porous double-layer capacitors : insights from Monte Carlo simulations," *Phys. Chem. Chem. Phys.*, vol. 13, pp. 11359–11366, 2011.
[19] Q. Ke and J. Wang, "Graphene-based materials for supercapacitor electrodes e A review," *J. Mater.*, vol. 2, no. 1, p. 37–54 2, 2016.
[20] P. Miao *et al.*, "Hydrothermal growth of 3D graphene on nickel foam as a substrate of nickel-cobalt-sulfur for high-performance supercapacitors," *J. Alloys Compd.*, vol. 732, pp. 613–623, 2018.
[21] W. R. H. and V. S. Lu Zhang, Derek DeArmond, Noe T. Alvarez, Daoli Zhao, Tingting Wang, Guangfeng Hou, Rachit Malik, "Beyond graphene foam, a new form of three-dimensional graphene for supercapacitor electrodes," *J. Mater. Chem. A*, vol. 4, pp. 1876–1886, 2016.
[22] S. Zheng *et al.*, "High Packing Density Unidirectional Arrays of Vertically Aligned Graphene with Enhanced Areal Capacitance for High-Power Micro-Supercapacitors," *ACS Nano*, vol. 11, no. 4, pp. 4009–4016, 2017.
[23] X. Zhang, H. Zhang, C. Li, K. Wang, X. Sun, and Y. Ma, "Recent advances in porous graphene materials for supercapacitor applications," *RSC Adv.*, vol. 4, no. 86, pp. 45862–45884, 2014.
[24] R. K. G. Sanket Bhoyate, Kwadwo Mansah-Darkwa, Pawan K. Kahol, "Recent Development on Nanocomposites of Graphene for Supercapacitor Applications," *Curr. Graphene Sci.*, vol. 1, pp. 26–43, 2017.
[25] Y. Gao, "Graphene and Polymer Composites for Supercapacitor Applications : a Review," *Nanaoscale Res. Lett.*, vol. 12, no. 387, pp. 1–17, 2017.
[26] W. B. K. Deepak P. Dubal, Jong Guk Kim, Youngmin Kim, Rudolf Holze, Chandrakant D. Lokhande, "Supercapacitors Based on Flexible Substrates : An Overview," *Energy Technol.*, vol. 2, pp. 325–341, 2014.
[27] A. González, E. Goikolea, J. A. Barrena, and R. Mysyk, "Review on supercapacitors: Technologies and materials," *Renew. Sustain. Energy Rev.*, vol. 58, pp. 1189–1206, 2016.
[28] A. Muza, M. B. Ahamed, K. Deshmukh, and J. Thirumalai, "A review on recent advances in hybrid supercapacitors : Design , fabrication and applications," *Renew. Sustain. Energy Rev.*, vol. 101, pp. 123–145, 2019.
[29] Z. Wu, L. Li, J. Yan, and X. Zhang, "Materials Design and System Construction for Conventional and New-Concept Supercapacitors," *Adv. Sci.*, vol. 4, no. 1600382, 2017.
[30] B. E. Conway, *Electrochemical Supercapacitors. Scientific Fundamentals and Technological Applications*. New York: Kluwer Academic/ Plenum Publishers, 1999.
[31] K. Jost, G. Dion, and Y. Gogotsi, "Textile energy storage in perspective," *J. Mater. Chem. A*, vol. 2, 2014.
[32] A. Amiri, M. Shanbedi, G. Ahmadi, H. Eshghi, S. N. Kazi, and B. T. Chew, "Mass production of highly-porous graphene for high-performance supercapacitors," *Sci. Rep.*, vol. 6, no. 32686, pp. 1–11, 2016.
[33] S. Zheng *et al.*, "Graphene-based materials for high-voltage and high-energy asymmetric supercapacitors," *Energy Storage Mater.*, vol. 6, pp. 70–97, 2017.
[34] Y. Chen, Z. Liu, L. Sun, Z. Lu, and K. Zhuo, "Nitrogen and sulfur co-doped porous graphene aerogel as an efficient electrode material for high performance supercapacitor in ionic liquid electrolyte," *J. Power Sources*, vol. 390, pp. 215–223, 2018.
[35] J. Wang, B. Ding, Y. Xu, L. Shen, H. Dou, and X. Zhang, "Crumpled Nitrogen-Doped Graphene for Supercapacitors with High Gravimetric and Volumetric Performances," *ACS Appl. Mater. Interfaces*, vol. 7, no. 40, pp. 22284–22291, 2015.
[36] E. A. Arkhipova *et al.*, "Effect of nitrogen doping of graphene nanoflakes on their efficiency in supercapacitor applications," *Funct. Mater. Lett.*, vol. 11, no. 06, p. 1840005, 2018.
[37] C. Ogata *et al.*, "All-Graphene Oxide Flexible Solid-State Supercapacitors with Enhanced Electrochemical Performance," *ACS Appl. Mater. Interfaces*, vol. 9, no. 31, pp. 26151–26160, 2017.
[38] N. Díez, C. Botas, R. Mysyk, E. Goikolea, T. Rojo, and D. Carriazo, "Highly packed graphene-CNT films as electrodes for

aqueous supercapacitors with high volumetric performance," *J. Mater. Chem. A*, vol. 6, 2018.
[39] Y. Wang *et al.*, "Graphene/carbon black hybrid film for flexible and high rate performance supercapacitor," *J. Power Sources*, vol. 271, pp. 269–277, 2014.
[40] Z. S. Wu, G. Zhou, L. C. Yin, W. Ren, F. Li, and H. M. Cheng, "Graphene/metal oxide composite electrode materials for energy storage," *Nano Energy*, vol. 1, no. 1, pp. 107–131, 2012.
[41] M. L.-C. Pedro Gomez-Romero, Malgorzata Chojak, Karina Cuentas-Gallegos, Juan A. Asensio, Pawel J. Kulesza, Nieves Casan-Pastor, "Hybrid organic – inorganic nanocomposite materials for application in solid state electrochemical supercapacitors," *Electrochem. commun.*, vol. 5, pp. 149–153, 2003.
[42] Nieves Casan-Pastor and Pedro Gomez-Romero, "POLYOXOMETALATES: FROM INORGANIC CHEMISTRY TO MATERIALS SCIENCE," *Front. Biosci.*, vol. 9, pp. 1759–1770, 2004.
[43] Y. Ji, L. Huang, J. Hu, C. Streb, and Y. Song, "Environmental Science," *Polyoxometalate-functionalized nanocarbon Mater. energy conversion, energy storage Sens. Syst.*, vol. 8, pp. 776–789, 2015.
[44] V. Ruiz, J. Suárez-guevara, and P. Gomez-romero, "Hybrid electrodes based on polyoxometalate – carbon materials for electrochemical supercapacitors Electrochemistry Communications Hybrid electrodes based on polyoxometalate – carbon materials for electrochemical supercapacitors," *Electrochem. commun.*, vol. 24, no. October, pp. 3–7, 2012.
[45] Ana Karina Cuentas-Gallegos, Rosa Martinez-Rosales, Mihaela Baibarac, Pedro Gomez-Romero, Marina E. Rincon, "Electrochemical supercapacitors based on novel hybrid materials made of carbon nanotubes and polyoxometalates," *Electrochem. commun.*, vol. 9, pp. 2088–2092, 2007.
[46] D. P. Dubal, N. R. Chodankar, A. Vinu, D.-H. Kim, and P. Gomez-Romero, "Asymmetric Supercapacitors Based on Reduced Graphene Oxide with Different Polyoxometalates as Positive and Negative Electrodes," *ChemSusChem*, vol. 10, no. 13, pp. 2742–2750, 2017.
[47] V. R. and P. G.-R. J. Suarez-Guevara, "Hybrid energy storage : high voltage aqueous supercapacitors based on activated carbon – phosphotungstate hybrid materials," *J. Mater. Chem. A*, vol. 2, pp. 1014–1021, 2014.
[48] J. Suárez-Guevara, V. Ruiz, and P. Gómez-Romero, "Stable Graphene-Polyoxometalate Nanomaterials for Application in Hybrid Supercapacitors.," *Phys. Chem. Chem. Phys.*, 2014.
[49] D. P. Dubal, J. Suarez-guevara, D. Tonti, E. Enciso, and P. Gomez-romero, "A high voltage solid state symmetric supercapacitor based on graphene – polyoxometalate hybrid electrodes with a hydroquinone doped hybrid gel-electrolyte," *J. Mater. Chem. A Mater. energy Sustain.*, vol. 3, pp. 23483–23492, 2015.
[50] D. P. Dubal *et al.*, "Ultrahigh energy density supercapacitors through a double hybrid strategy," *Mater. Today Energy*, vol. 5, no. September, pp. 58–65, 2017.
[51] Cheng Zhong, Yida Deng, Wenbin Hu, Jinli Qiao,c Lei Zhang and J. Zhangd, "A review of electrolyte materials and compositions for electrochemical supercapacitors," *Chem. Soc. Rev.*, vol. 44, pp. 7484–7539, 2015.
[52] M. Galiński, A. Lewandowski, and I. Stępniak, "Ionic liquids as electrolytes," *Electrochim. Acta*, vol. 51, no. 26, pp. 5567–5580, 2006.
[53] B. K. Kim, S. Sy, A. Yu, and J. Zhang, "Electrochemical Supercapacitors for Energy Storage and Conversion," in *Handbook of Clean Energy Systems*, American Cancer Society, 2015, pp. 1–25.
[54] Krzysztof Fic, Grzegorz Lota, Mikolaj Meller and Elzbieta Frackowiak, "Novel insight into neutral medium as electrolyte for high-voltage supercapacitors," *Energy Environ. Sci.*, vol. 5, no. 2, pp. 5842–5850, 2012.
[55] E. Frackowiak, Q. Abbas, and F. Béguin, "Carbon/carbon supercapacitors," *J. Energy Chem.*, vol. 22, no. 2, pp. 226–240, 2013.
[56] G. Wang, L. Zhang, and J. Zhang, "A review of electrode materials for electrochemical supercapacitors," *Chem. Soc. Rev.*, vol. 41, no. 2, pp. 797–828, 2012.
[57] S. Vaquero, R. Díaz, M. Anderson, J. Palma, and R. Marcilla, "Insights into the influence of pore size distribution and surface functionalities in the behaviour of carbon supercapacitors," *Electrochim. Acta*, vol. 86, pp. 241–247, 2012.
[58] V. Barranco *et al.*, "Amorphous Carbon Nanofibers and Their Activated Carbon Nanofibers as Supercapacitor Electrodes," *J. Phys. Chem. C*, vol. 114, no. 22, pp. 10302–10307, 2010.
[59] A. Eftekhari, "Supercapacitors utilising ionic liquids," *Energy Storage Mater.*, vol. 9, pp. 47–69, 2017.
[60] T. Romann, O. Oll, P. Pikma, K. Kirsimäe, and E. Lust, "4–10 V capacitors with graphene-based electrodes and ionic liquid electrolyte," *J. Power Sources*, vol. 280, pp. 606–611, 2015.
[61] D. R. McFarlane, J. Sun, J. Golding, P. Meakin, and M. Forsyth, "High conductivity molten salts based on the imide ion," *Electrochim. Acta*, vol. 45, no. 8, pp. 1271–1278, 2000.
[62] J. Sun, M. Forsyth, and D. R. MacFarlane, "Room-Temperature Molten Salts Based on the Quaternary Ammonium Ion," *J. Phys. Chem. B*, vol. 102, no. 44, pp. 8858–8864, 1998.
[63] A. Lewandowski and M. Galinski, "Practical and theoretical limits for electrochemical double-layer capacitors," *J. Power Sources*, vol. 173, no. 2, pp. 822–828, 2007.
[64] S. Maiti, A. Pramanik, and S. Mahanty, "Interconnected Network of MnO2 Nanowires with a 'Cocoonlike' Morphology: Redox Couple-Mediated Performance Enhancement in Symmetric Aqueous Supercapacitor," *ACS Appl. Mater. Interfaces*, vol. 6, no. 13, pp. 10754–10762, 2014.

[65] C. Zhao, W. Zheng, X. Wang, H. Zhang, X. Cui, and H. Wang, "Ultrahigh capacitive performance from both Co(OH) 2 /graphene electrode and K 3 Fe(CN) 6 electrolyte," *scientific*, vol. 3, no. 2986, pp. 3–8, 2013.

[66] G. Lota and E. Frackowiak, "Striking capacitance of carbon/iodide interface," *Electrochem. commun.*, vol. 11, no. 1, pp. 87–90, 2009.

[67] E. Frackowiak, M. Meller, J. Menzel, D. Gastol, and K. Fic, "Redox-active electrolyte for supercapacitor application," *Faraday Discuss.*, vol. 172, pp. 179–198, 2014.

[68] M. M. Masamitsu Tachibana, Takahiro Ohishi, Yasuhiro Tsukada, Aki Kitajima, Hideo Yamagishi, "Supercapacitor Using an Electrolyte Charge Storage System," *Electrochemistry*, vol. 79, no. 11, pp. 882–886, 2011.

[69] S. Chun *et al.*, "Design of aqueous redox-enhanced electrochemical capacitors with high specific energies and slow self-discharge," *Nat. Commun.*, vol. 6, pp. 1–10, 2015.

[70] L. Su, X. Zhang, C. Mi, B. Gao, and Y. Liu, "Improvement of the capacitive performances for Co – Al layered double hydroxide by adding hexacyanoferrate into the electrolyte.," *Phys. Chem. Chem. Phys.*, vol. 11, pp. 2195–2202, 2009.

[71] B. Akinwolemiwa, C. Peng, and G. Z. Chen, "Redox Electrolytes in Supercapacitors," *J. Electrochem. Soc.*, vol. 162, no. 5, pp. 5054–5059, 2015.

[72] X. Fang and D. G. Yao, "An Overview of Solid-Like Electrolytes for Supercapacitors," in *ASME International Mechanical Engineering Congress and Exposition, Proceedings (IMECE)*, 2013, vol. 6.

[73] R. Yuksel, Z. Sarioba, A. Cirpan, P. Hiralal, and H. E. Unalan, "Transparent and Flexible Supercapacitors with Single Walled Carbon Nanotube Thin Film Electrodes," *ACS Appl. Mater. Interfaces*, vol. 6, no. 17, pp. 15434–15439, 2014.

[74] Y. Yin, J. Zhou, A. N. Mansour, and X. Zhou, "Effect of NaI/I2 mediators on properties of PEO/LiAlO2 based all-solid-state supercapacitors," *J. Power Sources*, vol. 196, no. 14, pp. 5997–6002, 2011.

[75] X. Liu, Z. Wen, D. Wu, H. Wang, J. Yang, and Q. Wang, "Tough BMIMCl-based ionogels exhibiting excellent and adjustable performance in high-temperature supercapacitors," *J. Mater. Chem. A*, vol. 2, no. 30, pp. 11569–11573, 2014.

[76] P. Tamilarasan and S. Ramaprabhu, "Stretchable supercapacitors based on highly stretchable ionic liquid incorporated polymer electrolyte," *Mater. Chem. Phys.*, vol. 148, no. 1, pp. 48–56, 2014.

[77] G. P. Pandey, A. Rastogi, and C. R. Westgate, "Polyacrylonitrile and 1-Ethyl-3-Methylimidazolium Thiocyanate Based Gel Polymer Electrolyte for Solid-State Supercapacitors with Graphene Electrodes," *ECS Trans.*, vol. 50, no. 43, pp. 145–151, 2013.

[78] B. Francisco, C. M. Jones, S.-H. Lee, and C. Stoldt, "Nanostructured All-Solid-State Supercapacitor Based on Li2S-P2S5 Glass-Ceramic Electrolyte," *Appl. Phys. Lett.*, vol. 100, 2012.

[79] A. S. Ulihin, Y. G. Mateyshina, and N. F. Uvarov, "All-solid-state asymmetric supercapacitors with solid composite electrolytes," *Solid State Ionics*, vol. 251, pp. 62–65, 2013.

[80] Y. Shul'ga, S. Baskakov, V. A. Smirnov, N. Shulga, K. G. Belay, and G. Gutsev, "Graphene oxide films as separators of polyaniline-based supercapacitors," *J. Power Sources*, vol. 245, pp. 33–36, 2014.

[81] H.-C. Wu *et al.*, "High-performance carbon-based supercapacitors using Al current-collector with conformal carbon coating," *Mater. Chem. Phys.*, vol. 117, no. 1, pp. 294–300, 2009.

[82] S. Ye, I.-J. Kim, S. Yang, J. Lee, and W.-C. Oh, "CVD grown graphene/CNT composite as additive material to improve the performance of electric double layer capacitors (EDLCs)," *J. Mater. Sci. Mater. Electron.*, vol. 28, pp. 1–9, 2017.

Article 1: Ultrahigh energy density supercapacitors through a double hybrid strategy

Deepak P. Dubal, Bhawna Nagar, Jullieth Suarez-Guevara , Dino Tonti, Eduardo Enciso, Pablo Palomino, Pedro Gomez-Romero

Materials Today Energy, 5 (2017) 58-65

Materials Today Energy 5 (2017) 58–65

Contents lists available at ScienceDirect

Materials Today Energy

journal homepage: www.journals.elsevier.com/materials-today-energy/

Ultrahigh energy density supercapacitors through a double hybrid strategy

Deepak P. Dubal [a, b, *], Bhawna Nagar [a], Jullieth Suarez-Guevara [a], Dino Tonti [c], Eduardo Enciso [d], Pablo Palomino [d], Pedro Gomez-Romero [a, **]

[a] Catalan Institute of Nanoscience and Nanotechnology (ICN2), CSIC and the Barcelona Institute of Science and Technology, Campus UAB, Bellaterra, 08193 Barcelona, Spain
[b] School of Chemical Engineering, The University of Adelaide, Adelaide, South Australia 5005, Australia
[c] ICMAB (CSIC), Campus UAB, E-08193, Bellaterra, Barcelona, Spain
[d] Departamento de Química Física I, Facultad de Ciencias Químicas, Universidad Complutense de Madrid (UCM) Campus Moncloa, Madrid, Spain

ARTICLE INFO

Article history:
Received 23 November 2016
Received in revised form
29 April 2017
Accepted 3 May 2017
Available online 9 May 2017

Keywords:
Reduced graphene oxide-phosphotungstate hybrid
Hydroquinoe-doped gel electrolyte
Symmetric supercapacitors
Ultrahigh energy density

ABSTRACT

Herein, we are presenting all-solid-state symmetric supercapacitors (ASSSCs) with an innovative double hybrid strategy, where a hybrid material based on reduced graphene oxide (rGO) anchored with phosphotungstic acid, rGO-$H_3PW_{12}O_{40}$) is combined with hybrid electrolyte (hydroquinone-doped gel electrolyte). Initially, a hybrid electrode is fabricated by decorating $H_3PW_{12}O_{40}$ nanodots onto the surface rGO (rGO-PW_{12}). Next, a symmetric cell based on rGO-PW_{12} electrodes was assembled with PVA-H_2SO_4 polymer gel-electrolyte. Interestingly, rGO-PW_{12} symmetric cell revealed a substantial enhancement in the cell performance as compared to parent rGO systems. It featured a widened potential range of 1.6 V, thereby providing 1.05 mWh/cm^3 energy density. The electrochemical performance of rGO-PW_{12} cell was further advanced by introducing redox-active (hydroquinone) species in to the PVA-H_2SO_4 gel-electrolyte. Indeed, the performance of rGO-PW_{12} cell was surprisingly improved with an ultra-high energy density of 2.38 mWh/cm^3 (more than two-fold).

1. Introduction

Energy storage technologies are quickly maturing in order to effectively grow as key players in the forthcoming sustainable energy model. Electrical energy storage in particular will have to widen its target performance evolving from consumer electronics to a much broader set of applications, including grid, load-leveling, electric vehicles and other high-power applications. New materials, new devices and new systems will significantly contribute to satisfy this widened growth by making possible faster, more durable and cheaper high energy-density storage [1].

Combining high energy and power in a single device is a holy grail in energy storage but not an easy one to get through circuitry at a low price. Thus, materials and very especially electrode materials are explored to improve their intrinsic energy as well as power densities by means of various approaches from nanostructured design to hybridization. Nanostructure is a good way to increase and optimize electrode-electrolyte interfaces, whereas the development of hybrid materials allows for harnessing complementary properties of the components and even emerging synergic performances. Of course, these two approaches are not incompatible and can be used altogether reinforcing each other [1,2]. Indeed, there is a strong and growing research area dealing with energy storage systems based on hybrid nanocomposite electrodes [1].

Polyoxometalates (POMs) are clusters of anionic molecular metal oxide which includes variety of transition metals such as Mo, W, V etc. They have been well known in the realm of inorganic chemistry for a long time [3] but only recently have been recognized as useful nanosized blocks for the design of functional materials with outstanding applications in catalysis, energy conversion and molecular electronics [4–6]. Within the field of energy storage, they have found a particularly well-suited niche application in supercapacitors, initially integrated in conducting

* Corresponding author. Catalan Institute of Nanoscience and Nanotechnology (ICN2), CSIC and the Barcelona Institute of Science and Technology, Campus UAB, Bellaterra, 08193 Barcelona, Spain.
** Corresponding author.
E-mail addresses: dubaldeepak2@gmail.com (D.P. Dubal), pedro.gomez@icn2.cat (P. Gomez-Romero).

http://dx.doi.org/10.1016/j.mtener.2017.05.001
2468-6069/

polymers [7–9] and more recently forming hybrid electrodes with carbon materials [10–14]. POMs can exhibits high energy density for supercapacitors due to the rapid and reversible multi-electron redox reactions. However, the electrical connection of POMs trough conducting substrates is crucial to maximize their electron-transfer activity while preventing the dissolution of these clusters in the electrolytes. Therefore, researchers are currently exploring the anchoring of POMs on nanocarbons (carbon nanotubes CNTs, graphene etc.) to immobilize and integrate POMs in electrically conducting substrates. Keggin's structure (such as PMo_{12}, PW_{12} etc.) is the smallest and simplest version of POMs which electrochemically active and stable in aqueous acidic-media [15].

We first prepared a new hybrid electrode material based on Phosphotungstic acid ($H_3PW_{12}O_{40}$, in short, PW_{12}) and reduced Graphene Oxide (rGO). As it will be shown, these materials present a synergic combination with a dual charge storage mechanism: electrical double layer (EDL, nanocarbons) and redox (faradaic, PW_{12}). Related hybrid electrodes formed by Activated Carbons (AC) and polyoxometalates have shown how the anchoring of the inorganic clusters onto the carbon microporous surface effectively leads to increased (capacitive + faradaic) electrochemical behavior of the hybrid electrodes and to enhanced performance of symmetrical supercapacitor devices [11,12].

In addition to the preparation of these hybrid electrode materials we went one step further and tested the use of a hybrid electrolyte, that is, a gel electrolyte containing redox-active hydroquinone in addition to protons (1 M aqueous H_2SO_4) in order to achieve more advancement in rGO-PW_{12} based device performance. The use of electroactive redox species in EDLC supercapacitor electrolytes has been studied earlier, for instance using the I^-/I_3^- redox couple [16]. In the present paper though we have tried and report a specific combination of electrode and electrolyte, both incorporating different but compatible redox-active species.

2. Methods

2.1. Fabrication of rGO-PW_{12} hybrid materials based

Starting with the preparation of graphene oxide (GO) using a modified Hummers method: 2.5 g sodium nitrate ($NaNO_3$) was mixed with 125 ml of sulfuric acid (H_2SO_4) with continuous stirring. To which, 2.5 g graphite powder was added and the suspension was kept in an ice bath for next for 30 min. Later, 12.5 g of potassium permanganate ($KMnO_4$) was mixed in the above suspension and then the suspension was maintained at 50 °C for 2 h with constant stirring. In the next step, deionized water (500 ml) was gradually added in the above solution. To which, 15 ml of hydrogen peroxide (35% H_2O_2) was introduced to the resulting solution. The product was cleaned with 10% HCl solution and later with concentrated HCl (250 ml, 37%). The GO product was dried in vacuum oven at 80 °C for 24 h. To prepare reduced graphene oxide (rGO), 0.5 gm of GO was heat-treated at 800 °C for 1 h in nitrogen atmosphere.

Later, a hybrid material based on rGO and phosphotungstate (rGO-PW_{12}) was prepared as follows: The rGO suspension was prepared by sonicating rGO (0.25 g) in deionized water (100 ml) for 1 h using probe sonicator. We varied the concentration of phosphotungstic acid ($H_3PW_{12}O_{40}.3H_2O$, (PW_{12})) from 2 mM, 4 mM, 6 mM, 10 mM and 15 mM. Interestingly, the loading of PW_{12} was increased with concentration until 10 mM which saturates with further increase in concentration (15 mM). This might be attributed to the sufficient anchoring of PW_{12} on the rGO surface until the concentration of 10 mM phosphotungstic acid ($H_3PW_{12}O_{40}.3H_2O$, (PW_{12})) due to limited functional groups at the surface of rGO. Thus, the maximum and uniform loading of 0.38 mmol PW_{12} per gram of rGO was observed for 10 mM phosphotungstic acid. Hence, 10 mM of phosphotungstic acid ($H_3PW_{12}O_{40}.3H_2O$, (PW_{12})) was added to the above pre-sonicated 100 ml rGO dispersion. This resulting solution was sonicated for 5 h in bath sonicator and aged overnight. Finally, the rGO-PW_{12} samples was collected with centrifugation and dried at 80 °C for 24 h in vacuum oven.

2.2. Electrochemical properties

The pastes were prepared with the formulation of 85% of active material: 10% PVDF as binder: 5% Super P conducting additive. A small amount of *N*-Methyl-2-pyrrolidone was added to the above mixture and kept stirring overnight in order to prepare homogeneous paste. The electrodes were prepared by coating this paste on carbon cloth with doctor-blade method. A conventional Swagelok® cells were used to assemble solid state symmetric cells using rGO-PW_{12} electrodes and H_2SO_4/Polyvinyl alcohol (PVA) gel electrolyte. The electrochemical properties all the devices were tested with Biologic VMP3 potentiostat.

3. Results and discussion

3.1. Synthesis and characterizations

We have used three-dimensional (3D) interconnected open porous rGO nanosheets prepared by a modified Hummers' method as our base capacitive material. Subsequently, phosphotungstic acid ($H_3PW_{12}O40$) was uniformly and effectively decorated on the rGO nanosheets as it is shown in Fig. 1, which further shows tiny but enormous PW_{12} clusters anchored on very thin graphene nanosheets.

Further, the electrochemical performance of rGO-PW_{12} was studied by fabricating symmetrical supercapacitors with H_2SO_4/Polyvinyl alcohol (PVA) gel electrolyte.

XRD patterns shown in Fig. 2 (a) suggests two well-resolved peaks at 25.6° and 42.5° for both materials which can assigned to (002) and (001) planes, respectively [17]. Interestingly, no additional peak corresponding to PW_{12} is observed, suggesting uniform distribution of the molecular PW_{12} clusters on the surface of rGO.

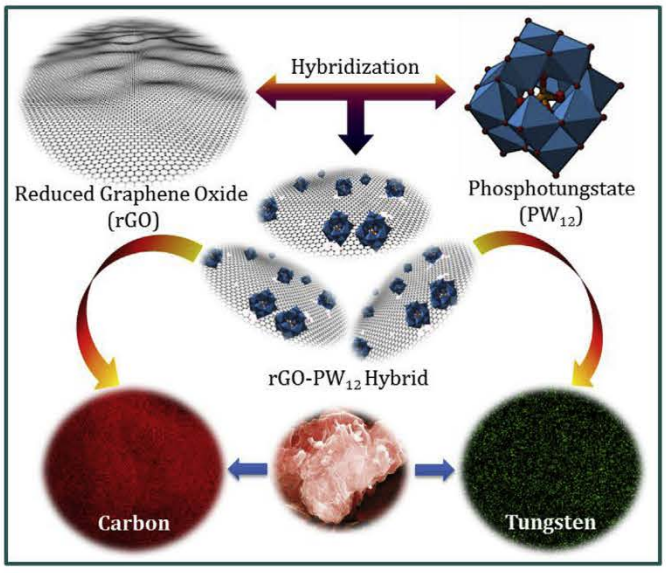

Fig. 1. Schematic illustration of steps involved in the synthesis of reduced graphene oxide (rGO) and phosphotungstate (PW_{12}) hybrid material (rGO-PW_{12}) with corresponding EDS mapping.

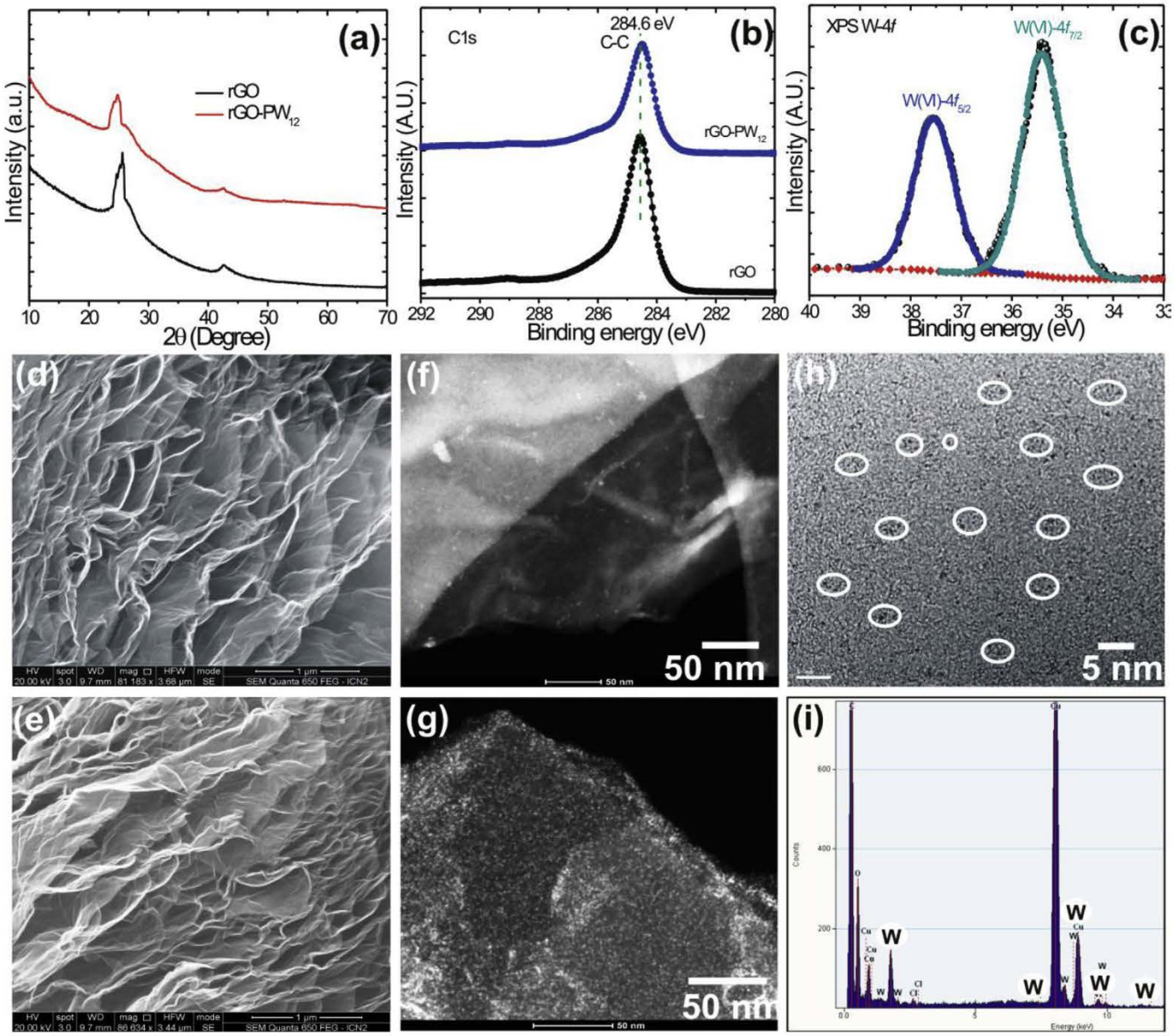

Fig. 2. (a) XRD patterns of rGO and rGO-PW_{12} hybrid materials, (b) core-level XPS spectra of C1s and (c) W4f of rGO-PW_{12} sample, respectively, (d, e) SEM images and (f, g) STEM images of rGO and rGO-PW_{12} hybrid samples, respectively (h) HR-TEM image of rGO-PW_{12} sample (i) EDS spectrum of rGO-PW_{12} sample measured from TEM.

Moreover, the broad and low intensity peaks for the rGO-PW_{12} hybrid further confirms less graphitization as compared to the rGO due to the anchoring of the PW_{12} molecular clusters. The rGO and rGO-PW_{12} samples were further analyzed with Raman spectroscopy (Supporting information S1). The intensity ratio of the Raman D band (at 1348 cm^{-1}) to G band (at 1591 cm^{-1}) is almost same (0.96–0.95) for both materials, thereby confirming the formation of reduced graphene oxide. Moreover, the intensity of bands is decreased for rGO-PW_{12} samples without any additional peaks associating to PW_{12} which supports to XRD results.

Two major and common peaks at 284.5 eV and 533.5 eV are observed in the overview of XPS spectra for rGO and rGO-PW_{12} which corresponds to C1s and O1s, respectively (Supporting information S2a). On the other hand, rGO-PW_{12} sample exhibits an additional peak at 35.71 eV (4f) which is assigned to tungsten. It is further interesting to note that, the peak intensity of core-level C1s spectra is considerably decreased with a minor shift towards low binding energy for rGO-PW_{12} (see Fig. 2(b)). Furthermore, core-level W4f spectrum shows two peaks at 37.54 eV ($W4f_{5/2}$) and 35.4 eV ($W4f_{7/2}$) with spin-orbit splitting of 2.14 eV (with a peak ratio 4:3). Thus, it is revealed that W atoms are in W(VI) oxidation state, confirming the presence of fully oxidized PW^{VI}_{12} in rGO-PW_{12} hybrid (Fig. 2(c)) [18,19].

The morphological analyses were performed in order to confirm and further characterize the anchoring of PW_{12} onto rGO nanosheets. It is evidenced that, rGO possesses interconnected ultrathin nanosheets which forms three dimensional open porous architectures (as seen in Fig. 2 d). This unique nanoarchitecture can provide highly conducting framework which is extremely favorable to enhance the electron transport. It is further interesting to note that, the open-porous structure of rGO is still maintained even after heavy decoration of PW_{12} clusters (see Fig. 2(e)). The detailed analysis of PW_{12} anchoring on to the rGO surface was further investigated with STEM and displayed in Fig. 2(f and g). The surface

of rGO looks more smooth and dustless as seen from Fig. 2(f) while on the complete contrary, huge number of white tiny dots of around nanometers size are clearly seen for rGO-PW_{12} hybrid (Fig. 2 g). Notably, the PW_{12} nanodots are uniformly anchored on to the surface of rGO nanosheets. Furthermore, black tiny nanoparticles of PW_{12} are clearly observed (few of them are marked with white circles) in HR-TEM image for rGO-PW_{12} hybrid (Fig. 2(h)). EDS mapping of rGO-PW_{12} hybrid (see Fig. 2(i)) further confirms the presence of 1 nm sized PW_{12} nanodots uniformly decorated on to the surface of rGO nanosheets (see supporting Figure. S2b).

We should keep in mind that all the twelve WO_6 species are on the surface in 1 nm sized PW_{12} clusters, underscoring the ultimate dispersion of the electroactive clusters in rGO-PW_{12} hybrids. Also, it is well known that the charges stored in the pseudo-capacitive materials rely on the surface redox reactions which means the energy is stored through the charge transfer near the electrode surface. In this context, the rGO-PW_{12} hybrid presented here is an ideal material which is a rational combination of open porous interconnected rGO nanosheets with redox active PW_{12} molecular clusters, thereby providing an exclusive foundation from a structural point of view.

The hybrid materials with excellent surface area and open-porosity are crucial parameters in order to achieve excellent electrochemical performances. The BET surface area for rGO and rGO-PW_{12} samples were found to be 242 m^2/g and 237 m^2/g, respectively (supporting information S3a). The negligibly small decrease in the BET surface area for rGO-PW_{12} samples might be ascribed to the anchoring of PW_{12} clusters, which considerable improves the final mass of the hybrid material. However, rGO-PW_{12} hybrid material still exhibits excellent BET surface area which is remarkably higher than the reported carbon based hybrid materials [3,20,21]. It is further seen that, both rGO and rGO-PW_{12} samples exhibit mesoporous nature (supporting information S3b), showing a pores in the range of 2–8 nm. Moreover, it is worth noting that there is substantial increase in the pore volume of the parent rGO material from 0.10 cm^3/g to 0.16 cm^3/g after anchoring the PW_{12} molecular cluster which can offer easy ionic transportation into the hybrid material.

Further, both the electrodes were tested by assembling all-solid state symmetric cells with H_2SO_4/PVA gel electrolyte. Fig. 3(a, b) summarizes the electrochemical properties of rGO and rGO-PW_{12} symmetric cells. The CV curves were measured for both symmetric cell based on rGO and rGO-PW_{12} electrodes and presented in Fig. 3(a). The anchoring of PW_{12} on the surface of rGO nanosheets dramatically improves the current density with an additional working voltage of 0.3 V than that for rGO based cell. Likewise, the rGO-PW_{12} cell exhibits noticeably longer discharging time as seen in Fig. 3(b), indicating a significantly greater specific capacitance. The larger working voltage (up to 1.6 V) of rGO-PW_{12} will lead to improved energy density of the cell. These excellent electrochemical properties can be assigned to the combined contribution from rGO (EDLC) and PW_{12} (faradic) in hybrid material. The CV curves for rGO-PW_{12} cell at various scan rate are displayed in Fig. 3(c). The shapes of CV curves are quasi-rectangular with strong redox peaks due to the faradic PW_{12} clusters overlapped with capacitive contribution from rGO which are extremely unlike than that for rGO based cell (supporting information S4). These CV shapes correspond to the combined charge storing behavior, faradaic (PW_{12}) and capacitive (EDLC). In addition, the rGO-PW_{12} cell retains their shapes of CV curves at high scan rate of 100 mV/s, suggesting excellent reversibility of rGO-PW_{12} cells for rapid charge/discharge rates. Galvanostatic charge/discharge measurements were carried out at different current densities for rGO-PW_{12} based cell and shown in Fig. 3(d). The non-triangular shapes of GCD curves for rGO-PW_{12} cell further suggests the inclusion of both capacitive from rGO and faradic from PW_{12} charge storing. The possible redox reactions of PW_{12} in hybrid rGO-PW_{12} as reported in our previous report [12] are as follows:

$$PW_{12}O_{40}^{3-} + e^- \Leftrightarrow PW_{12}O_{40}^{4-} \quad (1)$$

$$PW_{12}O_{40}^{4-} + e^- \Leftrightarrow PW_{12}O_{40}^{5-} \quad (2)$$

$$PW_{12}O_{40}^{5-} + 2e^- + H^+ \Leftrightarrow HPW_{12}O_{40}^{6-} \quad (3)$$

Thus, the anchoring of redox-active PW_{12} nanoparticle on the surface of rGO nanosheets provides extra faradaic contribution in addition to EDLC (from rGO) as well as extended working voltage window (up to 1.6 V) beyond thermodynamic limit of water reduction.

Moreover, in case of both cells, very small *iR* drop, suggests low internal resistance of both electrodes materials. In addition, the charging parts are almost symmetrical to their counter discharging parts, suggesting rapid and excellent electrochemical reversibility. For detailed calculations of electrochemical properties see supporting information S5. The plots of volumetric capacitances with respect to current density for both rGO and rGO-PW_{12} cells are shown in Fig. 3(e). The volumetric capacitance for rGO-PW_{12} cell was calculated to be 2.95 F/cm^3 (260 mF/cm^2) and 1.1 F/cm^3 (96 mF/cm^2) at 1.27 and 25.47 mA/cm^2 applied current densities, respectively. These values are significantly higher than that for rGO cell (0.7 F/cm^3 (60 mF/cm^2) and 0.33 F/cm^3 (28 mF/cm^2) at current density of 1.27 and 10.2 mA/cm^2, respectively). The whole credit for this great increase in specific capacitance goes to the redox contribution of PW_{12} clusters in the hybrid material. Furthermore, the cells retained around 32% (rGO) and 35% (rGO-PW_{12}) of initial capacitance after increase in scan rate from 5 to 100 mV/s, suggesting good rate capability of both the systems. There is obvious decrease in the specific capacitance values with scan rate which might be assigned to the slower electrochemical kinetics at higher scan rates. The capacitance values achieved in present investigation are extensively higher than the literature values for symmetric as well as asymmetric cells [7,8,21–23] and solid state gels based on metal oxides [24–29] (supporting information S6). The energy and power densities were calculated for both rGO and rGO-PW_{12} cells and shown in Fig. 3(f). As seen in the Ragone plots, the rGO-PW_{12} cell provides maximum energy density of 1.05 mWh/cm^3 at power of 11.5 mW/cm^3 which is significantly higher than that for rGO based cells (0.2 mWh/cm^3 at power of 9 mW/cm^3). Impressively, at a high power density of 231.6 mW/cm^3, the rGO-PW_{12} cell still delivers energy density of 0.4 mWh/cm^3 which is higher than rGO based cell. Thus, the results obtained here suggests that an innovative rGO-PW_{12} hybrid material is robust candidates to design high power and high energy supercapacitors. In addition, the symmetric cell design provides better results as compared to the complex asymmetric designs.

3.2. *Effect of hydroquinone doping in gel-electrolyte*

Recently, some interesting investigation showed the advancement in supercapacitive performance of electrodes using redox/active electrolytes [30,31] in particular conducting polymers [30]. In our recent investigation, we proved that, the inclusion of redox active species (hydroquinone) in gel-electrolyte significantly improves the performance of rGO-PMo_{12} symmetric device [32]. Herein, we are exploring the similar concept to further advance the supercapacitive performance of rGO-PW_{12} cell with redox-active species (hydroquinone) added PVA/H_2SO_4 gel-electrolyte. The *p*-

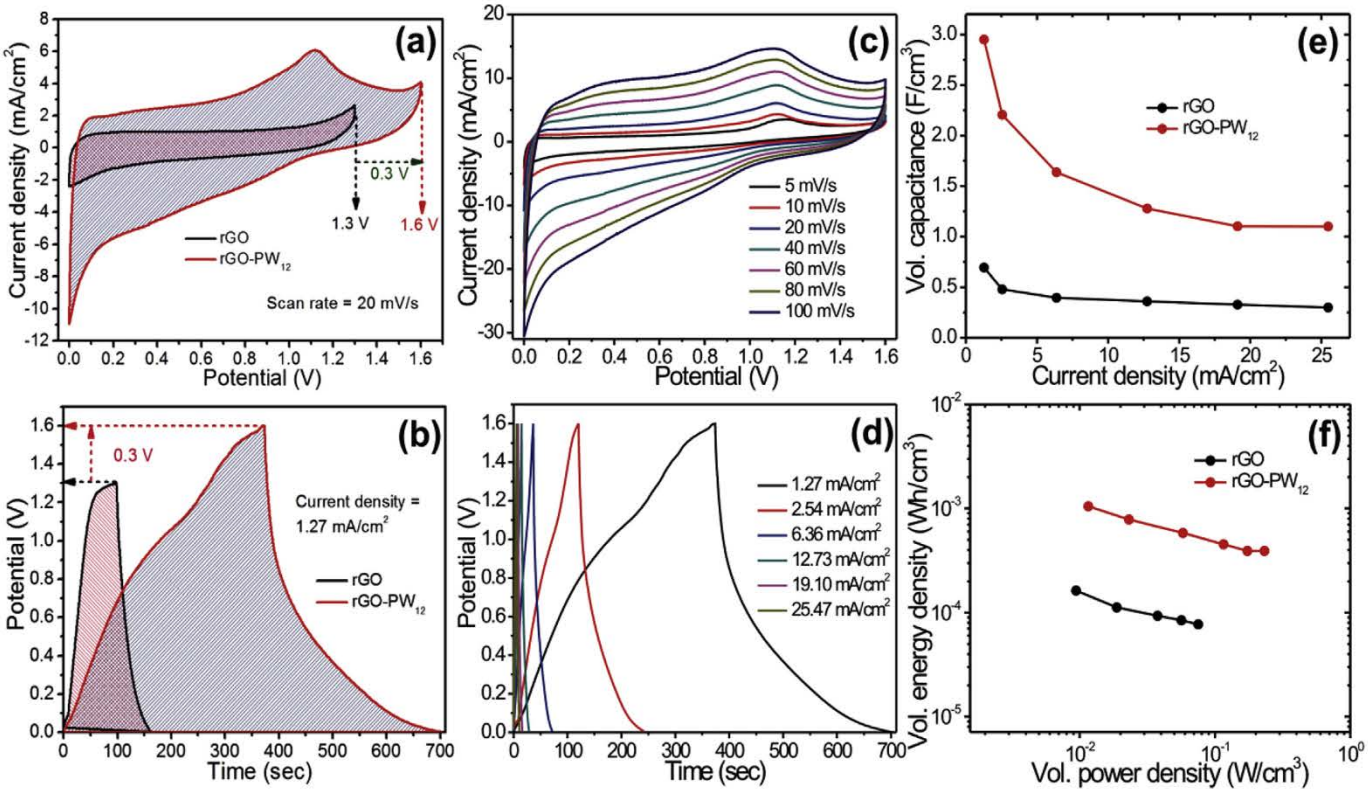

Fig. 3. (a, b) CV and GCD curves for rGO and rGO-PW_{12} symmetric cells at a fixed scan rate of 20 mV/s and a constant current density of 1.27 mA/cm^2, respectively, (c, d) CV and GCD curves for rGO-PW_{12} based cells at various scan rates and current densities, respectively. (e) Plots of variation of volumetric capacitance of rGO and rGO-PW_{12} based cells with scan rates, (f) Plots of energy and power densities for rGO and rGO-PW_{12} symmetric cells.

benzoquinone exhibits a redox couple of Quinone/Hydroquinone (Q/HQ) which is highly reversible. The hybrid electrolytes were prepared with three different concentrations of hydroquinone. The CV curves for rGO-PW_{12} cell with 0.2 M hydroquinone added gel-electrolyte are shown in Fig. 4(a). Strikingly, the shapes of CV curves are completely different than that observed for only PVA-H_2SO_4 electrolyte and shows very strong redox peaks, suggesting extra-ordinary improvement in the device performance. Obviously, this excellent advancement can be attributed to the Q/HQ redox reactions of *p*-benzoquinone which not only added redox species but also provides additional protons, thereby offers additional reaction sites for rapid as well as highly reversible redox processes [32].

The maximum area under the CV curves i.e. the maximum current density is obtained for 0.2 M concentration of HQ added gel-electrolyte which starts to decrease for higher concentration of HQ (supporting information S7). Likewise, the charge/discharge times for rGO-PW_{12} cell gradually improves till 0.2 M concentration of HQ which reduces for further increase in HQ concentration as shown in Fig. 4(b–d). The volumetric capacitance of rGO-PW_{12} cells at various current densities for all HQ concentrations were calculated and plotted in Fig. 4(e). The volumetric capacitances calculated for rGO-PW_{12} with 0.2 M HQ gel-electrolyte is 6.72 F/cm^3 (592 mF/cm^2) and 1.33 F/cm^3 (117 mF/cm^2) at current densities of 1.27 mA/cm^2 and 25.47 mA/cm^2, respectively, significantly higher than that with conventional gel-electrolyte. There is apparent decrease in the capacitance with current density which might be assigned to the slower kinetics at higher current densities (supporting information S8 and S9).

Thus, a double hybridization approach where rGO-PW_{12} hybrid electrode with redox-active species added hybrid gel electrolyte effectively enhances the performance of the device. The energy and power densities are shown in the Ragone plots (see Fig. 4(f)). The maximum energy density for rGO-PW_{12} cell was found to be 2.39 mWh/cm^3 (23.11 Wh/kg) at a power density of 11.58 mW/cm^3 (112 W/kg) with 0.2 M HQ added gel electrolyte. Surprisingly, at maximum power of 232 mW/cm^3 (2.23 kW/kg), rGO-PW_{12} cell delivers decent energy density values in the range of 0.4–0.8 mWh/cm^3 due to hybrid electrolyte, confirming the great potential for high energy and high power applications. Compared to the literature values reported for gel-electrolytes, present investigation offers excellent performances [24–26,28,29,32–35]. Thus, this innovative investigation open new opportunities for the further development of high performance supercapacitors.

In order to get deeper insights about the resistive and capacitive behavior of rGO-PW_{12} based symmetric cell in 0.2 M HQ doped H_2SO_4 gel-electrolyte, electrochemical impedance measurements were performed and presented in Fig. 5. The resulting Nyquist plot (see Fig. 5(a)) is composed of a semicircle in the high-frequency region and a straight line with the real axis in the low-frequency region. This line is called the Warburg line which is a result of the frequency dependence of ion diffusion in the electrolyte on the electrode interface. A simple equivalent circuit model to evaluate this kind of EIS result is shown in inset of Fig. 5(a). The real axis intercept at high frequency corresponds to the electrolyte resistance (Rs) and it is also known as equivalent series resistance (ESR). R_{ct} (also known as charge transfer resistance) characterizes the rate of redox reactions at the electrode-electrolyte interface [36]. Low charge transfer resistance suggests fast ion transport within the supercapacitor [37]. CPE_{dl} is the constant phase element (CPE) representing double layer capacitance, which occurs at interfaces between solids and ionic solutions due to separation of ionic and/or

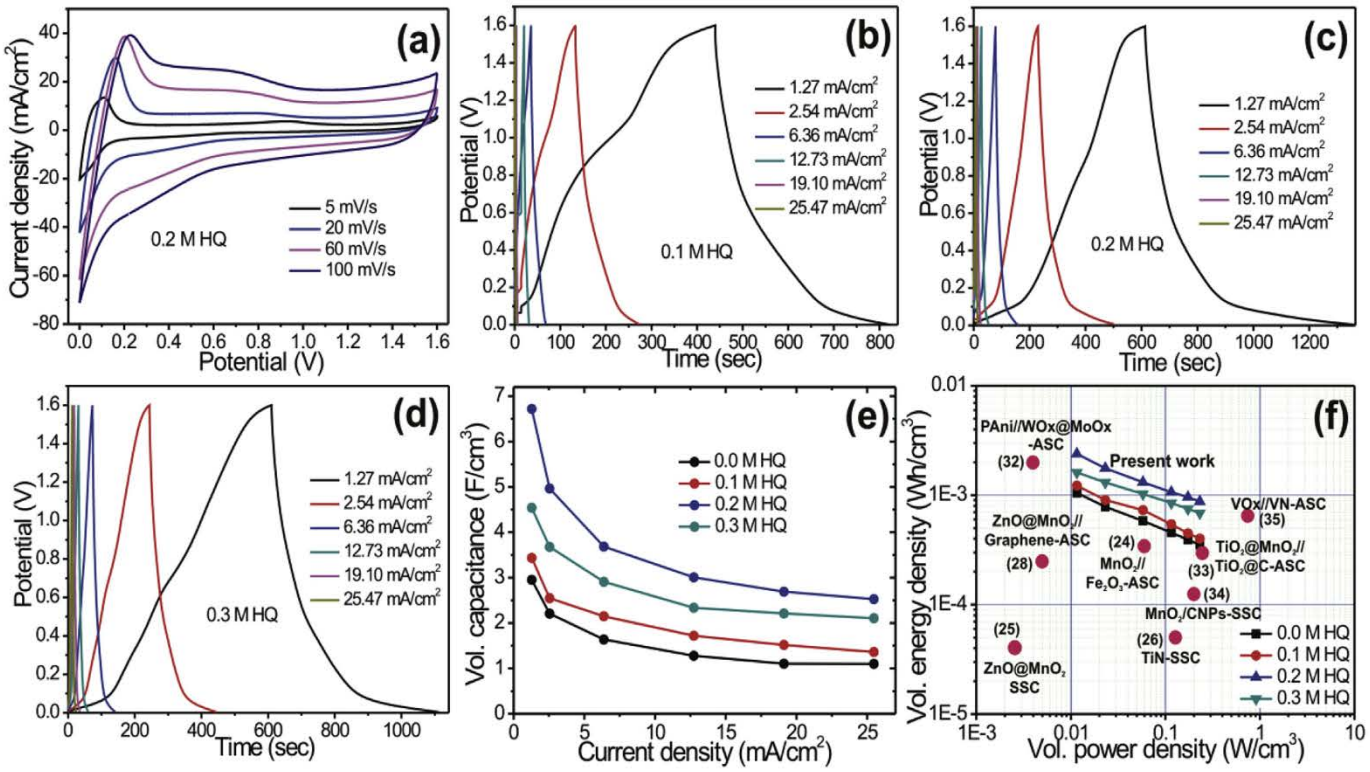

Fig. 4. (a) CV curves at various scan rates for rGO-PW_{12} symmetric cells with 0.2 M HQ doped gel-electrolyte, (b–d) CD curves of rGO-PW_{12} symmetric cells at different current densities with HQ doped gel-electrolyte of different concentrations, respectively, (e) Variation of volumetric capacitances of rGO-PW_{12} cell for different HQ concentrations with current densities, (f) volumetric energy density vs power density plots of rGO-PW_{12} symmetric cell with different concentration of HQ doped electrolytes in Ragone plot.

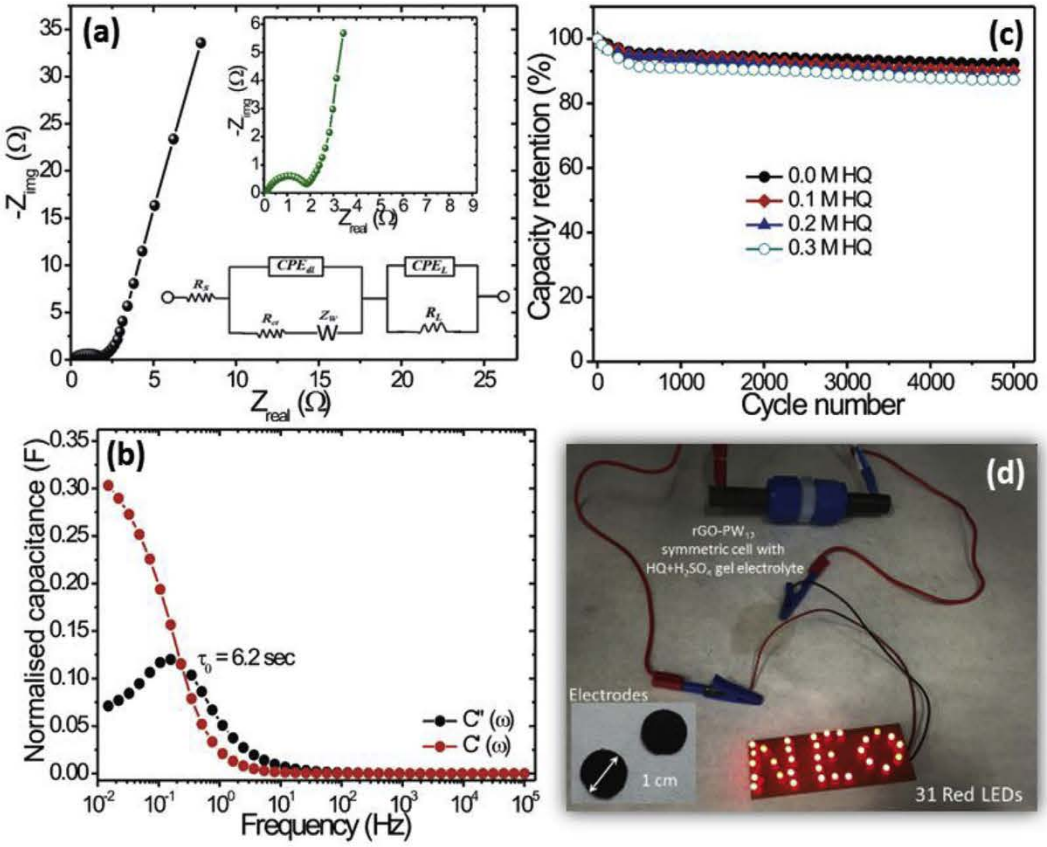

Fig. 5. (a) Nyquist plot of rGO-PW_{12} symmetric cell with enlarged view and equivalent circuit (in the inset) (b) real and imaginary capacitances (C′ and C″) vs. frequency (log f) with 0.2 M HQ doped polymer gel electrolyte (c) Capacity retention with number of cycles measured at 12.7 mA/cm^2 over 5000 cycles. (d) The practical demonstration by lighting Thirty-one (31) LED indicators with word "NEO" powered rGO-PW_{12} symmetric cell.

electronic charges [38]. W is the Warburg element, which represents the diffusion of ions into the porous electrode in the intermediate frequency region, and is a result of the frequency dependence of this diffusion. A possible reason for insensitivity to varying voltage scan rates is a short and equal diffusion path length of the ions in the electrolyte, as evidenced by a short Warburg region on the Nyquist plots. R_L is the leakage resistance which is placed in parallel with CPE_L. This is usually very high and can be ignored in the circuit. CPE_L denotes pseudocapacitance, which arises with voltage dependent Faradaic charge transfer processes. ESR and R_{ct} values for rGO-PW_{12} symmetric cell 0.56 and 1.58 Ω, respectively. These lower values indicate consistent interfacial contact between the rGO-PW_{12} electrode and electrolyte. In addition, anchoring of PW_{12} on to the surface of rGO nanosheets helps to facilitate electronic conduction from the PW12 anchored rGO to current collector; this results in a reduced ESR. Additionally, the resultant relatively small charge transfer resistance should be associated with increased contact area at the electrode-electrolyte interface. Thus, ion transfer and charge transfer is easily facilitated and reversibility is improved. Plots of normalized real capacitance vs. frequency and imaginary capacitance vs. frequency are shown in Fig. 5(b). The plot shows common relaxation-type dispersions where the real capacitance 'C' reduces with frequency while 'C‴' shows maxima. The relaxation time constant was evaluated using the following relation ($\tau_0 = 1/f_0$), which was found to be 6.2 s for rGO-PW_{12} symmetric cell.

The capacitance retention of the rGO-PW_{12} symmetric cell measured in the cycling charge-discharge test at a current density of 12.7 mA/cm^2 in redox-active electrolyte and shown in Fig. 5(c). Although the degradation of capacitance is a common problem in pseudo-capacitive materials, our rGO-PW_{12} hybrid cell exhibits capacity retention in the range of 88–93% with redox-active (HQ) electrolyte. This high cycling stability is mainly contributed by synergetic effect of rGO (EDLC) and PMo_{12} (redox-active molecular clusters). The practical application of rGO-PW_{12} cell with redox-active electrolyte is demonstrated by illuminating LEDs. The word "NEO" (NEO is short form of our group's name, Novel Energy Oriented-Materials) of 31 LEDs is lit by single rGO-PW_{12} cell with 0.2 M HQ added gel-electrolyte for almost 120 s after a charging the cell for about 30 s, suggesting excellent energy output on fast charging (see Fig. 5(d)). The reasons for this excellent electrochemical performances are listed as follows: 1) hybrid electrode, which is a combination of two best materials of two different charge storing behavior such as faradaic (PW_{12})and EDLC (rGO), 2) open-porous interconnected rGO nanosheets offers conducting channels for fast ionic transport, 3) excellent redox contribution from homogeneously anchored quantum sized PW_{12} molecular clusters 3) Large operational working voltage window (1.6 V) provided by unique cell design rGO-PW_{12}/PVA-H_2SO_4/rGO-PW_{12}, resulting in enhanced energy density, 4) Hybrid electrolyte: incorporation of H/HQ redox active species in polymer gel-electrolyte certainly provides extra protons and surplus redox active sites to store energy. Certainly, the addition of hydroquinone redox couple offers molecular moieties which can introduce battery-like properties in the cell and consequently improves the energy density of the device.

4. Conclusions

An innovative concept of double hybridization (hybrid electrode + hybrid electrolyte) in solid state supercapacitors is successfully explored including: i) design and synthesis of hybrid electrode by decorating redox-active PW_{12} nanodots onto the nanosheets of rGO and ii) applying a hybrid electrolyte, incorporating hydroquinone redox couple to PVA-H_2SO_4 gel-electrolyte. With the conventional gel-electrolyte, the symmetric cell based on rGO-PW_{12} hybrid shows considerable enhancement in the device performance, providing wider voltage window up to 1.6 V, which delivers an energy density of 1.05 mWh/cm^3. Furthermore, an incorporation of redox-active HQ into a gel electrolyte extraordinarily improves the performance of rGO-PW_{12} based device. Remarkably, a 2-fold increase in the energy density (2.38 mWh/cm^3) is achieved after introduction of redox-active species. Thus, overall results ensure that the double hybrid approach (rGO-PW_{12} hybrid electrode) and hybrid electrolyte (redox-active) is promising for the development of high performance supercapacitors.

Acknowledgments

Partial funding from Miisterio de Economía y Competitividad through Fondo Europeo de Desarrollo Regional (FEDER) (Grant MAT2015-68394-R, MINECO/FEDER) and from AGAUR (project NESTOR) are acknowledged. ICN2 acknowledges support of the Spanish MINECO through the Severo Ochoa Centers of Excellence Program under Grant SEV-2013-0295. Finally, the award to DPD of a Marie-Curie Fellowship through Beatriu de Pinos Program (BP-DGR-2013) from the Catalan system of science and technology, Spain, is gratefully acknowledged.

Appendix A. Supplementary data

Supplementary data related to this article can be found at http://dx.doi.org/10.1016/j.mtener.2017.05.001.

References

[1] D.P. Dubal, O. Ayyad, V. Ruiz, P. Gómez-Romero, Hybrid energy storage: the merging of battery and supercapacitor chemistries, Chem. Soc. Rev. 44 (2015) 1777–1790.
[2] P. Simon, Y. Gogotsi, B. Dunn, Where do batteries end and supercapacitors begin? Science 343 (2014) 1210–1211.
[3] L.C.W. Baker, D.C. Glick, Present general status of understanding of heteropoly electrolytes and a tracing of some major highlights in the history of their elucidation, Chem. Rev. 98 (1998) 3–50.
[4] P. Gomez-Romero, Polyoxometalates as photoelectrochemical models for quantum-sized semiconducting oxides, Sol. State Ionics 101 (1997) 243–248.
[5] D.-L. Long, R. Tsunashima, L. Cronin, Polyoxometalates: building blocks for functional nanoscale systems, Angew. Chem. Int. Ed. 49 (2010) 1736–1758.
[6] Y. Ji, L. Huang, J. Hu, C. Streb, Y.F. Song, Polyoxometalate-functionalized nanocarbon materials for energy conversion, energy storage and sensor systems, Energy Environ. Sci. 8 (2015) 776–789.
[7] P. Gomez-Romero, M. Chojak, K. Cuentas-Gallegos, J.A. Asensio, P.J. Kulesza, N. Casan-Pastor, M. Lira-Cantu, Hybrid organic-inorganic nanocomposite materials for application in solid state electrochemical supercapacitors, Electrochem. Commun. 5 (2003) 149–153.
[8] A.K. Cuentas-Gallegos, M. Lira-Cantu, N. Casan-Pastor, P. Gomez-Romero, Nanocomposite hybrid molecular materials for application in solid-state electrochemical supercapacitors, Adv. Funct. Mater. 15 (2005) 1125–1133.
[9] J. Vaillant, M. Lira-Cantu, K. Cuentas-Gallegos, N. Casan-Pastor, P. Gomez-Romero, Chemical synthesis of hybrid materials based on PAni and PEDOT with polyoxometalates for electrochemical supercapacitors, Prog. Sol. State Chem. 34 (2006) 147–159.
[10] A. Cuentas-Gallegos, R. Martinez-Rosales, M. Baibarac, P. Gomez-Romero, M.E. Rincon, Electrochemical supercapacitors based on Novel hybrid materials made of carbon nanotubes and polyoxometalates, Electrochem. Commun. 9 (2007) 2088–2092.
[11] V. Ruiz, J. Suarez-Guevara, P. Gomez-Romero, Hybrid electrodes based on polyoxometalates-carbon materials for electrochemical supercapacitors, Electrochem. Commun. 24 (2012) 35–38.
[12] J. Suarez-Guevara, V. Ruiz, P. Gomez-Romero, Hybrid energy storage: high voltage aqueous supercapacitors based on activated carbon-phosphotungstate hybrid materials, J. Mater. Chem. A 2 (2014) 1014–1021.
[13] M. Genovese, K. Lian, Pseudocapacitive behavior of keggin type polyoxometalate mixtures, Electrochem. Commun. 43 (2014) 60–62.
[14] M. Genovese, K. Lian, Polyoxometalate modified inorganic-organic nanocomposite materials for energy storage applications: a review, Curr. Opin. Solid State Mater. Sci. 19 (2015) 126–137.
[15] N. Casan-Pastor, P. Gomez-Romero, Polyoxometalates: from inorganic chemistry to materials science, Front. Biosci. 9 (2004) 1759–1770.

[16] G. Lota, K. Fic, E. Frackowiak, Alkali metal iodide/carbon interface as a source of pseudocapacitance, Electrochem. Commun. 13 (2011) 38–41.
[17] H. Kim, K.Y. Park, J. Hong, K. Kang, All-graphene-battery: bridging the gap between supercapacitors and lithium ion batteries, Sci. Rep. 4 (2014) 5278.
[18] D. Barreca, G. Carta, A. Gasparotto, G. Rossetto, E. Tondello, P. Zanella, A study of nanophase tungsten oxides thin films by XPS, Surf. Sci. Spectra 8 (2001) 258.
[19] L. Weinhardt, M. Blum, M. Bär, C. Heske, B. Cole, B. Marsen, E.L. Miller, Electronic surface level positions of WO_3 thin films for photoelectrochemical hydrogen production, J. Phys. Chem. C 112 (2008) 3078–3082.
[20] W. Wei, X. Cui, W. Chen, D.G. Ivey, Manganese oxide-based materials as electrochemical supercapacitor electrodes, Chem. Soc. Rev. 40 (2011) 1697–1721.
[21] H.Y. Chen, R. Al-Oweini, J. Friedl, C.Y. Lee, L. Li, U. Kortz, U. Stimming, M. Srinivasan, A Novel SWCNT-polyoxometalate nanohybrid material as an electrode for electrochemical supercapacitors, Nanoscale 7 (2015) 7934–7941.
[22] M. Skunik, M. Chojak, I.A. Rutkowska, P.J. Kulesza, Improved capacitance characteristics during electrochemical charging of carbon nanotubes modified with polyoxometallate monolayers, Electrochim. Acta 53 (2008) 3862–3869.
[23] G.M. Suppes, C.G. Cameron, M.S. Freund, A polypyrrole/phosphomolybdic acid//poly(3,4-ethylenedioxythiophene)/phosphotungstic acid asymmetric supercapacitor, J. Electrochem. Soc. 157 (2010) A1030–A1034.
[24] X. Lu, Y. Zeng, M. Yu, T. Zhai, C. Liang, S. Xie, M. Balogun, Y. Tong, Oxygen-deficient hematite nanorods as high-performance and Novel negative electrodes for flexible asymmetric supercapacitors, Adv. Mater. 26 (2014) 3148–3155.
[25] P. Yang, X. Xiao, Y. Li, Y. Ding, P. Qiang, X. Tan, W. Mai, Z. Lin, W. Wu, T. Li, H. Jin, P. Liu, J. Zhou, C.P. Wong, Z.L. Wang, Hydrogenated ZnO core-shell nanocables for flexible supercapacitors and self-powered systems, ACS Nano 7 (2013) 2617–2626.
[26] X.H. Lu, G.M. Wang, T. Zhai, M.H. Yu, S.L. Xie, Y.C. Ling, C.L. Liang, Y.X. Tong, Y. Li, Stabilized TiN nanowire arrays for high-performance and flexible supercapacitors, Nano Lett. 12 (2012) 5376–5381.
[27] M.F. El-Kady, V. Strong, S. Dubin, R.B. Kaner, Laser scribing of high-performance and flexible graphene-based electrochemical capacitors, Science 335 (2012) 1326–1330.
[28] W. Zilong, Z. Zhu, J. Qiu, S. Yang, High performance flexible solid-state asymmetric supercapacitors from MnO_2/ZnO core–shell nanorods//specially reduced graphene oxide, J. Mater. Chem. C 2 (2014) 1331–1336.
[29] X. Lu, M. Yu, G. Wang, T. Zhai, S. Xie, Y. Ling, Y. Tong, Y. Li, H-TiO_2@MnO_2//H-TiO_2@C core-shell nanowires for high performance and flexible asymmetric supercapacitors, Adv. Mater. 25 (2013) 267–272.
[30] W. Chen, R.B. Rakhi, H.N. Alshareef, Morphology-dependent enhancement of the pseudocapacitance of template-guided tunable polyaniline nanostructures, J. Phys. Chem. C 117 (2013) 15009–15019.
[31] S. Roldan, C. Blanco, M. Granda, R. Menendez, R. Santamaría, Towards a further generation of high-energy carbon-based capacitors by using redox-active electrolytes, Angew. Chem. Int. Ed. 50 (2011) 1699–1701.
[32] D.P. Dubal, J. Suarez-Guevara, D. Tonti, E. Enciso, P. Gomez-Romero, A high voltage solid state symmetric supercapacitor based on graphene–polyoxometalate hybrid electrodes with a hydroquinone doped hybrid gel-electrolyte, J. Mater. Chem. A 3 (2015) 23483–23492.
[33] X. Xiao, X. Peng, H. Jin, T. Li, C. Zhang, B. Gao, B. Hu, K. Huo, J. Zhou, Free-standing mesoporous VN/CNT hybrid electrodes for flexible all-solid-state supercapacitors, Adv. Mater. 25 (2013) 5091–5097.
[34] L.Y. Yuan, X.H. Lu, X. Xiao, T. Zhai, J.J. Dai, F.C. Zhang, B. Hu, X. Wang, L. Gong, J. Chen, C.G. Hu, Y.X. Tong, J. Zhou, Z.L. Wang, Flexible solid-state supercapacitors based on carbon nanoparticles/MnO_2 nanorods hybrid structure, ACS Nano 6 (2012) 656–661.
[35] X. Lu, M. Yu, T. Zhai, G. Wang, S. Xie, T. Liu, C. Liang, Y. Tong, Y. Li, High energy density asymmetric quasi-solid-state supercapacitor based on porous vanadium nitride nanowire anode, Nano Lett. 13 (2013) 2628–2633.
[36] M. Sluyters-Rehbach, Impedances of electrochemical systems: terminology, nomenclature and representation-Part I: cells with metal electrodes and liquid solutions, Pure Appl. Chem. 66 (1994), 1831–1831.
[37] L. Pan, G. Yu, D. Zhai, H.R. Lee, W. Zhao, N. Liu, H. Wang, B.C.K. Tee, Y. Shi, Y. Cui, Z. Bao, Hierarchical nanostructured conducting polymer hydrogel with high electrochemical activity, Proc. Natl. Acad. Sci. 109 (2012) 9287–9292.
[38] B. Conway, V. Birss, J. Wojtowicz, The role and utilization of pseudocapacitance for energy storage by supercapacitors, J. Power Sources 66 (1997) 1–14.

Supporting information

Ultrahigh energy density supercapacitors through a double hybrid strategy

Deepak P. Dubal,[a, b] Bhawna Nagar,[a] Jullieth Suarez-Guevara,[a] Dino Tonti,[c] Eduardo Enciso,[d] Pablo Palomino,[d] Pedro Gomez-Romero [a]***

[a]*Catalan Institute of Nanoscience and Nanotechnology (ICN2), CSIC and The Barcelona Institute of Science and Technology, Campus UAB, Bellaterra, 08193 Barcelona, Spain*

[b]*School of Chemical Engineering, The University of Adelaide, Adelaide, South Australia 5005, Australia*

[c]*ICMAB (CSIC), Campus UAB E-08193 Bellaterra, Barcelona, Spain*

[d]*Departamento de Química Física I, Facultad de Ciencias Químicas, Universidad Complutense de Madrid (UCM) Campus Moncloa, Madrid, Spain*

CORRESPONDING AUTHOR FOOTNOTE

Dr. Deepak Dubal, and Prof. Pedro Gomez-Romero

Tel.: +349373609/+34937373608 Fax: + 34936917640

E-mail: dubaldeepak2@gmail.com (D. Dubal),

pedro.gomez@icn2.cat (P. Gomez-Romero)

Supporting information S1

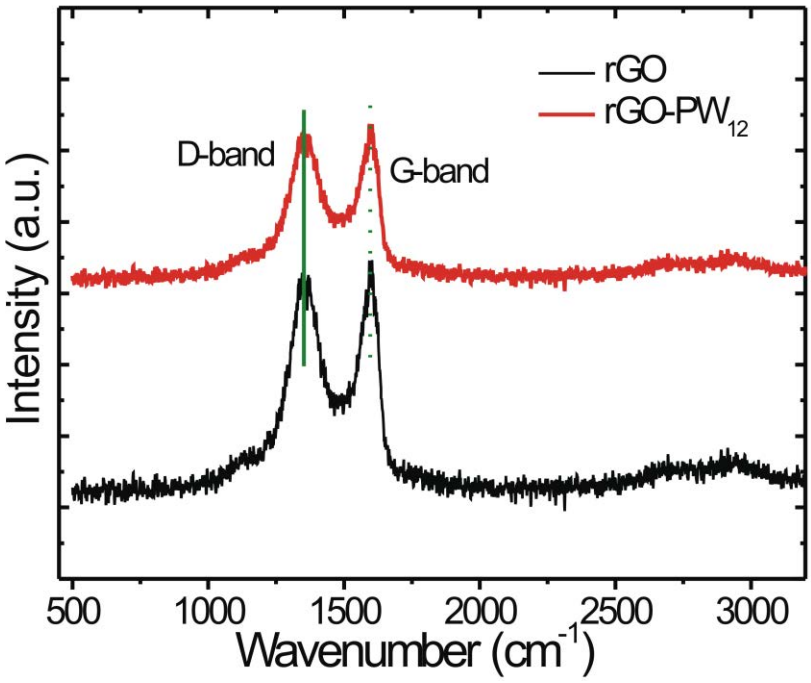

Fig. S1 Raman Spectra for rGO and rGO-PW_{12} hybrid materials

Supporting information S2

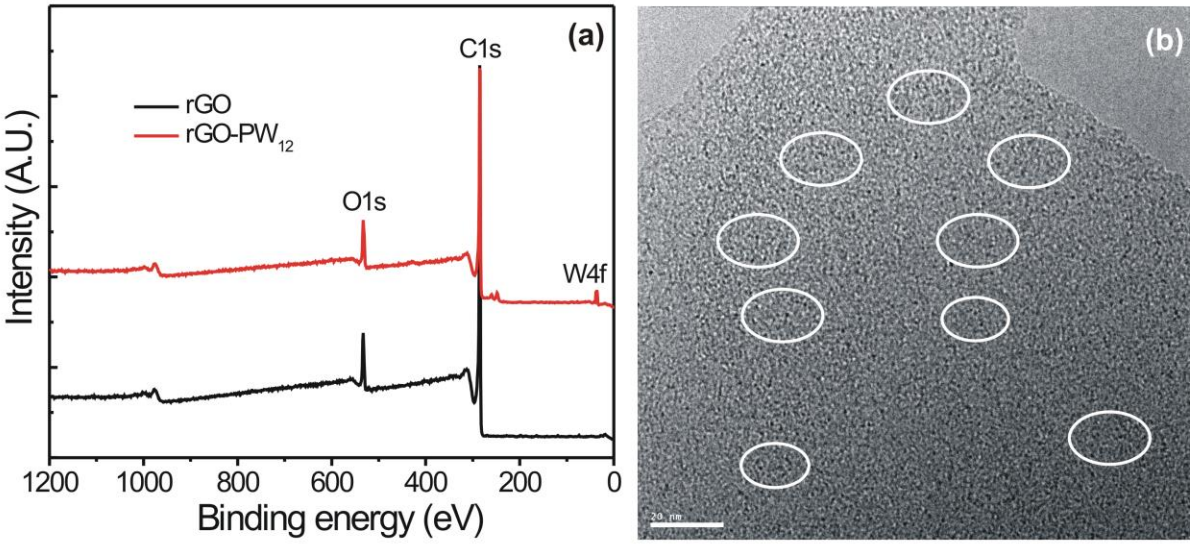

Fig. S2 (a) Full XPS spectra of rGO and rGO-PW_{12} samples, (b) HR-TEM image of rGO-PW_{12} sample.

Supporting information S3

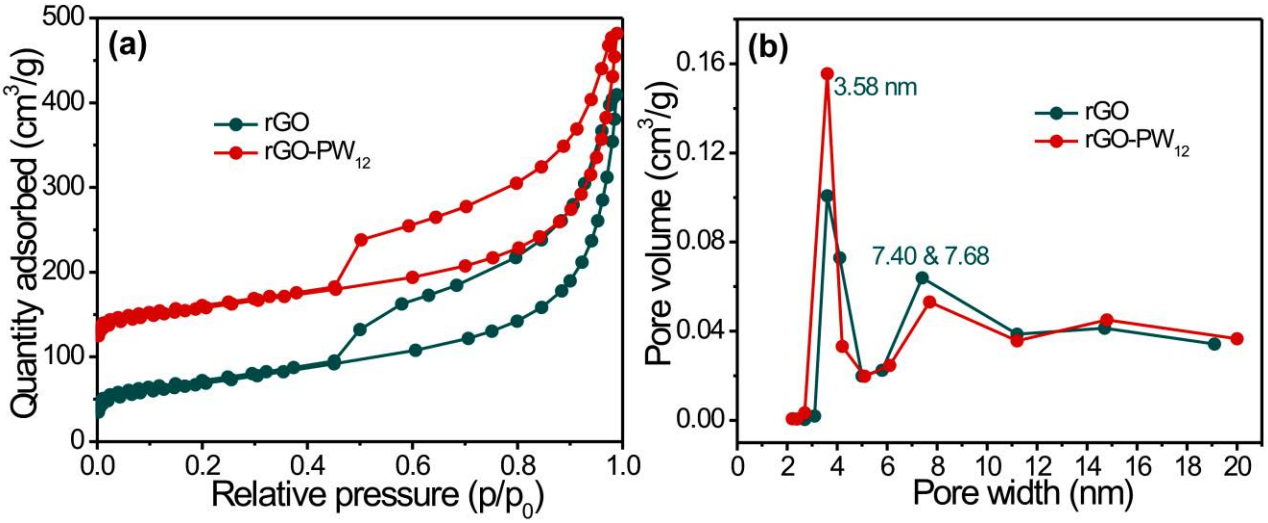

Figure S3 (a) Nitrogen adsorption-desorption isotherm of rGO and rGO-PW_{12} samples with (b) corresponding pore size distribution curves

Supporting information S4

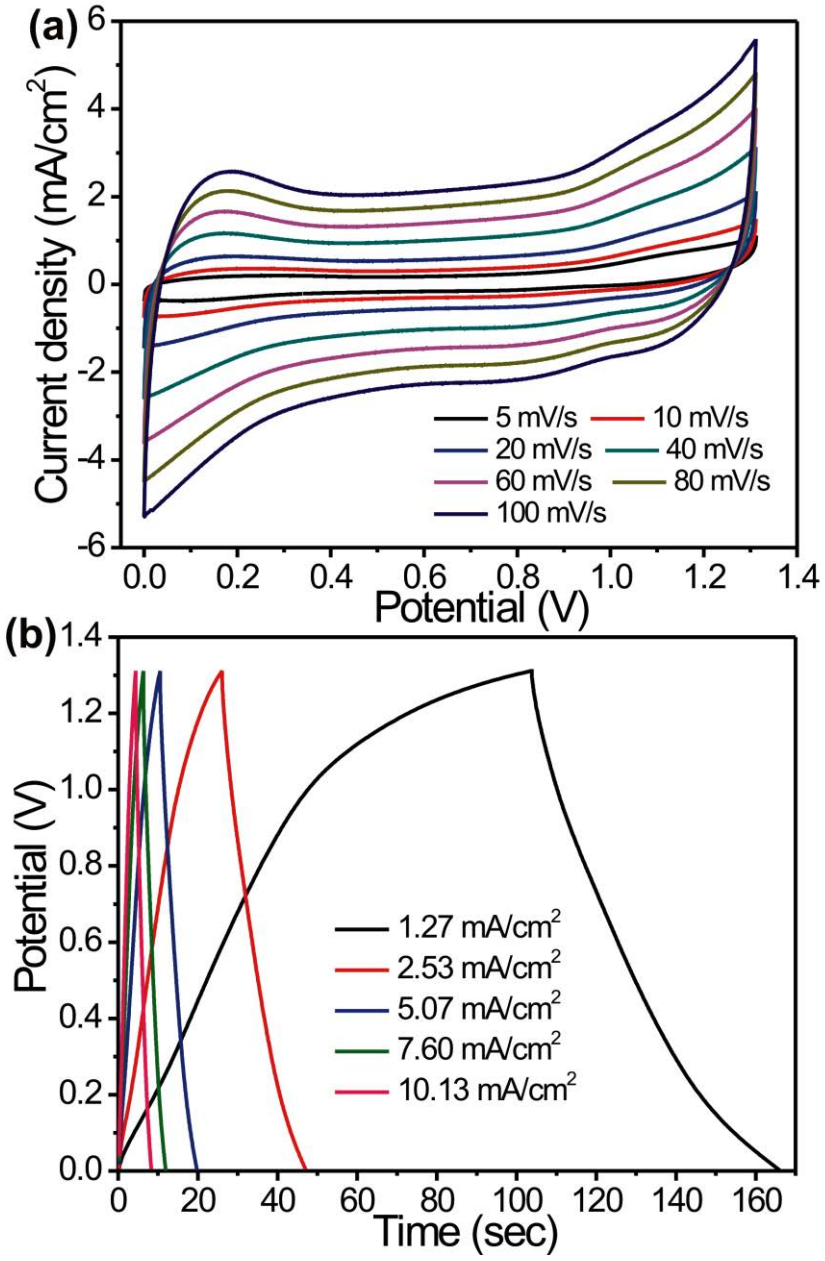

Figure S4 (a) Cyclic voltammetry curves at different scan rates, (b) Charge-discharge curves at different current densities for rGO based symmetric cell

Supporting information S5

Calculations:

The cell (device) capacitance (*C*) and volumetric capacitance of the symmetric devices were calculated from their CVs according to the following equation:

$$C_{cell} = \frac{Q}{\Delta V} \quad (1)$$

$$C_A = \frac{Q}{A \times \Delta V} \quad \text{and} \quad C_V = \frac{Q}{V \times \Delta V} \quad (2)$$

where, C_A and C_V are areal and volumetric capacitances, respectively. *Q* (C) is the average charge during the charging and discharging process, V is the volume (cm^3) of the whole device (The area and thickness of our symmetric cells is about 0.785 cm^2 (Area, $A=\pi r^2$, $3.14 \times (0.5)^2$) and 0.088 cm. Hence, the whole volume of device is about 0.069 cm^3, *ΔV* (V) is the voltage window. It is worth mentioning that the volumetric capacitances were calculated taking into account the volume of the device stack. This includes the active material, the flexible substrate and the separator with electrolyte.

Alternatively, the specific capacitance was estimated from the following equation:

$$C = \frac{I \cdot \int V \cdot dt}{m \cdot V^2} \quad (3)$$

where, *I* is the discharge current, *m* is the mass of the active material (both electrodes) and *V* is the potential window excluding the *iR* drop.

The volumetric (C_V) capacitance was further calculated by replacing 'm' by v- volume (cm^3) of the whole device (the whole volume of our device is about 0.069 cm^3), *Δt* is the discharging time, *ΔV* (V) is the voltage window.

Volumetric energy (E, Wh/cm^3) and power density (P, W/cm) of the devices were obtained from the following equations:

$$E = \frac{1}{2 \times 3600} C_V \Delta V^2 \quad (4)$$

$$P = \frac{3600 \times E}{\Delta t} \quad (5)$$

where *E* (Wh/cm^3*)* is the energy density, *CV* is the volumetric capacitance obtained from Equation (5) and *ΔV* (V) is the voltage window, P (W/cm^3) is the power density.

Furthermore, the capacitive behavior of $RuCo_2O_4$ can also be evaluated from EIS technique by calculating the real and imaginary capacitance at a corresponding frequency using following equations:

$$C(\omega) = C'(\omega) - jC''(\omega) \quad (6)$$

$$\text{Where, } C'(\omega) = \frac{Z''(\omega)}{\omega |Z(\omega)|^2} \quad (7)$$

$$C''(\omega) = \frac{Z'(\omega)}{\omega |Z(\omega)|^2} \quad (8)$$

where '*Z'* the complex impedance represented as *Z* (ω) = *Z*' (ω) + *Z*" (ω) and ω = 2πf where *f* is the frequency. *C*' (ω) is the real accessible capacitance of the electrode while *C*" (ω) is the energy loss due to the irreversible processes of the electrodes, *Z*' and *Z*" are the real and imaginary parts of the Nyquist plot, respectively.

Supporting information S6

Table 1 Comparison on supercapacitive values of POM as well as metal oxide based electrodes

Electrode	Device	Electrolyte	Capacitance	Ref.
SWCNT-TBA-PV_2Mo_{10}	Symmetric	H_2SO_4	317 mF/cm^2 at 0.1 mA/cm^2	[1]
$H_3PMo_{12}O_{40}$/MWCNT	Symmetric	H_2SO_4	38 F/g at 5 V/s	[2]
$H_3PMo_{12}O_{40}$/PPy//$H_3PW_{12}O_{40}$/PEDOT	Asymmetric	H_2SO_4	31 F/g at 1 mA	[3]
$H_3PMo_{12}O_{40}$/PAni	Symmetric	H_2SO_4	195 mF/cm^2 at 0.125 mA/cm^2	[4]
PAni/SiW_{12}	Symmetric	H_2SO_4	1.8 mF/cm^2 0.5 mA/cm^2	[5]
PAni/PW_{12}	Symmetric	H_2SO_4	15 mF/cm^2 0.5 mA/cm^2	[5]
MnO_2//Fe_2O_3	Asymmetric	Gel-electrolyte	1.21 F/cm^3 at 10 mV/s	[6]
ZnO@MnO_2	Symmetric	Gel-electrolyte	0.325 F/cm^3 at 0.5 mA/cm^2	[7]
TiN	Symmetric	Gel-electrolyte	0.33 F/cm^3 at 2.5 mA/cm^3	[8]
Graphene	Symmetric	Gel-electrolyte	0.42 F/cm^3 at 0.2 mA/cm^2	[9]
ZnO@MnO_2//graphene	Asymmetric	Gel-electrolyte	0.52 F/cm^3 at 10 mV/s	[10]

H-TiO_2@MnO_2//TiO_2@C	Asymmetric	Gel-electrolyte	0.70 F/cm^3 at 10 mV/s	[11]
rGO-PW_{12}	*Symmetric*	*Gel-electrolyte*	*2.95 F/cm^3 (260 mF/cm^2) at 1.27 mA/cm^2*	*Present work*
rGO-PW_{12} with HQ doping	*Symmetric*	*HQ doped gel-electrolyte*	*6.72 F/cm^3 (592 mF/cm^2) at 1.27 mA/cm^2*	*Present work*

References:

[1] H. Y. Chen, R. Al-Oweini, J. Friedl, C. Y. Lee, L. Li, U. Kortz, U. Stimming, M. Srinivasan, *Nanoscale*, **2015**, 7, 7934-7941.

[2] M. Skunik, M. Chojak, I. A. Rutkowska, P. J. Kulesza, *Electrochim. Acta*, **2008**, 53, 3862-3869.

[3] G. M. Suppes, C. G. Cameron, M. S. Freund, *J. Electrochem. Soc.,* **2010**, 157**,** A1030-A1034

[4] P. Gomez-Romero, M. Chojak, A. Cuentas-Gallegos, J. A. Asensio, P. J. Kulesza, N. Casan-Pastor, M. Lira-Cantu, *Electrochem. Commun.*, **2003**, 5, 149-153

[5] A. Cuentas-Gallegos, M. Lira-Cantu, N. Casan-Pastor, P. Gomez-Romero, *Adv. Funct. Mater.*, **2005**, 15, 1125-1133.

[6] X. Lu, Y. Zeng, M. Yu, T. Zhai, C. Liang, S. Xie, M. Balogun, Y. Tong, *Adv. Mater.* **2014**, *26*, 3148-3155.

[7] P. Yang, X. Xiao, Y. Li, Y. Ding, P. Qiang, X. Tan, W. Mai, Z. Lin, W. Wu,; T. Li, H. Jin, P. Liu, J. Zhou, C. P. Wong, Z. L. Wang, *ACS Nano* **2013**, 7, 2617-2626

[8] X. H. Lu, G. M. Wang, T. Zhai, M. H. Yu, S. L. Xie, Y. C. Ling, C. L. Liang, Y. X. Tong, Y. Li, *Nano Lett.* **2012**, 12, 5376-5381.

[9] M. F. El-Kady, V. Strong, S. Dubin, R. B. Kaner, *Science* **2012**, 335, 1326-1330.

[10] W. Zilong, Z. Zhu, J. Qiu, S. Yang, *J. Mater. Chem. C,* **2014**, 2, 1331-1336.

[11] X. Lu, M. Yu, G. Wang, T. Zhai, S. Xie, Y. Ling, Y. Tong, Y. Li, *Adv. Mater.* **2013**, *25*, 267-272.

Supporting information S7

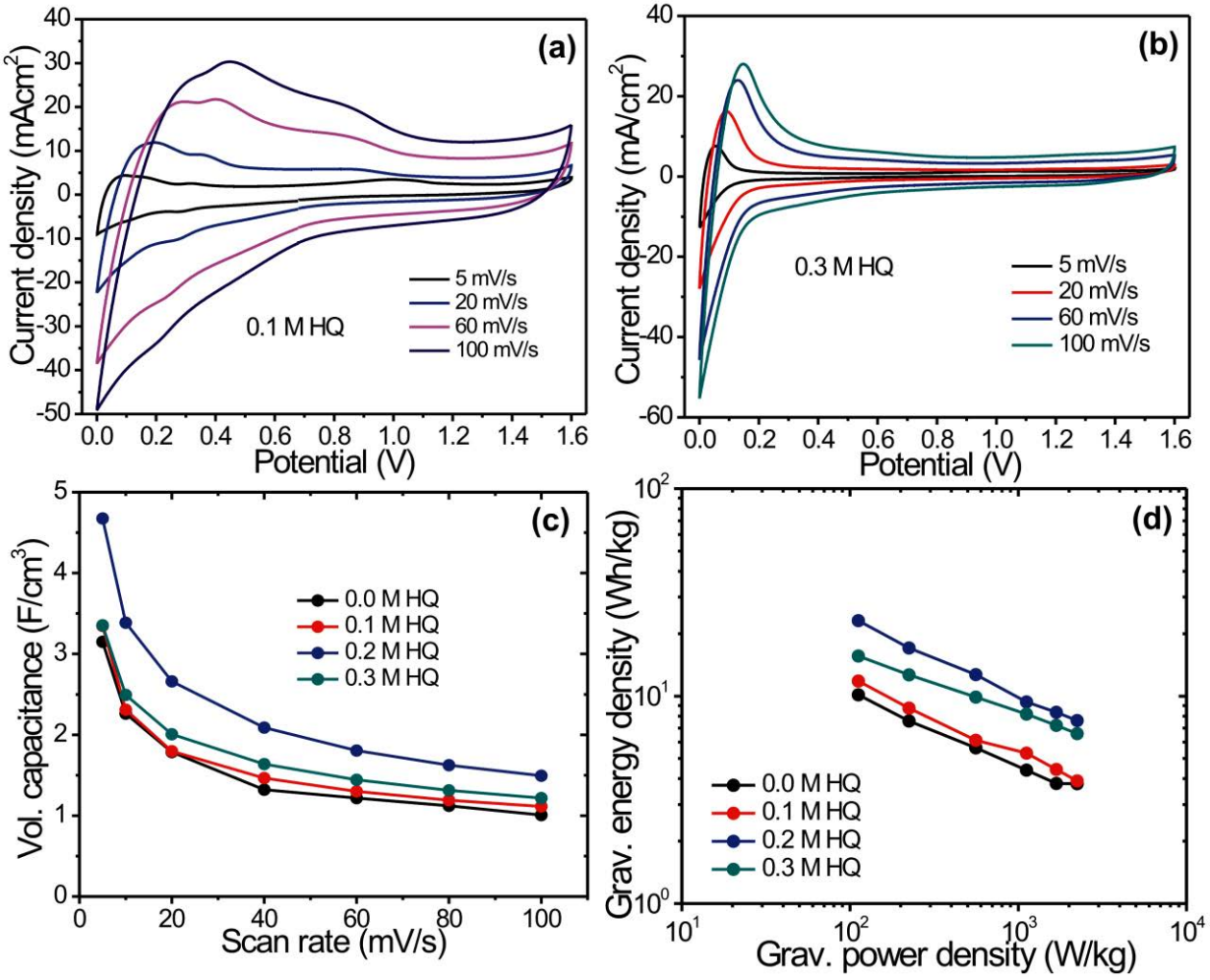

Figures S7 (a, b) CV curves of rGO-PW_{12} symmetric cell at different scan rates with HQ doped polymer gel-electrolyte with different concentrations. (c) Variation of volumetric capacitances of rGO-PW_{12} symmetric cell with scan rate for HQ doped polymer gel-electrolyte of different concentration, (d) Summary of volumetric energy and power of rGO-PW_{12} cell in Ragone plot for HQ doped polymer gel-electrolyte of different concentration

Supporting information S8

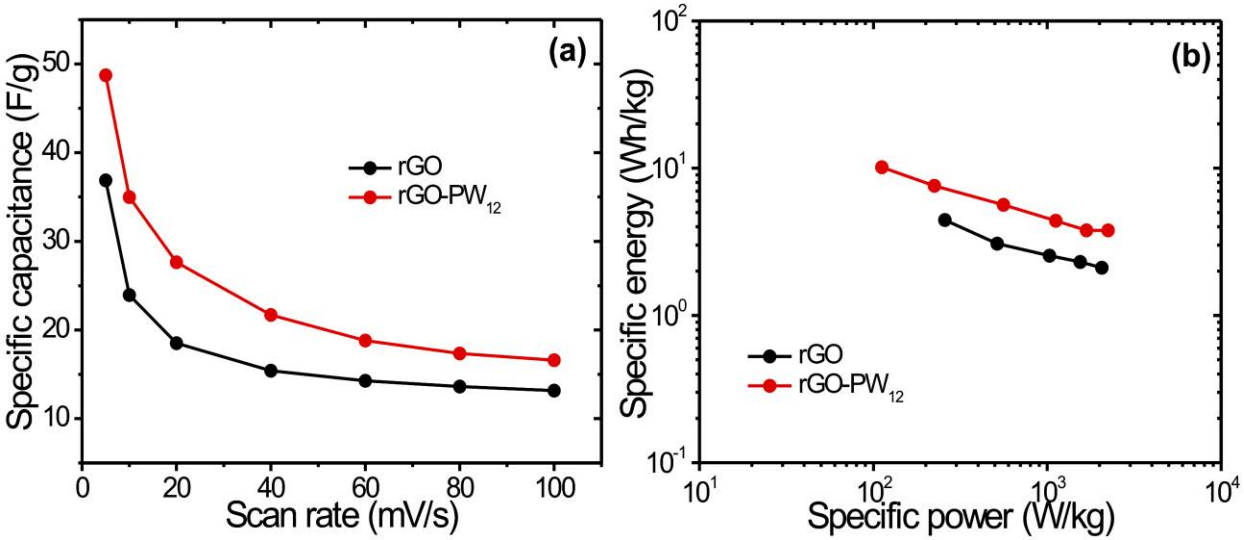

Figure S8 (a) Variation of specific capacitance with scan rates for rGO and rGO-PW_{12} symmetric cells, (b) Summary of specific energy and specific power for rGO and rGO-PW_{12} symmetric cells

Supporting information S9

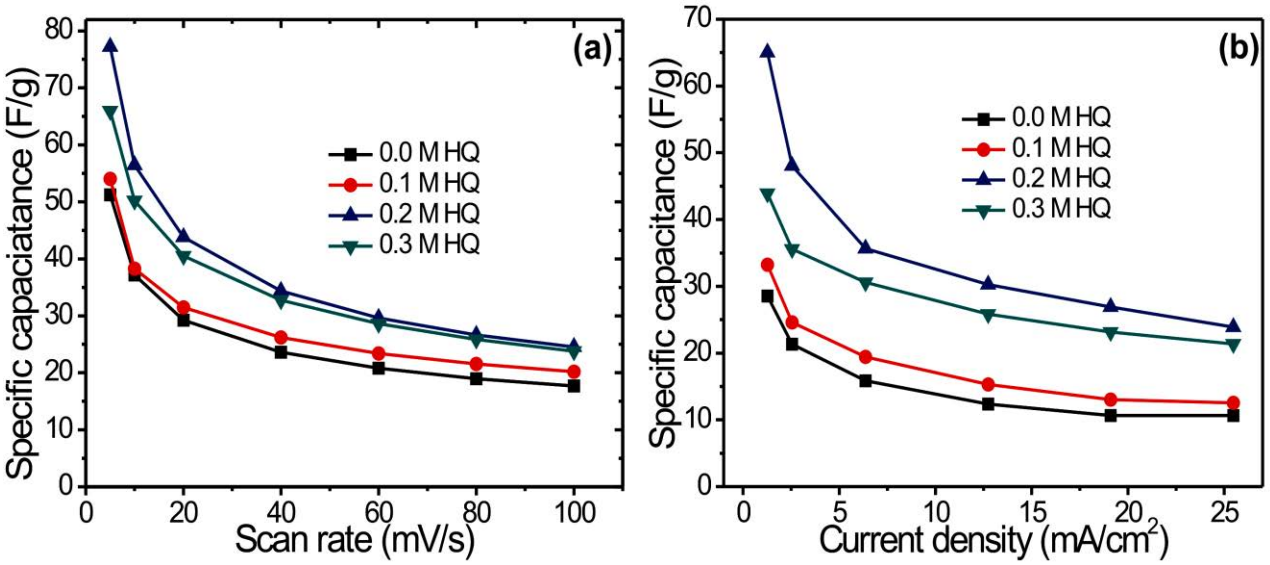

Figure S9 (a, b) Variation of specific capacitance of rGO-PW_{12} symmetric cells with scan rates and current densities for HQ doped gel electrolyte of different concentrations, respectively.

Article 2: Design and Fabrication of Printed Paper-Based Hybrid Micro-Supercapacitor by using Graphene and Redox-Active Electrolyte

Bhawna Nagar, Deepak P. Dubal, Luis Pires, Arben Merkoçi and Pedro Gómez-Romero

ChemSusChem 2018, 11, 1849 – 1856

ChemPubSoc Europe

DOI: 10.1002/cssc.201800426

CHEMSUSCHEM Full Papers

Design and Fabrication of Printed Paper-Based Hybrid Micro-Supercapacitor by using Graphene and Redox-Active Electrolyte

Bhawna Nagar,[a, b] Deepak P. Dubal,[a, c] Luis Pires,[b] Arben Merkoçi,[b, d] and Pedro Gómez-Romero*[a]

Inspired by future needs of flexible, simple, and low-cost energy storage devices, smart graphene-based micro-supercapacitors on conventional Xerox paper substrates were developed. The use of redox-active species (iodine redox couple) was explored to further improve the paper device's performance. The device based on printed graphene paper itself already had a remarkable maximum volumetric capacitance of 29.6 mF cm^{-3} (volume of whole device) at 6.5 mA cm^{-3}. The performance of the hybrid electrode with redox-active potassium iodide at the graphene surface was tested. Remarkably, the hybrid device showed improved volumetric capacitance of 130 mF cm^{-3}. The maximum energy density for a graphene + KI device in H_2SO_4 electrolyte was estimated to be 0.026 mWh cm^{-3}. Thus, this work offers a new simple, and lightweight micro-supercapacitor based on low-cost printed graphene paper, which will have great applications in portable electronics.

Introduction

The demand for highly efficient and cost-effective energy storage systems is on a steep rise. Consequently, research into energy storage technologies is trying to keep pace through the development of new materials and devices. Electrochemical energy storage devices—primarily batteries and supercapacitors—are some of the most promising technologies in this relentless race. The batteries work on a bulk storage mechanism, exhibiting a high energy density but a low power density and less cycling stability, whereas supercapacitors work on storing charges through non-faradaic surface adsorption and/or faradaic redox reactions (pseudocapacitive) and feature high power density with excellent cycling stabilities.[1,2] Graphene is a well-known two-dimensional (2D) nanocarbon material with outstanding thermal and electrical conductivity and high mechanical and chemical stability. Owing to its high surface area, graphene has a very high inherent electric-double-layer capacitance.[3] The calculated theoretical specific capacitance of single-layered graphene is approximately 21 μF cm^{-2} or 550 F g^{-1}.[4] In practice, however, these values are lower for several reasons, among which, the re-stacking of graphene layers, which hides and limits its active area, is one of the most detrimental. Thus, effective microstructuring of graphene electrodes is one of the primary approaches towards high-performance graphene supercapacitors. The other main approach is the reinforcement of its energy storage capability by hybridization, that is, through the incorporation of faradaic charge-storage components. Redox-active species can be incorporated into the device by means of three different approaches, namely, i) covalent attachment to graphene electrodes, ii) adsorption onto the capacitive carbon-based electrodes or iii) they can be added to the electrolyte, turning it into a hybrid redox-active electrolyte.

In this study, we designed a high-performance graphene micro-supercapacitor by tackling both the shaping of graphene electrodes by direct printing on a paper substrate and the improvement of energy storage by incorporation of a redox-active species, potassium iodide (KI). KI is a remarkably non-toxic and environmentally friendly redox-active species compared to other redox species used in energy storage research, like hydroquinone, catechol, ferro/ferricyanide etc. KI enhances the capacitance of the device by forming different redox pairs of iodide on the surface of the electrode $3I^-/I_3^-$, $2I^-/I_2$, $2I_3^-/3I_2$ and $I_2/2IO_3^-$.[5]

Flexibility and portability are two widely expected characteristics for modern industrial electronic technologies, which enable the fabrication a variety of sophisticated applications, such as flexible touchscreens, implantable sensors, flexible mobile phones, and flexible OLEDs.[6,7] Paper is among the

[a] B. Nagar, Dr. D. P. Dubal, Prof. P. Gómez-Romero
Novel Energy-Oriented Materials Group, Catalan Institute of Nanoscience and Nanotechnology (ICN2), CSIC and The Barcelona Institute of Science and Technology
Campus UAB, 08193 Bellaterra, Barcelona (Spain)
E-mail: pedro.gomez@icn2.cat

[b] B. Nagar, Dr. L. Pires, Prof. A. Merkoçi
Nanobioelectronics and Biosensors Group, Catalan Institute of Nanoscience and Nanotechnology (ICN2), CSIC and The Barcelona Institute of Science and Technology
Campus UAB, 08193 Bellaterra, Barcelona (Spain)

[c] Dr. D. P. Dubal
School of Chemical Engineering
University of Adelaide
Adelaide, South Australia 5005 (Australia)

[d] Prof. A. Merkoçi
ICREA
Pg. Lluís Companys, 23, Barcelona 08010 (Spain)

best-known substrate materials for such applications, as it is flexible, highly cost-effective, environmentally compatible, and easy to handle. It is composed of cellulose, with a size of 210 mm × 297 mm (DinA4 paper) and diameter of 20 μm. Papers has found a wide range of applications in electronics, solar cells, and energy devices and is also highly suitable for printing.[8]

Various printing techniques have been used for the fabrication of flexible electrodes for energy storage application, including roll-to-roll, screen printing, inkjet printing, and transfer techniques.[9–11] However, all of these printing methods have pros and cons and it is therefore very important to use the most appropriate printing technique for each specific application. In this study, a modified transfer technique using a wax printer and stamping mechanism was used in which a pattern was drawn over a nitrocellulose filter membrane and graphene was filtered through it and the pattern stamped over paper. This technique does not allow graphene sheets to move through the paper and they remain at the surface while the interior of the paper can be used as an electrolyte absorbent, as well as a separator. Thus, this strategy provides a unique means of fabrication for paper-based supercapacitors, which can be used in several portable and wearable applications.

We have designed and engineered a smart paper-based graphene supercapacitor device from the point of view of feasibility in industries that require easy and cheap fabrication along with enhanced supercapacitive properties in an aqueous electrolyte. The motivation is to enhance the capacitance and voltage of supercapacitors using aqueous electrolytes by shifting the oxygen evolution potential. In this context, we have used potassium iodide as a redox-active species (iodide/iodine redox pair), which stimulates the capacitance and widen the voltage window.[12–15] Most of the previous work has focused on the introduction of KI species in the electrolyte.[16–19] However, in the present study, we have investigated the effect of KI addition on the surface of printed graphene electrodes.

Results and Discussion

Morphological analysis

The transmission electron microscopy (TEM) image of the graphene nanosheet (Figure 1 a) shows that the nanosheets are thin and transparent with extra-large size and its selected-area electron-diffraction (SAED) pattern (Figure 1b) confirms the formation of graphene. Figure 1 c shows the scanning electron microscopy (SEM) image of a usual copy paper printed with graphene from the top view and a cross sectional view. The morphology of the paper is very rough and we took the advantage of this surface roughness to build an energy storage device that can absorb more electrolyte than the semipermeable filter membranes and can hence provide increased access to the exposed stamp-printed graphene. The SEM image in Figure 1 d shows the uniform printing of graphene sheets over the paper surface. With this printing technique, the graphene stays only at the surface of the paper and does not penetrate through to the other side, allowing us to stamp the prints on both sides of the paper, which serves as both a substrate and a separator (see cross-sectional view, Figure 1 c). Owing to strong binding forces in the paper, the adhesion of graphene layers to the paper is very strong and can be retained throughout a rubbing test.

Raman spectroscopy was used for verifying graphene layers. The distinctive G and 2D peaks appeared at 1580 and

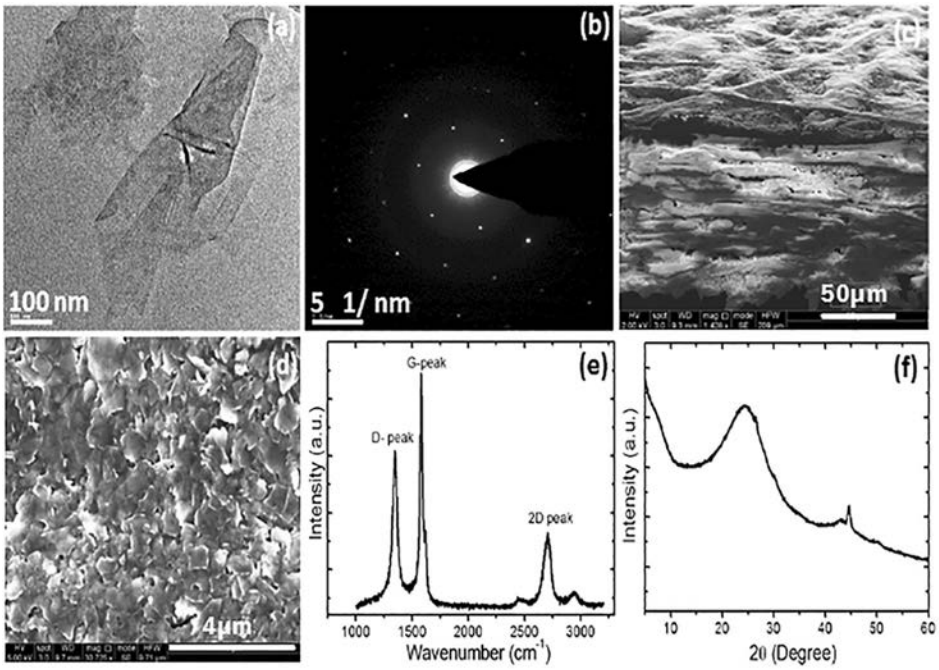

Figure 1. Investigation of the morphology of graphene used: a) TEM image of the graphene sheets. b) SAED pattern. c, d) SEM images of cross-section and top view of graphene print. e) Raman spectra of the graphene sheets. f) Corresponding XRD pattern.

2702 cm^{-1}, respectively, and correspond to few-layered graphene with a D-band at 1350 cm^{-1}, indicating few defects (Figure 1 e). The I_G/I_{2D} ratio suggested the formation of few-layered graphene.[20] The narrow 2D peak appears at 2700 cm^{-1}, which is different from 2D peak of graphite as it is a mixture of $2D_1$ and $2D_2$.[21,22] Moreover, the X-ray diffraction (XRD) pattern (Figure 1 f) showed a broad peak at 24.5°, which is associated with the characteristic (002) plane of graphene and represents an interlayer distance of 0.35 nm.[23]

Figure 2 shows some of the steps involved in the printing and fabrication of a device. Figure 2 a–c shows photographs of graphene printed on both sides of the paper, suggesting a highly flexible electrode design to be used in supercapacitors. Figure 2 d shows a schematic diagram of the supercapacitor cell assembly for testing.

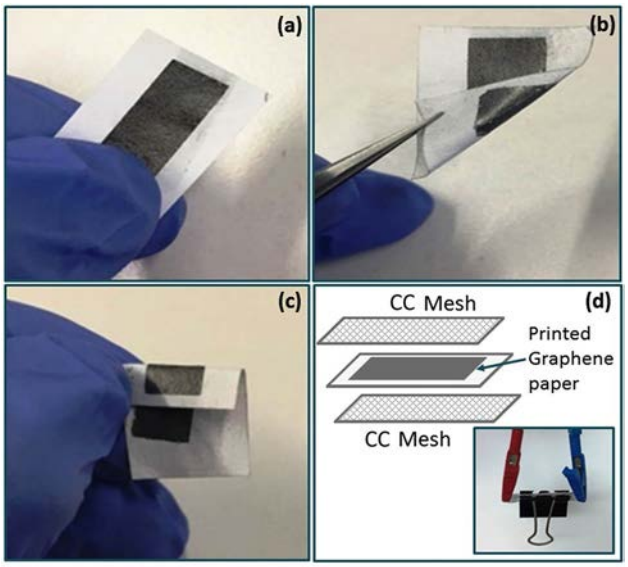

Figure 2. a–c) Graphene printed on both sides of the flexible paper. d) Schematic diagram of the device assembly. Inset shows an assembled device used for electrochemical measurements.

Electrochemical testing

All electrochemical testing of the device was performed in a two-electrode system by using 1 M H_2SO_4 electrolyte (see the Supporting Information, Figure S1). Figure 3 a shows the cyclic voltammetry (CV) curves of the paper based micro-supercapacitor device in a conventional 1 M H_2SO_4 electrolyte at various scan rates ranging from 5 to 100 mV s^{-1} in the voltage range of 0–0.8 V. The CV curve shapes are ideally rectangular with perfect symmetry, which corresponds to the inherent electric-double-layer capacitance (EDLC) of graphene sheets. The paper substrate did not interfere in the performance of the device and the capacitance increased with increasing scan rate. To assess the overall device performance in terms of energy storage, galvanostatic charge–discharge measurements were carried out at current densities from 6.5 to 10.5 mA cm^{-3} (Figure 3 b). The volumetric capacitance calculated from charge–discharge curves [see Experimental Section, Eqs. (5) and (6)] were 15.48, 19.6, 24, and 29.6 mF cm^{-3} at current densities of 6.5, 7.8, 9.2, and 10.5 mA cm^{-3}, respectively (areal capacitances were 1.2, 1.4, 1.8, and 2.2 mF cm^{-2} at 0.79, 0.69, 0.59, and 0.49 mA cm^{-2}, respectively). There is a decrease in the capacitance with applied current density with a maximum volumetric capacitance of 29.6 mF cm^{-3} (areal capacitance was 2.2 mF cm^{-2}) at 6.5 mA cm^{-3} in H_2SO_4 electrolyte. The calculated capacitance is significantly higher than that for some other reported supercapacitor devices. For example, Wu et al. reported a capacitance of 0.95 mF cm^{-2} for an interdigitated reduced graphene oxide hydrogel-patterned micro-supercapacitor over a metallic substrate.[24] Pech and co-workers reported a capacitance of 2.1 mF cm^{-2} for an inkjet-printed graphene micro-supercapacitor with an Et_4NBF_4 electrolyte,[25] whereas Bae et al. attained around 0.4 mF cm^{-2} areal capacitance by using graphene and ZnO nanowires.[26] Similarly, Gao et al. developed a flexible solid-state graphene supercapacitor with a capacitance of 12.4 μF cm^{-2}.[27]

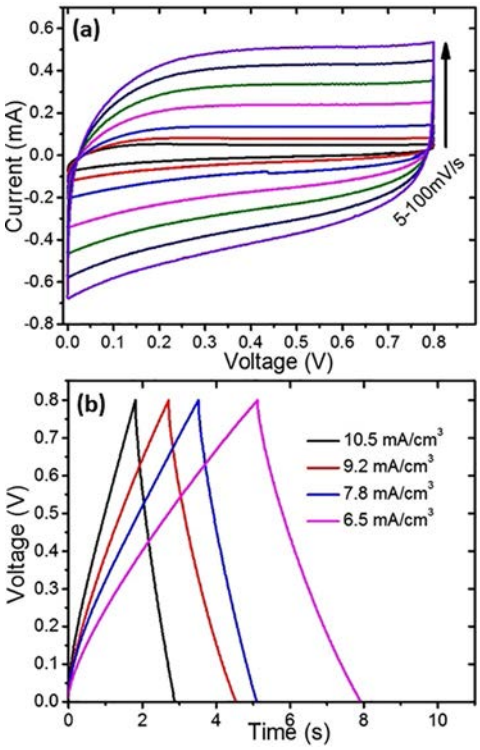

Figure 3. a) Cyclic voltammogram of the graphene device in conventional H_2SO_4 electrolyte. b) Charge–discharge curves.

The general goal of hybrid materials design is to combine the properties and identify synergies between two different materials. In energy storage devices, hybrid materials enhance the electrochemical performance of the device by complementing capacitive with pseudocapacitive materials.[2] In the present work, we adsorbed a redox-active species—particular potassium iodide—on the surface of graphene to improve the performance of the final device. We tested three different concentrations of KI adsorbed onto graphene and compared the results to those for the graphene + H_2SO_4 system. To confirm the presence and adsorption retention of iodide species on the surface of the graphene electrode, we carried out X-ray

photoelectron spectroscopy (XPS) of our positive (working) electrode at different stages, that is, before cycling, after the first charge, and after the first discharge (Figure 4a, b). The XPS spectra suggest the presence of C, O, and I peaks in all three graphene samples (Figure 4a). The two apparent I3d peaks at 619.4 and 631.0 eV can be assigned to $I3d_{5/2}$ and $I3d_{3/2}$ states, respectively (Figure 4b). The signal for $I3d_{5/2}$ at 619.6 eV correspond to bonding between carbon and iodine species, such as C–I and C–I^+–C as the oxidation products of I^- during the reaction process.[28,29] The amounts of iodide species adsorbed onto the graphene surface were found to be 86 at%, which slightly decreased after the first charge (to around 78 at%) and thereafter remained constant (at around 77 at%). These results suggest that only a very small percentage of the iodide species dissolved in the acidic electrolyte in the beginning, and the amount remained constant thereafter, indicating a very efficient attachment of iodide on the graphene surface. The electrochemical performances of the as-assembled device with iodide species adsorbed on graphene are presented in Figure 5 (for further details, see Figures S2–S4). Figure 5a shows the cyclic voltammetry (CV) curves for printed graphene device in conventional H_2SO_4 and KI-doped graphene electrode at a scan rate of 10 mV s^{-1}. The area under the CV curves increases significantly with the concentration of KI, suggesting a remarkable increase in the capacitance of the device. The device can be easily cycled up to 1.2 V, whereas for conventional electrochemical capacitors with aqueous electrolytes the working voltage range varies from 0.6 to 0.8 V.[30] Moreover, the shapes of the CV curves are distorted from the ideal rectangular shapes typical of electric-double-layer capacitors (carbon materials), which confirms the involvement of redox-active species (iodine/iodide) at the electrode/electrolyte interface.

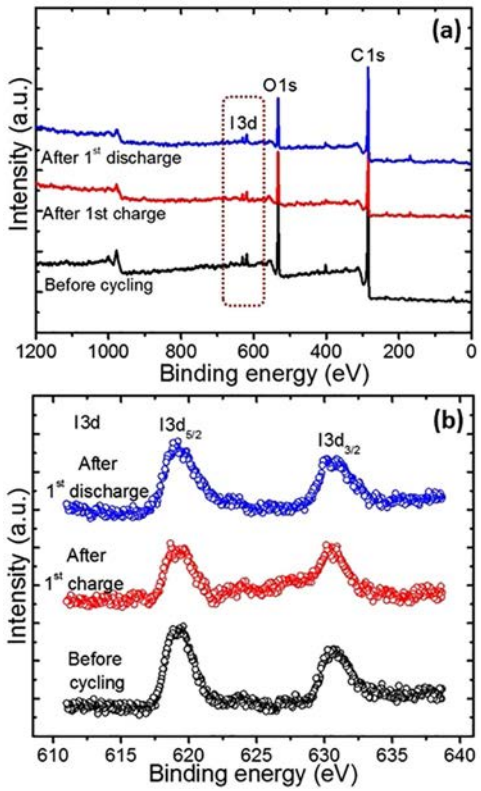

Figure 4. a) XPS spectra of graphene with KI adsorbed before and after electrochemical measurements. b) High-resolution magnification of the I3d signals.

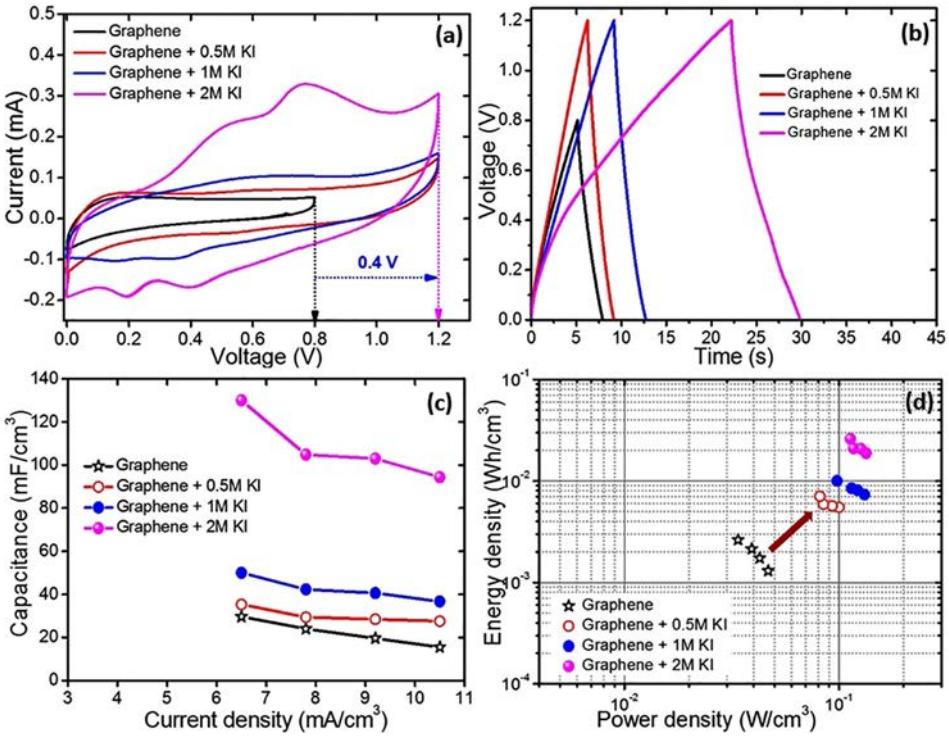

Figure 5. a) CV at 10 mV s^{-1} and b) charge–discharge curves at 6.5 mA cm^{-3} of the graphene device with different concentrations of KI. c) Comparative volumetric capacitance with unmodified graphene and graphene with different KI concentrations at different current values. d) Ragone plot of the device.

The charge storage mechanism of paper-based hybrid micro-supercapacitors is explained as follows: After initiation of the reaction (providing the required potential to the iodide species), both reactants and products (I^- and I_3^- ions) are negatively charged in the aqueous electrochemical oxidation of iodides. These species balance the charges in the electrochemical double layer (EDL) while electrostatically remaining in the positively charged electrode, hence increasing the charge storage capacity. The CV curves show the iodide redox reaction peaks, which are the source of the extra (redox) capacity and can be assigned to the reactions given by Equations (1)–(4) (with Eq. (2) predominating in aqueous media):[12]

$$2\,I^- \rightarrow I_2 + 2\,e^- \quad (1)$$

$$3\,I^- \rightarrow I_3^- + 2\,e^- \quad (2)$$

$$2\,I_3^- \rightarrow 3I_2 + 2\,e^- \quad (3)$$

$$I_2 + 6\,H_2O \rightarrow 2\,IO_3^- + 12\,H^+ + 10\,e^- \quad (4)$$

Considering that the ions can turn into polyions, the possibility of formation of polyiodides (I_3^-/I_5^-) cannot be ruled out, but, according to the Pourbaix diagram for iodine,[31,32] the possibility of their formation is low (it is more favorable in alkaline medium and at slightly higher potentials) and also the iodides have limited tendency for solvation. Moreover, the increase in the operating voltage can be further ascribed to the presence of KI, as reported by Fic et al.[33] The addition of KI extends the hydrogen evolution potential of the working electrode in the negative region and shows redox activity in the positive range. In the present investigation, we took advantage of this characteristic of KI and obtained an extended voltage window for our printed graphene device, although, with the extension of potential at the positive end, the hydrogen storage process becomes aggravated and the total potential window is compromised. However, these ranges can be further enhanced by using asymmetric electrodes, different electrode materials or electrolytes.[34–36]

The galvanostatic charge–discharge curves recorded at 6.5 mA cm^{-3} (Figure 5b) are in good agreement with the CV results (Figure 5a). The device with 2 M KI showed a prolonged discharge time over those with other concentrations, indicating high energy and capacitance. The maximum volumetric capacitance obtained for graphene device with 2 M KI is 130 mF cm^{-3} (9.8 mF cm^{-2}), which is almost 5 times higher than that for the conventional graphene electrode (Figure 5c). In addition, the device achieved maximum energy and power density values of 0.026 mWh cm^{-3} and 13.38 mW cm^{-3}, respectively, in the presence of 2 M KI + graphene in H_2SO_4 (Figure 5d). Among the three concentrations, the device showed maximum efficiency with 2 M KI added to H_2SO_4. To our knowledge, the maximum capacitance and the working potential range observed here are the highest reported to date for a paper-based graphene micro-supercapacitor device with aqueous electrolyte.

Electrochemical impedance spectroscopy (EIS) was carried out on the devices in the frequency range of 100 kHz–100 mHz at electrical open-circuit potential. The Nyquist plot obtained for the micro-supercapacitor device (Figure 6a) indicates that the devices acts like a pure capacitor without any sign of resistor-like behavior that blocks the transfer of charges

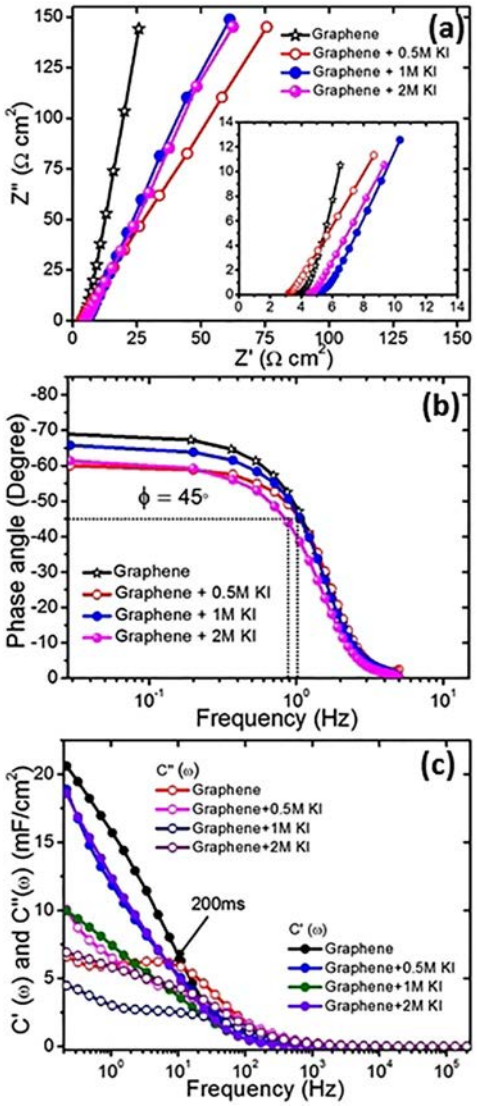

Figure 6. Electrochemical Impedance measurements: a) Nyquist Plot of the device with and enlarged view (inset). b) Bode plot of the micro-supercapacitor. c) Real and imaginary capacitances (*C′* and *C″*) vs. frequency (log *f*) of graphene- and graphene + KI-based micro-supercapacitors in 1 M H_2SO_4.

at the electrode/electrolyte interface. In theory, a vertical line at 90° must be observed as a sign of pure capacitor, but somehow due to few properties of the electrode like roughness, porosity etc., there can be some deviation from the vertical line. Roughness arising from the paper, addition of redox-active species and the pore size of graphene could be other possible reasons for non-vertical low frequency signal in this case. The Bode plot (Figure 6b) provides information of the phase-angle dependence on frequency. The phase angle approaches 73° in the case of graphene, for which EDLC is the sole mechanism of charge storage, whereas after addition of redox species the

phase angles shift to 61°, 67°, and 65° for 0.5 M KI, 1 M KI, and 2 M KI, respectively, indicating the dominance of faradaic processes as the charge storage mechanism. The phase angle approaching 90° represents ideal capacitive behavior and the frequency at which the phase angle crosses 45° is associated to the capacitive behavior of the graphene electrodes. The graphene electrode crosses 45° at a frequency of 1.1 Hz, which already shows a very fast frequency response, whereas the graphene with iodide species crosses 45° at even lower frequencies of 1.05, 1.05, and 0.85 for 0.5 M, 1 M, and 2 M KI, respectively, suggesting a swift frequency response owing to adsorbed iodide and excellent capacitive behavior.[37] Additionally, EIS can be used to study the electrochemical behavior of the fabricated device by using Equations (5)–(7) to calculate the real and imaginary capacitances at the corresponding frequencies:

$$C(\omega) = C'(\omega) - jC''(\omega) \quad (5)$$

$$C'(\omega) = \frac{Z''(\omega)}{\omega |Z(\omega)|^2} \quad (6)$$

$$C''(\omega) = \frac{Z'(\omega)}{\omega |Z(\omega)|^2} \quad (7)$$

where Z is the complex impedance given by $Z(\omega) = Z'(\omega) + Z''(\omega)$ and $\omega = 2\pi f$, f is the frequency, Z' and Z'' are the real and imaginary parts of the Nyquist plot and C' and C'' are the real and imaginary capacitances. In the plot of capacitance vs. frequency (Figure 6c), the capacitance decreases with increasing frequency. We determined the relaxation time constant (τ_e) by using Equation (8):

$$\tau_e = \frac{1}{f_e} \quad (8)$$

where τ_e is the minimum time needed by the device to discharge all of its energy with more than 50% efficiency of the maximum value and f_e is the frequency. It is taken from the frequency at maximum C''.[38,39] The lowest relaxation time constant was calculated for graphene electrodes to be 200 ms. This value is significantly lower than those for supercapacitors based on activated carbon (700 ms, 4.3 s),[40] reduced graphene oxide (1.034 s, 430 ms),[41–43] and hybrid graphene (392 ms).[44] The long-term cycling stability was investigated at a current density of 2 mA for 3000 galvanostatic charge–discharge cycles (Figure 7). Around 97% capacitance retention over 3000 cycles for the device with graphene in H_2SO_4 electrolyte was observed. In contrast, the capacitance declines quickly for graphene electrodes with KI added graphene SCs (90.4%, 84%, and 65% capacitance retention with 0.5 M, 1 M, and 2 M KI, respectively). This decrease in the capacitance might be attributed to the redox transitions of iodide species during the charge–discharge process.

These results demonstrate the feasibility of using a simple technique with cost-effective materials to fabricate highly efficient supercapacitors. In addition to the excellent electrochemical performances, this work opens a pool of possibilities to aiding advancements in the field of flexible paper-based devices. For example, the performances can be further improved by using different redox-active electrolytes, graphene based hybrids composites electrodes, different quality of papers and fabrication of handy pouch devices.

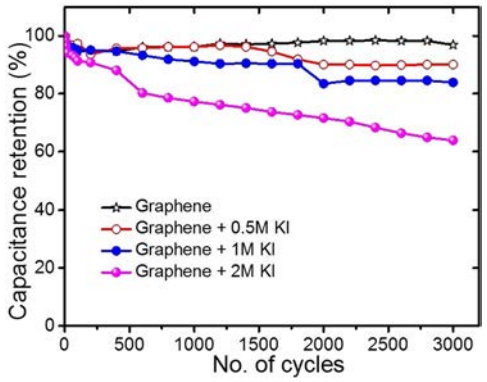

Figure 7. Capacitance retention of printed graphene device with and without KI species over 3000 charge–discharge cycles.

Conclusions

We have designed and engineered a paper-based graphene micro-supercapacitor device by introducing the redox-active species KI onto the surface of graphene electrodes. This strategy not only enhanced the capacitance but also extended the working voltage range, eventually leading to improved energy and power densities. The paper simultaneously served three functions: as substrate, separator, and electrolyte absorbent without any pre-treatment. This device is fabricated by using a facile stamping technique and provided a maximum volumetric capacitance of 130 mF cm^{-3} (areal capacitance of 10 mF cm^{-2}) at 6.5 mA cm^{-3}. Moreover, the maximum energy and power densities were calculated to be 0.026 mWh cm^{-3} and 13.4 mW cm^{-3}, respectively. The device exhibited very good cycling stability of around 97% capacitance retention over 3000 cycles. Since research on paper-based supercapacitor devices is in its early stages compared to that on devices based on other flexible substrates, these results show a very good combination of EDLC and redox mechanism by using this hybrid electrode concept, which opens a door for further research in this area.

Methods

Materials and reagents

Pristine graphene powder (< 20 μm), potassium iodide (≥ 99.0%), and sulfuric acid (99.999%) were purchased from Sigma Aldrich. Nitrocellulose filter membranes (pore size = 0.025 μm) were purchased from MF-Milipore, Merck.

Fabrication of graphene–KI hybrid

Graphene was synthesized by using similar procedure to that described in Ref. [45]. A 0.25 mg mL^{-1} graphene dispersion was prepared by sonication.0.5 M, 1 M, or 2 M KI was then added to the graphene suspension and the mixture sonicated for 1 h and left to settle overnight. The sediment was filtered off and re-dispersed in deionized water.

Stamp printing was used for printing of graphene on both sides of the paper by the method described in Ref. [46]. Briefly, graphene was dispersed in water at a concentration of 0.25 mg mL^{-1} and filtered through a hydrophilic 0.025 μm pore size nitrocellulose filter membrane with a diameter of 47 mm having had a pattern printed on it by using a Xerox ColorQube 8570 printer. This pattern was then transferred onto the paper by a roll-to-roll mechanism (built into the printer)

Fabrication and performance evaluation of graphene device

The printed electrodes were soaked in either conventional H_2SO_4 or KI-added H_2SO_4 for 5 min before each measurement. Carbon cloth was used as the current collector and was placed on both sides of the paper. The device was covered with a nonconducting parafilm tape and a clip was used to hold the device together before making connections for electrochemical measurements.

A Biologic potentiostat/galvanostat was used for all electrochemical measurements within the voltage range of 0–1.2 V. Electrochemical impedance spectroscopy (EIS) was carried in the frequency range of 100 kHz–100 mHz. The areal capacitance (C_a) and volumetric capacitance (C_v) of a two-electrode cell was calculated by using Equations (9) and (10):

$$C_V = \frac{I \times A_{cd}}{V_d \times V^2} \quad (9)$$

$$C_a = \frac{I \times A_{cd}}{A_d \times V^2} \quad (10)$$

where I is the current, t is the time, A_{cd} is the area of the charge–discharge curve, V_d and A_d are the volume and area of device, respectively, V represents the working voltage window. The areal and volumetric energy densities (E_a and E_v) and areal and volumetric power densities (P_a and P_v) were calculated by using Equations (11) and (12):

$$E_a = \frac{1}{2} C_a \times V^2, \qquad E_V = \frac{1}{2} C_V \times V^2 \quad (11)$$

$$P_a = \frac{E_a}{t}, \qquad P_V = \frac{E_V}{t} \quad (12)$$

Acknowledgements

Partial funding from MINECO (grants no. MAT2015-68394-R, and MAT2017-87202-P MINECO/FEDER) and recognition from AGAUR (2017 SGR 870) are acknowledged. The ICN2 is supported by the Severo Ochoa program of the Spanish Ministry of Economy, Industry, and Competitiveness (MINECO, grant no. SEV-2013-0295) and funded by the CERCA program/ Generalitat de Catalunya. This work has been carried out within the framework of doctoral program (PhD) of Material Science (Department of Chemistry) of Universität Autònoma de Barcelona (UAB).

Keywords: electrochemistry · electrolytes · graphene · portable electronics · supercapacitors

[1] a) P. H. Yang, W. J. Mai, *Nano Energy* **2014**, *8*, 274 – 290; b) D. P. Dubal, N. R. Chodankar, D. H. Kim, P. Gomez-Romero, *Chem. Soc. Rev.* **2018**, *47*, 2065 – 2129.
[2] D. P. Dubal, O. Ayyad, V. Ruiz, P. Gomez-Romero, *Chem. Soc. Rev.* **2015**, *44*, 1777 – 1790.
[3] Q. Ke, J. Wang, *J. Materiomics* **2016**, *2*, 37 – 54.
[4] J. Xia, F. Chen, J. Li, N. Tao, *Nat. Nanotechnol.* **2009**, *4*, 505 – 509.
[5] D. Madhabi, A. Kumar, *J. Phys. D* **2018**, *51*, 085501.
[6] Y. Xu, Z. Lin, X. Huang, Y. Wang, Y. Huang, X. Duan, *Adv. Mater.* **2013**, *25*, 5779 – 5784.
[7] W. K. Chee, H. N. Lim, Z. Zainal, N. M. Huang, I. Harrison, Y. Andou, *J. Phys. Chem. C* **2016**, *120*, 4153 – 4172.
[8] Y. Z. Zhang, Y. Wang, T. Cheng, W. Y. Lai, H. Pang, W. Huang, *Chem. Soc. Rev.* **2015**, *44*, 5181 – 5199.
[9] S. Lawes, A. Riese, Q. Sun, N. Cheng, X. Sun, *Carbon* **2015**, *92*, 150 – 176.
[10] B. Roth, R. R. Søndergaard, F. C. Krebs in *Handbook of Flexible Organic Electronics* (Ed.: S. Logothetidis), Woodhead, Oxford, **2015**, pp. 171 – 197.
[11] E. B. Secor, P. L. Prabhumirashi, K. Puntambekar, M. L. Geier, M. C. Hersam, *J. Phys. Chem. Lett.* **2013**, *4*, 1347 – 1351.
[12] F. Béguin, V. Presser, A. Balducci, E. Frackowiak, *Adv. Mater.* **2014**, *26*, 2219 – 2251.
[13] E. Frackowiak, M. Meller, J. Menzel, D. Gastol, K. Fic, *Faraday Discuss.* **2014**, *172*, 179 – 198.
[14] S. Roldán, Z. Gonzalez, C. Blanco, M. Granda, R. Menendez, R. Santamaria, *Electrochim. Acta* **2011**, *56*, 3401 – 3405.
[15] A. Singh, A. Chandra, *Sci. Rep.* **2016**, *6*, 25793.
[16] X. Cai, X. Cui, L. Zu, Y. Zhang, X. Gao, H. Lian, Y. Liu, X. Wang, *Polymers* **2017**, *9*, 288.
[17] D. Reber, R.-S. Kühnel, C. Battaglia, *Sustainable Energy Fuels* **2017**, *1*, 2155 – 2161.
[18] D. Xu, W. Hu, X. N. Sun, P. Cui, X. Y. Chen, *J. Power Sources* **2017**, *341*, 448 – 456.
[19] Y. Zhang, L. Zu, H. Lian, Z. Hu, Y. Jiang, Y. Liu, X. Wang, X. Cui, *J. Alloys Compd* **2017**, *694*, 136 – 144.
[20] W. Wang, S. Guo, M. Penchev, I. Ruiz, K. N. Bozhilov, D. Yan, M. Ozkan, C. S. Ozkan, *Nano Energy* **2013**, *2*, 294 – 303.
[21] A. C. Ferrari, *Solid State Commun.* **2007**, *143*, 47 – 57.
[22] L. M. Malard, M. A. Pimenta, G. Dresselhaus, M. S. Dresselhaus, *Phys. Rep.* **2009**, *473*, 51 – 87.
[23] T. Lan, H. Qiu, F. Xie, J. Yang, M. Wei, *Sci. Rep.* **2015**, *5*, 8498.
[24] Z.-K. Wu, Z. Lin, L. Li, B. Song, K.-S. Moon, S.-L. Bai, C.-P. Wong, *Nano Energy* **2014**, *10*, 222 – 228.
[25] D. Pech, M. Brunet, P.-L. Taberna, P. Simon, N. Fabre, F. Mesnilgrente, V. Conedera, H. Durou, *J. Power Sources* **2010**, *195*, 1266 – 1269.
[26] J. Bae, Y. J. Park, M. Lee, S. N. Cha, Y. J. Choi, C. S. Lee, J. M. Kim, Z. L. Wang, *Adv. Mater.* **2011**, *23*, 3446 – 3449.
[27] Y. Gao, Y. S. Zhou, W. Xiong, L. J. Jiang, M. Mahjouri-samani, P. Thirugnanam, X. Huang, M. M. Wang, L. Jiang, Y. F. Lu, *APL Mater.* **2013**, *1*, 012101.
[28] L. Demarconnay, E. Raymundo-Piñero, F. Béguin, *Electrochem. Commun.* **2010**, *12*, 1275 – 1278.
[29] K. Jayaramulu, D. P. Dubal, B. Nagar, V. Ranc, O. Tomanec, M. Petr, K. K. R. Datta, R. Zboril, P. Gómez-Romero, R. A. Fischer, *Adv. Mater.* **2018**, *30*, 1705789.
[30] C. Zhong, Y. Deng, W. Hu, J. Qiao, L. Zhang, J. Zhang, *Chem. Soc. Rev.* **2015**, *44*, 7484 – 7539.

[31] Y. Liu, H. R. von Gunten, *Migration Chemistry and Behaviour of Iodine Relevant to Geological Disposal of Radioactive Wastes: A Literature Review with a Compilation of Sorption Data*, PSI Bericht No. 16, **1988**, https://www.nagra.ch/data/documents/database/dokumente/$default/Default%20Folder/Publikationen/NTBs%201987-1988/e_ntb88-29.pdf.
[32] F. P. Glasser in *Chemistry and Microstructure of Solidified Waste Forms* (Ed.: R. D. Spence), CRC Press, Boca Raton, FL, **1993**, Chapter 1, pp. 1 – 40.
[33] K. Fic, M. Meller, E. Frackowiak, *J. Electrochem. Soc.* **2015**, *162*, A5140 – A5147.
[34] N. R. Chodankar, D. P. Dubal, A. C. Lokhande, A. M. Patil, J. H. Kim, C. D. Lokhande, *Sci. Rep.* **2016**, *6*, 39205.
[35] J. Menzel, K. Fic, E. Frackowiak, *Prog. Nat. Sci.* **2015**, *25*, 642 – 649.
[36] E. Frackowiak, K. Fic, M. Meller, G. Lota, *ChemSusChem* **2012**, *5*, 1181 – 1185.
[37] D. P. Dubal, N. R. Chodankar, R. Holze, D.-H. Kim, P. Gomez-Romero, *ChemSusChem* **2017**, *10*, 1771 – 1782.
[38] K. Byungwoo, C. Haegeun, K. Woong, *Nanotechnology* **2012**, *23*, 155401.
[39] K. Sheng, Y. Sun, C. Li, W. Yuan, G. Shi, *Sci. Rep.* **2012**, *2*, 247.
[40] T. M. Masikhwa, M. J. Madito, D. Y. Momodu, J. K. Dangbegnon, O. Guellati, A. Harat, M. Guerioune, F. Barzegar, N. Manyala, *RSC Adv.* **2016**, *6*, 46723 – 46732.
[41] K. Lee, D. Kim, Y. Yoon, J. Yang, H.-G. Yun, I.-K. You, H. Lee, *RSC Adv.* **2015**, *5*, 60914 – 60919.
[42] A. Muthurasu, P. Dhandapani, V. Ganesh, *New J. Chem.* **2016**, *40*, 9111 – 9124.
[43] K. P. Singh, D. Bhattacharjya, F. Razmjooei, Y.-S. Yu, *Sci. Rep.* **2016**, *6*, 31555.
[44] J. Yan, W. Sun, T. Wei, Q. Zhang, Z. Fan, F. Wei, *J. Mater. Chem.* **2012**, *22*, 11494 – 11502.
[45] H. Zhu, Y. Cao, J. Zhang, W. Zhang, Y. Xu, J. Guo, W. Yang, J. Liu, *J. Mater. Sci.* **2016**, *51*, 3675 – 3683.
[46] L. Baptista-Pires, C. Mayorga-Martinez, M. Medina-Sanchez, H. Monton, A. Merkoci, *ACS Nano* **2016**, *10*, 853 – 860.

Manuscript received: March 3, 2018
Revised manuscript received: April 5, 2018
Version of record online: May 22, 2018

Article 3: Screen-printed solid-state hybrid microsupercapcitor based on rGO/Nitrogen-doped carbon nanopipes electrodes and a redox electrolyte

Bhawna Nagar, Deepak P. Dubal, Marc Ballsells, Arben Merkoçi, Pedro Gómez-Romero

Screen-printed solid-state hybrid microsupercapcitor based on rGO/Nitrogen-doped carbon nanopipes electrodes and a redox electrolyte

Bhawna Nagar[a,b], Deepak P. Dubal[d], Marc Ballsells[b], Arben Merkoçi[bc] Pedro Gómez Romero[a]*

[a]Novel Energy Oriented Materials group at the Catalan Institute of Nanoscience and Nanotechnology (ICN2), CSIC and The Barcelona Institute of Science and Technology, Campus UAB, Bellaterra, 08193 Barcelona, Spain

[b]Nanobioelectronics and Biosensors Group at the Catalan Institute of Nanoscience and Nanotechnology (ICN2), CSIC and The Barcelona Institute of Science and Technology, Campus UAB, Bellaterra, Barcelona 08193, Spain

[c]ICREA, Pg. Lluís Companys, 23, Barcelona 08010, Spain

[d]School of Chemistry, Physics and Mechanical Engineering, Queensland University of Technology (QUT), 2 George Street, Brisbane, QLD 4001, Australia

CORRESPONDING AUTHOR FOOTNOTE

Prof. Pedro Gomez-Romero

Tel.: +34937373608 Fax: + 34936917640

E-mail: pedro.gomez@cin2.es (P. Gomez-Romero)

Abstract

This work demonstrates a functional flexible solid-state microsupercapacitor fabricated by screen-printing a negative reduced graphene oxide (rGO) and a positive nitrogen-doped carbon nanopipes (N-CNPipes) composite electrode . Inks of rGO, N-CNPipes and their composite rGO/N-CNPipes were formulated and printed using an ionic liquid as a binder. The composite exhibited an enhanced capacitance in comparison with rGO and N-CNPipes, along with 0.2 V extension in the working voltage window. As and additional upgrade, different concentrations of redox-active potassium iodide (KI) were introduced into the aq. KOH electrolyte to improve the device performance. As expected, remarkable enhancement in the capacitance from 6 to 95.34 mF/cm^2 was obtained for the composite electrode without and with KI additive, respectively, together with high energy and power densities (19 $\mu Wh/cm^2$ and 11.2 mW/cm^2 respectively). This easily scalable and simple technique to fabricate such a high-performing device can offer great advantages in the field of flexible, portable and miniaturized electronics.

Introduction

There is an intensive research going on finding sustainable solutions to provide high-performing energy storage devices. As a result, new materials and composites are being extensively and continuously developed. Supercapacitors are electrochemical energy storage devices that store energy in form of an electric double layer (EDL) or through surface faradaic redox reactions i.e. pseudocapacitance. In principle, supercapacitors are high power-density devices with excellent cyclability when compared to rechargeable batteries. The capacitance, energy and power performance of a supercapacitor can be enhanced by designing a hybrid system that exhibits both double layer and pseudocapacitance [1-2], [3]. Graphene, is a perfect material for its use in energy storage devices due to its unique combination of extraordinary properties like excellent electrical conductivity, high surface

area, excellent mechanical and chemical stability etc [3]. Although these properties of graphene are highly advantageous for its application in energy storage, the single/exfoliated graphene sheets are not able to perform to their theoretical limit as they suffer re-stacking of the sheets [3, 5]. This precludes the material to show 100% efficiency. One way to avoid this is by using different graphene-based structures like 3D foam or vertically aligned sheets, or by synthesizing graphene based hybrid composites, this would obstruct the restacking of the sheets and at the same time provide additional benefits to the device. Different 0D, 1D, 2D and 3D nanostructures and materials can be combined with graphene in order to improve the overall device performance [5][6]. For instance, CNTs are 1D structures that offer the advantages of their high aspect ratio, high surface area and good electron and ion conduction. Their combination has been well applied for numerous applications like energy storage[7][8], biosensors [9][10], transistors[11][12] etc. Also, by producing defects or doping these nanostructures great improvements have been shown in the capacitance and energy densities of the resulting supercapacitive devices [13][14][15]

For applications in electronics, wearables, touch screens etc., it is crucial for a device to be flexible, portable and scalable. In order to prepare devices that meet the requirement of flexibility and industrial scalability, simple yet innovative solutions need to be researched[16]. A variety of printing techniques can be employed for this purpose of printing graphene or graphene based composites depending on the end applications [17][18][19]. Our work focuses on scalable screen printing methods to get interdigitated patterns of graphene and N-CNPipes composite over flexible and transparent PET substrates. Another interesting way to enhance the device performance that has gained a lot of attention in recent years is the modification of the electrolyte. Conventionally, hybrids of nanocarbons with a redox active species can be prepared to take advantage of both EDL and pseudocapacitive storage mechanisms; however, as an alternative, a redox active species can be incorporated into the electrolyte rather than the electrode causing the device to store energy through faradaic reactions in

solution or through adsorbed species (pseudocapacitance)[20][21][22][23]. This approach results not only in the enhancement of specific capacitance but also leads to increased specific energy and power density of the device by expanding the working voltage range.

In this work, we report the fabrication of a hybrid nanocomposite formed by graphene and N-doped carbon nanopipes. The latter were prepared by using a soft template method where Methyl orange molecules self-assemble into nanorods in the presence of FeCl3 serving as nucleation and growth sites for pyrrole polymerization. The composite of polypyrrole/graphene oxide initially formed was pyrolized to yield conformal reduced graphene oxide/Nitrogen doped CNPipes (rGO/N-CNPipes)[24][25]. A flexible interdigitated microsupercapacitor was assembled using a screen-printing technique. Screen printable inks of the materials were formulated and tested. Herein, the conventional binder was replaced by an ionic liquid with the intention of increasing the active sites of the material. Ionic liquids are salts that are liquid at room temperatures and are generally used as electrolytes for supercapacitors[26]; however, some reports have shown their advantageous use as binders to utilize the active areas in materials that become inactive due to addition on insulating binders[27][28]. For electrochemical testing, solid-state KOH gel electrolyte was used and later different concentrations of KI were tested.

Methods

N-CNPipes and rGO/ N-CNPipes synthesis

Polypyrrole nano-pipes (PPy-NPipes) were prepared using the procedure described elsewhere [13]. In which 5mM methyl orange and 1.5mM $FeCl_3$ (0.243 g)were dissolved in 30 ml double distilled water. 1.5mM (0.1 ml)of pyrrole monomer was then added to the flocculent precipitate and kept it stirring at room temperature for 24 h. For the PPy/GO composite synthesis, the above procedure was kept the same with addition of GO (0.005 to 5mg/ml), just before the addition of pyrrole monomer. The formed precipitates (PPy-NPipes and PPy-NPipes/GO) were filtered-off using Sohxlet filtration using ethanol

until the pH was neutral. Following the cleaning, filtrates as well as dried GO were pyrolysed in a tubular furnance at 800 °C for 1 h in N_2 gas with a heating rate of 5 °C/min to produce N-CNPipes, rGO and rGO/N-CNPipes hybrid

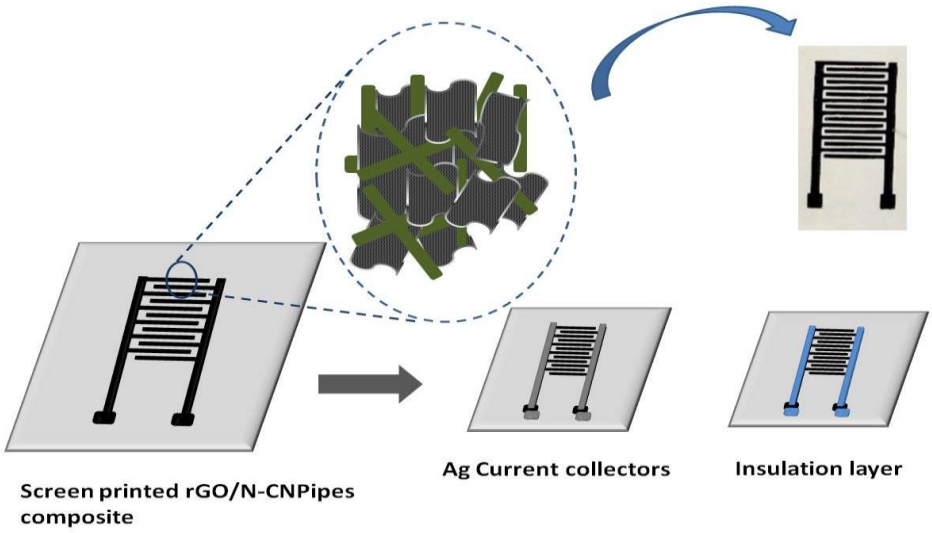

Figure 1: Schematic of the device fabrication.

Ink formulation

Inks of all the products were prepared using a combination of 70% active material (AM), 20% binder or IL, and 10% filler (acetylene black). The powders were mixed using NMP as the solvent to make a thick screen printable paste. The formulated inks were printed over PET (Polyethylene terephthalate) substrates using a DEK 248 semi-automatic screen printer (England) through an interdigitated patterned mask as shown in Fig. 1

Electrolyte Preparation

KOH gel electrolyte was prepared by first dissolving 1g PVA in 10 ml mili-Q water at 80 °C with continuous stirring. Once the powder was completely dissolved and the solution became transparent

and viscous, 2ml of 10M KOH was added to it and stirred for another 10 mins. This gel was then casted over the printed PET substrate and dried at RT for 1h. In case of KI modified gel-electrolyte, potassium iodide with different concentrations such as 0.5 and 1M were dissolved in the heated mili-Q water before addition of PVA.

Equipments used

Characterisations of the materials were performed using Scanning Electron Microscopy (SEM) FEI Quanta 650 FEG ESEM, Transmission electron Microscopy (TEM) FEI Tecnai F20, X-ray Diffraction (XRD), X'Pert MPD from PANalytical and X-ray photoelectron Sepctroscopy (XPS), SPECS PHOIBOS 150 analyser (SPECS GmbH, Berlin, Germany).

Electrochemical measurements

A VMP3 Bio-logic potentiostat/galvanostat was used for all the electrochemical measurements within the voltage range of 0 to 1.2 V. Electrochemical Impedance spectroscopy was carried in the frequency range of 100kHz to 100mHz. The areal capacitances (C_a), energy density (E_a) and power density (P_a) of a two electrode cell was calculated using the equations (1), (2) and (3) given in the supporting information (S).

Results and Discussions

Fig. 2 (a and b) shows SEM images of rGO/N-CNpipes hybrid material at two different magnifications. A uniform composite formation is deduced from the images; graphene sheets are either rolling the pipes or are covering them. This provides good connections between the two materials, which should lead to

better performance. This can be seen more clear from TEM analysis, Fig.2 (c and d). The diameter of the nanopipes is approximately 80 to 100 nm.

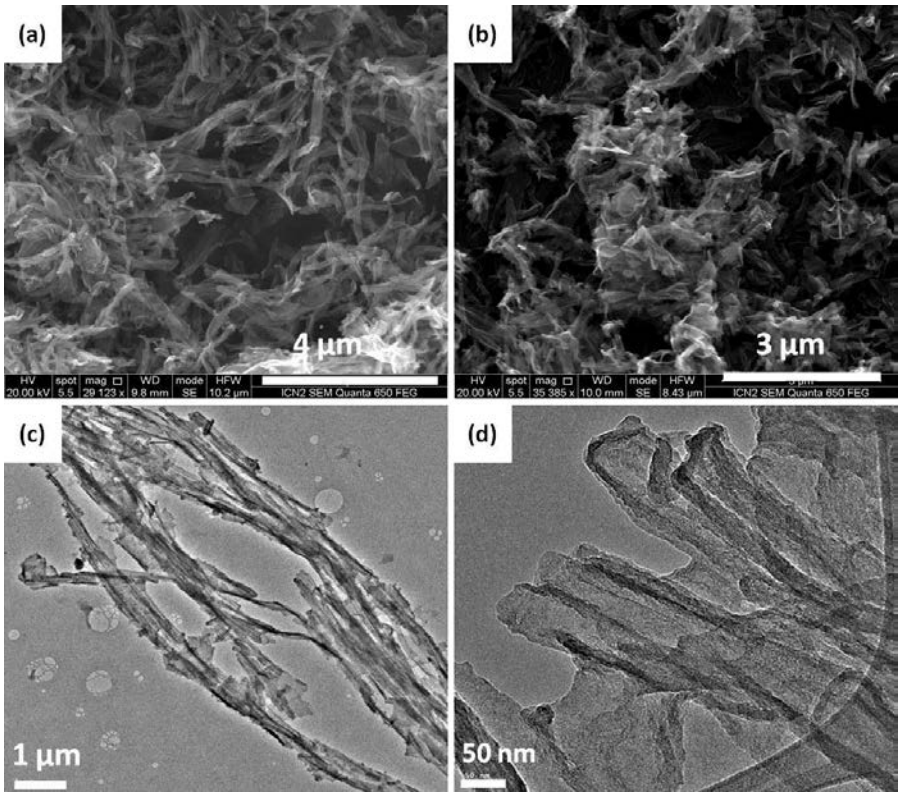

Figure 2: (a and b) are the SEM images and (c and d) are the TEM images of the rGO/N-CNPipes composite.

In addition, the attachment of graphene sheets to N-CNPipes can be clearly confirmed. XRD patterns of rGO, N-CNPipes, and rGO/N-CNpipes are shown in Fig. 3(a). All the three materials show amorphous nature with a hump at 25.4 º that corresponds to 002 planes with an interlayer spacing of about 0.4nm [29], indicating their graphitic texture[13]. In order to get further insights, XPS spectra of the materials were obtained. Fig, 3(b) gathers the full XPS spectra of rGO, N-CNPipes and rGO/N-CNPipes, which shows the characteristic C1s, O1s and N1s peaks. The core level C1s and N1s spectra of the composite material is shown in Fig. 3 (c) and (d). The C1s spectra is fitted with three peaks at 284.6, 285.4 and 287.3 eV that correspond to the graphitic C=C, C-N and C-O bonds respectively [30] while the N1s

spectra shows two clear peaks at 398.2 and 400.8 eV that which indicate the presence of pyridinic and graphitic nitrogen [31][32]. Core level C1s, O1s, N1s XPS spectra of rGO and N-CNPipes are presented in the supporting information S1.

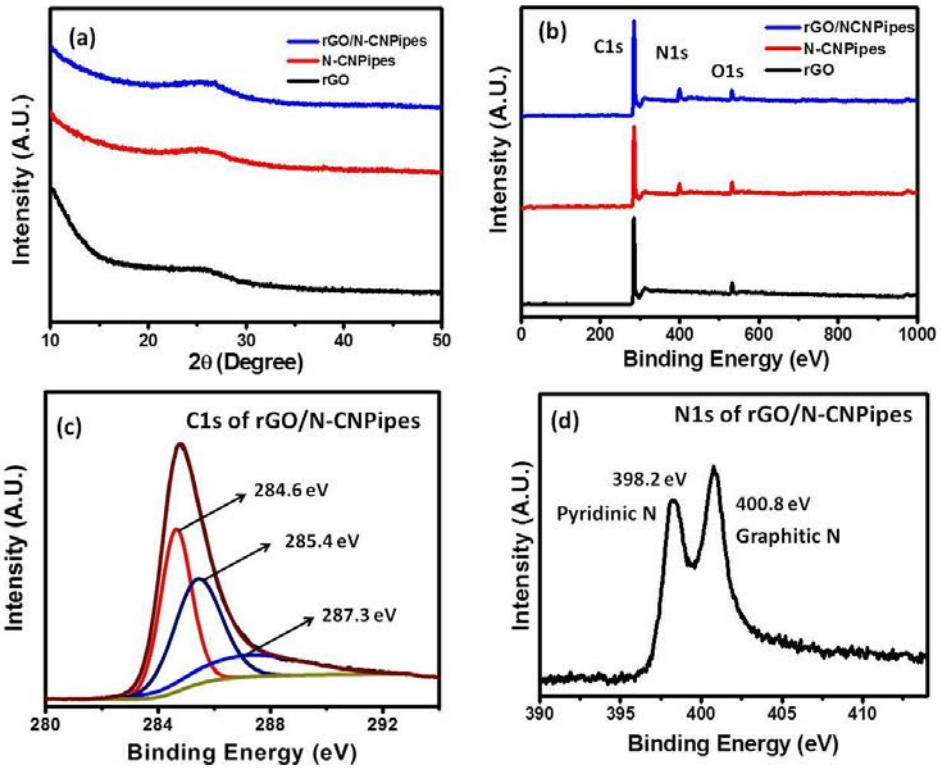

Figure 3: (a) is the full range XPS spectra comparing rGO, N-CNPipes and rGO/N-CNPipes, (b and c) are the core level O1s and N1s spectra of the composite materials and (d) is the XRD pattern of the three materials

Electrochemical testing

Two-electrode tests of the symmetric device were carried out in solid-state KOH gel electrolyte. Fig. 4 (a, b) compares the electrochemical properties of different materials such as rGO, N-CNPipes and rGO/N-CNPipes hybrid in KOH-based gel-electrolyte... It can be seen that rGO shows a typical square shaped CV curve, characteristic of electric double layer capacitance whereas N-CNPipes deviate from this behaviour and give a distorted square shape with the appearance of broad oxidation and reduction waves due to

the presence of nitrogen groups. This suggests the presence of pseudocapacitance. The composite however, shows increased capacitance as well as an increased voltage window from 1 to 1.2 V. This increase in the electrode performance can be explained due to the synergic effect obtained by combining the two materials, and is also apparent from their charge discharge curves (Fig. 4 b). The electrochemical behaviour of the electrodes made with the three materials (rGO, N-CNPipes and rGO/N-CNPipes hybrid) at varying scan rates and current densities is shown in the supporting information S2. In order to improve the performance of the prepared composite, the electrodes were tested in KOH-gel-electrolyte with KI as an added redox-active species. The CV curves for the symmetric device based on rGO/N-CNPipes are shown in Fig. 4 (c) where an increase in the peak currents is observed by increasing the KI concentration to 1M. In addition, the small and broad peaks of iodide redox reactions can be seen from the voltammograms that provides the added pseudocapacitance to the electrodes. The possible redox reactions happening on the electrodes due to iodide can be[20]:

$$2I^- \longrightarrow I_2 + 2e^-$$

$$3I^- \longrightarrow I_3^- + 2e^-$$

$$2I_3^- \longrightarrow 3I_2 + 2e^-$$

A detailed study of the cyclic voltammetric response of the composite electrode in 2M KOH, 2M KOH/0.5M KI and 2M KOH/1M KI at different scan rates and charge discharge cycles at varying current densities is provided in the supporting information S(3). Fig. 4 (e) represents the areal capacitances obtained at different current densities with and without redox active KI, with the maximum areal capacitance achieved for the rGO/N-CNPipes electrode in presence of KOH electrolyte containing 1M KI is 53.8, 73.5, 76.5, and 95.3 mF/cm^2 at 1.2, 0.8, 0.4 and 0.2 mA/cm^2, respectively. Moreover, the device can deliver maximum values of energy and power density of 19 µWh/cm^2 and 11.2 mW/cm^2 for KI added KOH-gel electrolyte. A comparison of energy and power densities delivered by the composite electrode in different electrolytes and concentrations is shown in Fig. 4 (f).

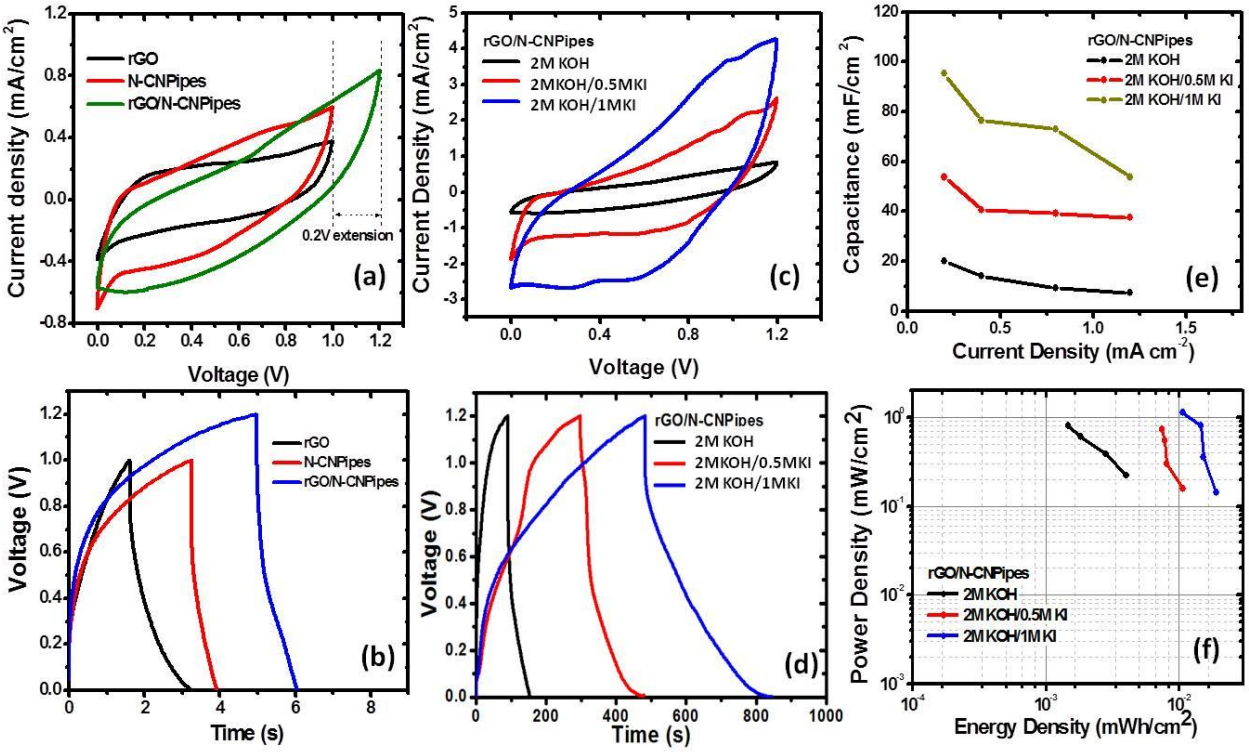

Figure 4: ELectrochemical performance of the symmetrical supercapacitor device. (a and b) are the CV and CD curves of the three materials tested while (c and d) are the CV and CD curves of the device with rGO/N-CNPipes (e) is the calculated capacitance at different current densities with and without different KI concentrations. (d) is the obtained ragone plot.

Fig. 5(a) and (b) represent the electrochemical impedance measurements in terms of (a) Nyquist plot and (b) Bode plot obtained from rGO/N-CNPipes hybrid carried out in the frequency range of 100 kHz-100 mHz. The materials shows capacitor like behaviour at low frequencies as the slope of the vertical line approaches 90° with highest electrode equivalent series resistance shown by rGO/N-CNPipes in KOH electrolyte of 68.3 Ω compared to 0.5 and 1MKI (26 and 16 Ω). From the Bode plot it can be seen that the phase for the hybrid material, with and without KI is far from 90° which implies that the faradaic process are dominating the charge storing processes [33]. Finally, in Fig. 5 (a and b), we can see the performance of the device in terms of capacity retention and self-discharge which is seen to decrease with the increase in concentration of KI. The device was cycled up to 2000 charge discharge cycles with

and without KI-based gel-electrolyte. It can be seen that the addition of KI (1M) shows only 53 % of initial capacity after 2000 cycles, whereas, 0.05M and blank KOH retains 70 and 80 % of the initial capacity respectively. This can be due to the fact that higher concentrations of Iodide ions are not efficiently adsorbed during charging and discharging cycles resulting in loss of capacitance over time. This is in accordance with the study shown by et al, where they have shown that the concentration of redox species in the electrolyte directly impacts the reversibility and stability in repeated cycles [34].

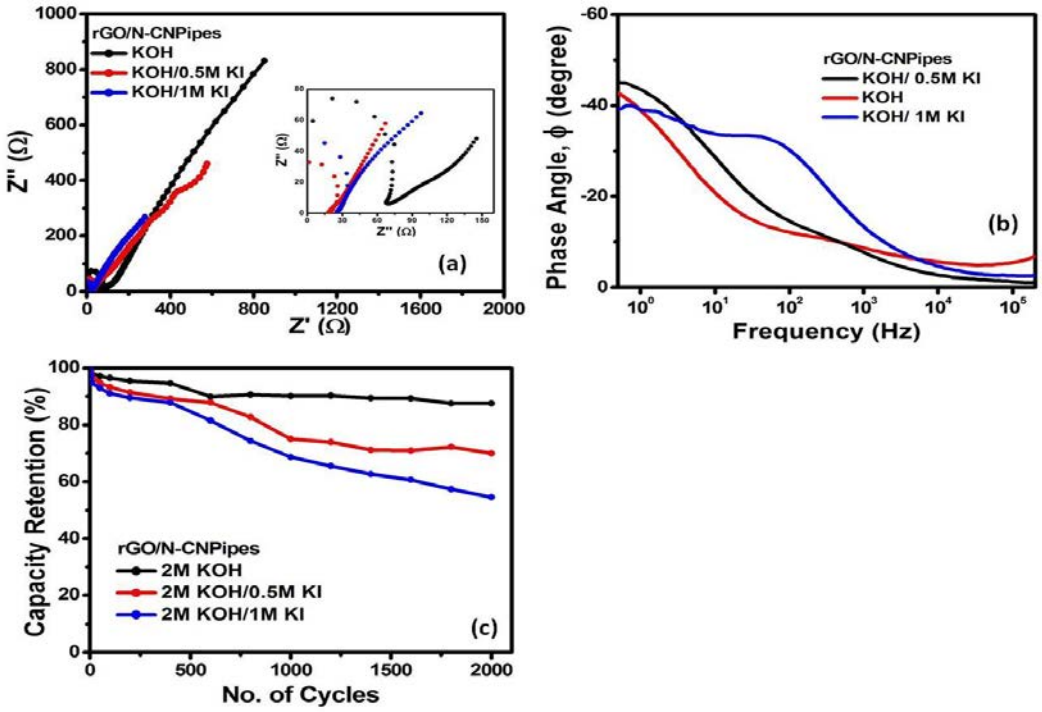

Figure 5: Showing the Electrochemical impedance measurement of the composite device (a) Nyquist plot (with enlarged image at low frequency in the inset) and (b) bode Plot and (c) stability performance upto 2000 CD cycles

Conclusions

In summary, we have designed here an interdigitated pattern over flexible PET substrate using rGO/N-CNPipes hybrid electrode that delivered high specific capacitance of 95.3 mF/cm^2 as well as good energy

and power densities. The device can be used up to a minimum of 2000 cycles with capacity retention of 80 % with an inert electrolyte. The stability of the KI-containing system can be increased further by either decreasing the concentration of KI or by improving the attachment of KI to the composite material. The solid-state device fabricated benefitted from a double hybrid strategy by using a composite exhibiting EDL and pseudocapacitance along with the electrolyte that consists of redox active species, thus providing additional capacitance to the system. Combinations of these two strategies can be highly advantageous in an area where scalable production of flexible and high performing devices is required.

References

[1] D. P. Dubal, O. Ayyad, V. Ruiz, and P. Gómez-Romero, "Hybrid energy storage: The merging of battery and supercapacitor chemistries," *Chem. Soc. Rev.*, vol. 44, no. 7, pp. 1777–1790, 2015.

[2] A. González, E. Goikolea, J. A. Barrena, and R. Mysyk, "Review on supercapacitors: Technologies and materials," *Renew. Sustain. Energy Rev.*, vol. 58, pp. 1189–1206, 2016.

[3] Novoselov K. S. and Geim A. K, "The Rise of Graphene," *Nat. Mater.*, vol. 6, pp. 1–14, 2007.

[4] G. Xiong, C. Meng, R. G. Reifenberger, P. P. Irazoqui, and T. S. Fisher, "A review of graphene-based electrochemical microsupercapacitors," *Electroanalysis*, vol. 26, no. 1, pp. 30–51, 2014.

[5] X. Chen, R. Paul, and L. Dai, "Carbon-based supercapacitors for efficient energy storage," *Natl. Sci. Rev.*, vol. 4, no. 3, pp. 453–489, 2017.

[6] Q. Cheng, J. Tang, J. Ma, H. Zhang, N. Shinya, and L. C. Qin, "Graphene and carbon nanotube composite electrodes for supercapacitors with ultra-high energy density," *Phys. Chem. Chem. Phys.*, vol. 13, no. 39, pp. 17615–17624, 2011.

[7] Y. H. Lee, D. T. Pham, T. H. Lee, D. H. Luong, F. Yao, A. Ghosh, and V. T. Le, "Carbon Nanotube-Bridged Graphene 3D Building Blocks for Ultrafast Compact Supercapacitors," *ACS Nano*, no. March, 2016.

[8] A. Ansaldo, P. Bondavalli, S. Bellani, A. E. Del Rio Castillo, M. Prato, V. Pellegrini, G. Pognon, and F. Bonaccorso, "High-power graphene–Carbon nanotube hybrid supercapacitors," *ChemNanoMat*, vol. 3, no. 6, pp. 436–446, 2017.

[9] S. Palanisamy, S. Cheemalapati, and S. M. Chen, "Amperometric glucose biosensor based on glucose oxidase dispersed in multiwalled carbon nanotubes/graphene oxide hybrid biocomposite," *Mater. Sci. Eng. C*, vol. 34, no. 1, pp. 207–213, 2014.

[10] J. Chen, X. Zheng, F. Miao, J. Zhang, X. Cui, and W. Zhen, "Engineering graphene/carbon nanotube hybrid for direct electron transfer of glucose oxidase and glucose biosensor," *J. Appl. Electrochem.*, vol. 42, no. 10, pp. 875–881, 2012.

[11] B. Li, X. Cao, H. G. Ong, J. W. Cheah, X. Zhou, Z. Yin, H. Li, J. Wang, F. Boey, W. Huang, and H. Zhang, "All-carbon electronic devices fabricated by directly grown single-walled carbon nanotubes on reduced graphene oxide electrodes," *Adv. Mater.*, vol. 22, no. 28, pp. 3058–3061, 2010.

[12] S. H. Kim, W. Song, M. W. Jung, M. A. Kang, K. Kim, S. J. Chang, S. S. Lee, J. Lim, J. Hwang, S. Myung, and K. S. An, "Carbon nanotube and graphene hybrid thin film for transparent electrodes and field effect transistors," *Adv. Mater.*, vol. 26, no. 25, pp. 4247–4252, 2014.

[13] D. P. Dubal, N. R. Chodankar, Z. Caban-Huertas, F. Wolfart, M. Vidotti, R. Holze, C. D. Lokhande, and P. Gomez-Romero, "Synthetic approach from polypyrrole nanotubes to nitrogen doped pyrolyzed carbon nanotubes for asymmetric supercapacitors," *J. Power Sources*, vol. 308, pp. 158–165, 2016.

[14] K. Gopalakrishnan, K. Moses, A. Govindaraj, and C. N. R. Rao, "Supercapacitors based on nitrogen-doped reduced graphene oxide and borocarbonitrides," *Solid State Commun.*, vol. 175–176, pp. 43–50, 2013.

[15] J. Zhu, A. S. Childress, M. Karakaya, S. Dandeliya, A. Srivastava, Y. Lin, A. M. Rao, and R. Podila, "Defect-Engineered Graphene for High-Energy- and High-Power-Density Supercapacitor Devices," *Adv. Mater.*, pp. 7185–7192, 2016.

[16] K. D. Harris, A. L. Elias, and H. J. Chung, "Flexible electronics under strain: a review of mechanical characterization and

durability enhancement strategies," *J. Mater. Sci.*, vol. 51, no. 6, pp. 2771–2805, 2016.
[17] D. P. Dubal, N. R. Chodankar, D.-H. Kim, and P. Gomez-Romero, "Towards flexible solid-state supercapacitors for smart and wearable electronics," *Chem. Soc. Rev.*, vol. 47, no. 6, pp. 2065–2129, 2018.
[18] A. V Eletskii, I. M. Iskandarova, A. A. Knizhnik, J. S. Ponraj, Z. Xu, and S. Chander, "2D printing technologies using graphene-based materials."
[19] W. Yang and C. Wang, "Graphene and the related conductive inks for flexible electronics," *J. Mater. Chem. C*, vol. 4, no. 30, pp. 7193–7207, 2016.
[20] F. Béguin, V. Presser, A. Balducci, and E. Frackowiak, "Carbons and electrolytes for advanced supercapacitors," *Adv. Mater.*, vol. 26, no. 14, pp. 2219–2251, 2014.
[21] E. Frackowiak, M. Meller, J. Menzel, D. Gastol, and K. Fic, "Redox-active electrolyte for supercapacitor application," *Faraday Discuss.*, vol. 172, pp. 179–198, 2014.
[22] S. Roldán, Z. González, C. Blanco, M. Granda, R. Menéndez, and R. Santamaría, "Redox-active electrolyte for carbon nanotube-based electric double layer capacitors," *Electrochim. Acta*, vol. 56, no. 9, pp. 3401–3405, 2011.
[23] B. Nagar, D. P. Dubal, L. Pires, A. Merkoçi, and P. Gómez-Romero, "Design and Fabrication of Printed Paper-Based Hybrid Micro-Supercapacitor by using Graphene and Redox-Active Electrolyte," *ChemSusChem*, vol. 11, no. 11, pp. 1849–1856, 2018.
[24] Y. Yan, H. Li, Y. Zhang, J. Kan, T. Jiang, H. Pang, Z. Zhu, and H. Xue, "Facile synthesis of polypyrrole nanotubes and their supercapacitive application," *Int. J. Electrochem. Sci.*, vol. 12, no. 10, pp. 9320–9334, 2017.
[25] T. Dai and Y. Lu, "Water-soluble methyl orange fibrils as versatile templates for the fabrication of conducting polymer microtubules," *Macromol. Rapid Commun.*, vol. 28, no. 5, pp. 629–633, 2007.
[26] A. Eftekhari, "Supercapacitors utilising ionic liquids," *Energy Storage Mater.*, vol. 9, pp. 47–69, 2017.
[27] N. Maleki, A. Safavi, and F. Tajabadi, "Print - High-Performance Carbon Composite Electrode Based on an Ionic Liquid as a Binder - Analytical Chemistry (ACS Publications).pdf," vol. 78, no. 11, pp. 3820–3826, 2006.
[28] S. Bag, A. Samanta, P. Bhunia, and C. R. Raj, "Rational functionalization of reduced graphene oxide with imidazolium-based ionic liquid for supercapacitor application," *Int. J. Hydrogen Energy*, vol. 41, no. 47, pp. 22134–22143, 2016.
[29] A. Jabbar, G. Yasin, W. Q. Khan, M. Y. Anwar, R. M. Korai, M. N. Nizam, and G. Muhyodin, "Electrochemical deposition of nickel graphene composite coatings effect of deposition temperature on its surface morphology and corrosion resistance," *RSC Adv.*, vol. 7, no. 49, pp. 31100–31109, 2017.
[30] Y. Li, Y. Zhao, H. Cheng, Y. Hu, G. Shi, L. Dai, and L. Qu, "Ja206030C.Pdf," pp. 18–21, 2012.
[31] M. Scardamaglia and C. Bittencourt, "Metal-free catalysis based on nitrogen-doped carbon nanomaterials: a photoelectron spectroscopy point of view," *Beilstein J. Nanotechnol.*, vol. 9, pp. 2015–2031, 2018.
[32] F. Davodi, M. Tavakkoli, J. Lahtinen, and T. Kallio, "Straightforward synthesis of nitrogen-doped carbon nanotubes as highly active bifunctional electrocatalysts for full water splitting," *J. Catal.*, vol. 353, no. August, pp. 19–27, 2017.
[33] D. P. Dubal, N. R. Chodankar, R. Holze, D. H. Kim, and P. Gomez-Romero, "Ultrathin Mesoporous RuCo2O4Nanoflakes: An Advanced Electrode for High-Performance Asymmetric Supercapacitors," *ChemSusChem*, vol. 10, no. 8, pp. 1771–1782, 2017.
[34] L. Su, X. Zhang, C. Mi, B. Gao, and Y. Liu, "Improvement of the capacitive performances for Co – Al layered double hydroxide by adding hexacyanoferrate into the electrolyte.," *Phys. Chem. Chem. Phys.*, vol. 11, pp. 2195–2202, 2009.

Supporting Information

Calculations:

Areal Capacitance Ca

$$\mathrm{Ca} = \frac{\mathrm{I} \times \mathrm{Acd}}{\mathrm{Ae} \times \mathrm{V}^2} \quad (1)$$

Equations used for calculating areal energy density (E_a) and power density (P_a) were

$$\mathrm{Ea} = \frac{1}{2}\mathrm{Ca} \times \mathrm{V}^2 \quad (2)$$

$$\mathrm{Pa} = \frac{\mathrm{Ea}}{\mathrm{t}} \quad (3)$$

Here, I is the Current, t is the time, A_{CD} is the area of the charge discharge curve, A_e is the area of the electrode, ΔV represents the voltage window and d is the film thickness

Supporting information S1

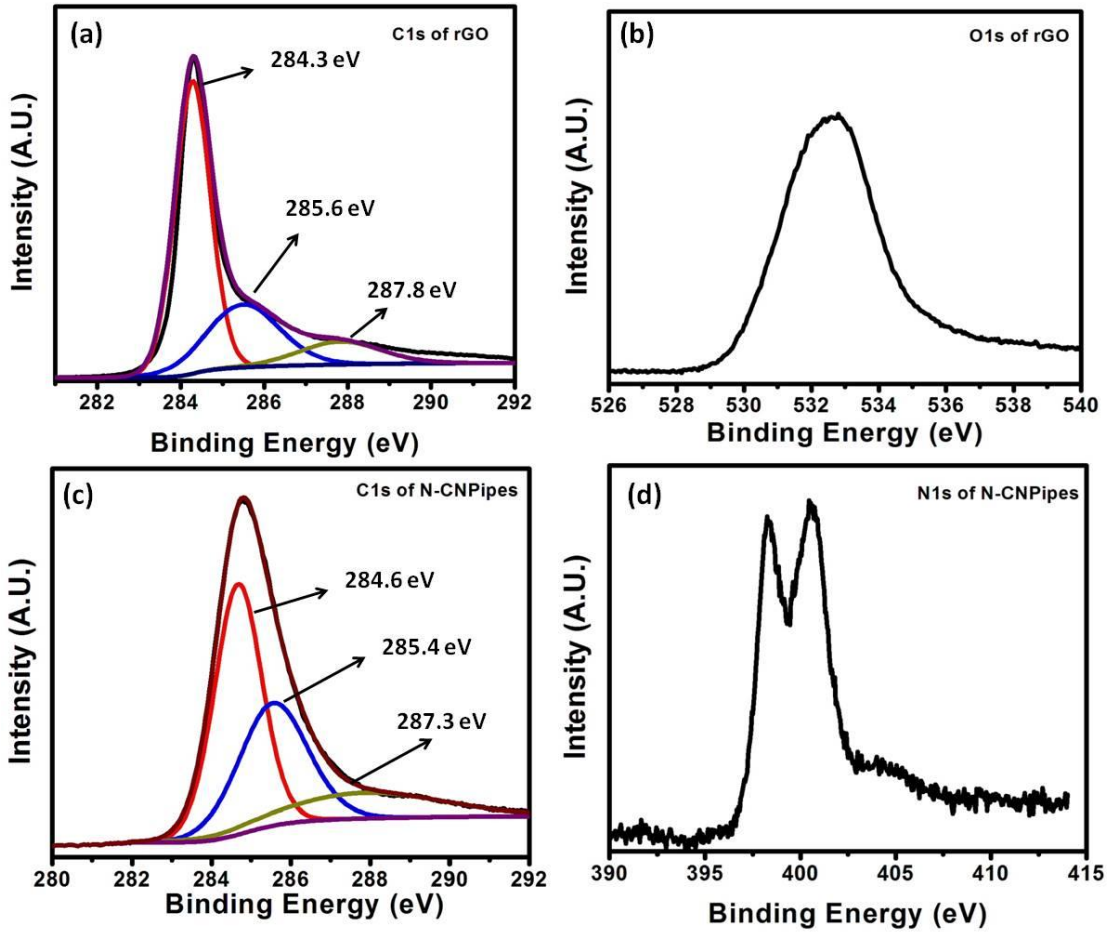

Figure 6: (a) and (b) are the Core level (a) C1s and (b) O1s spectra of rGO , (c) C1s (d) N1s of N-CNPipes.

Supporting information S2

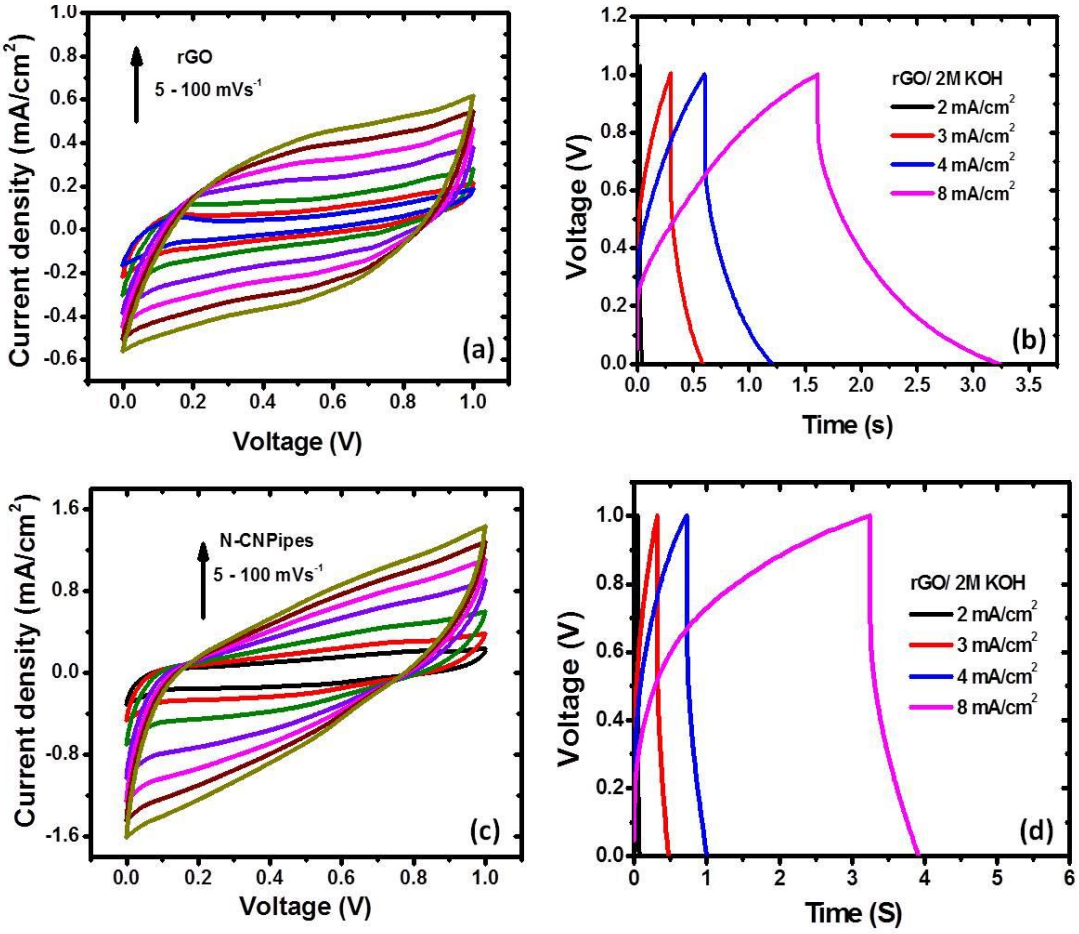

Figure 7: Cyclic Voltammetry Curves (a) and (c) at different scan rates from 5- 100 mV/s and (b) and (d) galvanostatic charge/discharge cycles at different current densities of rGO and N-CNPipes respectively.

Supporting information S3

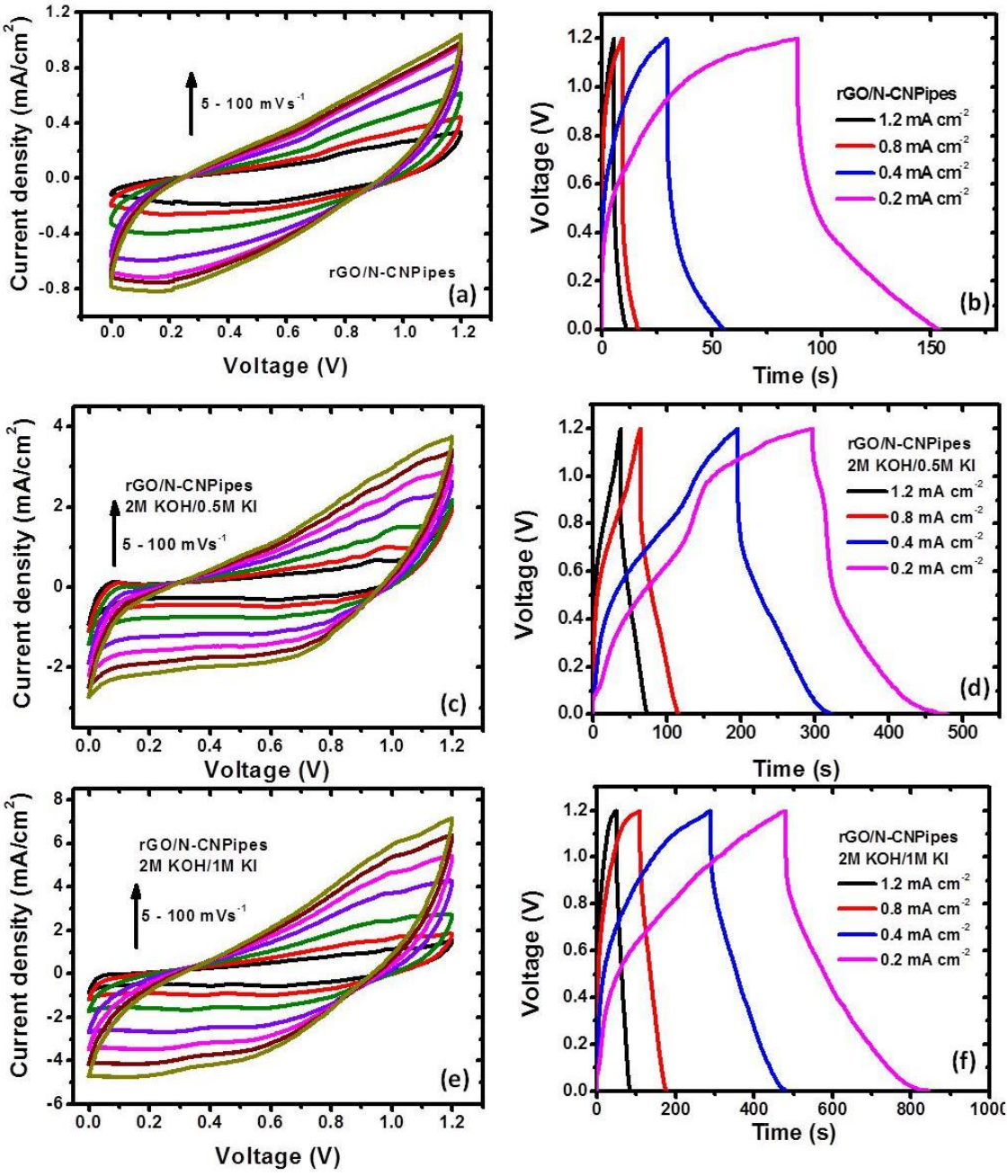

Figure 8: Cyclic Voltammograms (a), (c) and (e) at different scan rates from 5- 100 mV/s and (b), (d) and (f) galvanostatic charge/discharge cycles at different current densities of the composite (rGO/N-CNPipes) in 2M KOH, 2M KOH/0.5M KI and 2M KOH/1M KI respectively.

Supporting information S4

Electrode	Device	Electrolyte	Capacitance	Ref.
rGO/Ni	Symmetric	PVA/LiCl gel electrolyte	12.5 mF/cm^2 at a scan rate of 5 mV/s	[1]
Hydrophilic N-doped graphene	Symmetric	PVA-H_3PO_4 gel electrolyte	37.5 mF/cm^2 at a scan rate of 5 mV s^{-1}	[2]
Sulfur-Doped Graphene	Symmetric	H_2SO_4/PVA gel electrolyte	~553 μF/cm^2 at 10 mV s-1	[3]
Graphene SC by Laser Ablation	Symmetric	PVA-H2SO	80.5 μF/cm^2.	[4]
N-doped rGO	Symmetric	PVA–H3PO4	3.4 mF/cm^2 at 20 mF/cm^2	[5]
rGO	Symmetric	PVA-H2SO4 gel electrolyte	19.8 mF/cm2	[6]
Graphene	Symmetric	Ion- gel ink (ionic liquid, [EMIM][TFSI]) and a gelling triblock copolymer, PS-PMMA-PS)	268 μF/cm^2 at 10mV/s	[7]
Graphene/PEDOT	Symmetric	PVA/H2SO4	37.08 mF cm^{-2} at 0.05 mA cm-2	[8]
rGO/N-doped CNTs	*Symmetric*	*KI doped PVA-KOH gel-electrolyte*	95.3 mF/cm^2 at 0.2 mA/cm^2	*Present work*

References

[1] Y. Chen, B. Xu, J. Xu, J. Wen, T. Hua, C.-W. Kan, Graphene-based in-planar supercapacitors by a novel laser-scribing, in-situ reduction and transfer-printed method on flexible substrates, J. Power Sources. 420 (2019) 82–87. doi:https://doi.org/10.1016/j.jpowsour.2019.02.096.

[2] Q. Chang, L. Li, L. Sai, W. Shi, L. Huang, Water-Soluble Hybrid Graphene Ink for Gravure-Printed Planar Supercapacitors, Adv. Electron. Mater. 4 (2018) 1800059. doi:10.1002/aelm.201800059.

[3] Z.-S. Wu, Y.-Z. Tan, S. Zheng, S. Wang, K. Parvez, J. Qin, X. Shi, C. Sun, X. Bao, X. Feng, K. Müllen, Bottom-Up Fabrication of Sulfur-Doped Graphene Films Derived from Sulfur-Annulated Nanographene for Ultrahigh Volumetric Capacitance Micro-Supercapacitors, J. Am. Chem. Soc. 139 (2017) 4506–4512. doi:10.1021/jacs.7b00805.

[4] S.M. Djuric, G. Kitic, G. Dubourg, R. Gajic, T. Tomasevic-Ilic, V. Minic, M. Spasenovic, Miniature graphene-based supercapacitors fabricated by laser ablation, Microelectron. Eng. 182 (2017) 1–7. doi:https://doi.org/10.1016/j.mee.2017.08.005.

[5] S.-Y. Liu, J. Xie, H. Li, Y. Wang, H. Yang, T. Zhu, S. Zhang, G. S. Cao, X. B. Zhao, Nitrogen-doped reduced graphene oxide for high-performance flexible all-solid-state micro-supercapacitors, J. Mater. Chem. A. 2 (2014) 18125–18131. doi:10.1039/C4TA03192J.

[6] G. Sun, J. An, C.K. Chua, H. Pang, J. Zhang, P. Chen, Layer-by-layer printing of laminated graphene-based interdigitated microelectrodes for flexible planar micro-supercapacitors, Electrochem. Commun. 51 (2015) 33–36. doi:https://doi.org/10.1016/j.elecom.2014.11.023.

[7] W.J. Hyun, E.B. Secor, C.-H. Kim, M.C. Hersam, L.F. Francis, C.D. Frisbie, Scalable, Self-Aligned Printing of Flexible Graphene Micro-Supercapacitors, Adv. Energy Mater. 7 (2017) 1700285. doi:10.1002/aenm.201700285.

[8] H.U. Lee, J.-H. Jin, S.W. Kim, Effect of gel electrolytes on the performance of a minimized flexible micro-supercapacitor based on graphene/PEDOT composite using pen lithography, J. Ind. Eng. Chem. 71 (2019) 184–190. doi:https://doi.org/10.1016/j.jiec.2018.11.021.

Chapter 3
Printed Electrochemical (Bio)sensors

3.1. Introduction

Pursuit of a healthy and long life has motivated humans to continuously advance the research in the field of medical science and biotechnology. It is of high importance to find cures and alternatives to current medicines for some diseases, however, it is also equally important to detect the signs of diseases at earlier stages or to check the symptoms of an ongoing condition, because "prevention is always better than cure". One of the ways to stay protected is to have a health monitoring system that can give us information about the impending or an ongoing condition. On the other hand are the changes in the environment and surroundings that can be a cause of many serious damages on the ecosystem, directly or indirectly affecting humans. Detection of changes in levels of certain compounds is necessary to control the effects which can be a cause of harmful diseases if above a certain limit. This can be realized by employing sensing devices that are capable to monitor the chemical changes in the surrounding medium and can transfer the signals in many forms that are readable and understandable to the user. According to International Union of Pure and Applied Chemistry (IUPAC), **Chemical sensor** is defined as a "**device that transforms chemical information, ranging from the concentration of a specific sample component to total composition analysis, into an analytically useful signal"**[1] and when biochemical processes are used for analyzing the signals using a bio or biologically derived receptor, it can be classified into as a *Biosensor* [2]. These utilize a bioreceptor for recognizing bioanalytes from bodily fluids such as sweat, blood, urine etc. In case of a chemical sensor, it may or may not use a bioreceptor to detect and convert chemical changes from the surroundings into readable analytical signals.

Applications of Internet of Things (IOTs), in particular, for medical devices especially sensing devices has been of interest due to the need of real time, easy, non-invasive health monitoring [3].

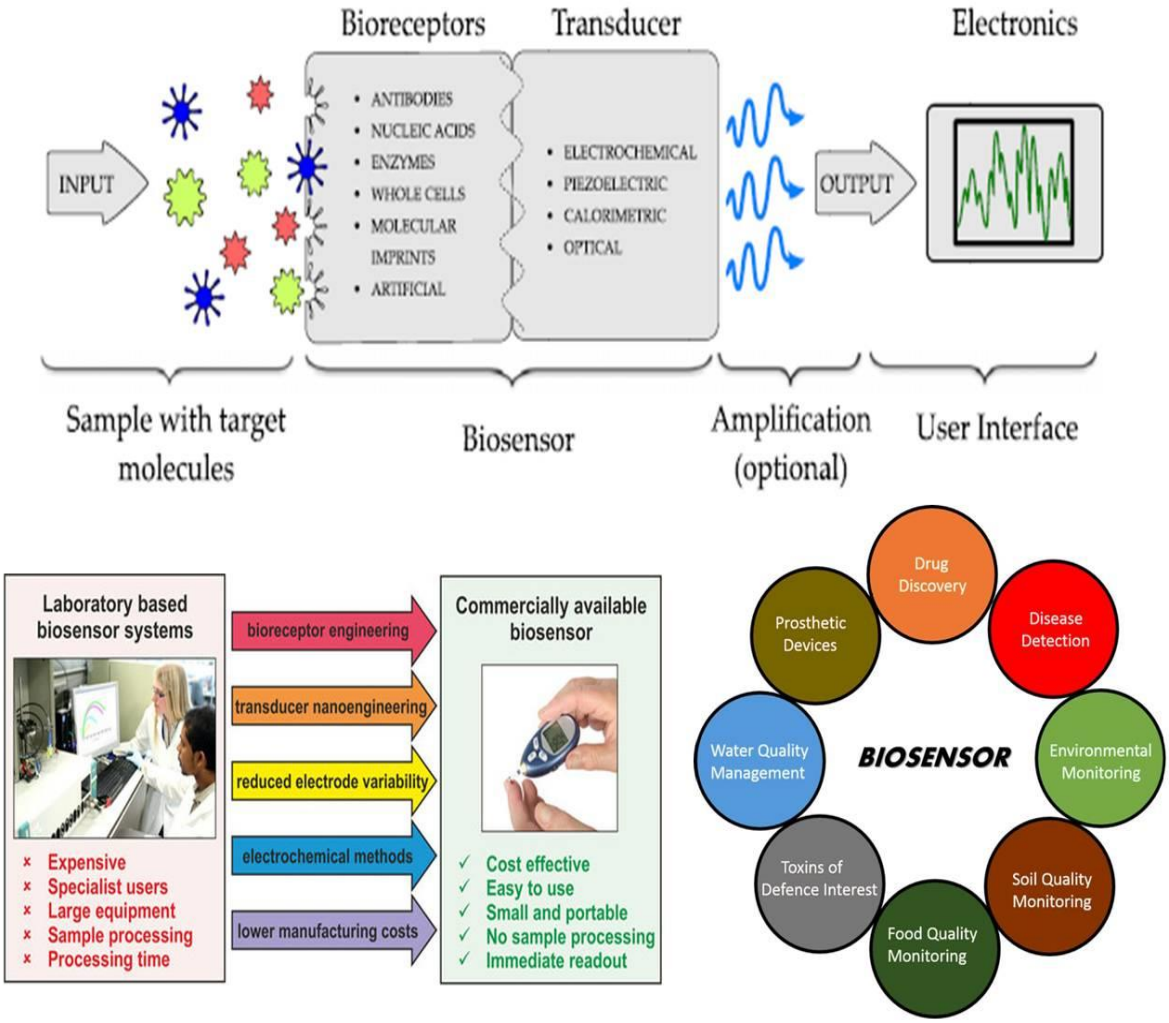

Figure 1: (Bio)Sensing device components, the advantages of biosensors over the conventional analytical techniques and application of biosensors [4][5]

These flexible, quick, one-time-use sensors are much in demand [6][7][8] as an alternative to the traditional sensing systems as they can be very expensive, use complex instruments that need a skilled personnel and are very time consuming. (Bio)Sensors utilize a sensing element which after contact with

the analyte generates signals (it is a result of change in either mass, proton concentrations, gases absorption/desorption, heat generation etc.) which are further converted into measurable and readable response using a transducer, through electrochemical, electrical, thermal, optical or piezoelectric means. These signals coming from the transducer are readable and proportional to the analyte concentration. A comprehensive image of the sensing device components are shown in fig.1. The receptor receives the changes (physical or chemical) from the analytes while the transducer functions to transfer the signals that can be further analyzed for understanding.

3.2. Biosensors

Different bioreceptors are employed for the task of interacting specifically with the bio-analytes, note the biochemical changes and transfer them to the transducer. These can be enzymes, antibodies, nucleic acids, cells or organelles [9][10]. Enzymes are the most commonly used bioreceptors that are selected specifically to the analyte of interest. There is direct electron transfer from the enzyme catalyzed reaction to the transducer electrode

Different transduction systems are used for transmitting the signals from the receptors. Transducer can be of various types: (i) electrochemical/electrical, in which the redox reaction occurring at the electrode or electrode/electrolyte interface are measured by amperometry, potentiometry, conductometry or impedimetry. The transducer generates electrical response after interaction of the analyte with the receptor, (ii) Piezoelectric, it is based on a mass sensitive piezoelectric crystal in which the changes in oscillating frequency of the crystal happening due to addition of the mass (positive or negative) caused by binding of the analytes is detected in form of electrical signals. (iii) Thermometric transducers rely on the heat production or absorption during the reaction/interaction of the analyte with the receptor molecule on the electrode. Heat is measured using a thermistor which is proportional to the analyte

concentration. (iv) Optical transducer, these send out the signals in form of light, can be fluorescence or optical diffraction [10][9].

3.2.1. Electrochemical Sensors

In electrochemical sensors, the detection is done using generally a three electrode setup comprising of a Working, Reference and Counter/Auxiliary electrodes. It measures the changes via Amperometry, when measurable current is generated from the electrochemical reactions at the transducer, by Potentiometry when there is generation of measurable potential due to accumulation of charges or by measuring the conductive or impedimetric properties.

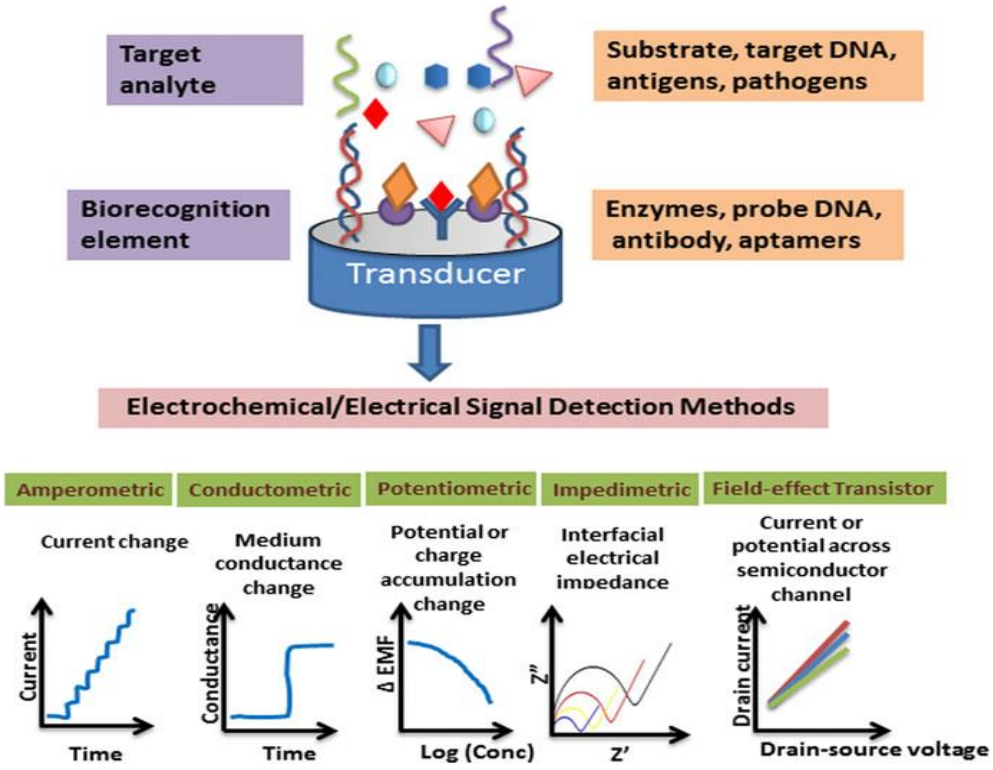

Figure 2: Electrochemical sensor and components along with the different electrochemical techniques employed

3.2.1.1. Amperometric Sensors

They are self-contained integrated devices that transform biochemical reactions going on the electrode surface into current signals i.e. it measures current generated from the oxidation or reduction of the electroactive species at the working electrode. When current is measured at constant potential value, it is called as Amperometry and when the current is measured at varied potentials, the technique is known as voltammetry [11]. The peak current values over the linear potential ranges corresponding to oxidation/reduction of the electroactive species are directly proportional to the analyte concentration. The research on Amperometric biosensors was initiated by Clark in 1956 where he showed the rise in concentration at the oxygen electrode proportional to the Oxygen concentration [12], this is perhaps used as the simplest platform for amperometric sensors, Clark later in 1962 entrapped Glucose Oxidase enzyme into his Oxygen electrode using dialysis membrane to use an amperometric glucose sensor [13].

3.2.1.2. Potentiometric Sensors.

Change in potential at the working electrode compared to the reference at equilibrium in an electrochemical reaction is determined using Potentiometric biosensors and it works on constant current mode. In other words, charges accumulated at the working electrode with respect to the reference electrode are measured at a zero or negligible current flow between them. Concentrations and Potential values here are related using the Nernst equation []:

$$EMF\ or\ E_{cell} = \mathrm{E}^{0}_{\mathrm{cell}} - \frac{RT}{nF} lnQ$$

Where E_{cell} is the cell potential at zero current, also known as Electromotive Force (EMF), $\mathrm{E}^{0}_{\mathrm{cell}}$ is the constant potential contribution to the cell, T is absolute Temperature in Kelvin, R is the gas constant, n is no. of charges and F is Faraday constant and Q is the ratios of ion concentration at anode and cathode.

Ion selective electrodes like pH electrode, ammonia or CO_2 sensitive electrodes are used to measure the changes in ion concentrations. Many types of Field effect Transistors (FET) based potentiometric devices have also been studied for measuring the changes in the pH, ion concentrations and to check the kinetics of enzymes based catalytic reactions. Light Addressable Potentiometric sensor (LAPS) is another Potentiometric sensor that uses the photovoltaic effect for the point of measurement determination [14]. Achievable detection limits using potentiometric sensors is usually between 10^{-8} and 10^{-11} M [15].

3.2.1.3. Conductometric/Impedimetric sensors

Many enzymes reactions or reception of biological receptors can be monitored by ion conductometry or impedimetric devices. Conductometric measurements are used when the medium conductivity (conductance or resistivity) is altered during a reaction. Sensing is conducted when the analyte (like the electrolyte solution) or the electrode is able to carry electrical current when an alternating potential has been applied between inert electrodes[16][17]. In case of enzymes, ionic strength of the solution changes due to the enzymatic reactions i.e. changes in concentration of the charged species can be directly monitored using these sensors [16][18]. Apart from this, conductance at the electrode due to antibody/Antigen interactions DNA hybridizations or other receptor immobilizations can also be measured [19]. Electrochemical impedance spectroscopy (EIS) is the most common technique to measure the change in conductivity/resistivity or charging capacity at the electrode/electrolyte interface, impedance is measured over a wide range frequency range, mostly from 100 kHz to 1 mHz. This frequency dependent response of the changes occurring at the electrode/electrolyte interface gives information about the solution resistance, charge transfer between electrode/electrolyte, double layer capacitance and diffusion transport of the species to and from bulk of the solution. Two types of EIS measurements can be performed that are faradaic and non-faradaic. Faradaic EIS relies on the increased or decreased charge transfer resistance occurring due to binding of receptors to the electrode surface or

analyte to the receptor using redox probes whereas in the latter one, no redox probes are used and the measurements are based on changes in formation of double layer i.e. double layer capacitance upon binding of receptors or analytes at the electrode surface[20]. Interdigitated two electrodes system for capacitive sensing have garnered particular interest since sometime [21][22][23]. EIS gives us the advantage of label free sensing as well as real time monitoring of binding affinities and the EIS based sensors have been used in detection of cancer, pollutants, bacterias, toxins etc. [20]. For instance, Bertok *et al* [24] used EIS to study for the changes in charge transfer resistance at the gold electrode modified with Au nanoparticles for detection of glycoproteins and achieved an ultra-low detection limit of ~1 aM. Hang *et al* prepared a low density DNA microarray over inderdigitated electrodes to detect low density, label-free detection of DNAs using EIS [25]. Disadvantages of using EIS is its variable reproducibility maybe due to non-specific binding and high limit of detections [26]

3.3. Graphene based Electrochemical sensors

Graphene possess many fine qualities like easy processability and homogenous distribution of electrochemical active sites at nano-level, fast heterogeneous electron transfer kinetics (ETK), wide electrochemical potential window (~2.5V in 0.1mM Phosphate buffer saline) [27], high electrical conductivity, edge plane sites/defects, biocompatibility etc. that makes it an interesting material for electrochemical sensors. Papakonstantinou *et al.* in their work showed that the multilayer graphene prepared over Si substrates without any catalysts with 2-3nm sharp knife like edges showed very fast ETK and electrocatalytic activity. They used the electrode for electrochemical sensing of Dopamine in presence of ascorbic acid and uric acid. The sensor could simultaneously detect the three chemical compounds and the sensing ability was better than other unmodified and un-treated carbon electrodes like HOPG (highly Ordered Pyrolytic Graphite) and Glassy carbon electrode and was comparable only with the EPPG (Edge Plane Pyrolytic Graphite) [28]. This faster and favorable electron transfer kinetics in

graphene compared to graphite was also demonstrated by Zhou *et al* [27]. As mentioned earlier, (bio)receptor molecules that interacts with the analytes are immobilized onto the electrode surface (graphene in this case) by either chemical bonding [29], entrapment into the graphene surface [30][31] or by simple adsorption [32][33][34]. Also, modifications to the graphene sheets like electrodeposition, polymerization, doping etc. to impart specific properties to graphene needed for the particular application can be done. This functionalization can provide direct electron transfer (DET) between the electrode and the receptor molecule. Enzymatic biosensors a major class of biosensors has been significant for research purposes as well as commercially for disease diagnosis. Here the redox enzymes are wired directly into the graphene electrodes for a direct electron transfer. Graphene have been conjugated with different metal nanoparticles [35], polymers [36], chitosan [37], metal oxides [38] etc. for enzymatic sensing of glucose cholesterol, hemoglobin etc. Apart from providing the advantage of DET, enzyme loading capacity is increased due to the large surface area of graphene increasing the device sensitivity. DET between the receptor and functionalized Graphene can take place without the use of any mediator. Ping *et al.* reported the use of Graphene for detection of H_2O_2, where they deposited electrochemically exfoliated rGO over ionic liquid doped screen printed electrode (SPE) and successfully detected the enzymatic product H_2O_2 in the linear range of 0.15 µM to 1.8 mM with the detection limit of oxidation/reduction of H_2O_2 0.05 µM/0.08 µM. Carrying on with this strategy, they prepared an enzymatic glucose sensor by immobilizing glucose oxidase that produces H_2O_2 as the enzyme by-product, they were able to detect glucose levels with a sensitivity of 22.78 mA/mM/cm^2 with detection limit of glucose of 1 µM [39]. The DET from gluscose oxidase using graphene was studied by Wisitsoraat *et al*. In their work they used a composite of graphene/poly(3,4-ethylenedioxythiophene): polystyrene sulfonic modified SPE, where the direct electrochemical resposnse of the enzyme at the fabricated electrode was studied using Cyclic Voltammetry (CV) and the electrode exhibited an amperometric sensitivity of 7.23 µA/mM [40]. Park *et al*, created a thin film transistor (TFT) based

sensor using a composite of Graphene and carboxylated polypyrrole nanotubes, the composite microelectrode created better electrical connections resulting in enhanced electron transfer. This Glucose detection using Glucose oxidase exhibited a very fast response within <1 s with a detection limit of 1 nM. Enzymatic biosensors are highly sensitive, however, the disadvantages of using enzymes are their instability in different conditions like pH, temperature, chemical etc., their inactivation affecting the device performance along with being expensive [41][42]. This can be overcome by using non-enzymatic biosensors that are easy to fabricate, have better stabilities and can achieve continuous monitoring. For instance, for glucose monitoring, the electrocatalytic responses of various materials like noble metals, metal oxides, graphene, polymers or their hybrids have been investigated for oxidation of glucose. In one of the example demonstrated by Sun *et al* [43] a composite of CuO/graphene to modify screen printed electrode for non-enzymatic glucose sensing with superior sensitivities and limit of detection compared to the glassy carbon electrodes was prepared. Other examples of graphene based non-enzymatic sensors can be seen from the reviews [44][45]. DNAs are arguably one of the most important bio-elements owing to the unique and inherent base pair interactions between the two complimentary strands. Hybridization between two single stranded complimentary DNAs is the basis of detection in DNA biosensors. Typically, a single stranded probe (ssDNA) is immobilized uniformly onto the recognition layer where the interaction with the target strand occurs generating a signal (mechanically, electrically or optically) which is then read and presented in an understandable manner by the transducer. It is therefore necessary for the overall device performance to align and immobilize DNAs in an organized way that their base pairs are available for the hybridization with the target probes. When graphene is concerned, in an easy labelled or label free optical detection of DNA hybridization is studied by simple adsorption [46][47][33] whereas for electrical or electrochemical detection most of the work is usually focussed on single stranded DNA (ssDNA), RNA, aptamers conjugated with graphene [48][49][50][51]. In the study by Zhou *et al.* showed that the detection of four free bases was better at

graphene modified GCE compared to the graphite modified GCE [27]. One of the most used strategies is the use of Gold Nanoparticles (AuNPs) for attachment of thiolated DNAs via thiol-Au chemistry [52][53]. Immunosensors relies on the specific conjugation of antigens and antibodies. Just like enzymatic sensor, graphene helps in higher loading of antibodies along with enhanced electrochemical performances. Borisova *et al*. prepared an amperometric immunosensor using AuNPs/rGO composite coated over SPE for detection of Brettanomyces Bruxellensis in buffered solution and red wine. The specific antibodies were immobilized onto the electrode surface via carbodimide coupling with the help of 3-mercaptopropionic acid. This design led them to obtained very low detection limits of 8 CFU/mL and 56 CFU/mL in buffer and red wine solutions respectively [54]. Another similar work was done by Mehta *et al* where graphene modified SPE was used for impedimetric detection of Parathion with very low detection limits of 52 pg/L and the sensing range of 0.1–1000 ng/L was shown [55]. Quite recently, graphene based immunosensors have been developed for detection viruses and disease causing micr-organisms, for instance Zika Virus [56], Dengue Virus [57], Rotavirus [58], E.Coli [59]. Numerous other labelled and label-free graphene based electrochemical immunosenosrs can be found in the literarture [60][61][62][63][64]. Other bioreceptors can be the cells or micro-organism (whole cell biosesnors) [65]. These sensors can detect wider ranges of substances, hence are more sensitive to the modifications in the surrounding environment and are stable in comparatively broader range of pH and temperatures [10]. Due to these advantages, they are highly studied and employed for food and environmental monitoring, drug screenings etc. [66][65]. But the maintenance, selection and cultures of the cells, micro-organisms can be a complex task [67]. Apart from detection of bio-compounds or molecules, many chemical compounds or environmental pollutants from the surrounding can be detected with high sensitivity using graphene or graphene hybrids such heavy metals, pesticides, explosives industrial compounds etc. Heavy metals like Lead (Pb), Cadmium (Cd), Zinc (Zn) Arsenic (As) etc. pose a great danger to humans and the environment, exposure to even very little amounts of these ions can be life

threatening [68][69][70][71], because of which their detection at low concentrations is highly needed. Graphene for the reasons of high surface area, metal ions-sorption properties and high electrical conductivity, has been used widely for their electrochemical detection using Anodic Stripping Voltammetry (ASV). Xuan *et al* had prepared a micro patterns of rGO using lithography followed by electrodeposition of Bismuth over Au coated Silicon substrate and obtained the detection limits of 0.4 and 1 ppb for Pb and Cd respectively [72]. Bismuth has been known to make alloys, either binary or multi-component with the heavy metals which results in enhanced sensitivity of sensor [73][74], this is why a lot of articles have worked on preparing composites of graphene and Bismuth in different forms for detection of heavy metals [75][76][77][78]. Another highly uniform size composite of SnO_2/rGO was prepared by Wei *et al* [79] where the composite also acted as the electrochemical catalyst for square wave anodic stripping voltammetry for simultaneous detection of Cd^{2+}, Pb^{2+}, Cu^{2+}, and Hg^{2+} with the detection limit 0.1, 0.18, 0.23, and 0.28 nM respectively. There have been a lot of reviews studying the use of graphene and their composites for heavy metals detection [80][81][81][82]. Modifications of graphene using ion-exchange polymers like PSS (poly(styrene-sulfonate)) [83] or nafion [84] have been also done to have advantages of large surface, high conductivity and metal adsorption properties of Graphene and cation exchange properties from the polymer. Chalupniak and Merkoçi prepared a lab-on-chip microfluidic platform using graphene oxide-poly(dimethylsiloxane) (GO-PDMS) composite for higher loading/preconcentration of the metal ions for their detection exhibiting a reversible adsorption and desorption of the ions. The system could achieve a very low concentrations of 0.5ppb Pb, and because of mechanical durability of the device and ions reversible adsorption/desorption, the device was re-useable [85]. Graphene has been utilised for sensing of other compounds such as phenol containing compounds, Uric acids, dopamine Anti-oxidants like Ascorbic acids, etc. [86][87][87]

3.4. Flexible wearable and wireless Graphene based sensors

Flexible and wearable sensors can be employed as an alternative to the traditional expensive and time-consuming analytical tools that also require large volumes of testing samples. These devices also hold the benefit of being non-invasive that can be applied for continuous real time monitoring. The active material must be biocompatible in order to be applied along with easy proccessability for printing and mass production purposes. For this reason, Graphene is one of the most suitable materials, as described since the beginning. Graphene possesses all the properties to be used as an active material like the easy and cost effective mass production techniques providing good and acceptable conductivities along with ability to be printed by various different methods.

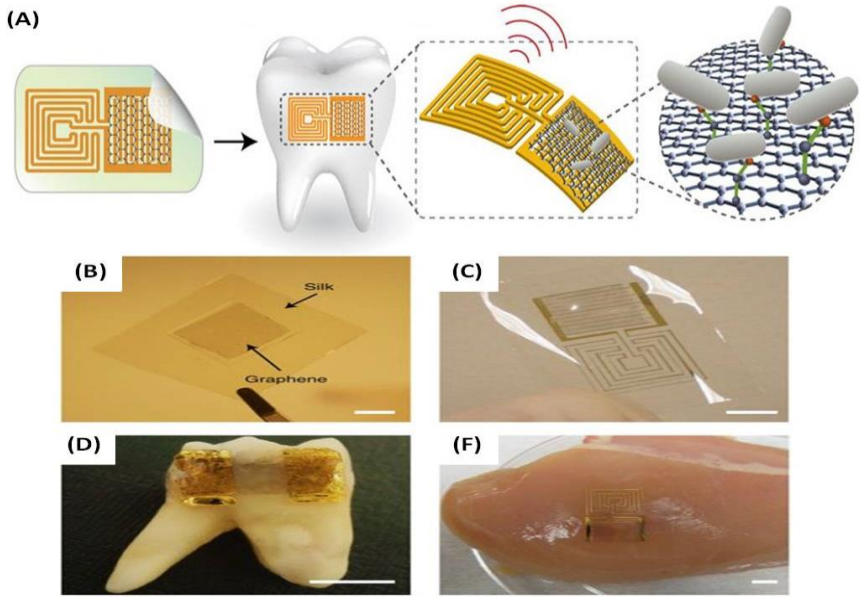

Figure 3: (A) Schematic of the fabricated device, (B) Printed graphene over Bioresorbable Silk, (C) Printed device with Au and Graphene electrodes, (D) Graphene sensor transferred over the (E) tooth and skin [88]

A wireless bacterial graphene sensor was proposed by Mannoor *et al* (Fig. 3), which was integrated with the Au Inductive coil for wireless transmission, Au interdigitated capacitor electrodes that were connected with the Graphene resistance sensor over a bioresorbable silk substrate. They demonstrated

in their work that the Graphene patterns were attached and transferred to the desired area (tooth enamel) when silk dissolved in Liquid media. Measuring the resistance of the graphene Au electrode modified with a bi-functional peptide, they could achieve the detection of bacteria at single cell level [88].

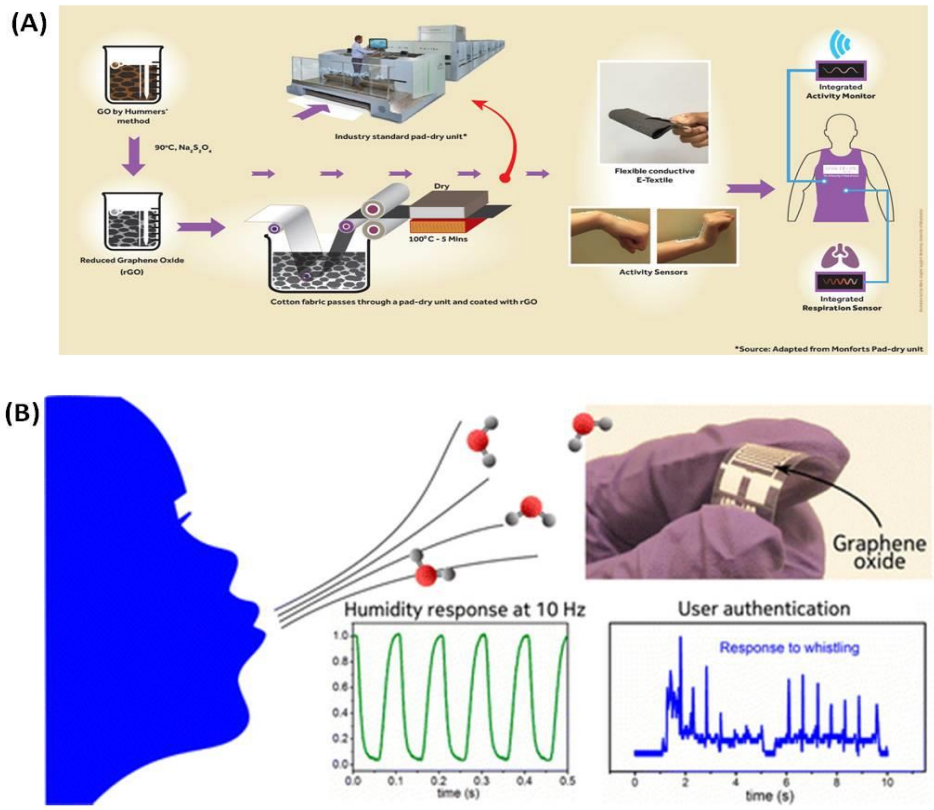

Figure 4: (A) Schematic of the scalable production of Graphene based activity monitoring sensor [89] (B) Printed graphene oxide based humidity sensor [90]

A Battery free, wireless Radio Frequency Identification Humidity sensor was fabricated by Huang *et al* [91] using the dielectric properties of GO. In this, Insulating GO was screen printed over Graphene RFID antenna and the sensor showed increase in the relative dielectric permittivity of GO with change in humidity as a result of uptake of water by GO. Inkjet printed enzymatic graphene electrochemical sensor for detection paraoxan, an organophosphate was fabricated, achieving a low detection limit of 3 nM with

a rapid response of 5 s. They electrodeposited Platinum nanoparticles (Pt NPs) for enhancing the electrical conductivity, surface area and electro-active nature of the electrode. The enzyme phosphotriesterase (PTE) was immobilised using Gluteraldehyde cross linking for the amperometric detection [92]. Karim *et al*, from the group of Novoselov, had fabricated activity monitoring (motion) sensors over textiles (Fig. 4(A)) using a pad-dry coating technique for its scalable productions by measuring the changes in resistance of the material during stretching, bending or twisting [89]. To prepare a humidity sensor, Borini *et al.* used hydrophilic properties of GO along with the transparency and flexibility to fabricate the sensor with an ultra-fast response of ∼30 m, Fig. 4(B) [90]. A wearable and stretchable patch for detection of glucose level from sweat was prepared by Lee *et al*,. Their device was integrated with multiple sensors, actuators and sweat control layers. At first humidity is monitored, which, when increases by more than 80% activates the other sensors like the pH, temperature and electrochemical Glucose sensor. In addition, the patch is integrated with micro-needles containing the drugs for diabetes that can be activated with another integrated thermal actuator (Fig. 5(A)) [93]. Another example of flexible Glucose sensor was demonstrated by Park *et al* in which they integrated the electrochemical glucose sensor in a transparent and flexible contact lens for glucose detection from tears. The graphene hybrid with Ag nanowires improved the conductivity, transparency and strechability of the contact lens, Fig. 5(B). The sensor was able to achieve the detection limit of approximately 12.57 µM with a response time of 1.3s [94]. Another example of integrated glucose sensor includes a microfluidic chip integrated with an electrochemical sensor using Graphene Au hybrid for continuous monitoring of glucose level was fabricated by Pu *et al* [95].

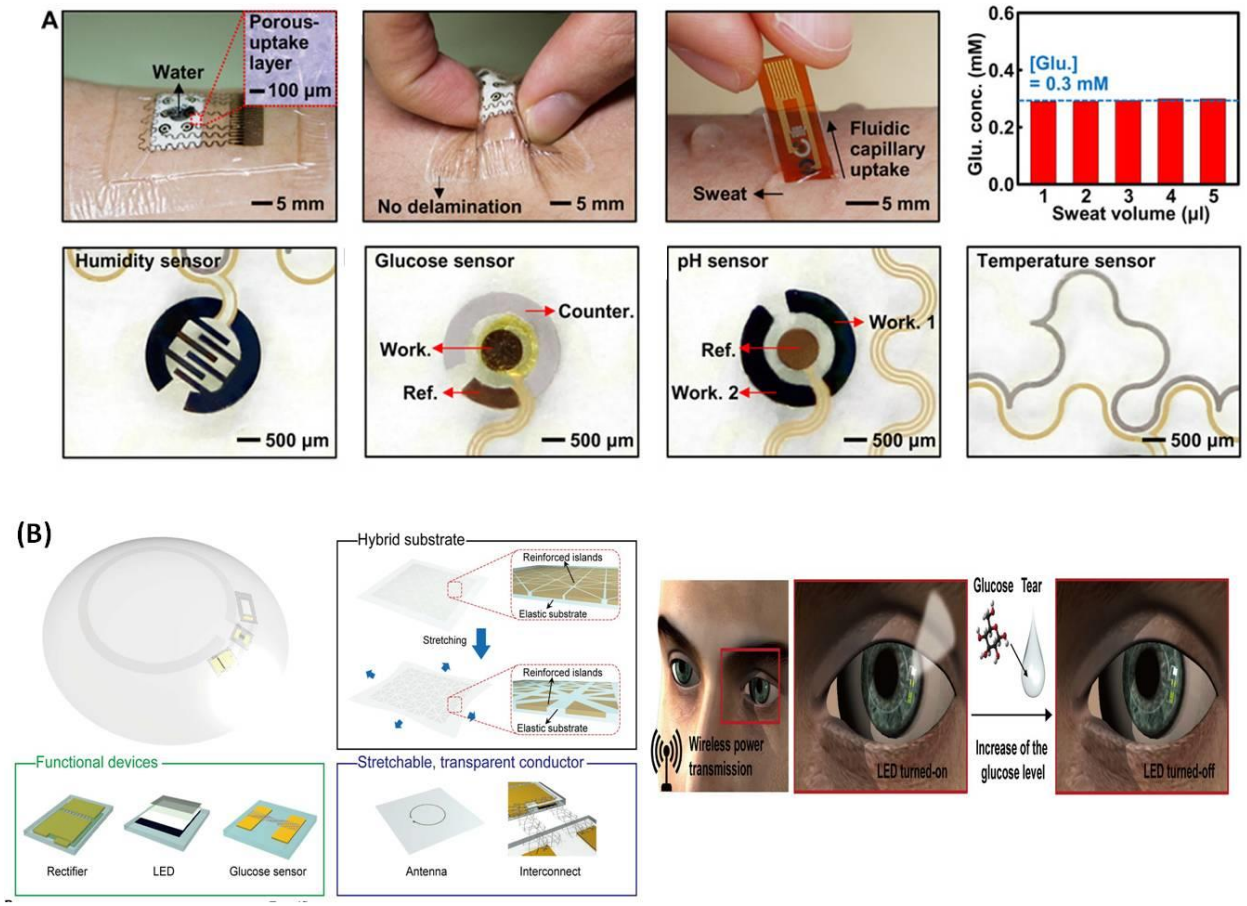

Figure 5: (A) wearable sweat analysis patch showing the adhesion over skin and sweat uptake (above) and the integrated different sensors (below) [93]. (B) Schematic and the operation of the soft, smart and wireless contact lense for Glucose sensing from the tear analysis [94]

Screen printed Graphene and Carbon nanotubes (CNTs) pastes over textile for improved conductive properties and sensing towards chemical vapors was shown by Skrzetuska *et al* [96] Another rGO based wireless, battery-free gas (ammonia vapour) sensor was demonstrated by [97] using inkjet printing technique over paper and Kapton substrates. Numerous other examples of graphene used for sensing of glucose, breath, wound, strain, motion, humidity etc for wireless and flexible devices application can be found [98][99][100][28][29].

3.5. Refrences

[1] A. Hulanicki, S. and Glab, and F. Ingman, "Chemical Sensors: Definitions and Classifications," *Pure Appl. Chem.*, vol. 63, no. 9, pp. 1247–1250, 1991.

[2] J. R. Stetter, W. Penrose, and S. Yao, "Sensors, Chemical Sensors, Electrochemical Sensors, and ECS," *J. Electrochem. Soc. - J Electrochem SOC*, vol. 150, 2003.

[3] N. Sheikh and O. Sheikh, "Forecasting of Biosensor Technologies for Emerging Point of Care and Medical IoT Applications Using Bibliometrics and Patent Analysis," 2016.

[4] A. Ahmed, J. V Rushworth, N. A. Hirst, and P. A. Millner, "Biosensors for Whole-Cell Bacterial Detection," *Clin. Microbiol. Rev.*, vol. 27, no. 3, pp. 631–646, 2014.

[5] N. Bhalla, P. Jolly, N. Formisano, and P. Estrela, "Introduction to biosensors," *Essays Biochem.*, vol. 60, no. 1, pp. 1–8, 2016.

[6] J. Andreu, D. Leff, H. Ip, and G.-Z. Yang, "From Wearable Sensors to Smart Implants-–Toward Pervasive and Personalized Healthcare," *IEEE Trans. Biomed. Eng.*, vol. 62, 2015.

[7] A. J. Bandodkar and J. Wang, "Non-invasive wearable electrochemical sensors: a review," *Trends Biotechnol.*, vol. 32, no. 7, pp. 363–371, 2014.

[8] T. Q. Trung and N.-E. Lee, "Flexible and Stretchable Physical Sensor Integrated Platforms for Wearable Human-Activity Monitoringand Personal Healthcare," *Adv. Mater.*, vol. 28, no. 22, pp. 4338–4372, 2016.

[9] R. Monosik, M. Streansky, and E. Surdik, "Biosensors-classification, characterization and new trends," *Acta Chim. Slovaca*, vol. 5, pp. 109–120, 2012.

[10] A. A. Zuber, E. Klantsataya, and A. Bachhuka, "3.06 - Biosensing," in *Comprehensive Nanoscience and Nanotechnology (Second Edition)*, Second Edition., D. L. Andrews, R. H. Lipson, and T. Nann, Eds. Oxford: Academic Press, 2019, pp. 105–126.

[11] D. Grieshaber, R. MacKenzie, J. and Voros, and E. Reimhult, "Electrochemical Biosensors - Sensor Principles and Architectures," *Sensors*, vol. 8, pp. 1400–1458, 2008.

[12] L. C. Clark, "Monitor and Control of Blood and Tissue Oxygen Tensions," *Am. Soc. Artif. Intern. Organs*, vol. 2, no. 1, pp. 41–48, 1956.

[13] L. C. Clark Jr. and C. Lyons, "ELECTRODE SYSTEMS FOR CONTINUOUS MONITORING IN CARDIOVASCULAR SURGERY," *Ann. N. Y. Acad. Sci.*, vol. 102, no. 1, pp. 29–45, 1962.

[14] J. C. Owicki, L. J. Bousse, D. G. Hafeman, G. L. Kirk, J. D. Olson, H. G. Wada, and J. W. Parce, "The Light-Addressable Potentiometric Sensor: Principles and Biological Applications," *Annu. Rev. Biophys. Biomol. Struct.*, vol. 23, no. 1, pp. 87–114, 1994.

[15] E. Bakker and E. Pretsch, "Potentiometric sensors for trace-level analysis," *TrAC Trends Anal. Chem.*, vol. 24, no. 3, pp. 199–207, 2005.

[16] P. D'Orazio, "Biosensors in clinical chemistry," *Clin. Chim. Acta*, vol. 334, no. 1, pp. 41–69, 2003.

[17] S. Dzyadevych and N. Jaffrezic-Renault, "6 - Conductometric biosensors," in *Biological Identification*, R. P. Schaudies, Ed. Woodhead Publishing, 2014, pp. 153–193.

[18] X. Luo and J. J. Davis, "Electrical biosensors and the label free detection of protein disease biomarkers," *Chem. Soc. Rev.*, vol. 42, no. 13, pp. 5944–5962, 2013.

[19] E. bahadır and M. Kemal Sezgintürk, "A review on impedimetric biosensors," *Artif. cells, nanomedicine, Biotechnol.*, vol. 44, pp. 1–15, 2014.

[20] J. Hammond, N. Formisano, P. Estrela, S. Carrara, and J. Tkac, "Electrochemical biosensors and nanobiosensors," *Essays Biochem.*, vol. 60, pp. 69–80, 2016.

[21] N. S. Mazlan, M. Ramli, M. M. A. B. Abdullah, D. S. Che Halin, S. S. Mat Isa, L. F. A. Talip, N. Danial, and S. A. Zainol Murad, "Interdigitated electrodes as impedance and capacitance biosensors: A review," in *AIP Conference Proceedings*, 2017, vol. 1885, p. 20276.

[22] H. Cui, X. Xiong, B. Gao, Z. Chen, Y. Luo, F. He, S. Deng, and L. Chen, "A Novel Impedimetric Biosensor for Detection of Lead (II) with Low-cost Interdigitated Electrodes Made on PCB," *Electroanalysis*, vol. 28, no. 9, pp. 2000–2006, 2016.

[23] N. Couniot, D. Flandre, L. A. Francis, and A. Afzalian, "Bacteria Detection with Interdigitated Microelectrodes: Noise Consideration and Design Optimization," *Procedia Eng.*, vol. 47, pp. 188–191, 2012.

[24] T. Bertok, A. Sediva, J. Katrlik, P. Gemeiner, M. Mikula, M. Nosko, and J. Tkac, "Label-free detection of glycoproteins by the lectin biosensor down to attomolar level using gold nanoparticles," *Talanta*, vol. 108, pp. 11–18, 2013.

[25] T. C. Hang and A. Guiseppi-Elie, "Frequency dependent and surface characterization of DNA immobilization and hybridization," *Biosens. Bioelectron.*, vol. 19, no. 11, pp. 1537–1548, 2004.

[26] J. S. Daniels and N. Pourmand, "Label-Free Impedance Biosensors: Opportunities and Challenges," *Electroanalysis*, vol. 19, no. 12, pp. 1239–1257, 2007.

[27] M. Zhou, Y. Zhai, and S. Dong, “Electrochemical Sensing and Biosensing Platform Based on Chemically Reduced Graphene Oxide,” *Anal. Chem.*, vol. 81, no. 14, pp. 5603–5613, 2009.

[28] N. G. Shang, P. Papakonstantinou, M. McMullan, M. Chu, A. Stamboulis, A. Potenza, S. S. Dhesi, and H. Marchetto, “Catalyst-Free Efficient Growth, Orientation and Biosensing Properties of Multilayer Graphene Nanoflake Films with Sharp Edge Planes,” *Adv. Funct. Mater.*, vol. 18, no. 21, pp. 3506–3514, 2008.

[29] S. L. Hirsh, M. M. M. Bilek, N. J. Nosworthy, A. Kondyurin, C. G. dos Remedios, and D. R. McKenzie, “A Comparison of Covalent Immobilization and Physical Adsorption of a Cellulase Enzyme Mixture,” *Langmuir*, vol. 26, no. 17, pp. 14380–14388, 2010.

[30] S. Liébana Girona and G. Drago, “Bioconjugation and stabilisation of biomolecules in biosensors,” *Essays Biochem.*, vol. 60, pp. 59–68, 2016.

[31] M. M. Barsan, M. David, M. Florescu, L. Ţugulea, and C. M. A. Brett, “A new self-assembled layer-by-layer glucose biosensor based on chitosan biopolymer entrapped enzyme with nitrogen doped graphene,” *Bioelectrochemistry*, vol. 99, pp. 46–52, 2014.

[32] B. Liu, S. Salgado, V. Maheshwari, and J. Liu, “DNA adsorbed on graphene and graphene oxide: Fundamental interactions, desorption and applications,” *Curr. Opin. Colloid Interface Sci.*, vol. 26, pp. 41–49, 2016.

[33] M. Wu, R. Kempaiah, P.-J. J. Huang, V. Maheshwari, and J. Liu, “Adsorption and Desorption of DNA on Graphene Oxide Studied by Fluorescently Labeled Oligonucleotides,” *Langmuir*, vol. 27, no. 6, pp. 2731–2738, 2011.

[34] W. Putzbach and N. J. Ronkainen, “Immobilization Techniques in the Fabrication of Nanomaterial-Based Electrochemical Biosensors: A Review,” *Sensors*, vol. 13, no. 4, pp. 4811–4840, 2013.

[35] P. Yin, T.-H. Kim, J.-W. Choi, and K.-B. Lee, “Prospects for graphene-nanoparticle-based hybrid sensors,” *Phys. Chem. Chem. Phys.*, vol. 15, 2013.

[36] L. A. Mercante, M. H. M. Facure, R. C. Sanfelice, F. L. Migliorini, L. H. C. Mattoso, and D. S. Correa, “One-pot preparation of PEDOT:PSS-reduced graphene decorated with Au nanoparticles for enzymatic electrochemical sensing of H2O2,” *Appl. Surf. Sci.*, vol. 407, pp. 162–170, 2017.

[37] A. Rabti, W. Argoubi, and N. Raouafi, “Enzymatic sensing of glucose in artificial saliva using a flat electrode consisting of a nanocomposite prepared from reduced graphene oxide, chitosan, nafion and glucose oxidase,” *Microchim. Acta*, vol. 183, 2016.

[38] F. Parnianchi, M. Nazari, J. Maleki, and M. Mohebi, “Combination of graphene and graphene oxide with metal and metal oxide nanoparticles in fabrication of electrochemical enzymatic biosensors,” *Int. Nano Lett.*, vol. 8, no. 4, pp. 229–239, Dec. 2018.

[39] X. Zhu, X. Niu, H. Zhao, and M. Lan, “Doping ionic liquid into Prussian blue-multiwalled carbon nanotubes modified screen-printed electrode to enhance the nonenzymatic H2O2 sensing performance,” *Sensors Actuators B Chem.*, vol. 195, pp. 274–280, 2014.

[40] A. Wisitsoraat, S. Pakapongpan, C. Sriprachuabwong, D. Phokharatkul, P. Sritongkham, T. Lomas, and A. Tuantranont, “Graphene–PEDOT:PSS on screen printed carbon electrode for enzymatic biosensing,” *J. Electroanal. Chem.*, vol. 704, pp. 208–213, 2013.

[41] G. Rocchitta, A. Spanu, S. Babudieri, G. Latte, G. Madeddu, G. Galleri, S. Nuvoli, P. Bagella, M. I. Demartis, V. Fiore, R. Manetti, and P. A. Serra, “Enzyme Biosensors for Biomedical Applications: Strategies for Safeguarding Analytical Performances in Biological Fluids,” *Sensors*, vol. 16, no. 6, 2016.

[42] G. Rocchitta, A. Spanu, S. Babudieri, G. Latte, G. Madeddu, G. Galleri, S. Nuvoli, P. Bagella, M. Ilaria Demartis, V. Fiore, R. Manetti, and P. Andrea Serra, “Analytical Problems in Exposing Amperometric Enzyme Biosensors to Biological Fluids,” *Sensors*, vol. 16, p. 780, 2016.

[43] C.-L. Sun, W.-L. Cheng, T.-K. Hsu, C.-W. Chang, J.-L. Chang, and J.-M. Zen, “Ultrasensitive and highly stable nonenzymatic glucose sensor by a CuO/graphene-modified screen-printed carbon electrode integrated with flow-injection analysis,” *Electrochem. commun.*, vol. 30, pp. 91–94, 2013.

[44] G. Gnana kumar, G. Amala, and S. M. Gowtham, “Recent advancements, key challenges and solutions in non-enzymatic electrochemical glucose sensors based on graphene platforms,” *RSC Adv.*, vol. 7, no. 59, pp. 36949–36976, 2017.

[45] C. I. L. Justino, A. R. Gomes, A. C. Freitas, A. C. Duarte, and T. A. P. Rocha-Santos, “Graphene based sensors and biosensors,” *TrAC Trends Anal. Chem.*, vol. 91, pp. 53–66, 2017.

[46] J. S. Park, N.-I. Goo, and D.-E. Kim, “Mechanism of DNA Adsorption and Desorption on Graphene Oxide,” *Langmuir*, vol. 30, no. 42, pp. 12587–12595, 2014.

[47] B. Liu, Z. Sun, X. Zhang, and J. Liu, “Mechanisms of DNA Sensing on Graphene Oxide,” *Anal. Chem.*, vol. 85, no. 16, pp. 7987–7993, 2013.

[48] Y. Hu, F. Li, X. Bai, D. Li, S. Hua, K. Wang, and L. Niu, “Label-free electrochemical impedance sensing of DNA hybridization based on functionalized graphene sheets,” *Chem. Commun.*, vol. 47, no. 6, pp. 1743–1745, 2011.

[49] M. Arvand, M. Sanayeei, and S. Hemmati, “Label-free electrochemical DNA biosensor for guanine and adenine by ds-DNA/poly(L-cysteine)/Fe3O4 nanoparticles-graphene oxide nanocomposite modified electrode,” *Biosens. Bioelectron.*, vol. 102, pp. 70–79, 2018.

[50] Q. Gong, H. Yang, Y. Dong, and W. Zhang, "A sensitive impedimetric DNA biosensor for the determination of the HIV gene based on electrochemically reduced graphene oxide," *Anal. Methods*, vol. 7, 2015.
[51] P. A. Rasheed and N. Sandhyarani, "Graphene-DNA electrochemical sensor for the sensitive detection of BRCA1 gene," *Sensors Actuators B Chem.*, vol. 204, pp. 777–782, 2014.
[52] E. Pensa, E. Cortés, G. Corthey, P. Carro, C. Vericat, M. H. Fonticelli, G. Benítez, A. A. Rubert, and R. C. Salvarezza, "The Chemistry of the Sulfur–Gold Interface: In Search of a Unified Model," *Acc. Chem. Res.*, vol. 45, no. 8, pp. 1183–1192, 2012.
[53] J. I. A. Rashid and N. A. Yusof, "The strategies of DNA immobilization and hybridization detection mechanism in the construction of electrochemical DNA sensor: A review," *Sens. Bio-Sensing Res.*, vol. 16, pp. 19–31, 2017.
[54] B. Borisova, M. L. Villalonga, M. Arévalo-Villena, A. Boujakhrout, A. Sánchez, C. Parrado, J. M. Pingarrón, A. Briones-Pérez, and R. Villalonga, "Disposable electrochemical immunosensor for Brettanomyces bruxellensis based on nanogold-reduced graphene oxide hybrid nanomaterial," *Anal. Bioanal. Chem.*, vol. 409, no. 24, pp. 5667–5674, Sep. 2017.
[55] J. Mehta, P. Vinayak, S. K. Tuteja, V. A. Chhabra, N. Bhardwaj, A. K. Paul, K.-H. Kim, and A. Deep, "Graphene modified screen printed immunosensor for highly sensitive detection of parathion," *Biosens. Bioelectron.*, vol. 83, pp. 339–346, 2016.
[56] S. Afsahi, M. B. Lerner, J. M. Goldstein, J. Lee, X. Tang, D. A. Bagarozzi, D. Pan, L. Locascio, A. Walker, F. Barron, and B. R. Goldsmith, "Novel graphene-based biosensor for early detection of Zika virus infection," *Biosens. Bioelectron.*, vol. 100, pp. 85–88, 2018.
[57] K. Navakul, C. Warakulwit, P. Yenchitsomanus, A. Panya, P. A. Lieberzeit, and C. Sangma, "A novel method for dengue virus detection and antibody screening using a graphene-polymer based electrochemical biosensor," *Nanomedicine Nanotechnology, Biol. Med.*, vol. 13, no. 2, pp. 549–557, 2017.
[58] J. H. Jung, D. S. Cheon, F. Liu, K. B. Lee, and T. S. Seo, "A Graphene Oxide Based Immuno-biosensor for Pathogen Detection," *Angew. Chemie Int. Ed.*, vol. 49, no. 33, pp. 5708–5711, 2010.
[59] Y. Huang, X. Dong, Y. Liu, L.-J. Li, and P. Chen, "Graphene-based biosensors for detection of bacteria and their metabolic activities," *J. Mater. Chem.*, vol. 21, no. 33, pp. 12358–12362, 2011.
[60] G. Wang, G. Xu, X. Zhou, G. Zhang, H. Huang, X. Zhang, and L. Wang, "Electrochemical immunosensor with graphene/gold nanoparticles platform and ferrocene derivatives label," *Talanta*, vol. 103, pp. 75–80, 2013.
[61] C. Gan, Z. Sun, L. Ling, Z. He, H. Lei, and Y. Liu, "Construction of portable electrochemical immunosensors based on graphene hydrogel@polydopamine for microcystin-LR detection using multi-mesoporous carbon sphere-enzyme labels," *RSC Adv.*, vol. 6, 2016.
[62] Y. Wang, Y. Zhang, D. wu, H. Ma, X. Pang, D. Fan, Q. Wei, and B. Du, "Ultrasensitive Label-free Electrochemical Immunosensor based on Multifunctionalized Graphene Nanocomposites for the Detection of Alpha Fetoprotein," *Sci. Rep.*, vol. 7, p. 42361, 2017.
[63] N. Alarfaj and M. F. El-Tohamy, "A label-free electrochemical immunosensor based on gold nanoparticles and graphene oxide for the detection of tumor marker calcitonin," *New J. Chem.*, vol. 41, 2017.
[64] K. Mao, D. Wu, Y. Li, H. Ma, Z. Ni, H. Yu, C. Luo, Q. Wei, and B. Du, "Label-free electrochemical immunosensor based on graphene/methylene blue nanocomposite," *Anal. Biochem.*, vol. 422, no. 1, pp. 22–27, 2012.
[65] Q. Gui, T. Lawson, S. Shan, L. Yan, and Y. Liu, "The Application of Whole Cell-Based Biosensors for Use in Environmental Analysis and in Medical Diagnostics," *Sensors*, vol. 17, p. 1623, 2017.
[66] L. Bousse, "Whole cell biosensors," *Sensors Actuators B Chem.*, vol. 34, no. 1, pp. 270–275, 1996.
[67] P. Wang, G. Xu, L. Qin, Y. Xu, Y. Li, and R. Li, "Cell-based biosensors and its application in biomedicine," *Sensors Actuators B Chem.*, vol. 108, no. 1, pp. 576–584, 2005.
[68] P. Tchounwou, C. Yedjou, A. K Patlolla, and D. Sutton, "Heavy Metal Toxicity and the Environment," *EXS*, vol. 101, pp. 133–164, 2012.
[69] C. M. Stansfield, "LEGISLATION | Contaminants and Adulterants," in *Encyclopedia of Food Sciences and Nutrition (Second Edition)*, Second Edition., B. Caballero, Ed. Oxford: Academic Press, 2003, pp. 3507–3513.
[70] F. M. Badr and O. El-Habit, "Chapter 18 - Heavy Metal Toxicity Affecting Fertility and Reproduction of Males," in *Bioenvironmental Issues Affecting Men's Reproductive and Sexual Health*, S. C. Sikka and W. J. G. Hellstrom, Eds. Boston: Academic Press, 2018, pp. 293–304.
[71] A. F. Abiola, "Chapter 20 - Risk Factors for Kidney Disease in Disadvantaged Populations—Communicable Diseases, Environmental Factors, and Pollutants," in *Chronic Kidney Disease in Disadvantaged Populations*, G. García-García, L. Y. Agodoa, and K. C. Norris, Eds. Academic Press, 2017, pp. 191–207.
[72] X. Xuan, M. F. Hossain, and J.-Y. Park, "A Fully Integrated and Miniaturized Heavy-metal-detection Sensor Based on Micro-patterned Reduced Graphene Oxide," *Sci. Rep.*, vol. 6, p. 33125, 2016.
[73] J. Wang, "Stripping Analysis at Bismuth Electrodes: A Review," *Electroanalysis*, vol. 17, pp. 1341–1346, 2005.
[74] M. Cadevall, J. Ros, and A. Merkoçi, "Bismuth nanoparticles integration into heavy metal electrochemical stripping sensor," *Electrophoresis*, vol. 36, no. 16, pp. 1872–1879, 2015.

[75] J. Ping, Y. Wang, J. Wu, and Y. Ying, "Development of an electrochemically reduced graphene oxide modified disposable bismuth film electrode and its application for stripping analysis of heavy metals in milk," *Food Chem.*, vol. 151, pp. 65–71, 2014.

[76] L. Shi, Y. Li, X. Rong, Y. Wang, and S. Ding, "Facile fabrication of a novel 3D graphene framework/Bi nanoparticle film for ultrasensitive electrochemical assays of heavy metal ions," *Anal. Chim. Acta*, vol. 968, pp. 21–29, 2017.

[77] G.-J. Lee, H.-M. Lee, and C. K. Rhee, "Bismuth nano-powder electrode for trace analysis of heavy metals using anodic stripping voltammetry," *Electrochem. Commun. - Electrochem COMMUN*, vol. 9, pp. 2514–2518, 2007.

[78] S. Lee, S.-K. Park, E. Choi, and Y. Piao, "Voltammetric determination of trace heavy metals using an electrochemically deposited graphene/bismuth nanocomposite film-modified glassy carbon electrode," *J. Electroanal. Chem.*, vol. 766, pp. 120–127, 2016.

[79] Y. Wei, C. Gao, F.-L. Meng, H.-H. Li, L. Wang, J.-H. Liu, and X.-J. Huang, "SnO2/Reduced Graphene Oxide Nanocomposite for the Simultaneous Electrochemical Detection of Cadmium(II), Lead(II), Copper(II), and Mercury(II): An Interesting Favorable Mutual Interference," *J. Phys. Chem. C*, vol. 116, no. 1, pp. 1034–1041, 2012.

[80] Y. Zhi-yu, D. Ning-ning, L. Rui-tao, H. Zheng-hong, and K. Fei-yu, "A review of graphene composite-based sensors for detection of heavy metals," *Xinxing Tan Cailiao/New Carbon Mater.*, vol. 30, pp. 511–518, 2015.

[81] J. Chang, R. Zhou, E. Christensen, R. Heideman, and J. Chen, "Graphene-based sensors for detection of heavy metals in water: A review Chemosensors and Chemoreception," *Anal. Bioanal. Chem.*, vol. 406, 2014.

[82] L. Cui, J. Wu, and H. Ju, "Electrochemical sensing of heavy metal ions with inorganic, organic and bio-materials," *Biosens. Bioelectron.*, vol. 63, pp. 276–286, 2015.

[83] C. Huangfu, L. Fu, Y. Li, X. Li, H. Du, and J. Ye, "Sensitive Stripping Determination of Cadmium(II) and Lead(II) on Disposable Graphene Modified Screen-Printed Electrode," *Electroanalysis*, vol. 25, no. 9, pp. 2238–2243, 2013.

[84] S. Lee, S. Bong, J. Ha, M. Kwak, S.-K. Park, and Y. Piao, "Electrochemical deposition of bismuth on activated graphene-nafion composite for anodic stripping voltammetric determination of trace heavy metals," *Sensors Actuators B Chem.*, vol. 215, pp. 62–69, 2015.

[85] A. Chałupniak and A. Merkoçi, "Graphene Oxide–Poly(dimethylsiloxane)-Based Lab-on-a-Chip Platform for Heavy-Metals Preconcentration and Electrochemical Detection," *ACS Appl. Mater. Interfaces*, vol. 9, no. 51, pp. 44766–44775, 2017.

[86] N. Tukimin, J. Abdullah, and Y. Sulaiman, "Review—Electrochemical Detection of Uric Acid, Dopamine and Ascorbic Acid," *J. Electrochem. Soc.*, vol. 165, pp. B258–B267, 2018.

[87] K. Chen, Z.-L. Zhang, Y.-M. Liang, and F. Sgdsg, "A Graphene-Based Electrochemical Sensor for Rapid Determination of Phenols in Water," *Sensors (Basel).*, vol. 13, pp. 6204–6216, 2013.

[88] M. S. Mannoor, H. Tao, J. D. Clayton, A. Sengupta, D. L. Kaplan, R. R. Naik, N. Verma, F. G. Omenetto, and M. C. McAlpine, "Graphene-based wireless bacteria detection on tooth enamel," *Nat. Commun.*, vol. 3, p. 763+, Mar. 2012.

[89] N. Karim, S. Afroj, S. Tan, P. He, A. Fernando, C. Carr, and K. S. Novoselov, "Scalable Production of Graphene-Based Wearable E-Textiles," *ACS Nano*, vol. 11, no. 12, pp. 12266–12275, 2017.

[90] S. Borini, R. White, D. Wei, M. Astley, S. Haque, E. Spigone, N. Harris, J. Kivioja, and T. Ryhänen, "Ultrafast Graphene Oxide Humidity Sensors," *ACS Nano*, vol. 7, no. 12, pp. 11166–11173, 2013.

[91] X. Huang, T. Leng, T. Georgiou, J. Abraham, R. Raveendran Nair, K. S. Novoselov, and Z. Hu, "Graphene Oxide Dielectric Permittivity at GHz and Its Applications for Wireless Humidity Sensing," *Sci. Rep.*, vol. 8, 2017.

[92] J. A. Hondred, J. C. Breger, N. J. Alves, S. A. Trammell, S. A. Walper, I. L. Medintz, and J. C. Claussen, "Printed Graphene Electrochemical Biosensors Fabricated by Inkjet Maskless Lithography for Rapid and Sensitive Detection of Organophosphates," *ACS Appl. Mater. Interfaces*, vol. 10, no. 13, pp. 11125–11134, 2018.

[93] H. Lee, C. Song, Y. Seok Hong, M. Sung Kim, H. R. Cho, T. Kang, K. Shin, S. Hong Choi, T. Hyeon, and D.-H. Kim, "Wearable/disposable sweat-based glucose monitoring device with multistage transdermal drug delivery module," *Sci. Adv.*, vol. 3, p. e1601314, 2017.

[94] J. Park, J. Kim, S.-Y. Kim, W. H. Cheong, J. Jang, Y.-G. Park, K. Na, Y.-T. Kim, J. H. Heo, C. Y. Lee, J. H. Lee, F. Bien, and J.-U. Park, "Soft, smart contact lenses with integrations of wireless circuits, glucose sensors, and displays," *Sci. Adv.*, vol. 4, no. 1, 2018.

[95] Z. Pu, C. Zou, R. Wang, X. Lai, H. Yu, K. Xu, and D. Li, "A continuous glucose monitoring device by graphene modified electrochemical sensor in microfluidic system," *Biomicrofluidics*, vol. 10, no. 1, p. 11910, 2016.

[96] E. Skrzetuska, M. Puchalski, and I. Krucińska, "Chemically Driven Printed Textile Sensors Based on Graphene and Carbon Nanotubes," *Sensors (Basel).*, vol. 14, pp. 16816–16828, 2014.

[97] T. Le, V. Lakafosis, Z. Lin, C. P. Wong, and M. Tentzeris, "Inkjet-Printed Graphene-Based Wireless Gas Sensor Modules," *Proc. - Electron. Components Technol. Conf.*, 2012.

[98] B. Melai, P. Salvo, N. Calisi, L. Moni, A. Bonini, C. Paoletti, T. Lomonaco, V. Mollica, R. Fuoco, and F. Di Francesco, "A graphene oxide pH sensor for wound monitoring," in *Conference proceedings: ... Annual International Conference of the IEEE Engineering in Medicine and Biology Society. IEEE Engineering in Medicine and Biology Society. Conference*, 2016, vol. 2016.

[99] L. Wang, J. A. Jackman, J. H. Park, E.-L. Tan, and N.-J. Cho, “A flexible, ultra-sensitive chemical sensor with 3D biomimetic templating for diabetes-related acetone detection,” *J. Mater. Chem. B*, vol. 5, no. 22, pp. 4019–4024, 2017.

[100] C. Karuwan, A. Wisitsoraat, P. Chaisuwan, D. Nacapricha, and A. Tuantranont, “Screen-printed graphene-based electrochemical sensor for microfluidic device,” *Anal. Methods*, vol. 9, 2017.

[101] R. Singh, E. Singh, and H. S. Nalwa, “Inkjet printed nanomaterial based flexible radio frequency identification (RFID) tag sensors for the internet of nano things,” *RSC Adv.*, vol. 7, no. 77, pp. 48597–48630, 2017.

[102] S. Oren, H. Ceylan, P. S. Schnable, and L. Dong, “High-Resolution Patterning and Transferring of Graphene-Based Nanomaterials onto Tape toward Roll-to-Roll Production of Tape-Based Wearable Sensors,” *Adv. Mater. Technol.*, vol. 2, no. 12, p. 1700223, 2017.

Article 4: Fully printed one-step biosensing device using graphene/AuNPs composite

Bhawna Nagar, Marc Balsells, Alfredo de la Escosura, Pedro Gómez-Romero and Arben Merkoçi.

Biosensors and Bioelectronics, 129(2019), 238-244

Biosensors and Bioelectronics 129 (2019) 238–244

Contents lists available at ScienceDirect

Biosensors and Bioelectronics

journal homepage: www.elsevier.com/locate/bios

Fully printed one-step biosensing device using graphene/AuNPs composite

Bhawna Nagar[a,b], Marc Balsells[a], Alfredo de la Escosura-Muñiz[a], Pedro Gomez-Romero[b], Arben Merkoçi[a,c,*]

[a] Nanobioelectronics and Biosensors group, Catalan Institute of Nanoscience and Nanotechnology (ICN2), CSIC and The Barcelona Institute of Science and Technology, Campus UAB, Bellaterra, 08193 Barcelona, Spain
[b] Novel Energy-Oriented Materials Group, Catalan Institute of Nanoscience and Nanotechnology (ICN2), CSIC and The Barcelona Institute of Science and Technology, Campus UAB, Bellaterra, 08193 Barcelona, Spain
[c] ICREA, Pg. Lluís Companys, 23, Barcelona 08010, Spain

ARTICLE INFO

Keywords:
RGO
Wax stamping
Screen printing
Electrochemistry
DNA
Biosensing

ABSTRACT

Driven by the growing need of simple, cost efficient and flexible sensing systems, we have designed here a fully printed Reduced Graphene Oxide (rGO) based impedimetric sensor for one step sensing of DNA. The DNA sensor was fabricated by stamping of layered rGO and rGO/gold nanoparticles/single stranded DNA (rGO/AuNPs/ssDNA) composites over PET substrates using wax-printing technique. rGO works as an excellent working electrode, while the AuNPs create a suitable environment for ssDNA immobilization. Counter and reference electrodes were previously screen-printed on the plastic substrate, making thus a compact and highly integrated sensing platform. The change in electron transfer resistance after hybridization with a target ssDNA specific of Coxsackie B3 virus was monitored using electrochemical impedance spectroscopy (EIS), finding a linear response in the range of concentrations 0.01–20 μM. The novel, simple and straightforward one-step printing process for fabrication of a biosensing device developed keeps in mind the growing need of large scale device manufacturing. The successful proof-of-concept for the detection of DNA hybridization can be extended to other affinity biosensors, taking advantage of the integration of the bioreceptor on the sensor surface. Such ready-to-use biosensor would lead to a one-step electrochemical detection.

1. Introduction

Graphene is a well-known one-atom thick two dimensional carbon layer that possess outstanding inherent properties like high mechanical and chemical stability, high thermal and outstanding electrical and thermal conductivity (Novoselov et al., 2004; Geim and Novoselov, 2007). It has a high theoretical surface area of about $\sim 2600\ m^2\ g^{-1}$ that is higher than that of carbon or CNTs (10 or $1315\ m^2\ g^{-1}$). It is sp^2 hybridized and the out of plane π bonds are responsible for the high conductivity. Although these properties are interesting and highly useful for research purposes in different areas, they vary greatly with the quality of graphene (Chen et al., 2011; Bollella et al., 2017) that is, number of layers, sheet size, degree of oxidation or defects, all of which depend in turn of the production procedures. Indeed, graphene materials with varied quality and price can be prepared in different ways considering the end application; broadly by mechanical or chemical exfoliation of graphite, vapor deposition or epitaxial growth etc (Lee et al., 2017). All this has made possible the use of graphene in broad range of applications (Randviir et al., 2014) like solar cells (Roy-Mayhew and Aksay, 2014), energy storage (Dubal et al., 2017; Li and Zhi, 2018), electronics (Lee et al., 2015), (bio)sensing (Shao et al., 2010; Justino et al., 2017) to name a few. Owing to such great properties of graphene, especially due to its high conductivity and high biomolecule loading as a result of high surface area, it is widely explored in the research of (electrochemical) biosensings (Pumera, 2011; Bo et al., 2017), for instance, Huang et al. demonstrated the use of rGO composite with single-walled carbon nanotubes as an effective electrode material for electrochemical sensing (Huang et al., 2013). Apart from this, graphene can interact with the biomolecules using non covalent interactions like π-π or Hydrogen bonding making it more suitable for sensors application.

Two formats are widely followed for DNA sensing by taking advantage of rGO, either attaching (labelled or non-labelled) ssDNAs directly over Graphene sheet via π-π bonding or by modifying Graphene surface by using polymers, nanoparticles etc. that have available groups or sites for binding to the DNA. Most commonly used nanomaterial for

* Corresponding author at: Nanobioelectronics and Biosensors group, Catalan Institute of Nanoscience and Nanotechnology (ICN2), CSIC and The Barcelona Institute of Science and Technology, Campus UAB, Bellaterra, 08193 Barcelona, Spain.
E-mail address: arben.merkoci@icn2.cat (A. Merkoçi).

https://doi.org/10.1016/j.bios.2018.09.073
Received 1 July 2018; Received in revised form 10 September 2018; Accepted 20 September 2018
Available online 21 September 2018
0956-5663/

this purpose are gold nanoparticles (AuNPs) which are typicaly attached to the modified ssDNA at one end via thiol-Au interactions (Lin et al., 2011; Singh et al., 2013).

Flexibility and portability are characteristics most expected for wearable electronic systems and has been used in fancy applications like implantable/wearable sensors (Ray and Joseph, 2013; Singh et al., 2017) Joseph, OLEDs (Lee et al., 2016), transistors (Seo et al., 2016), energy devices (Nagar et al., 2018) etc. Material of interest is usually printed over a flexible substrate (usually plastics) to make a cost efficient, compatible, flexible and easy to handle or use device. The ability to form nanoscale patterns and features over the flexible substrates offers us the advantage of more sensitivity and precision in the sensing devices along with low cost and easy handling. Several printing techniques like screen printing, inkjet printing, roll-to-roll, wax transfer/stamping technique etc. (Søndergaard et al., 2012; Li et al., 2015; Baptista-Pires et al., 2016; Mattana and Briand, 2016) are being used for the fabrication of electrodes. However, it is important to select a particular technique for a particular application. Particularly, our objective is the development of a Point-of-Care (POC) device, which requires a fabrication technique that doesn't need any post printing step for keeping the biomaterial unharmed, being wax stamping technique ideal in this case. POC have been widely used for decades now but is yet continuously refined according the user and manufacturer's needs. The important features to be fulfilled for POCs are (a) ease of fabrication, (b) cost effectiveness and (c) easy handling. The advancements in recent years have provided us with loads of new technological strategies to make improved devices for biorecognition, interactions and sensing (Quesada-Gonzalez and Merkoci, 2018).

In this work, we used chemically exfoliated graphite as it promotes cost effective, large scale production of Graphene Oxide (GO; graphene sheets containing Oxygenated groups such as epoxides, alcohols or carboxyl groups on the surface or the edges of the sheets). The presence of these groups makes GO water dispersible which further helps in making water based inks for printing purposes. Such material was later reduced to reduced Graphene Oxide (rGO) and mixed with already conjugated gold nanoparticle/single stranded DNA probe (AuNPs/ssDNA). Later, wax stamping technique was applied to create the working electrode pattern made of the rGO/AuNPs/ssDNA composite over already screen-printed counter (carbon) and reference (Ag/AgCl) electrodes, allowing us to have a ready-to-use one-step electrochemical biosensor This strategy for patterning rGOe composite doesn't require harsh or toxic solvents helping us to get rid of the post printing steps (annealing) that could affect the functioning of the biorecognition element (DNA in this case). At the end, we get a sensing platform with uniform patterns integrated with the biorector,which is ready to be tested without any further steps (Fig. 1).

2. Experimental section

2.1. Oligonucleotides

Synthetic oligonucleotides were obtained for Sigma-Aldrich. The target sequence employed corresponds to a region characteristic of the ECHO ^{virus} (Coxsackie virus B3).

Probe: 5′-Thi CCTGAATGCGGCTAATCCTA – 3′
Target: 5′-TAGGATTAGCCGCATTCA – 3′
Non-Complementary DNA: 5′ GCATCATAGGCAGTCAGGT 3′

Oligonucleotide solutions were prepared in TE buffer, pH 8 (10 mM Tris-HCl buffer solution, 1 mM in EDTA) and maintained at − 20 °C. Working solution of the oligonucleotide probe was made in 0.1 M Tris. pH 7.2 buffer, while thiol labelled oligonucleotide target strand was diluted in a 2× SSC buffer (300 mM sodium chloride/30 mM sodium citrate),pH 7.2. This solution was stored at 4 °C.

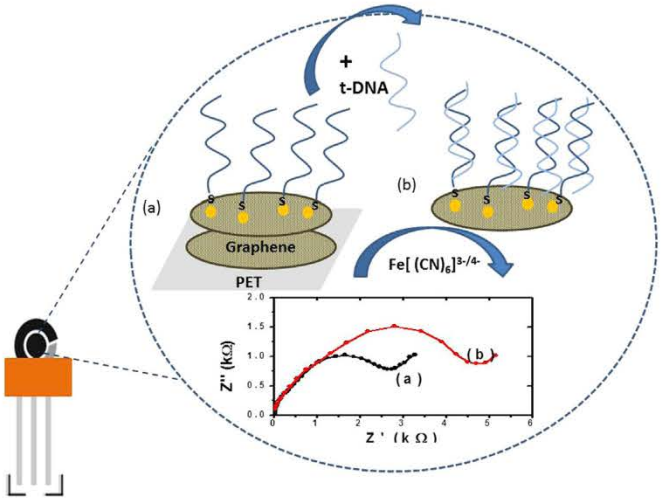

Fig. 1. DNA sensing principle. After stamping on the PET substrates, rGO/AuNPs/ssDNA is incubated with the target ssDNA. DNA duplex formation causes an increase in impedance that is related with the amount of analyte.

2.2. Chemicals and equipment

The GO (Graphenea Graphene Oxide, 4 mg/mL) was purchased from Graphenea Inc (Cambridge, MA 02142, U.S.A). Sodium Citrate ($HOC(COONa)(CH_2COOH)_2$, Sodium chloride (NaCl), ascorbic acid (C6H8O6), BSA (Bovine serum albumin), Trizma® base ($NH_2C(CH_2OH)_3$) and Gold(III) chloride hydrate ($HAuCl4{\cdot}H2O$) were purchased from Sigma-Aldrich Quimica SL (Madrid, Spain). Potassium Hexanocyanoferrate $K_3[Fe(CN)_6]$/ $K_4[Fe(CN)_6]$, was purchased from Panreac Quimica S.L.U. Rest of the general chemicals were purchased from Sigma Aldrich (Spain). All chemicals were of analytical grade and used as received and all the aqueous solutions were prepared in Milli-Q water.

Characterization of the materials, composites and prints were performed using Scanning Electrochemical Microscopy FEI Quanta 650 FEG ESEM and FEI Magellan 400 L (high resolution, HR-SEM) (The Netherlands), High resolution transmission electron microscopy (TEM) FEI Tecnai F20, ultra-violet visible spectroscopy (UV–vis),Cary 4000 UV–vis Spectrophotometer, Agilent technologies, X-ray photoelectron Sepctroscopy (XPS), SPECS PHOIBOS 150 analyser (SPECS GmbH, Berlin, Germany).

Xerox ColourQube 8570 wax printer (compatible with Windows™, MacOS™ and UNIX) and Corel draw software, Screen printing was performed using DEK 248 semi-automatic screen-printer (England) and the electrochemical studies were carried out using Autolab302 Potentiostat/galvanostat PGST30 with the software GPES for cyclic voltammetry and FRA for impedace measurements.

2.3. Methods

2.3.1. Synthesis of rGO

10 mg/mL Graphene oxide (GO) was provided by Angstrom materials. It was reduced by exposing 100 mL of 1 mg/mL GO (solution to 100 mg of ascorbic acid in an autoclave at 121 °C for 45 min).

2.3.2. AuNPs synthesis and conjugation with probe single-stranded DNA (ssDNA)

16 nm sized AuNPs were synthesized using Turkevich's method (Turkevich et al., 1951). Briefly, 50 mL of 1% $HAuCl_4$ solution was heated in an Erlenmeyer flask under vigorous stirring until boiling starts. Then, 1.25 mL of 1% sodium citrate was added while stirring continued. The reaction was kept under same conditions until 10 min and then the heating was stopped and the reaction was let to cool. The

color of the solution changes from deep blue to wine red, indicating AuNPs formation. AuNPs suspension was stored at 4 °C protected from light until further use.

2.3.3. Conjugation of AuNPs with probe DNA (ssDNA)

The particles were then conjugated with the thiol modified ssDNA probe sequence using the protocol described and pioneered by (Mirkin et al. 1996). For this, 190 µL of AuNPs were mixed with 10 µL of 1500 µg/mL thiolated sequence at 250 rpm for 20 h at 25 °C. Later 50 µL of 10 mM phosphate buffer (pH 7)/0.1 M NaCl was added to the above solution and let it stand for 44 h. Finally a centrifugation step at 14,000 rpm at 4 °C for 20 min was carried out to extract the conjugated DNA which was reconstituted in 200 µL Mili-Q water for further use. Later, 0.1% BSA solution in milli-Q water was added to graphene and conjugated AuNPs in separate eppendorf tubes and mixed for 1 h at 600 rpm at room temperature and 4° C respectively.

2.3.4. rGO and rGO/AuNPs/ssDNA patterning

A hydrophilic nitrocellulose membrane (purchased from Merck) with a pore size of 25 µm and diameter of 47 mm was used for making patterns using the wax printer followed by filtration of the water based solutions were done - i) First, a layer of 3 mL solution containing 1.7 mL rGO (1.7 mL; 0.25 mg/mL) hand mixed with 300 µL AuNPs/ssDNA was filtered and then ii) second layer was formed by adding 10 mL of 0.6 mg/mL rGO solution very carefully (not to disturb the already filtered layer) over the first layer. This was removed from the vacuum machine and then stamped over the already patterned (counter and reference) screen printed electrodes. Fig. 2(a-e) shows the schematic printing steps (top) and corresponding pictures of the sensing platform (bottom). The procedure is done in the following way: at first, a specific design is wax printed onto the 25 nm pore sized filter membranes (a), (b) which is then used for filtration of two solutions sequentially (First the mixture of rGO/AuNPs/ssDNA and on top just rGO), (c) this filtererd membrane is then attached to the desired substrate (PET) and passed through the rollers that are already installed in the wax printer to provide the pressure. The substrate is made ready for this step by printing the other electrodes prior to wax stamping, that consisted of 2 steps (i) printing of silver layer for better conductivity and (ii) printing of counter layer (carbon) and reference layer (Ag/AgCl). (R.E and C.E respectively) using a screen-printer. the patterns were left to dry at 100° C overnight to dry the solvents The working area however was left blank intentionally for stamping of Graphene or Graphene composites later. (d) is the printed electrode that is insulated with the kapton tape (e), ready to use for further measurement. Without any further modifications, these electrodes were used for electrochemical tests and biosensing. For hybridization step, 30 µL of different concentrations of complementary and non-complementary DNA (in 2 x SSC buffer, pH 7.2) (De la Escosura-Muñiz et al., 2007) were added to the working electrode of the sensor and incubated for 1 h at room temperature. It was then washed using PBS solution pH 7.4 before obtaining the electrochemical response.

Long-term stability of the sensors was evaluated by storing rGO/AuNPs/ssDNA electrodes at 4 °C when not used and hybridizing with the complementary ssDNA after 0, 5, 10, 15 and 20 days.

2.3.5. Electrochemical set-up

Once the electrodes were fabricated, their electrochemical performance was evaluated. The electrochemical studies of the printed electrodes were always performed in a solution of 10 mM PBS (Phosphate Buffer Saline) containing 20 mM $[Fe(CN)_6]^{3-/4-}$ as redox active probe. Firstly, Cyclic Voltammetry was performed within the voltage range − 0.5–0.8 V vs Ag/AgCl that provided us the oxidation and reduction peaks of Fe(III)/(II) which were taken as the reference peaks. It involved a preliminary study on the graphene concentrations as well as the behavior of different modified printed electrodes. Later, DNA quantification studies were made using Electrochemical Impedance Spectroscopy (EIS) with the software FRA, carried out in the frequency range of 1000–0.05 Hz. For all the measurements, 200 µL of the electrolyte solution was placed on the electrode area (covering all the electrodes) under room temperature without interruption. The electrodes were connected with the potentiostat using a homemade edge connector module.

3. Results and discussion

3.1. Morphological characterizations

Fig. 3 **(a and b)** shows the high resolution scanning electron microscopy (HR-SEM) top view images of printed rGO and rGO/AuNPs, whereas Fig. 3 **(c and d)** shows SEM images corresponding to cross sectional view of the prints over the PET susbtrate. It was observed that the two layers were placed uniformly over the desired area of the electrode and that the conjugated AuNPs appeared only on the surface and not in the bulk.

This was a strategy adopted to have mainly two benefits a) uniform deposition of the conjugated nanoparticles throughout the working electrode and b) to minimize quantity of the biorecognition element used. Another option was to use the rGO/AuNPs/ssDNA directly as the working electrode instead of filtering 2 layers. The transmission electron microscopy (TEM) image of graphene and its mixture with AuNPs

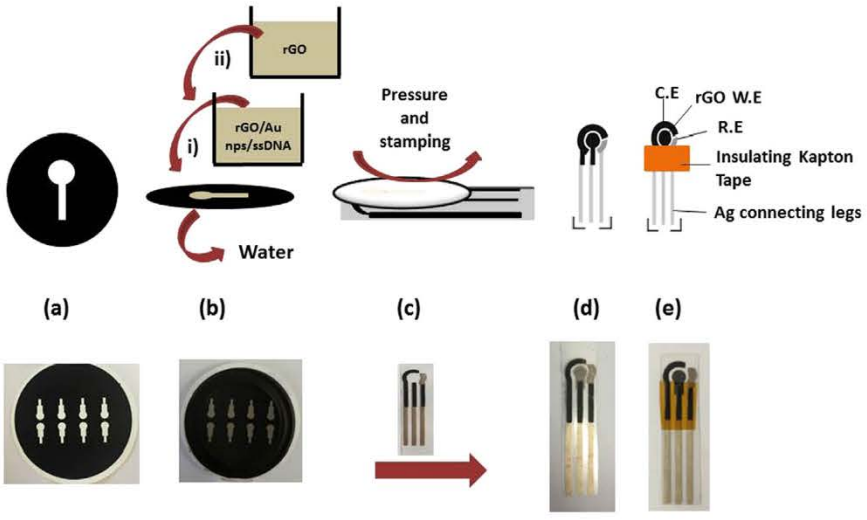

Fig. 2. Schematic of the printing strategy (top) pictures of the sensing platform (bottom). (a) wax printed design over the filter membrane; (b) sequential filtering of the two solutions to form two layers; (c) stamping of the filtered layer; (d) fully-printed electrode consisting of fully functional 3 electrodes for electrochemical measurements; (e) attachment of Kapton layer for insulation.

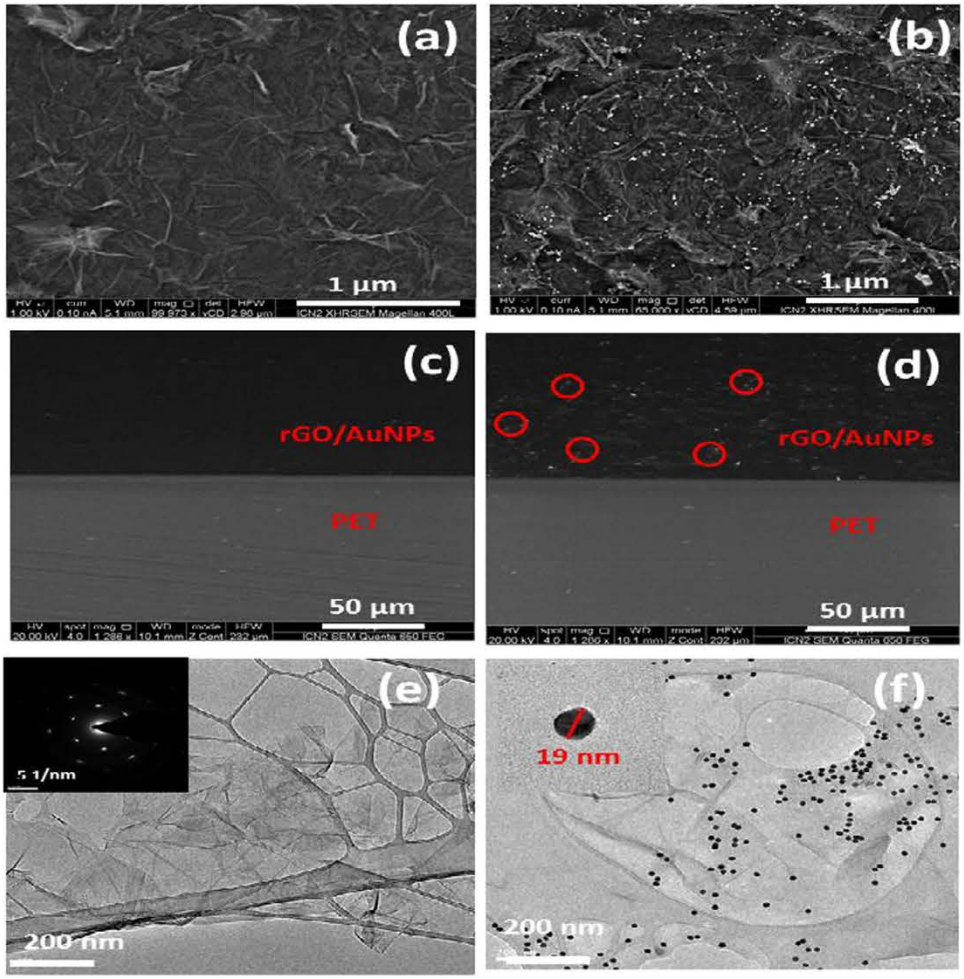

Fig. 3. Optical characterizations. HR-SEM images of the top view (a and b), cross sectional view (c and d), TEM images (e and f) of printed rGO and AuNps/rGO respectively. Insets SAED patters of rGO Fig. 3(e) and AuNps size Fig. 3(f).

is shown in Fig. 3(e and f respectively). It shows a thin and transparent morphology of the graphene nanosheets along with large size **3(e)** and uniform AuNPs distributions in **3(f)**. The selected area electron diffraction pattern confirms the formation of graphene (inset). From Fig. 3 **(f)** inset, it can be seen that AuNPs have a diameter of ~20 nm and are uniformly attached/adsorbed onto the graphene sheets.

X-ray Photoelectron spectroscopy was utilized further to evaluate the elemental ratios of the binding states of the materials, as shown at Fig. 4 **(a-e)**. To prepare it, layer of GO, rGO and rGO/AuNPs/ssDNA were filtered on different nitrocellulose filter membranes and used directly for the measurement. A very high degree of oxidation is shown for GO as seen from its C 1 s spectra, Fig. 4**(b)**. It shows the different carbon oxygen bonds like Carboxyl (289 eV), epoxide/hydroxl bonds (286.7 eV). These peaks were changed after the reduction of GO in ascorbic acid was performed. In Fig. 4 **(c)**, a highest peak at 284.8 eV was observed after the reduction procedure which corresponded to the graphitic carbon i.e. the energy of sp^2 C-C bonds along with drastic decrease in all the peaks related to the oxygen species (Hossain and Park, 2014; Arul et al., 2016; Xu et al., 2017; Yu et al., 2018). Also, mixture of rGO/AuNPs/ssDNA with BSA (used as blocking reagent for avoiding unspecific adsorptions) was studied using this technique. Two obvious peaks observed at 84 eV and 87.6 eV for Au 4 $f_{7/2}$ and Au 4 $f_{5/2}$ respectively with a difference of 3.6 eV is an indication for the presence of Au nanoparticles, Fig. 4**(e)** (H H Mevold et al., 2015; Krishnan and John, 2015; Govindaraju et al., 2017). Fig. 4 **(d)** shows the N 1 s spectra of the mixture that corresponds to tertiary amines at 400.3 eV and protonated primary amines at 401.6 eV (Zhang and Srinivasan, 2004; Yang et al., 2009; Stevens et al., 2013; Yu et al., 2014) most likely coming from the BSA that is used to modify Graphene and AuNPs. Fig. 4**(f)** shows the UV–vis spectra of GO, rGO and rGO/AuNPs with BSA. Reduction of GO to rGO is visible from the spectra where GO shows typical humps at 230 and 300 nm that corresponds to π-π * transitions of C=C bonds and n- π * transitions of C=O bonds respectively and changes to only one peak at 273 nm due to a red shift and the peak at 300 nm is disappeared indicating the reduction of graphene oxide. The presence of AuNPs can be confirmed with the peak spotted at 525 nm, however, after modifying the particles with BSA, the peaks shifted slightly to 528 nm suggesting successful modification with the protein. The interaction of BSA with AuNPs can be explained by the hydrophobic interactions, the thiol-Au interactions (thiol or disulfide groups present in the amino acids of BSA; cysteine) or due to the interaction of amines or carboxylate groups with AuNPs (Zhang et al., 2011; Tabrizi et al., 2014; Binaymotlagh et al., 2016).

3.2. Electrochemical Testing

3.2.1. Electrodes characterization using Cyclic voltammetry (CV)

Cyclic voltammetry (CV) was initially employed to test the performance of the electrodes using 5.0 mM $[Fe(CN)_6]^{3-4-}$/0.1 M PBS as redox probe. At first, different concentrations of GO were tested in order to optimize the best thickness needed for conductivity and robustness. Fig. 5 **(a)** shows the optical images (inset) and the CV for rGO filtered ranging from 0.1 to 1 mg/mL. It was observed that at higher concentrations (> 0.6 mg/mL), the prints were non-uniform and uneven

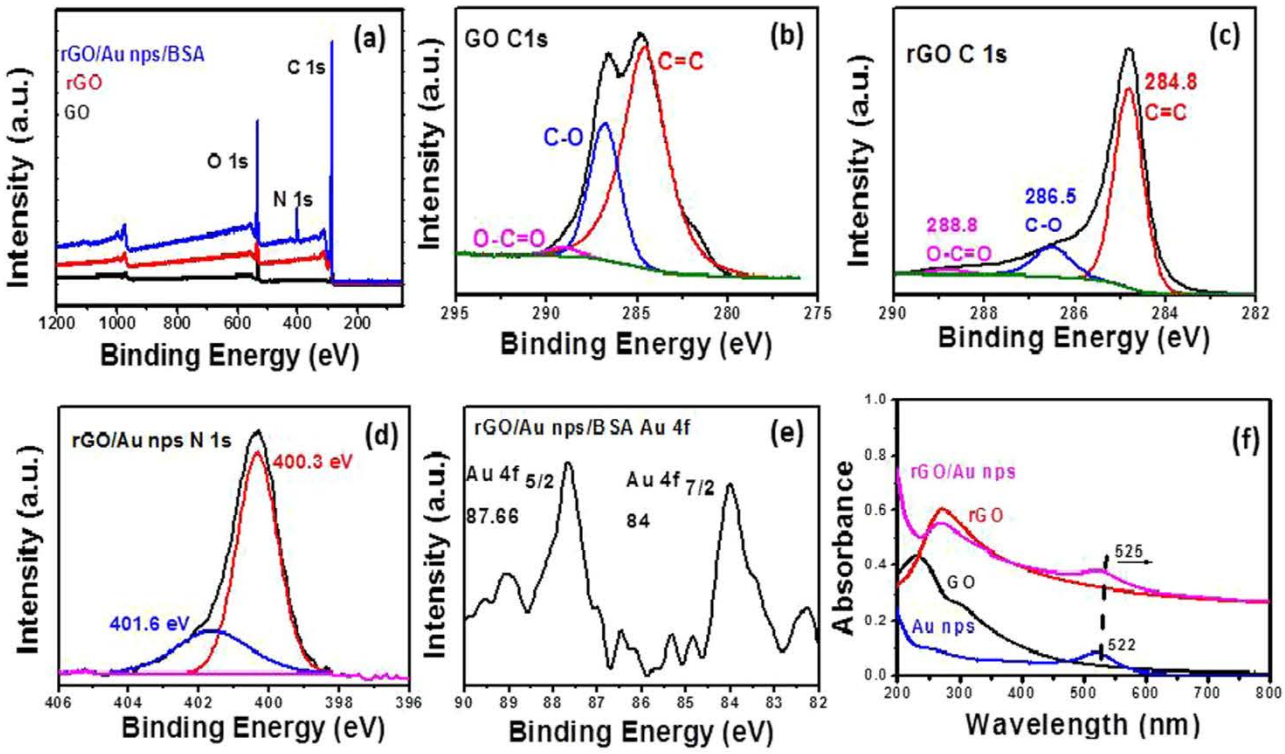

Fig. 4. X-ray Photoelectron spectroscopy (a)overall spectra of GO, rGO and rGO/AuNPs with BSA, core level XPS spectra of C 1s of (b) GO and (c) rGO, (d)N 1s and (e)Au 4f of rGO/Au nps modified with BSA. (f) UV–Visible spectra of GO, rGO, AuNPs and rGO/AuNPs.

(inset) and the oxidation/reduction peaks shifted towards more positive/negative potential respectively without any considerable increase in the current values. At low concentrations (< 0.6 mg/mL), the current values were extremely low making it inefficient for further measurements (CV in Fig. 5**a**). Consequently. 0.6 mg/mL was chosen as optimum concentration for all the final measurements. Next, study on

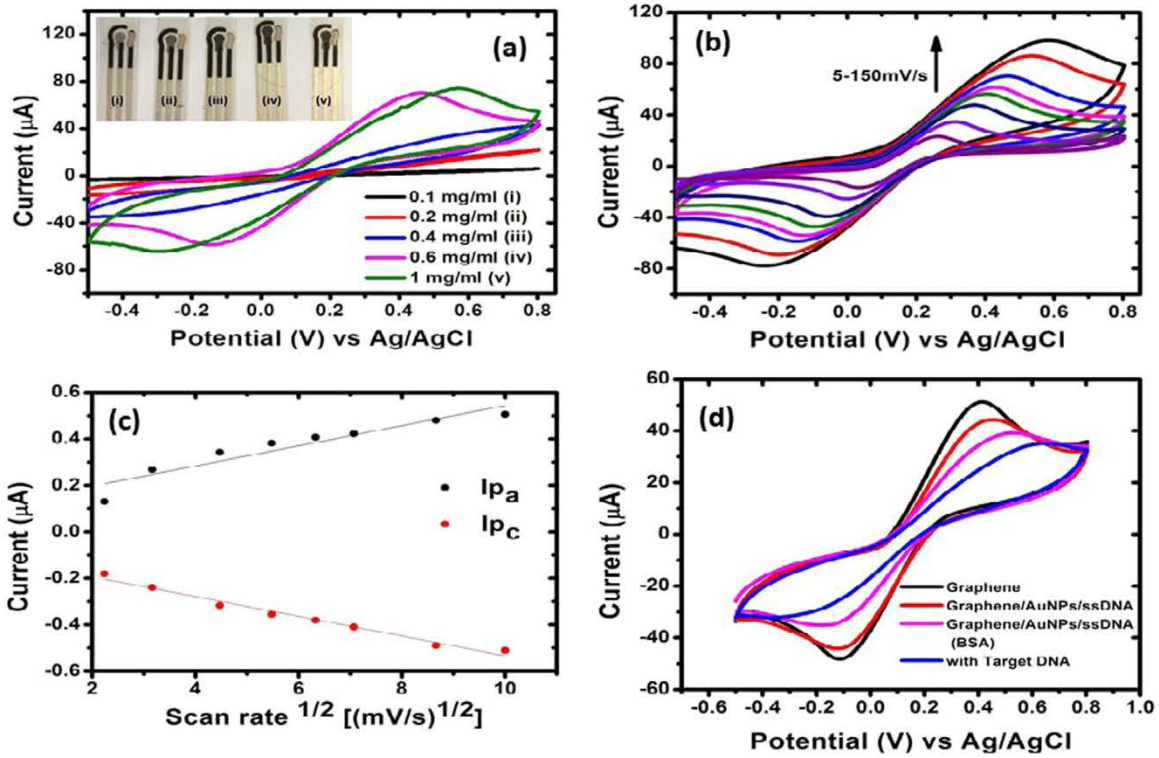

Fig. 5. (a) optimization of the rGO concentrations from 0.1 to 1 mg/mL (i – v) with the images in the inset and their corresponding CV response, CV response of the electrode studied at (a) different scan rates from 5 to 150 mV/s b), Plot of Current vs the square root of scan rate. Furthermore, at figure (c) is the response of different materials and target analytes at 50 mV/s (d).

electrochemical behavior of the optimized electrode was continued using CV. Fig. 5**(b)** shows that the peak currents (Ip_a and Ip_c) linearly increase with the increasing scan rate. This is indicative of the fact that the ongoing electrochemical process of Fe(II) to Fe(III) was diffusion controlled. Also, the shift in oxidation/reduction peak positions with increasing scan rates demonstrates a quasi- reversible process since in a reversible process, the peak position is independent of the scan rate. This linear dependency of peak potential was plotted against the square root of scan rate, given in Fig. 5**c**. Fig. 5**(d)** are the signals obtained from electrodes of different printed materials. The signal decreases after the presence of ssDNA due to electrostatic repulsion from negatively charged DNA strands. This was decreased further after modifying the material with BSA, evidencing successful blocking of free sites that could cause non-specific adsorption. Later, after addition of 1 μM target ssDNA, the current was seen decreasing more due to enhanced repulsion between the negatively charged DNA and negative ions from the electrolyte that hinders the charge transfer at electrode/electrolyte interface.

3.2.2. DNA quantification using Electrochemical Impedance Spectroscopy (EIS)

After optimizing the graphene electrode and its quality testing, the electrodes were further used for performing impedance measurements. Electrochemical impedance spectroscopy (EIS) is very useful electrochemical technique that is generally performed to obtain more sensitive information about the changes and interactions going on at the interface. One of the way to interpret the data is through the Nyquist plot which typically consists of a semicircle at high frequency regions corresponding to blocking of the transferred charges at electrode/electrolyte interface. This is called the charge transfer resistance (R_{CT}) which can be calculated by directly measuring the diameter of the semicircle. At high frequency regions it shows a line with a slope of around 45° which demonstrates a diffusion controlled process. This typical behavior was exhibited by our graphene electrodes (as displayed in Fig. 1). Graphene electrodes showed a very low charge transfer resistance of 2.5 kΩ which was seen increasing after modifying its surface by addition of conjugated AuNPs (rGO/AuNPs/ssDNA) to 4.6 kΩ. This correlates with the CV results and the explanation that the coated layer was blocking the electron transfer from $[Fe(CN)_6]^{3-/4-}$ to the electrode surface as a result of electrostatic repulsion. It was observed that AuNPs treated with BSA exhibited larger Rct value than without the treated ones, implying that the free sites on the synthesized AuNPs were successfully covered and the non-specific adsorption/attachment was minimized if not completely eliminated. Fig. 6**(a)** shows the increase of resistance observed with increasing concentrations of the target probe from 0.01 to 25 μM increases of 3.5, 4.7, 5.6, 6.5 and 7.6 kΩ were observed for 0.01, 0.1, 1, 10, 20 μM target ssDNA respectively. For normalizing the response of the different electrodes, the increase in Rct for each sensor before and after the hybridization is considered as the analytical signal. Fig. 6**(b)** gives the quantitative information on the increase in the value of such analytical signal with the amount of target ssDNA. A logarithmic range of response from 0.01 to 20 μM was observed, adjusted to the following equation:

$$Increase\ in\ R_{ct}(K\Omega) = 148.82\ ln\ [conc.\ \ ssDNA\ (\mu M)] + 1344.5$$

with a correlation coefficient (r) of 0.994, with an average relative standard deviation (RSD) of 13%. A limit of detection (LOD, calculated as the analyte concentration giving a signal equal to the blank signal + three times its standard deviation) of 0.18 nM of ssDNA is estimated. A linear range from 0.01 to 20 μM was observed with a correlation coefficient (r) of 0.97. A non-significant increase in resistance was observed with the addition of blank buffer and 0.1 μM non complementary ssDNA, demonstrating the specificity ssDNA due to electrostatic repulsion from negatively charged DNA strands. Long-term stabilty study results suggest that the sensor performance remain unaffected during at least up to three weeks (see supporting information).

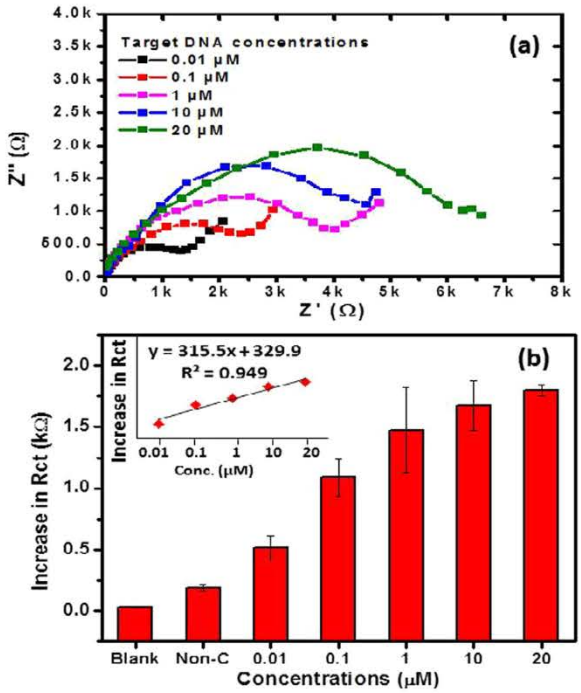

Fig. 6. a) Impedimetric response of the electrode towards different concentrations of the complementary DNA (0.01–20 μM) on different electrodes and (b) the change of resistance for different target ssDNA concentrations as well as for the blank and the negative control.

Longer times were not evaluated in this preliminary work.

The proposed biosensor showed comparable or enhanced performance than recently reported DNA sensors on conventional screen printed electrodes, where detection limits at the nM levels are achieved i.e. 4.7 nM for ebola Virus (Ilkhani and Farhad, 2018) and 35 and 21 nM for influenza genes (Subak and Ozkan-Ariksoysal, 2018). Although, modifying graphene surfaces prior to printing and later DNA detection has result in sensors with higher sensitivities, even at fM levels, (Chen et al., 2016, 2018);, our approach exhibit clear advantages in terms of integration, simplicity and low time of analysis It must also be noted that in this work, no additional conducting layer has been utilized for transfer of charges: graphene is the sole carrier for conduction as well as for anchoring AuNPs and ssDNA. This also opens the possibility directly adsorbing probe ssDNA (labelled or un labelled) via π-π bonding onto graphene substrates and checking the electrochemical or optical signals.

4. Conclusion

An innovative strategy of printed sensing platform that requires only one step modification of the working electrode has been proposed and demonstrated. A composite containing the electrode material (rGO) as well as AuNPs connected with the biorecognition element (ssDNA), was stamped onto a PET substrate. Such strategy eliminates the need of conventional modification steps of the electrode prior to testing. The electrode properties and materials were characterized and the printing procedure was carefully optimized. ssDNA characteristic of a virus was selected as model analyte, for the demonstration of the proof-of-concept, based on changes in the impedimetric signal of the electrode, reaching a detection limit of 0.18 nM. The performance of the system is comparable with those previously reported using conventional screen-printed carbon electrodes, but with clear advantages in terms of simplicity, integration and time of analysis. This successful proof-of-concept can be extended to other affinity biosensors, taking advantage of the integration of the bioreceptor (antibody, enzyme, etc) on the sensor

surface. Such ready-to-use biosensor would lead to a one-step electrochemical detection.

Acknowledgments

We acknowledge support from MINECO, Spain for MAT2017-87202-P, the Severo Ochoa program (Grant No. SEV-2013-0295) and Graphene Flagship Core Project 2 (Ref.: 785219). This work is also funded by the CERCA Programme/Generalitat de Catalunya. Bhawna Nagar also acknowledges Autonomous University of Barcelona (UAB) for the possibility of performing this work under the framework of Material Science (Department of Chemistry) PhD Programme.

Appendix A. Supplementary material

Supplementary data associated with this article can be found in the online version at doi:10.1016/j.bios.2018.09.073

References

Arul, R., Oosterbeek, R., Robertson, J., Xu, G., Jin, J., Simpson, C., 2016. Carbon 99, 423–431.
Baptista-Pires, L., Mayorga-Martínez, C.C., Medina-Sánchez, M., Montón, H., Merkoçi, A., 2016. ACS Nano 10 (1), 853–860.
Binaymotlagh, R., Hadadzadeh, H., Farrokhpour, H., Haghighi, F.H., Abyar, F., Mirahmadi-Zare, S.Z., 2016. Mater. Chem. Phys. 177, 360–370.
Bo, X., Zhou, M., Guo, L., 2017. Biosens. Bioelectron. 89, 167–186.
Bollella, P., Fusco, G., Tortolini, C., Sanzò, G., Favero, G., Gorton, L., Antiochia, R., 2017. Biosens. Bioelectron. 89, 152–166.
Chen, S., Frank Cheng, Y., Voordouw, G., 2018. Sens. Actuators B 262, 860–868.
Chen, M., Hou, C., Huo, D., Bao, J., Fa, H., Shen, C., 2016. Biosens. Bioelectron. 85, 684–691.
Chen, X.-m., Wu, G.-h., Jiang, Y.-q., Wang, Y.-r., Chen, X., 2011. Analyst 136 (22), 4631–4640.
De la Escosura-Muñiz, A., González-García, M.B., Costa-García, A., 2007. Biosens. Bioelectron. 22, 1048–1054.
Dubal, D.P., Nagar, B., Suarez-Guevara, J., Tonti, D., Enciso, E., Palomino, P., Gomez-Romero, P., 2017. Mater. Today Energy 5, 58–65.
Geim, A.K., Novoselov, K.S., 2007. Nat. Mater. 6, 183.
Govindaraju, S., Ankireddy, S.R., Viswanath, B., Kim, J., Yun, K., 2017. Sci. Rep. 7, 40298.
H H Mevold, A., Hsu, W.-W., Hardiansyah, A., Huang, L.-Y., Yang, M.-C., Liu, T.-Y., Chan, T.-Y., Wang, K.-S., Su, Y.-A., Jeng, R.-J., Wang, J., Wang, Y.-L., 2015. Nanoscale Res. Lett. 10, 397.
Hossain, M.F., Park, J.Y., 2014. Electroanalysis 26 (5), 940–951.
Huang, T.Y., Huang, J.H., Wei, H.Y., Hoa, K.C., Chu, C.W., 2013. Biosens. Bioelectron. 43, 173–179.
Ilkhani, H., Farhad, S., 2018. Anal. Biochem. https://doi.org/10.1016/j.ab.2018.06.010.
Justino, C.I.L., Gomes, A.R., Freitas, A.C., Duarte, A.C., Rocha-Santos, T.A.P., 2017. TrAC Trends Anal. Chem. 91, 53–66.
Krishnan, G., John, S.A., 2015. RSC Adv. 5, 42369–42375.
Lee, J., Han, T.-H., Park, M.-H., Jung, D.Y., Seo, J., Seo, H.-K., Cho, H., Kim, E., Chung, J., Choi, S.-Y., Kim, T.-S., Lee, T.-W., Yoo, S., 2016. Nat. Commun. 7, 11791.
Lee, S.-M., Kim, J.-H., Ahn, J.-H., 2015. Mater. Today 18 (6), 336–344.
Lee, H.C., Liu, W.-W., Chai, S.-P., Mohamed, A.R., Aziz, A., Khe, C.-S., Hidayah, N.M.S., Hashim, U., 2017. RSC Adv. 7 (26), 15644–15693.
Li, J., Rossignol, F., Macdonald, J., 2015. Lab Chip 15 (12), 2538–2558.
Li, X., Zhi, L., 2018. Chem. Soc. Rev. 47 (9), 3189–3216.
Lin, L., Liu, Y., Tang, L., Li, J., 2011. Analyst 136 (22), 4732–4737.
Mattana, G., Briand, D., 2016. Mater. Today 19 (2), 88–99.
Mirkin, C.A., Letsinger, R.L., Mucic, R.C., Storhoff, J.J., 1996. Nature 382, 607.
Nagar, B., Dubal, D.P., Pires, L., Merkoçi, A., Gomez-Romero, P., 2018. ChemSusChem 11 (11), 1849–1856.
Novoselov, K.S., Geim, A.K., Morozov, S.V., Jiang, D., Zhang, Y., Dubonos, S.V., Grigorieva, I.V., Firsov, A.A., 2004. Nat. Mater. 306 (5696), 666.
Pumera, M., 2011. Mater. Today 14 (7), 308–315.
Quesada-Gonzalez, D., Merkoci, A., 2018. Chem. Soc. Rev. https://doi.org/10.1039/c7cs00837f.
Randviir, E.P., Brownson, D.A.C., Banks, C.E., 2014. Mater. Today 17 (9), 426–432.
Ray, W.J., Joseph, W., 2013. Electroanalysis 25 (1), 29–46.
Seo, J.-H., Ling, T., Gong, S., Zhou, W., Ma, A.L., Guo, L.J., Ma, Z., 2016. Sci. Rep. 6, 24771.
Shao, Y., Wang, J., Wu, H.-X., Jun Liu, J., Aksay, I.A., Lin, Y., 2010. Electroanalysis 22 (10), 1027–1036.
Singh, E., Meyyappan, M., Nalwa, H.S., 2017. ACS Appl. Mater. Interfaces 9 (40), 34544–34586.
Singh, A., Sinsinbar, G., Choudhary, M., Kumar, V., Pasricha, R., Verma, H.N., Singh, S.P., Arora, K., 2013. Sens. Actuators B 185, 675–684.
Søndergaard, R., Hösel, M., Angmo, D., Larsen-Olsen, T.T., Krebs, F.C., 2012. Mater. Today 15 (1), 36–49.
Stevens, J.S., Luca, A.C., Pelendritis, M., Terenghi, G., Downes, S., Schroeder, S.L.M., 2013. Surf. Interface Anal. 45 (8), 1238–1246.
Subak, H., Ozkan-Ariksoysal, D., 2018. Sens. Actuators B 263, 196–207.
Tabrizi, M.A., Tavakkoli, A., Dhand, V., Rhee, K.Y., Park, S.-J., 2014. J. Ind. Eng. Chem. 20 (6), 4327–4331.
Turkevich, J., Stevenson, P.C., Hillier, J., 1951. J. Discuss. Faraday Soc. 11, 55–75.
Xu, J., Li, D., Chen, Y., Tan, L., Kou, B., Wan, F., Jiang, W., Li, F., 2017. Nanomaterials 7 (12), 450.
Yang, Y., Wang, J., Zhang, J., Liu, J., Yang, X., Zhao, H., 2009. Langmuir 25 (19), 11808–11814.
Yu, B., Wang, X., Qian, X., Xing, W., Yang, H., Ma, L., Lin, Y., Jiang, S., Song, L., Hu, Y., Lo, S., 2014. RSC Adv. 4 (60), 31782–31794.
Yu, X., Wu, Q., Zhang, H., Zeng, G., Li, W., Qian, Y., Li, Y., Yang, G., Chen, M., 2018. Materials 11 (1), 38.
Zhang, Z., Chen, H., Xing, C., Guo, M., Xu, F., Wang, X., Gruber, H.J., Zhang, B., Tang, J., 2011. Nano Res. 4 (6), 599–611.
Zhang, F., Srinivasan, M.P., 2004. Langmuir 20 (6), 2309–2314.

Fully Printed One-Step Biosensing Device Using Graphene/AuNPs Composite.

Bhawna Nagar[a,b] , Marc Balsells[a], Alfredo de la Escosura-Muñiz[a] , Pedro Gomez-Romero[b], and Arben Merkoçi[a,c]*

[a]Nanobioelectronics and Biosensors group, Catalan Institute of Nanoscience and Nanotechnology (ICN2), CSIC and The Barcelona Institute of Science and Technology, Campus UAB, Bellaterra, 08193 Barcelona, Spain

[b] Novel Energy-Oriented Materials Group, Catalan Institute of Nanoscience and Nanotechnology (ICN2), CSIC and The Barcelona Institute of Science and Technology, Campus UAB, 08193 Bellaterra, Barcelona (Spain)

[c]ICREA, Pg. Lluís Companys, 23, Barcelona 08010, Spain

* Corresponding author. Tel.: +34 937374604; e-mail: arben.merkoci@icn2.cat (A.Merkoçi)

Supporting information

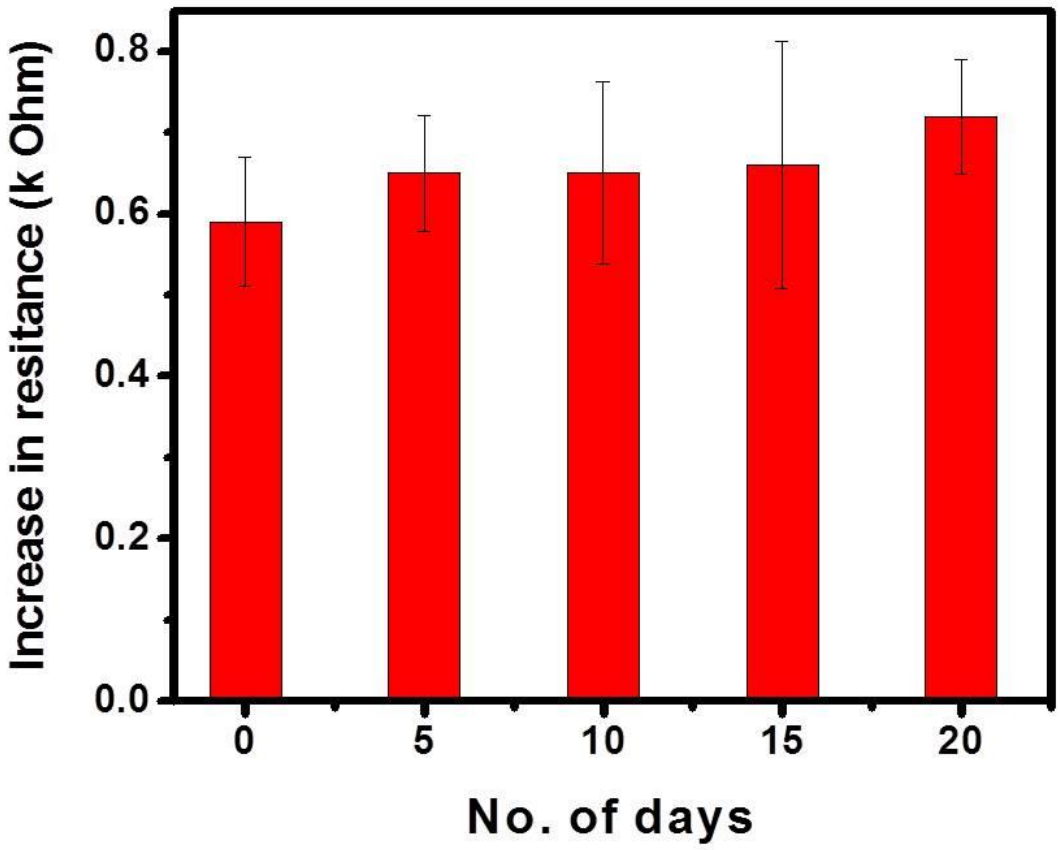

Figure 1: Stability measurements; signals obtained for detection of 1µM target DNA (t-DNA) over a period of 3 weeks.

Article 5: Highly concentrated, additive-free dispersions of reduced graphene oxide for inkjet printing of amperometric sensors

Bhawna Nagar, Victor Costa Bassetto, Milica Jović, Yingdi Zhu, Pedro Gómez-Romero , Arben Merkoçi, Hubert H. Girault and Andreas Lesch

Highly concentrated, additive-free dispersions of reduced graphene oxide for inkjet printing of amperometric sensors

*Bhawna Nagar,[a,b] Victor Costa Bassetto[c] Milica Jović,[c] Yingdi Zhu,[c] Pedro Gómez Romero[a] , Arben Merkoçi,[b] Hubert H. Girault[c] and Andreas Lesch[d,]**

[a]Novel energy oriented Materials group Catalan Institute of Nanoscience and Nanotechnology (ICN2), CSIC and The Barcelona Institute of Science and Technology, Campus UAB, Bellaterra, 08193 Barcelona, Spain.

[b] Nanobioelectronics and Biosensors Group, Catalan Institute of Nanoscience and Nanotechnolgy (ICN2), CSIC and The Barcelona Institute of Science and Technology, Campus UABm Bellaterra, Barcelona 08193, Spain

ICREA, Pg. Lluís Companys, 23, Barcelona 08010, Spain

[c] Ecole Polytechnique Fédérale de Lausanne (EPFL) Valais Wallis, Laboratory of Physical and Analytical Electrochemistry, Rue de l'Industrie 17, 1950 Sion, Switzerland.

[d] University of Bologna, Department of Industrial Chemistry "Toso Montanari", Viale del Risorgimento 4, 40136 Bologna, Italy.

CORRESPONDING AUTHOR FOOTNOTE

Dr. Andreas Lesch

Tel.: +39 051 20 9 3701

E-mail: andreas.lesch@unibo.it

Abstract

The facile inkjet printing of highly concentrated reduced graphene oxide (rGO) without the use of dispersion stabilizing additives, polymeric binders or surfactants for amperometric sensor fabrication is reported. Research in the field of printed flexible electronics is ongoing tremendously to cater the needs of good quality conductive patterns, for instance for wearable sensors and batteries. Inkjet printing of graphene and its derivatives is a promising digital mask- and contact-less way of producing such devices, but faces challenges in terms of keeping production costs low for materials, ink composition and production. Achieving stable inks does often not reach or adulterate the electrochemical properties of graphene and its derivatives. This work addresses these issues and a stable dispersion of rGO with an exceptionally high concentration of 30 mg/mL was achieved using a combination of N-methyl pyrrolidone and 1,2-propanediol. An all inkjet printed three-electrode viable bacteria detection sensor was printed over flexible polyimide substrates using rGO as the working and counter electrode and silver chloride as the quasi-reference electrode. Bacteria detection was enabled by using (5-cyano-2,3-di-(p-tolyl) tetrazolium chloride (CTC), 2-(4-iodophenyl)-3-(4-nitrophenyl)-5-(phenyl) tetrazolium chloride (INT), 2,3,5-triphenyl tetrazolium chloride (TTC) and resazurin (RS) redox indicators whose reduction by the bacterial respiration was electrochemically followed. Four redox dyes were successfully applied to *E.Coli* samples.

Graphical Abstract

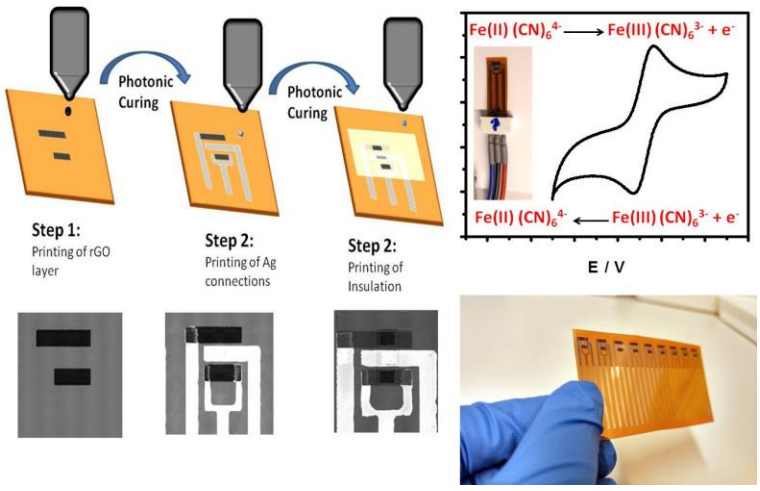

Introduction

Printing techniques like screen printing, roll-to-roll, inkjet printing etc. have become crucial for making functional working electrodes or circuits in electronic industry owing to their low cost and scalability. These techniques can effectively produce patterns over a rigid or flexible substrate[1]. Electrochemical sensors operate by reacting with the analyte of interest and producing an electrical signal proportional their concentration. A typical electrochemical sensor consists of a sensing electrode (or working electrode), and a counter electrode separated by a thin layer of electrolyte, it provide several advantageous like high sensitivity, selectivity, accuracy, time efficiency, miniaturization and uncomplicated route compared to the molecular, culture dependent conventional approach. The three main electrochemical routes for bacterial detection are Voltammetric, Amperometric/Potentiometric and Impedimetric among which Amperometry measures current generated from the oxidation or reduction of the electroactive species at the working electrode at constant potential values and are directly proportional to the analyte concentration[2][3]. Different metallic (Pt, Au) or carbon based electrodes (Glassy Carbon electrodes, graphite or graphene) have been used as working electrodes where the Metallic electrodes have shown highly sensitive sensors owing to their high conductivity, but are expensive, rigid and have smaller electrochemical window (instability) [4]. These reasons influenced the use of alternative carbon electrodes like GCEs which have been widely exploited as electrodes for electrochemical sensor, however, these also suffer from few drawbacks, the main being rigidity and lower analyte loading due to their highly compact nature and the absence of active surface groups does not favors direct attachment of the biomaterial to the electrode surface or the possibility of surface modifications. For flexibility purposes Screen printed carbon electrodes [5][6] and Graphene [7] are being used at a tremendous rate as they provide easy processability, printing and flexibility in addition to high conductivity, wider electrochemical window, chemical inertness etc. Graphene can provide much higher loadings and conductivity as compared to graphite due its exceptionally high surface area and

fast electron transfer and also provides more functionalization possibilities [8].

Depending on the final application of the printed device, some of the mentioned deposition techniques can be superior to the others considering the typical advantages and drawbacks of those. For instance, screen printing can be used for making thick patterns where high precision of the layer roughness and lateral micrometric resolution are not the primary concerns [9][10][11]. The ink formulation can be less complex compared to inkjet printing where the fluid properties are more strict in order to provide precise and accurate deposition of picoliter droplets, without nozzle clogging, and consequently providing high micrometric resolution [12][13][14][15]. Inkjet printing is an emerging printing technique for patterning a wide range of nanomaterials at large scale. However, the particle size, level of particle aggregation, and the selection as well as mixtures of solvents is crucial to attain appropriate fluid properties for jetting. For instance, Drop on Demand Dimatix printer requires the ink surface tension and viscosity to be in the range of 28 – 33 mN/m and 10-12 cPs respectively [16]. Inkjet printing has further the possibility of upscaling of a production from a prototype level to reach commercialization purposes, simply by increasing the number of nozzles in a printhead. Further features of inkjet printing include that it is maskless, contactless, compatibility with various substrates and avoids wastage (due to drop-on-demand operation). The main challenge of inkjet printing is the formulation of reproducible and stable inks [17][18], which is mostly hindered by nanoparticle aggregating or sedimentation in the printhead blocking irreversibly the nozzle orifice. This leads often to the formulation of inks with low loadings and, as a result, multiple layers have to be printed in order to obtain a conductive layer of conductive nanoparticles. Other issues are based on obtaining homogeneous patterns, i.e. without local particle sedimentation due to coffee ring effect-related phenomena. Furthermore, the adhesion of the printed layer to the substrate, e.g. when being into contact with a liquid or when being bent, has to be considered.

The inkjet printing of different materials ranging from metal/metal oxide nanoparticles[19][20], polymers[21] or carbonaceous materials like carbon nanotubes (CNTs) [22][23] or graphene[24] have been reported. Nanoparticles of Ag, Pt, Au or Cu are attractive for many applications in circuits or sensing, but often expensive or unstable (e.g. due to chemical oxidation). An alternative group of conductive materials, which at the same time is advantageous for the electrochemical detection of organic molecules, are carbon-based nanomaterials, such as CNTs or graphene, which are further chemically and mechanically stable, possess exceptional thermal and electronic properties [25][26]. Graphene can easily be produced on large scale by different production techniques like chemical oxidation, liquid-phase exfoliation of graphite[27][28], but is generally difficult to disperse due strong inter sheet attraction based on π-π-interactions [29][30]. The particle aggregate size should generally be one hundred times smaller than the dimension of the nozzle orifice (rule of thumb), which in case of many printers is equal to 200 nm particles for 20 µm nozzles. Replacing graphene by graphene oxide (GO), which is hydrophilic, leads to aqueous dispersion of high stability. However, GO is characterized by non-conductivity or at least by high resistance values (depending on the degree of oxidation of the graphene sheets). After printing, GO can be thermally, chemically or photonically reduced [31], but this represents an additional working step that can degrade other sensor layers and the substrate. Certain solvents, such as N-Methyl-Pyrrolidone (NMP) result in graphene dispersions without the need for stabilisers due to the matching Hansens solubility parameters[32] with the additional advantage of reducing the coffee ring effect [33]. The aggregation of graphene sheets in inks can further be avoided by adding so-called stabilizers (e.g. surfactants or polymers) [34][35] These modification blocks the graphene sheets from aggregating, but can result in either enhanced conductivities, synergistic effect resulting from the composite or large inter-particle resistances and even insulating patterns. Consequently, thermal post-processing steps (>100 ºC) are applied for the removal of the stabilizers and for annealing/sintering the conductive particles forming a conductive layer [15][36]. This represents an

additional process step and thermal processing is restricted by the thermal stability of the substrates, in particular when low melting point plastics are used. In many cases, researchers prepare graphene based hybrid inks with conducting polymers or metal NPs that not only avoids aggregation but also provide synergistic effects to enhance the performance of the electrodes for particular applications: for example hybrids with Conducting polymers are commonly used for enhancing capacitance of the electrode, or even provide surface for functionalization or entrapment of a biomolecule for biosensing applications. With metal NPs, the overall conductivity can be enhanced providing higher loading or catalytic effects for electrochemical sensing (REF).

In this work, be formulated an ink with high concentration of reduced graphene oxide for printing amperometric three-electrode cells used for the detection of viable bacteria. Specific for bacterial detection, different strategies are usually employed by using enzymes, antibodies (labelled or un-labelled), DNAs or even whole cell (micro-organism) as the bioreceptors where the response arising from the bacterial metabolic activities or the change in charges due to their attachment at the working electrode can be directly studied. Apart from these direct approaches, redox mediator assisted electrochemical sensing is also performed where oxidation/reduction changes of the mediator occurring due to the presence of analyte are studied [37]. Our goal was to produce in a simple and straightforward way an inkjet-printable ink with rGO that can be scaled-up in ink volume. The shelf life of the ink should allow long-term, high-throughput printing with large numbers of parallel nozzles. Besides NMP 1,2-propanediol was added to the ink to adjust the viscosity and improve jetting and the resulting ink exhibited a density, viscosity qnd surface tension of 1.05 g/cm^3, 3.8 mPa·s and of 38 mN/m respectively with the Z value of 7.5 at a concentration of 30mg/ml. Three-electrode amperometric sensors were printed and electrochemically characterized in aqueous solutions containing a redox mediator. As a proof-of-concept, the sensors were applied to detect viable bacteria. In proof-of-concept measurements, test solutions contained viable and metabolically active *E. coli* and specific redox

indicators. The redox indicator molecules were reduced by the respiratory chain of the bacteria decreasing thus the redox dye concentration in the solution, which was electrochemically followed by voltammetry using the printed sensors.

Experimental Methods

Materials and Reagents

Graphene oxide (15-20 sheets, 4-10% edge-oxidized, Sigma Aldrich), commercial silver ink (Silverjet DGP-40LT-15C, 30-35 wt.%, Sigma Aldrich), UV curable dielectric ink (jettable insulator EMD 6201, Sun Chemical), N-methyl pyrrolidone (NMP), 1,2-Propanediol, potassium hexacyanoferrate(III) ($K_3[Fe(CN)_6]$), potassium hexacyanoferrate(II) ($K_4[Fe(CN)_6]$), ferrocenemethanol (FcMeOH), hexaammineruthenium(III) chloride ($[Ru(NH_3)_6]Cl_3$), potassium hexachloroiridate(III) (K_3IrCl_6), potassium nitrate (KNO_3), lysogeny broth (Sigma-Aldrich), four metabolic activity indicators (5-cyano-2,3-di-(p-tolyl) tetrazolium chloride (CTC), 2-(4-iodophenyl)-3-(4-nitrophenyl)-5-(phenyl) tetrazolium chloride (INT), 2,3,5-triphenyl tetrazolium chloride (TTC) and resazurin (RS); all Sigma-Aldrich), were of analytical grade and used as received. Polyimide (PI, Kapton HN, thickness 125 μm) were used as substrates for inkjet printing after rinsing with isopropyl alcohol and drying with a stream of nitrogen.

Ink Preparation

The graphene ink was prepared by adding 30 mg of the as-purchased rGO powder per mL of a mixture of NMP and 1,2-Propanediol in the volume ratio 7:3. The mixture was then sonicated for 30 min at 40% amplitude with an on/off pulse cycle of 5 s using a Sonics Vibra Cell 505 in the "Cup horn" arrangement. The viscosity and surface tension of the inks were characterized with an SV-10 A series viscometer (A&D Instruments Limited) and a drop shape analyzer DSA-30 (Krüss).

Inkjet printing of rGO patterns and three-electrode sensors

A drop-on-demand DMP-2850 materials deposition printer (Fujifilm Dimatix) with disposable DMC-11610 cartridges (16 individually addressable nozzles, 10 pL nominal droplet volume), which operate under piezoelectric actuation were used for the inkjet printing of the rGO inks. Printing parameters, such as piezoelectric actuation, jetting frequency and cleaning cycles for the nozzles were optimised. The substrate temperature was kept at 60 ºC for fast evaporation of the ink solvents. The rGO layers were then subjected to photonic curing (PulseForge 1300, NovaCentrix), which was integrated into an X-Serie CeraPrinter (Ceradrop). The parameters of the high intensity pulsed light were 400 V for the lamp charging with a pulse width of 18 µs resulting in a theoretical total energy density of 6.9 J/cm^2.

Three electrode sensors, composed of Ag connection paths, Ag/AgCl quasi-reference electrode (QRE), rGO working electrode (WE) and counter electrode (CE), dielectric ink for insulation and electrode area definition, were printed using both the CeraPrinter (Ag, dielectric ink) and DMP-2850 (rGO). Printing designs and process steps for Ag and the dielectric were adapted from our previous works [38] [39]. Briefly, after printing and curing rGO (as purchased reduced graphene oxide (rGO), 4 to 5 % edge functionalised into a mixture of N-Methyl-2-Pyrrolidone and 1,2-Propanediol), patterns of Ag were printed with a Q-Class Sapphire QS-256 printhead followed by photonic curing, then the UV curable insulation was printed with a DMC-11610 cartridge and simultaneously photo-polymerized using an UV lamp (FireEdge FE300 380-420 nm, Pheseon Technology) integrated into the printhead carrier. Rectangular electrode areas were obtained in this way with an active area of 1mm^2.

Materials characterizations

The printed sensors were first characterized by using scanning electron microscopy (SEM, FEI Quanta 650 FEG ESEM) and high-resolution transmission electron microscopy (TEM, FEI Tecnai F20). X-ray

photoelectron spectroscopy (XPS) was performed using a SPECS PHOIBOS 150 analyser (SPECS GmbH). Optical micrographs were taken with the built-in cameras of the CeraPrinter and DMP printer.

Bacterial culture and incubation

Bacterial cultures were prepared by adding to 250 µL of a E.Coli bacterial stock solution to lysogeny broth, followed by 2-3 h incubation under shaking at 650 rpm at 37°C. Bacteria counting was done by measuring the UV-Vis absorbance at 600nm. The optical density of 1.2 at 600 nm corresponded to approximately 8.3×10^8 cells/mL.

Electrochemical measurements

A MultiEmStat (PalmSens) in a three electrode configuration (rGO as WE and CE, Ag/AgCl as QRE) was used for all electrochemical measurements, *i.e.*, cyclic voltammetry (CV) and differential pulse voltammetry (DPV). The general electrochemical performance of the rGO-based sensors was investigated with CV using the four redox mediators FcMeOH, $K_3(IrCl_6)$, a 1:1 mixture of $K_3[Fe(CN)_6]/K_4[Fe(CN)_6]$ and $[Ru(NH_3)_6]Cl_3$ (concentration of all 2 mM) in 0.1 M KNO_3. The electrochemical performance of the four redox indicators RS, CTC, TTC and INT (all 5 mM) was studied using CV and DPV. The functionality of the sensors as viable bacteria sensors was evaluated by DPV dropping 30 µL of lysogeny broth without and with incubated bacteria (30 min incubation time with finally ~8.3×10^8 *E. coli* cells/mL) onto the sensor.

Results and Discussions

Ink formulation and inkjet printing

First, an ink was formulated fulfilling the following requirements: high dispersibility of rGO, stable jetting

with piezoelectric driven printheads, fast drying of printed patterns, homogeneous rGO patterns after printing and drying, conductive rGO patterns with good adhesion to Kapton in aqueous solutions. NMP (Viscosity 1.65 mPas at 25 ºC) was chosen as one of the solvents due to its known positive properties for dispersing graphene. 1,2-propanediol (viscosity 40.4 mPa·s at 25 °C) was used to lower the viscosity of the ink. Finally, an NMP:1,2-propanediol mixture of 7:3 reaching rGO loadings of 30 mg/mL, which to the best of our knowledge overcomes at least ten times the loadings of the current commercial and yet reported inkjet printable graphene and graphene derivate-based inks [40][12][41][42]. In parallel to achieving the high rGO loading, the physical and rheological properties of the ink were adjusted to match the narrow operability window of piezoelectric inkjet printing ranging from 10-12 cPs and 28 – 33 mN/m for viscosity and surface tension, respectively. The final ink exhibited a density (ρ) of 1.05 g/cm^3, dynamic viscosity (η) of 3.8 mPa·s and surface tension (γ) of 38 mN/m. A non-dimensional *Z*-parameter, which is the inverse of the Ohnesorge number (Oh) that is derieved from Reynolds(Re) and Weber (We) number, was calculated using the following formula [43] :

$$Re = \frac{\upsilon \rho a}{\eta}$$

$$We = \frac{\upsilon^2 \rho a}{\gamma}$$

$$Oh = \frac{\sqrt{We}}{Re} = \frac{\eta}{\sqrt{\gamma \rho a}}$$

to estimate if the ink is within the printability range of $1 < Z < 10$ as defined by Derby [44] .A too high *Z*-value (larger than 10 or 16) [45] can result in satellite formation whereas a *Z*-value lower than 1 represents inks of extreme viscous impeding the formation of stable droplets [44] [46]. The *Z* number of 7.5 (nozzle diameter 21.5 µm) for the rGO formulated herein fell indeed in the printability range and stable jetting could be observed for 6 parallel nozzles (**Fig. 1a**, note that the printer camera can only visualize six nozzles at a time). Spherical 0.113 pL droplets at a distance of 150-180 µm from the nozzles

was generated allowing to print first arrays of separated droplets on a Kapton substrate (**Fig. 1b**). The ink dried within few minutes, as supported by using 1,2-propanediol as one ink solvent with relatively high vapour pressure (0.08 mmHg at 20 °C), and circular droplets of ~60 µm diameter with nearly homogeneous darkness were obtained with the grayscale printer camera indicating a homogeneous distribution of the rGO flakes in all droplets. The latter was supported by the presence of NMP [33][47]. The good wetting of the Kapton substrate with the rGO ink was characterized by a contact angle of 15% (**Fig. 1c**). Rectangular patterns of rGO were then printed and dried on Kapton using different numbers of printed layers ranging from one to 20 (**Fig. 1d**). Fig. 1e is the printer camera image of the patterns for 10 L. Please note that one layer refers to the deposition of one droplet per coordinate and not to a single layer of rGO. Even with just 1L of rGO the pattern is clearly visible to the eye with increasing darkness with layer number.

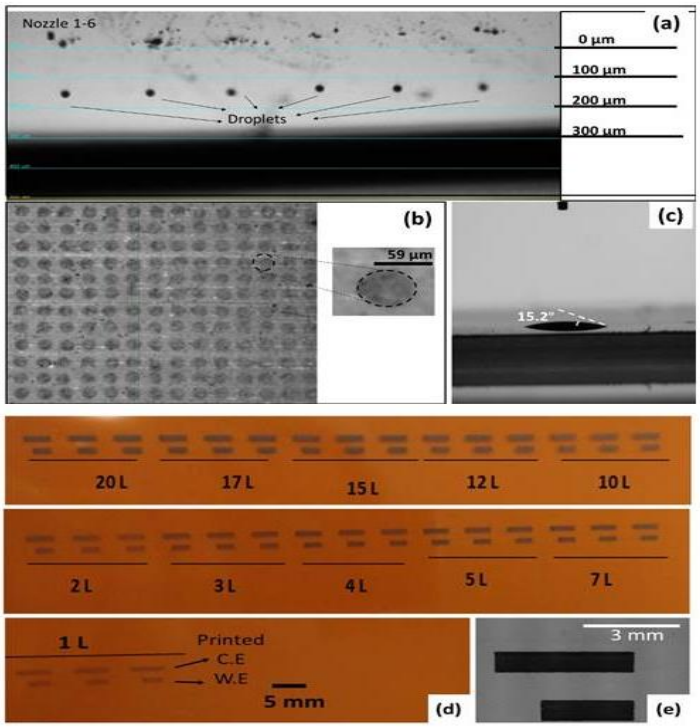

Figure 1. a) Representative simultaneous jetting of droplets of the rGO ink (30 mg/mL) from six consecutive nozzles. b) Dried droplet array on Kapton with a lateral droplet separation of 100 µm. c) Contact angle measurement of an rGO ink droplet on Kapton. d) Patterns of rGO inkjet printed with 1 to 20 printed ink layers L.

Graphene after sonication falls within the printable ranges of the DMP printer (nozzle diameter 21.5 µm) that maybe acts more like particles than flakes, additionally being highly dispersible in NMP and Propanediol (due to the the edge functionalities of rGO). Finally, a three electrode pattern was printed as shown in fig. 2, in 3 steps, i) printing of Graphene working and counter electrode, ii) printing of the Ag connecting legs and (pseudo)reference electrode and iii) printing of the insulation layer. Photonic curing was applied after each step except in the case of insulating layer which was cured using the UV lamp.

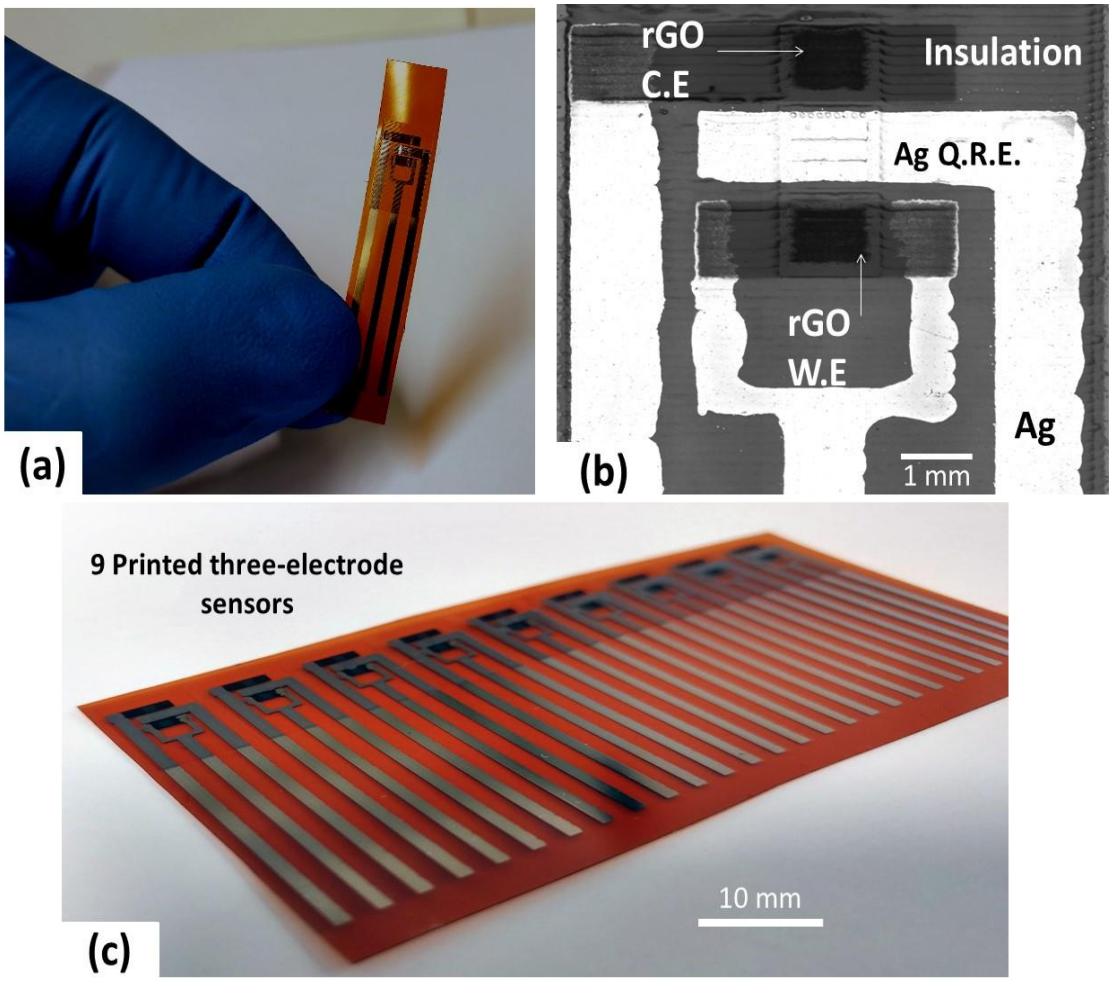

Figure 2. (a) photograph of a single printed electrode (b)Printer images of the three printed layers to make final device(c) multiple fabricated electrodes taken with a mobile phone.

Morphological Characterization

An SEM image of the raw rGO powder with a flake size of ~4 µm is shown in **Fig. 3a**. **Fig. 3b** shows the TEM image of rGO from the inkjet ink. Different numbers of graphene layers could be observed from 2 to 20 layers which is in correspondence with the SAED (selected area electron diffraction, **Fig. 3c**). Hexagonal rings exhibiting a six fold symmetric pattern, attributing to graphene, with different and multiple spot sizes. This can be credited to the multilayer graphene stackings, presence of domain boundaries and /or intrinsic rotational [48]. The first hexagon of reflections refers to an inter-plane distance of 2.13 Å and the outer hexagon refers to 1.23 Å corresponding to the {0110} to {1210} planes[i] Further, the size of the rGO flakes have been reduced considerably in order to make the final ink compatible with printing. In the final prints, e.g. with 10 L (**Fig. 3d**), the size of the rGO flakes ranged from 200 - 400 nm resulting in a compact film morphology.

Fig. 3e shows the XPS spectra of the printed rGO pattern before (i.e. after removing the patterns from printer hot plate, 60°C) and after photonic curing using a 400V pulse a width of 18 µs generating a theoretical total shot energy of 6.9 J/cm^2. Apart from facilitating the drying of the printed film, a small reduction in the oxygen content from 9 to 6.2 % was observed, indicating a reduction of the rGO induced by the light from the Xe flash lamp. Such reductive, light induced curing has recently been described by [49][49] and Costa Bassetto et al. [50] where certain compounds, such as alcohols can act as reducing agents. The temperature in the irradiated materials can reach several hundred degrees (ref). The rapidity of the flash light-induced process avoids the formation of oxides although the high temperature process is carried out under ambient conditions. In general, several works on curing/reducing graphene oxide films as a cost and time effective process have been reported [51][52][53]. In the Core level C1s spectra of both printed patterns, the peaks corresponding to C=C graphitic carbon at 284.X eV, C-C sp^3 at 285.5 and C=O carbonyl groups at 288.7 can be seen, however,

with reduction of the oxygen content from 9 to 6.2%. Also, a peak at 291.3 eV appears that can be attributed to the π- π* shape-up satellite peak or the tail corresponding to C=C graphitic peaks after photonic curing[54][55]. For thermal treatments, the prints were subjected to 100 and 300 ºC.

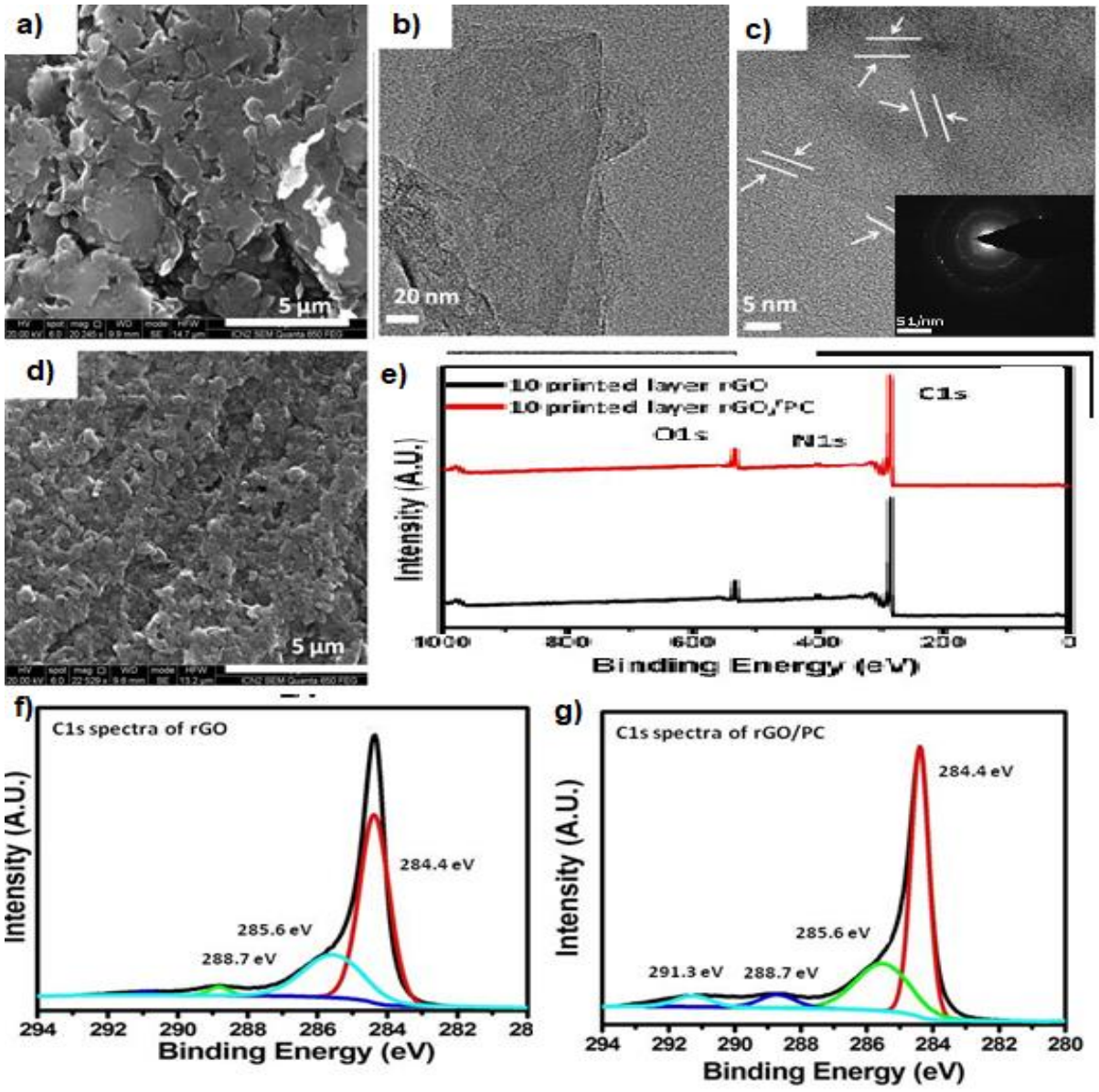

Figure 3. a) SEM image of raw rGO powder. b) TEM image of the rGO taken from the rGO ink. c) Selected area electron diffraction (SAED) pattern of rGO taken from the rGO ink. d) SEM image of inkjet-printed rGO pattern. e) XPS spectra of printed rGO patterns before (black) and after (red) photonic curing. f) Core level C1s of XPS spectrum of rGO before photonic curing. g) Core level C1s of XPS spectrum of rGO after photonic curing.

Electrochemical characterization

The three-electrode sensors were analysed by cyclic voltammetry (CV) in 2mM ferro/ferri containing 0.1 M KNO_3 solution (**Fig. 4a**). The electrochemical oxidation and reduction of Ferri/Ferro can be seen at ~0.13 and~ 0.04V respectively for the 1st, 15th and 25th electrode with similar current values proving high repeatability for several electrodes. Effect of layers was studied and optimised next (**Fig. 4b**). It can be seen from fig. 2 (b) that the current increased with increasing no. of prints and clear signals could be observed at as low as just 2 prints, this implied that with just two printed layers, decent graphene coverage for connectivity could be achieved which could be further improved by printing more layers.

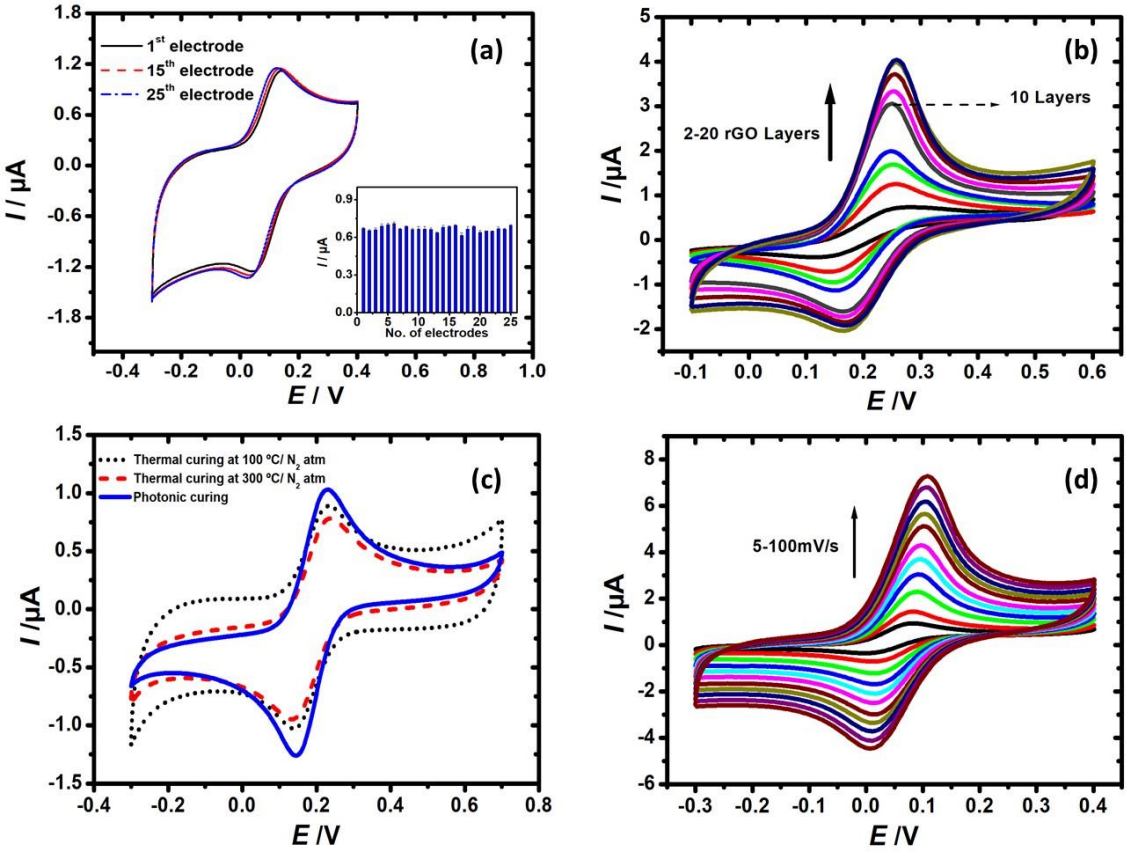

Figure 4. a) Sensor reproducibility study with 25 inkjet printed sensors with 20L rGO photonically cured in 2 mM /ferro//ferri and 0.1 M KNO_3 at 50 mV/s,. b) Effect of the number of printed layers in 2 mM FcMeOH and 0.1 M KNO_3. at 50 mV/s . c) Effect of thermal and photonic curing. d) Effect of scan rate from 5 to 100 mV/s. in 2 mM FcMeOH and 0.1 M KNO_3, at 50 mV/s

However, not a considerable increase in peak current was observed after 10 prints and the peak-to-peak separation was the best at and after this point (76 ± 2 mV at 50 mV/s) that implies the film just got thicker without significant increase in the real surface anymore, therefore further tests and sensing measurements were performed with 10 rGO prints always. In future, printing parameters can be modified to change the printing process, for instance, by playing with the jetting voltages, droplet volumes or drop spacing etc different prints could be obtained or the quality could be further enhanced. Effect of thermal and photonic curing is shown in (**Fig. 4c**). For thermal treatments, the prints were subjected to 100 and 300 ºC under N_2 flow for 1 h and the patterns were compared in 2 mM ferro/ferri solution in 0.1M KNO_3 and at 50 mV/s from -0.3 to 0.8 V. From the obtained voltammograms, we can see that that curing photonically and thermally at high temperature provided comparable results with slightly closer peak separation potentials after photonic treatment, 80mV for PC, 86 and 88 mV for TC at 300 and 100 ºC respectively at 50mV/s. Additionally, the reduction in capacitive signals suggests that the edge functionalities/defects on the graphene sites were reduced with partial restoration of the sp2 structure. This has been shown by many studies that the capacitance of Graphene is higher at the edges than the basal planes as the edges provide greater accessibility to the solvent ions and large inhomogeneities of the charges allow greater ion adsorption [56][57][58]. Reduction of capacitive current could also indicate that the film gets more compact = less porous, as also thermal curing at 300 °C shows the reduction of the capacitive current. Less double layer charging, but still linear diffusion during CV. For all the above optimisations, an external Ag/AgCl R.E was used instead of the Ag to avoid any uncertainty. Finally, a scan rate dependency study was made of the sensors with an all inkjet printed and integrated three electrode system (printed Ag was used as the R.E). Response towards different

redox mediators and a scan rate dependency study was tested as shown in the supporting information(S 1-4). Except for FCMeOH (Fig. 4d), a linear function -of the anodic peak currents (Ip_a) towards the square root of the scan rates ($\upsilon^{1/2}$) was observed for $[Fe(CN_6)]^{3-/4-}$, $IrCl^{3-}_6$, $[Ru(NH_3)_6]^{3+}$ with high reproducibility of the scans, suggesting a semi-infinite diffusion controlled process. For oxidation and reduction of FCMeOH, value of the slope obtained from the log (Ipa) vs log (υ) was 0.72 indicating the presence of adsorption processes, this could also be verified by calculating the ratio of anodic and cathodic peak currents Ipa/IPc which was ~1.4, far away from the ideal 1 suggesting not all the reduced FCMeOH species while oxidation was reduced back to its original form[59]. Furthermore, the peak-to-peak separation potentials (ΔE = Epa - Epc) for oxidation and reduction at different scan rates of all the redox mediators exceeded the theoretical value 59mV for one electron transfer process. The deviated values obtained for Ferro/ferri (83.4 ± 4mV), FCMeOH (74.7 ± 8.4 mV), $IrCl^{3-}_6$ (74.3 ± 4.8 mV) and $[Ru(NH3)6]^{3+}$ (63.4 ± 2.8 mV) can be due to the IR drop and kinetic limitations at the electrode or due to the defects present in Graphene during its preparation, printing or post printing treatments (boundary defects or the present oxygen functionalities)[60][59]. The sensors showed a very high reproducibility when the peak currents and the peak potential separation was calculated for 25 different electrodes with average peak-to-peak separation and anodic peak intensity of 72.6 ± 5.1 mV and 0.67 ± 0.014 µA (see Fig. 6) and each electrode was useable atleast 5-6 times.

Viable bacterial detection

Metabolically active bacteria can be detected using redox dyes that permeate into the cell where they under reduction by the respiratory chain [61][62]. This concept is used since long in colorimetric bacteria assays. However, since recently, this concept has also found application in electrochemical sensing, as many of the known redox dye molecules are electro-active and thus detectable with amperometric electrodes [63]. Resazurin (RS) and the three tetrazolium based indicator dyes TTC, CTC and INT were

analysed measuring CVs and DPVs of blank samples (redox indicator in LB) and test solutions (redox indicator in LB with 8.3×10^8 *E. coli* cells (strain DH5alpha)/mL (**Fig. 5**)). Electrochemical measurements of all the redox indicators with or without the bacteria was performed by cycling from 0 to -0.8V and concentration of the redox indicators was in all cases 5 mM. Reverse cycling was performed using cyclic voltammetry for understanding the behavior of indicators, it shows clear oxidation and reduction peaks (humps) during the reverse (negative) and forward (towards positive) scans respectively. Differential Pulse Voltammetry (DPV) was performed for quantifying purposes. Characteristic reduction peaks of the four redox indicators RS, CTC, TTC and INT are evident from Fig. 5. Cyclic voltammetry was carried out by scanning towards negative potential in order to electrochemically reduce the indicators, demonstrated irreversibility for TTC, CTC and INT characterized by the missing oxidation peaks. These tetrazolium salts showed reduction peaks of different shapes and at different potentials owing to different reaction kinetics. RS reduction, on the other hand, demonstrates two peaks (at ~ 0.2V and ~ 0.36V), it is first reduced to irreversible resorufin and then reversibly to dihydroresorufin [64].

Higher activity of reduction by bacteria were observed with RS and CTC exhibiting higher activity with peak reduction of 60.6 and 68.9% whereas TTC and INT showed lower reduction activity with only 40 and 32.1 % after incubation with live bacteria (E.Coli) on the rGO electrode surface. The electrochemical reduction of the redox indicators showed similar behavior reported by Zhu et al where sensing was performed using Inkjet printed CNT electrodes [63].

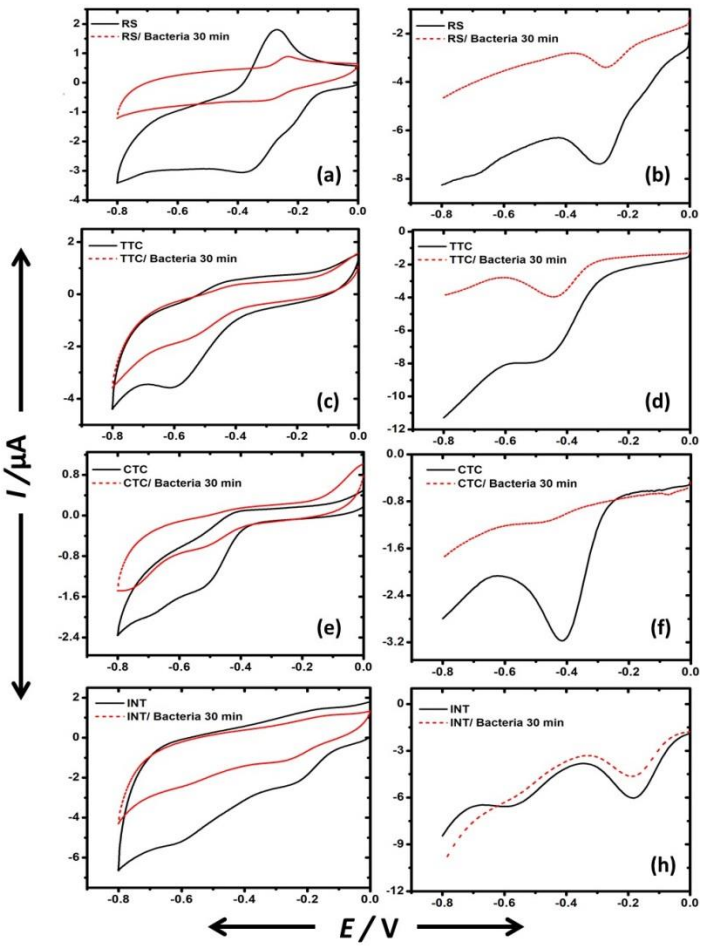

Figure 5. Electrochemical detection of viable bacteria (8.3×10^8 *E. coli* cells (strain DH5alpha)/mL) using the rGO-based sensors (10 L rGO) with CV (left panels) and DPV (right panels) for RS (a, b), TTC (c, d), CTC (e, f) and INT (g, h). Blanks (no bacteria) are shown in black/solid and test solutions with bacteria after 30 min of incubation are shown in red/dashed. Experimental conditions: lysogeny broth, CV parameters: scan rate 50 mV/s; DPV parameters: scan rate 50 mV/s, step potential 5 mV, potential pulse 100 mV and pulse time 0.05 s.

Conclusions

A very simple and straightforward yet highly effective inkjet printing of graphene electrodes by formulating a highly concentrated (30mg/ml), surfactant free graphene ink has been achieved. This prudent selection of the materials solvents and parameters led to fabrication of electrodes that demonstrated very good reproducibility, excellent and uniform prints over Kapton substrates with very high resolutions with less time consumption. This strategy eliminates the use of harsh post treatment

steps making it applicable to variety of substrates, in turn, applicable to numerous applications. Electrochemically, the electrodes exhibit quasi-reversible behavior with close small peak-to-peak separations. These inks can be patterend and used for variety for flexible electrical or electrochemical application, out of which, the sensing ability is demonstrated here by performing few preliminary measurements for detection of live E.Coli. The work has great potential for efficient and low cost (<20 cents/ rGO/sensor) mass production of flexible electronics. Furthermore, the prepared electrodes are not limited to just bacterial sensing, they can be used for various other electrical or electrochemical applications that includes chemical or biosensing or energy storage applications etc.

References

[1] G. Hu *et al.*, "Functional inks and printing of two-dimensional materials," *Chem. Soc. Rev.*, vol. 47, no. 9, pp. 3265–3300, 2018.

[2] D. Grieshaber, R. MacKenzie, J. and Voros, and E. Reimhult, "Electrochemical Biosensors - Sensor Principles and Architectures," *Sensors*, vol. 8, pp. 1400–1458, 2008.

[3] M. Pohanka and P. Skládal, "Electrochemical Biosensors-Principles and Applications," *J. Appl. Biomed.*, vol. 6, 2008.

[4] R. S. Kelly, "Analytical Electrochemistry: Basic concepts," 2019.

[5] K. Yamanaka, M. C. Vestergaard, and E. Tamiya, "Printable Electrochemical Biosensors: A Focus on Screen-Printed Electrodes and Their Application," *Sensors*, vol. 16, p. 1761, 2016.

[6] K. Honeychurch, "Printed thick-film biosensors," *Print. Film. Mater. Sci. Appl. Sensors, Electron. Photonics*, pp. 366–409, 2012.

[7] S. Cinti and F. Arduini, "Graphene-based screen-printed electrochemical (bio)sensors and their applications: Efforts and criticisms," *Biosens. Bioelectron.*, vol. 89, pp. 107–122, 2017.

[8] M. Pumera, "Graphene in biosensing," *Mater. Today*, vol. 14, no. 7–8, pp. 308–315, 2011.

[9] S. Centi, A. I. Stoica, S. Laschi, and M. Mascini, "Development of an electrochemical immunoassay based on the use of an eight-electrodes screen-printed array coupled with magnetic beads for the detection of antimicrobial sulfonamides in honey," *Electroanalysis*, vol. 22, no. 16, pp. 1881–1888, 2010.

[10] A. I. Zamaleeva *et al.*, "A whole-cell amperometric herbicide biosensor based on magnetically functionalised microalgae and screen-printed electrodes," *Anal. Methods*, vol. 3, no. 3, pp. 509–513, 2011.

[11] B. Nagar, M. Balsells, A. de la Escosura-Muñiz, P. Gomez-Romero, and A. Merkoçi, "Fully printed one-step biosensing device using graphene/AuNPs composite," *Biosens. Bioelectron.*, 2018.

[12] P. He *et al.*, "Fully printed high performance humidity sensors based on two-dimensional materials," *Nanoscale*, vol. 10, no. 12, pp. 5599–5606, 2018.

[13] Y. Aleeva and B. Pignataro, "Recent advances in upscalable wet methods and ink formulations for printed electronics," *J. Mater. Chem. C*, vol. 2, no. 32, pp. 6436–6453, 2014.

[14] S. Lawes, A. Riese, Q. Sun, N. Cheng, and X. Sun, "Printing nanostructured carbon for energy storage and conversion applications," *Carbon N. Y.*, vol. 92, pp. 150–176, 2015.

[15] G. Hu *et al.*, "Functional inks and printing of two-dimensional materials," *Chem. Soc. Rev.*, vol. 47, no. 9, pp. 3265–3300, 2018.

[16] Anonymous, "FUJIFILM Dimatix Materials Printer DMP-2800 Series User Manual," *2010*. User Manual ed. U.S.A.: FUJIFILM Dimatix, Inc., 2010.

[17] H. Yoo and C. Kim, "Colloids and Surfaces A : Physicochemical and Engineering Aspects Experimental studies on formation , spreading and drying of inkjet drop of colloidal suspensions," *Colloids Surfaces A Physicochem. Eng. Asp.*, vol. 468, pp. 234–245, 2015.

[18] B. Derby, "Inkjet Printing of Functional and Structural Materials: Fluid Property Requirements, Feature Stability, and Resolution," *Annu. Rev. Mater. Res.*, vol. 40, no. 1, pp. 395–414, 2010.

[19] A. Kamyshny and S. Magdassi, "Conductive nanomaterials for printed electronics," *Small*, vol. 10, no. 17, pp. 3515–3535, 2014.

[20] I. Reinhold, "Inkjet Printing of Functional Materials and Post-Processing," in *Nanomaterials for 2D and 3D Printing*, John Wiley & Sons, Ltd, 2017, pp. 27–49.

[21] B.-J. de Gans, P. C. Duineveld, and U. S. Schubert, "Inkjet Printing of Polymers: State of the Art and Future Developments," *Adv. Mater.*, vol. 16, no. 3, pp. 203–213, 2004.

[22] R. P. Tortorich and J.-W. Choi, "Inkjet Printing of Carbon Nanotubes," *Nanomaterials*, vol. 3, pp. 453–468, 2013.

[23] O.-S. Kwon *et al.*, "Fabrication and characterization of inkjet-printed carbon nanotube electrode patterns on paper," *Carbon N. Y.*, vol. 58, pp. 116–127, 2013.

[24] L. Dybowska-Sarapuk *et al.*, "Efficient Inkjet Printing of Graphene-Based Elements: Influence of Dispersing Agent on Ink Viscosity," *Nanomaterials*, vol. 8, no. 8, p. 602, 2018.

[25] Novoselov K. S. and Geim A. K, "The Rise of Graphene," *Nat. Mater.*, vol. 6, pp. 1–14, 2007.

[26] A. K. Geim, "Graphene : Status and Prospects," *Science (80-.).*, vol. 1530, no. 2009, pp. 1530–1534, 2014.

[27] C. N. R. Rao, U. Maitra, and H. S. S. R. Matte, "Synthesis, Characterization, and Selected Properties of Graphene," *Graphene Synth. Prop. Phenom.*, pp. 1–47, 2012.

[28] S. Gambhir, R. Jalili, D. L. Of, and G. G. Wallace, "Chemically converted graphene : scalable chemistries to enable processing and fabrication," no. March, 2015.

[29] S. Kholghi, A. Chinnappan, W. A. D. M. Jayathilaka, M. Khatibzadeh, E. Kowsari, and S. Ramakrishna, "A review on inkjet printing of CNT composites for smart applications," *Appl. Mater. Today*, vol. 9, pp. 372–386, 2017.

[30] A. V Eletskii, I. M. Iskandarova, A. A. Knizhnik, J. S. Ponraj, Z. Xu, and S. Chander, "2D printing technologies using graphene-based materials."

[31] R. K. Singh, R. Kumar, and D. P. Singh, "Graphene oxide: strategies for synthesis, reduction and frontier applications," *RSC Adv.*, vol. 6, no. 69, pp. 64993–65011, 2016.

[32] D. W. Johnson, B. P. Dobson, and K. S. Coleman, "Current Opinion in Colloid & Interface Science A manufacturing perspective on graphene dispersions," *Curr. Opin. Colloid Interface Sci.*, vol. 20, no. 5–6, pp. 367–382, 2015.

[33] M. V. Bracamonte, G. I. Lacconi, S. E. Urreta, and L. E. F. Foa Torres, "On the nature of defects in liquid-phase exfoliated graphene," *J. Phys. Chem. C*, vol. 118, no. 28, pp. 15455–15459, 2014.

[34] P. Li, C.-A. Tao, B. Wang, J. Huang, T. Li, and J. Wang, "Preparation of Graphene Oxide-Based Ink for Inkjet Printing," *J. Nanosci. Nanotechnol.*, vol. 18, no. 1, pp. 713–718, 2018.

[35] Y. Gao, W. Shi, W. Wang, Y. Leng, and Y. Zhao, "Inkjet Printing Patterns of Highly Conductive Pristine Graphene on Flexible Substrates," *Ind. Eng. Chem. Res.*, vol. 53, no. 43, pp. 16777–16784, 2014.

[36] W. Yang and C. Wang, "Graphene and the related conductive inks for flexible electronics," *J. Mater. Chem. C*, vol. 4, no. 30, pp. 7193–7207, 2016.

[37] S. Kuss, H. M. A. Amin, and R. G. Compton, "Electrochemical Detection of Pathogenic Bacteria—Recent Strategies, Advances and Challenges," *Chem. – An Asian J.*, vol. 13, no. 19, pp. 2758–2769, 2018.

[38] A. Lesch *et al.*, "Large scale inkjet-printing of carbon nanotubes electrodes for antioxidant assays in blood bags," *J. Electroanal. Chem.*, vol. 717–718, pp. 61–68, 2014.

[39] M. Jović *et al.*, "Inkjet-printed microtiter plates for portable electrochemical immunoassays," *J. Electroanal. Chem.*, vol. 786, pp. 69–76, 2017.

[40] T. Carey *et al.*, "Fully inkjet-printed two-dimensional material field-effect heterojunctions for wearable and textile electronics," *Nat. Commun.*, vol. 8, no. 1, 2017.

[41] D. McManus *et al.*, "Water-based and biocompatible 2D crystal inks for all-inkjet-printed heterostructures," *Nat. Nanotechnol.*, vol. 12, no. 4, pp. 343–350, 2017.

[42] E. B. Secor, P. L. Prabhumirashi, K. Puntambekar, M. L. Geier, and M. C. Hersam, "Inkjet printing of high conductivity, flexible graphene patterns," *J. Phys. Chem. Lett.*, vol. 4, no. 8, pp. 1347–1351, 2013.

[43] J. E. Fromm, "Numerical Calculation of the Fluid Dynamics of Drop-on-Demand Jets," *IBM J. Res. Dev.*, vol. 28, no. 3, 1984.

[44] B. Derby, "Inkjet Printing of Functional and Structural Materials : Fluid Property Requirements , Feature Stability , and Resolution" no. August 2015, 2010.

[45] B. Derby, "Inkjet printing ceramics: From drops to solid," *J. Eur. Ceram. Soc.*, vol. 31, no. 14, pp. 2543–2550, 2011.

[46] P. He and B. Derby, "Inkjet printing ultra-large graphene oxide flakes," *2D Mater.*, vol. 4, no. 2, p. aa629e, 2017.

[47] F. Torrisi *et al.*, "Inkjet-printed graphene electronics," *ACS Nano*, vol. 6, no. 4, pp. 2992–3006, 2012.

[48] A. W. Robertson and J. H. Warner, "Hexagonal single crystal domains of few-layer graphene on copper foils," *Nano Lett.*, vol. 11, no. 3, pp. 1182–1189, 2011.

[49] E. B. Secor, B. Y. Ahn, T. Z. Gao, J. A. Lewis, and M. C. Hersam, "Rapid and Versatile Photonic Annealing of Graphene Inks for Flexible Printed Electronics," *Adv. Mater.*, vol. 27, no. 42, pp. 6683–6688, 2015.

[50] V. Costa Bassetto *et al.*, "Rapid inkjet printing of high catalytic activity Co3O4/N-rGO layers for oxygen reduction reaction," *Appl. Catal. A Gen.*, vol. 563, pp. 9–17, 2018.

[51] E. B. Secor, T. Z. Gao, M. H. Dos Santos, S. G. Wallace, K. W. Putz, and M. C. Hersam, "Combustion-Assisted Photonic Annealing of Printable Graphene Inks via Exothermic Binders," *ACS Appl. Mater. Interfaces*, vol. 9, no. 35, pp. 29418–29423, 2017.

[52] S. J. Choi, S. J. Kim, and I. D. Kim, "Ultrafast optical reduction of graphene oxide sheets on colorless polyimide film for wearable chemical sensors," *NPG Asia Mater.*, vol. 8, no. 9, pp. 1–10, 2016.

[53] C. L. J, C.-S. R, and H. J, "Flash Reduction and Patterning of Graphite Oxide and Its Polymer Composite," *J. Am. Chem. Soc.*, vol. 131, no. 31, pp. 11027–11032, 2009.

[54] W. Gao, L. B. Alemany, L. Ci, and P. M. Ajayan, "graphite oxide," *Nat. Chem.*, vol. 1, no. 8, pp. 403–408, 2009.

[55] J. M. Chem, "Journal of Materials Chemistry," pp. 23227–23231, 2012.

[56] C. Zhan, Y. Zhang, P. T. Cummings, and D. en Jiang, "Computational insight into the capacitive performance of graphene edge planes," *Carbon N. Y.*, vol. 116, pp. 278–285, 2017.

[57] D. A. C. Brownson, L. J. Munro, D. K. Kampouris, and C. E. Banks, "Electrochemistry of graphene: Not such a beneficial electrode material?," *RSC Adv.*, vol. 1, no. 6, pp. 978–988, 2011.

[58] A. J. Pak, E. Paek, and G. S. Hwang, "Impact of graphene edges on enhancing the performance of electrochemical double layer capacitors," *J. Phys. Chem. C*, vol. 118, no. 38, pp. 21770–21777, 2014.

[59] D. a. C. Brownson and C. E. Banks, *The Handbook of Graphene Electrochemistry - Chapter 2 - Interpreting Electrochemistry*, no. Cvd. 2014.

[60] J. Electroanal, U. Parts, and P. Cedex, "(Received 26th August 1982; in revised form 27th October 1982)," vol. 147, pp. 39–51, 1983.

[61] T. Bernas and J. W. Dobrucki, "The Role of Plasma Membrane in Bioreduction of Two Tetrazolium Salts , MTT , and CTC," vol. 380, no. 1, pp. 108–116, 2000.

[62] J. L. Chen, T. W. J. Steele, and D. C. Stuckey, "Metabolic reduction of resazurin; location within the cell for cytotoxicity assays," *Biotechnol. Bioeng.*, vol. 115, no. 2, pp. 351–358, 2018.

[63] Y. Zhu *et al.*, "Immuno-affinity Amperometric Detection of Bacterial Infections," *Angew. Chemie Int. Ed.*, vol. 57, no. 45, pp. 14942–14946, 2018.

[64] R. S. Twigg, "Oxidation-Reduction Aspects of Resazurin," *Nature*, vol. 155, pp. 401–402, 1945.

Supplementary Information

S1

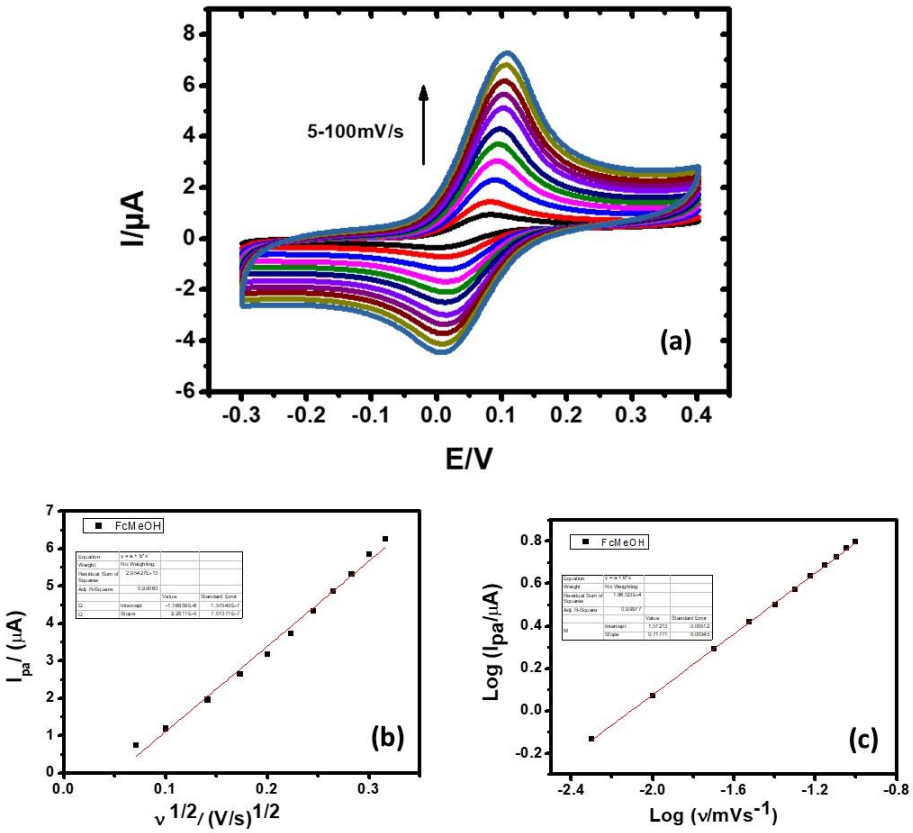

Figure 1: (a) Scan rate dependency of rGO electrode 10 printed L (b) Anodic Current (Ipa) vs square root of scan rate (υ) and (c) Log of anodic current (Ipa) vs square root of scan rate (υ) in in 2mM FcMeOH/0.1M KNO_3

S2

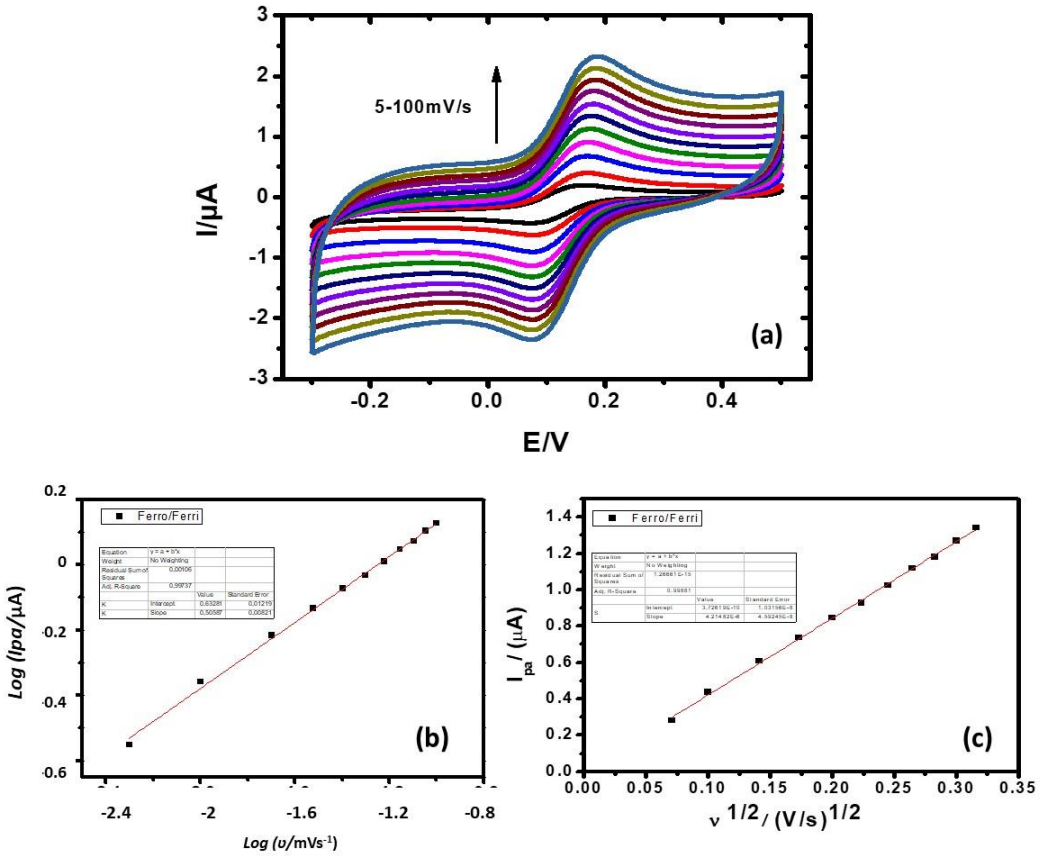

Figure 2: (a) Scan rate dependency of rGO electrode 10 printed L (b) Log of anodic current (Ipa) vs square root of scan rate (υ) and (b) Anodic Current (Ipa) vs square root of scan rate (υ) in 2mM Ferro/Ferri/0.1M KNO_3

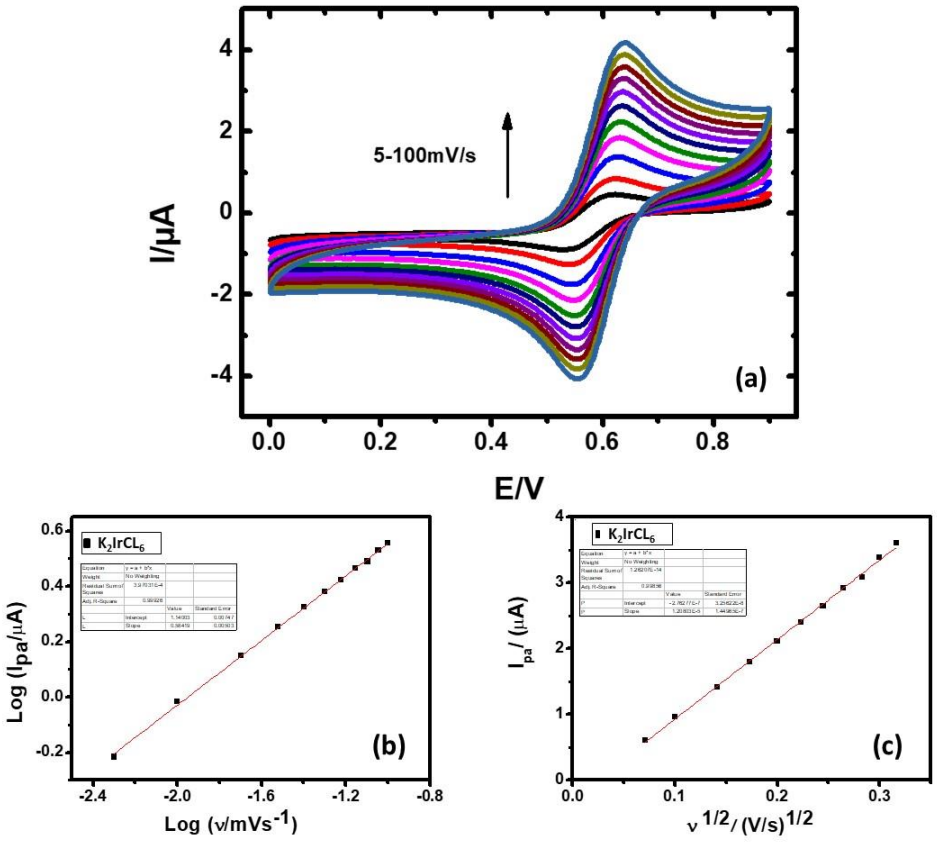

Figure 3: (a) Scan rate dependency of rGO electrode 10 printed L (b) Log of anodic current (Ipa) vs square root of scan rate (υ) and (b) Anodic Current (Ipa) vs square root of scan rate (υ) in 2mM (K_3IrCl_6)/0.1M KNO_3

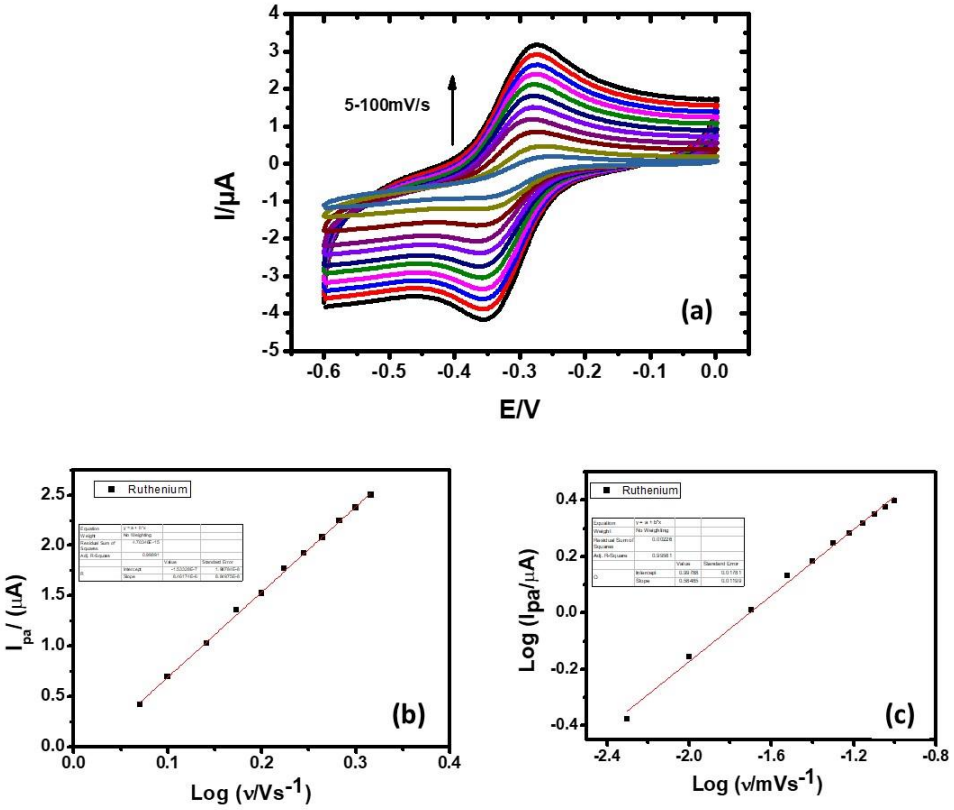

Figure 4: (a) Scan rate dependency of rGO electrode 10 printed L (b) Anodic Current (Ipa) vs square root of scan rate (υ) and (c) Log of anodic current (Ipa) vs square root of scan rate (υ) in in 2mM ($[Ru(NH_3)_6]Cl_3$)/0.1M KNO_3

CHAPTER 4
Conclusions and Future Perspectives

Detailed conclusions are mentioned at the end of each work presented. In this chapter, general conclusions, shortcomings and future perspective on the fabricated devices are discussed. Enhanced performance characteristics of proof of concept devices have been demonstrated along with unique strategies employed that can be used as initial trials for further research. Some shortcomings that must be overcome for the proposed technologies to be used for commercial applications along with the possible solutions are mentioned below:

Energy Storage

We were able to demonstrate the fabrication and working of three different supercapacitor devices using different technologies and materials.

(i) In the first example, easiest coating method was used to develop supercapacitor device using double hybrid technology over flexible Textile substrates. Technically, the device showed great performance in terms of capacitance, energy and power densities and in principle the fabrication can be done for large scale and low-cost applications .The symmetric cell composed of rGO modified with anchored phoshotungstic acid (rGO-$H_3PW_{12}O_{40}$) and combined with hybrid electrolyte (hydroquinone-doped gel electrolyte; HQ doped PVA-H_2SO_4) exhibited a wide working potential of 1.6V and an ultra-high energy density of 2.38 mWh/cm^3. The self-discharge of the device for long term application due to redox- active electrolyte might be an issue.

(ii) The second work presented showed a very good response and performance of the graphene printed paper electrode supercapacitor device. In this case, we used the hybrid electrode technology which aided the enhanced overall performance like the high volumetric capacitance of 130 mF cm^{-3} at a current density of 6.5 mA cm^{-3} and maximum energy and power density of 0.026 mWh cm^{-3} and 13.4 mW cm^{-3}, respectively of the graphene electrode with Redox active KI along with 97% capacitance retention after 3000 charge/discharge cycles. However, for its practical application, a lot of key factors still need to be worked upon. Some of these factors are, (a) the self-discharge of the device was tested to be very high (due to the solubility of KI that led to its migration through the paper), (b) concerning the paper substrate, conventional paper was used to demonstrate the device performance, but the paper incorporates different additives, binders etc during its fabrication which could give different and unwanted signals directly affecting the reproducibility, plus the poor mechanical strength in aqueous electrolytes doesn't make it possible to be industrially used. For this purpose different kinds of paper substrates or solid electrolytes can be tested as part of future work. Solid electrolytes can not only help in maintaining the device stability but can also help in easy and leakage-free packaging.

(iii) The third work showed the use of N-doped CNPipes/Graphene composite printed through screen printing using Ionic liquid as the binder. Screen printing method was highly efficient in preparing the micro-interdigitated patterns reproducibly and the symmetric cells of the hybrid exhibited a high capacitance value of 95.34 mF/cm^2 in redox-active aqueous electrolyte (KI/KOH) with high energy and power densities of 19 μWh/cm^2 and 11.2 mW/cm^2 respectively with 80% capacity retention for 2000 charge/discharge cycles. In this work, the N-doped CNTs were prepared by pyrolyzing previously synthesised polypyrrole nanotubes, but the Polypyrrole nanotubes were not studied as the electrode material due

to the lack of its ability to form a stable ink. Numerous efforts were made to make polypyrrole based inks but it was extremely difficult to find a suitable solvent for its uniform dispersion without making structural or chemical changes. Also, the use of ionic liquid undoubtedly resulted in better performance of the device, however, its binding capabilities compared to the conventional polymer based binders is not comparable and often the patterns could easily be scratched off from the substrate surface. Future steps here might include formulation of polypyrrole nanotubes inks and compare its behaviour with graphene as well as with the N-doped CNTs along with trying different ILs and different concentrations or perhaps the mixtures with other binders.

Electrochemical sensors

(i) An DNA sensor fully printed in one step was demonstrated using an rGO/Au composite. The proposed sensor promises a number of advantages like high sensititivity (reaching a detection limit of 0.18 nM), wide concentration range (linear response in the range of concentrations 0.01–20 μM) and integrated immobilisation technique, environmentally friendly device fabrication and no need for post printing steps that gives us the advantage of using any type of substrate regardless of its thermal or mechanical stability. Another major benefit of the technique is that it is not just limited for DNA sensing, it can be applied to make immunosenosrs, whole cell or enzymatic electrochemical sensors. The weak point of the technique is the reproducibility. Because of the mechanism proposed, there are certain unavoidable deviations in each transfer like the concentration or the distribution of AuNPs can vary since the AuNPs and Graphene is not chemically bonded, which directly affects the reproducibility. It is very important to very carefully monitor each transferring step to obtain

reproducible results. One way to avoid this is by transferring as many electrodes as possible in one transferring step.

(ii) Other work is focussed on the preparation of Graphene-based inks for inkjet application. The prepared highly concentrated ink of 30 mg/ml shows excellent and reproducible electrochemical performance in different redox mediated electrolytes. Combination of photonic curing gave an additional benefit to the device by making the use of different flexible substrates like PET that do not have very high melting points possible. The ability of the prepared electrode as a sensing platform was tested for detection of bacteria. Bacterial detection (E. Coli; strain DH5alpha cells) at high concentrations was performed electrochemically as a proof of concept and the results exhibited decrease in peak current values upon incubation of the redox indicators with bacterial cells demonstrating effective reduction by live bacteria. Additionally, the proposed electrodes can be used for other bio or chemical sensing, especially for heavy metals detection. The ink was very stable during the printing procedure (long hours), however, if kept idle overnight, troubles (including aggregation, blocked nozzle, etc.) in printing later occurred. This was avoided by cleaning the whole cartridge everytime if the ink was kept idle overnight or by using fresh ink for each printing. Generally, enough electrodes (80 – 90) electrodes could be printed with one filled cartridge. Another disadvantage is the use of NMP, which is a toxic organic solvent. Although, the ink was printed with the combination of 1,2 Propanediol (Propylene Glycol), research for other suitable solvents must be done in order to make an eco-friendly